Granites from the Midyan terrain, NW Saudi Arabia: Petrology, geochemistry and geochronology

Rami A. M. Bakhsh

Thesis submitted to Royal Holloway, University of London

for the degree of Doctor of Philosophy

Declaration of Authorship

I, Rami Bakhsh, herby declare that this thesis and the work presented in it is entirely my own. Where I have quoted the work of others, this is always clearly stated. This work has not been submitted for any other degree or award in any other university or educational establishment.

Signed:

(Rami A. M. Bakhsh)

Date:

Acknowledgements

I would like to thank God, the Most Gracious, and the Most Merciful for helping me to accomplish my doctoral studies. I would like to thank my parents, my wife and my son Rayan, my cousin Alaa Hakeem and my friend Naser Al-Jahdali for their support, my government for sponsoring me and my home university (King Abdul Aziz) for facilitating the field trips.

I am deeply grateful to my supervisor, Dr. David Alderton, for maintaining high standards in supervision, guidance, academic knowledge and attitude. In addition, I would like to thank Prof. Martin Menzies for his helpful comments during the upgrade period, Prof. Margaret Collinson for following up the progress of my thesis, Prof. Matthew Thrilwall for allowing me to attend his intensive courses in geochemistry and for giving me the opportunity to use the facilities in the geochemistry laboratory, Dr. Christina Manning for her supervision of my isotopic work and Dr. Nathalie Grassineau for her assistance with the geochemical analysis using the ICP-MS and AES.

I would like also to thank Dr. Inga Sevastjanova for instructing me in the techniques of mineral separation, Sue Hall for instructing me in the geochemical analysis, Neil Holloway who prepared all the thin- and polished sections and resin blocks, Sharon Gibbons for her assistance with the scanning electron microscope, Kevin D'Souza for showing me how to take photos in the optics lab, and Dr. Andy Beard and Dr. Martin Ritner from UCL who gave me the opportunity and helped me in using the electron-probe and to use the laser ablation ICPMS, respectively.

Finally, I will not forget to thank the lecturers, secretaries and students in the Earth Sciences department for providing me with a healthy and productive research environment during my Ph.D study.

List of Contents

List of Figures

List of Tables

Granites from the Midyan terrain, NW Saudi Arabia: Petrology, geochemistry and geochronology

Five, Neoproterozoic, poorly-studied felsic intrusives from NW Saudi Arabia have been subjected to a detailed geological study to understand their characteristics, evolutionary history, tectonic setting, ages and economical potential for rare metal mineralization.

The work has utilized field observations, mapping, mineralogy, petrography, geochemistry (ICP-AES and MS, XRF, scanning electron microscopy and microprobe) and geochronology (Rb/Sr whole rock isochrons and U-Pb zircon analysis).

The results have indicated that the individual plutons in the region are each quite different. This is mainly displayed by the existence of different types of granites, based on chemistry and petrography (peralkaline, alkaline and calc-alkaline) and mineralogy (particularly the presence of different types of amphibole, both sodic and calcic). The plutons probably formed at low crystallizaton pressures (~ 1.2 to 3.4 Kbar) and at shallow (~4 to 12 km ±0.5 km) depths, but seem to have been derived from similar source regions. The granites were most likely derived by low-pressure, partial melting of crustal rocks with possible crustal contamination, followed by fractional crystallization and later sub-solidus alteration by fluids. The plutons' ages span a range from 630Ma (Cryogenian) to 554Ma (Ediacaran). The geochemical differences between the granites could be related to their formation during different stages of the region's evolution. A gradual change in tectonic setting is indicated, from island arc accretion in the middle stages of the Panafrican orogen, to a post-collisional setting in the early stages of the Panafrican event. Economically, the granites contain relatively high contents of rare earths elements (REEs) and rare-metals (RMs), mostly hosted by phosphates (monazite-Ce and xenotime), Nb-oxide (fergusonite-Y) and possible rare earth carbonates (synchysite). These elevated REEs and Nb contents and their mineralogical forms highlight the presence of suitable exploration targets for rare earth elements late stage deposits.

I. Introduction

I.1. The importance of granites

Granitic rocks are a very common igneous lithology, covering large parts of the Earth's continental crust. Studying granites is important for two reasons. Firstly, their study gives an indication of the formation processes (e.g. fractional crystallization, partial melting, and magma mixing). As granite is a product and indicator of crustal processes and evolution it's study may therefore allow the tectonic setting and evolution of a region to be determined. There are several mineralogical and chemical schemes for the classification of granites (e.g. the quartz-alkali feldspar-plagioclase-feldspathoid or the QAPF of Strekeisen, 1976, the modified alkali-lime index or the MALI and the Fe number of Frost *et al*., 2001). Some of these mineralogical/chemical classifications have been used to suggest the geological environments in which these magmas were generated and emplaced. The best known of these is the alphabetic scheme which initially introduced I (igneous) - and S (sedimentary)-type granites (Chappell and White, 1974), and later the M (mantle)-type, the A (alkaline)-type and its subdivisions (A1 and A2) (Loiselle and Wones, 1979; Eby, 1992). Chemical classifications were also developed by Pearce *et al*. (1984), through using trace elements to determine the tectonic environments in which various types of granites may form.

The second important feature of granites is their common association with deposits of important mineral commodities and in particular deposits of the rarer elements. Some examples of such metal deposits associated with granites are the Sn and W deposits in SW England (Alderton and Moore, 1981), the Fe-F (Cu, Mo, Cu-Pb-Zn, Ag, Au and REE) concentrations in the Bushveld granite in South Africa (Robb *et al*., 2000) and the biotite granites hosting deposits of columbite (and minor cassiterite, sphalerite, molybdenite, chalcopyrite and galena) in the Ririwai complex of northern Nigeria (Kinnaird *et al*., 1985). More specifically, some of the Cretaceous, calc-alkaline, granitic masses and alkali ring complexes that occupy the southern part of the Egypt Desert exhibit Sn mineralization and enrichments in other rarer metals (U, Th, Pb, W, Nb, Y, Be and Mo; Soliman, 1987).

In the Arabian shield, certain types of granites (e.g. albite-microcline microgranite, alkali microgranite, alkali-feldspar granite, alkali granite) display a distinct association

with rare metal (RM) and rare earth element (REE) deposits. The mineralization in these granites is commonly hosted in felsic veins and is closely associated with various postmagmatic, hydrothermal processes, such as albitization, greisenization, silicification, propylitic and phyllic alteration (Jackson, 1986). Many of these granite-associated deposits are of major economic significance and are set to become more important in the coming years. The study of granites and associated rare metal mineralization is thus of more than academic interest; it also has economic and industrial relevance.

RM is here considered to be any metal that is normally present in low concentrations in most rock types and is both difficult and expensive to extract from its ore (e.g. Ta, Nb, Au and Ag). In contrast, most of the REEs are not actually as rare as the RM in the earth's crust and they are more abundant than many other relatively common metals (Cu, Pb). The REE group consists of 17 REEs, 15 within the lanthanide chemical group, plus yttrium and scandium. They consist of two sub-groups, the Light rare earths (LREE) that range from lanthanum with an atomic number of 57 to gadolinium (64), and the heavy rare earths (HREE) that range from Yttrium with an atomic number of 39 to terbium (65) (Humphries, 2010). Until fairly recently the usage of these REEs was mostly restricted to certain industrial applications, such as ferrous and nonferrous metallurgy (Harben and Kuzvart, 1996), this has now all changed and they have wide and increasing applications, particularly in the telecommunications and electronics industries.

I.2. Justification for the selection of the study area

There has been a dramatic increase in the use of the REEs and RMs in technology over the past few decades. The world demand for rare earth elements is estimated at 134,000 tons annually and it is expected to rise to 180,000 tons by 2012 (Humphries, 2010). Other elements, such as zirconium and niobium, are also now in high demand (Info mine research group, 2008). However, most of the discovered deposits are currently located in a few countries, such as China, Australia and Brazil. As the market for such metals is mainly controlled by relatively few producers, this has promoted a major exploration impetus to find new deposits in other countries to satisfy the global demand for these commodities.

Various types of granite can be good hosts for concentrations of RMs and REEs and one region that contains large numbers of granites is the Arabian Shield in Saudi Arabia. However, many of these granites are not well studied and due to this lack of geological data, their geology and tectonic evolution have remained unclear. Therefore, a detailed geological study is needed to characterize these intrusives, determine their nature and ages and discover if they have any economic potential.

An initial study of some plutons from the Midyan terrain has indicated that some granites here are associated with RM and REE mineralization (e.g. the Nb-Th-Zr mineralization in a microgranite-microsyenite at Jabal Tawlah; Drysdall and Douch, 1986, and the Nb-Th-Zr-REE mineralization in the microgranite at the Ghurayyah prospect; Drysdall *et al*., 1984). Therefore, the locations for the present study were chosen with the aim of providing a better understanding of the geological history of the terrain and to investigate the potential for economic concentrations of metals.

I.3. Location of the Study area

Geographically, Saudi Arabia is located in southwest Asia, occupying an area of 2.25 million km^2 (Al-Shanti, 2003)**.**

Geologically, the Arabian shield occupies one-third (covering the western area) of the total area of Saudi Arabia and younger sedimentary cover occupies the remaining portion. Precambrian rocks underlie an area of 650,000 km^2 of the Western Arabian Peninsula. On its northern, eastern and southern sides, the Precambrian basement is covered by flat-lying, early to Late Paleozoic sediments and is bounded on its western side by Cenozoic formations along the Red Sea Coastal Plain. Tertiary and Quaternary alkali basalt flows and trachytes form several lava fields (the Harrats) along the Red Sea Coast, with an area of 80,000 km^2 (Al-Shanti, 2003).

The study areas are located in different parts of the Midyan terrain in the most northwestern part of the Arabian Shield (Longitude 26^o 40`E to $28^o$ 20` E; latitude from 35^o 10` N to $36^o$ 50` N; Fig. 1.1) and are mainly composed of Neoproterozoic felsic igneous plutons emplaced into Pre-Cambrian strata.

I.4. Aims of Project

1) To describe and characterize selected granitic masses from the Midyan region by observing field features, understanding their petrography and determining their mineralogy and geochemistry.
2) To define the ages of granite emplacement.
3) To use the chemistry and ages of the granites to fit them into a model for the tectonic evolution of the Arabia Shield.
4) To study the chemistry and mineralogy of these intrusives to determine if they could have any economic potential and warrant more detailed exploration.

I.5. Methodology

1- Field studies (aided by field reconnaissance, recent satellite images and detailed field sampling) to characterize the different granitic masses and collect material for further analysis.
2- Petrographic and mineralogical studies to characterize the main rock varieties and identify any variations in mineralogical composition. Electron probe microanalysis is used to identify individual minerals.
3- Geochemical analysis.
   a- Major elements, trace elements and REE. These are crucial to define the chemical variations, magmatic affinity and tectonic setting.
   b- Radiogenic isotopes (Rb-Sr in granites and U-Pb in zircon) will assist in defining the source region and ages.

All the above methods will be used to investigate the economic potential of the studied plutons and to see if previously published models for the tectonic evolution of the region are valid.

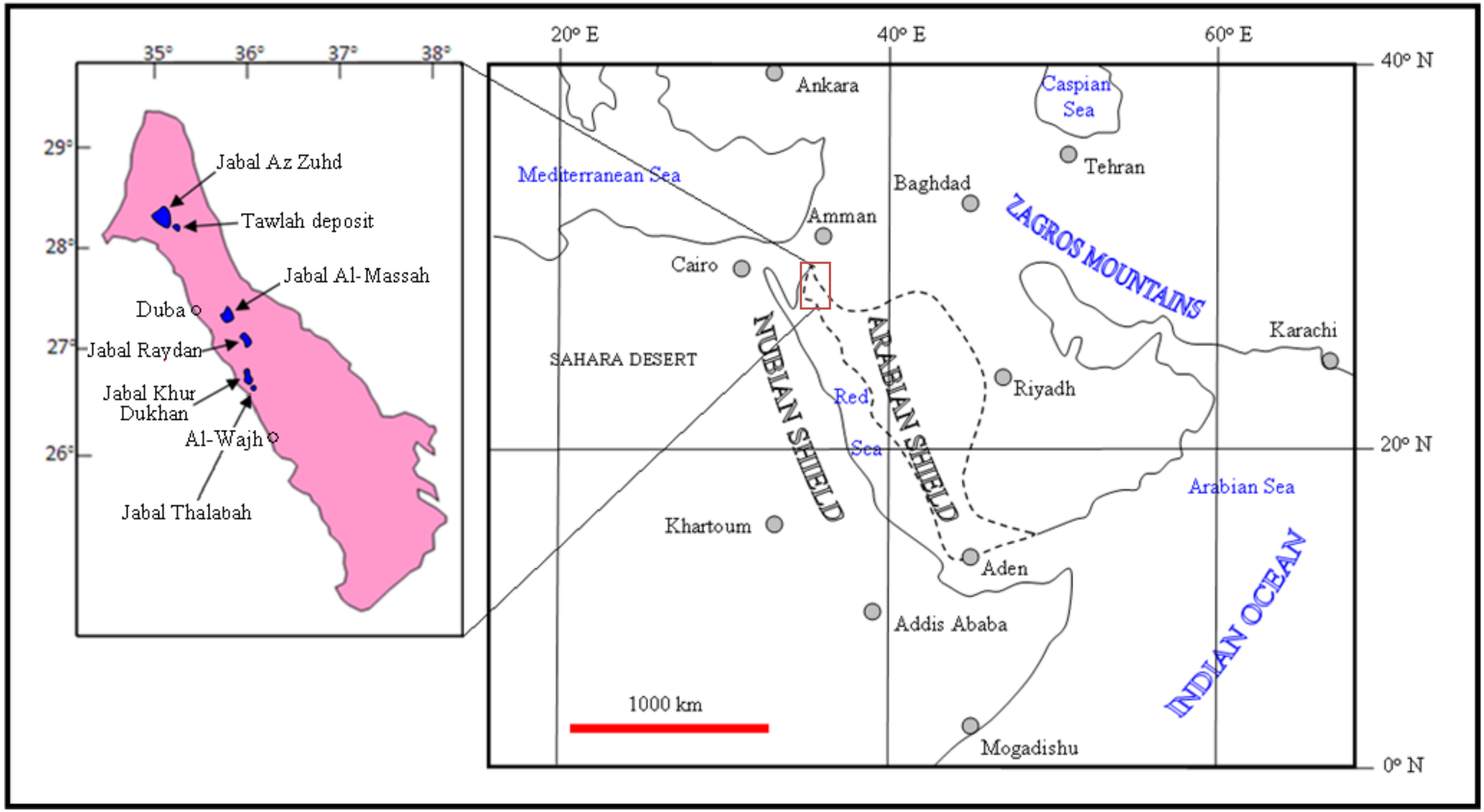

Figure 1.1: Map showing location of the Arabian shield & Midyan Terrain and the granites selected for this study (after Drysdall *et al*., 1986)

I.6. Structure of the thesis

- Chapter one simply defines the project, clarifying its importance, giving a brief introduction to the location of the areas of interest and justifying their selection. Finally it mentions the aims of the project and the methods used to obtain these goals.

- Chapter two covers the evolution of the Arabian Shield (discussing the different theories of formation), its geology, its classification, its major structural features and the constituent terrains.

- Chapter three covers the field observations, including sampling, basic geological mapping, and rock description in the field.

- Chapter four describes the petrographic study to characterize and distinguish the different masses.

- Chapter five is a mineralogical study, characterising the amphiboles and identifying the opaque and other, accessory, fine-grained mineral phases.

- Chapter six is mainly concerned with granite chemistry and uses the major and trace element data to achieve rock classification, and to determine magmatic series, magmatic affinity and tectonic environment. It also investigates the affect of alteration on granite chemistry and discusses the economical potential of the studied plutons

- Chapter seven is a geochronological study, using and comparing both whole rock Rb-Sr radiogenic isotopes and U-Pb zircon dating. These data are then used to clarify the granites' geological evolution.

- Chapter eight concludes with a discussion about how this study has advanced our understanding of the granites and the geological evolution of the Midyan terrain.

II. Geology of the Arabian Shield

II.1. Introduction

The Arabian shield is mainly composed of five terrains (see below), which have amalgamated along ophiolitic zones which were associated with East and West Gondwana convergence (Fig 2.1). Sedimentation and volcanism in several overlapping basins later contributed to the development of the larger tectonic unit. Subsequently the Arabian Shield separated from the Nubian shield during the early Tertiary Red Sea rifting event (Saudi Geological Survey, 2012).

Saudi Arabia (the host country of the Arabian Shield) is generally composed of Paleoproterozoic (older than 900 Ma) basement igneous and metamorphic lithologies (the latter with igneous and sedimentary protoliths), Neoproterozoic igneous and metamorphic rocks (900 to 500 Ma) and a cover of Cambrian to Tertiary sedimentary rocks. The Arabian Shield (Fig. 2.2) gets narrower towards the northern and southern regions. Its width in the north ranges between 50 and 100 km and is about 200 km in the south, but it gets wider in the central region (approximately 700 km) (Al-Shanti, 2003).

During its history the Arabian shield has been subjected to several orogenic events which have resulted in uplift and subsidence in basins, as illustrated by the vertical and lateral changes in their sedimentary facies. These events were accompanied by major plutonic intrusives, which also deformed and contact metamorphosed the surrounding rocks (Al-Shanti, 2003).

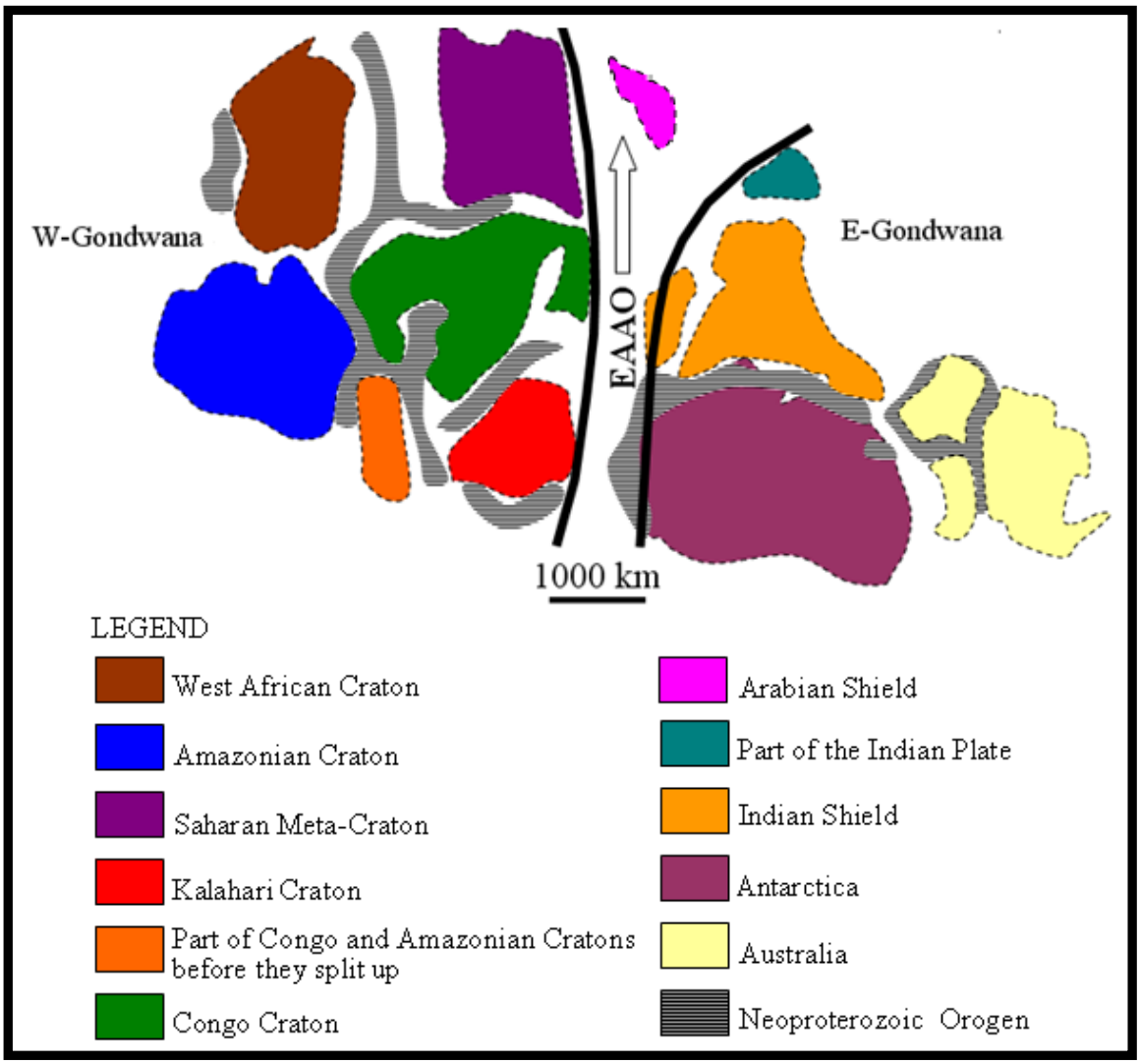

Figure 2.1: Location of the Arabian Shield during the evolution of the Neoproterozoic East Africa–Antarctic Orogene (EAAO), the beginning of the Rodinia supercontinent break-up and reconstruction of the Gondwana supercontinent (After Stern and Johnson, 2010).

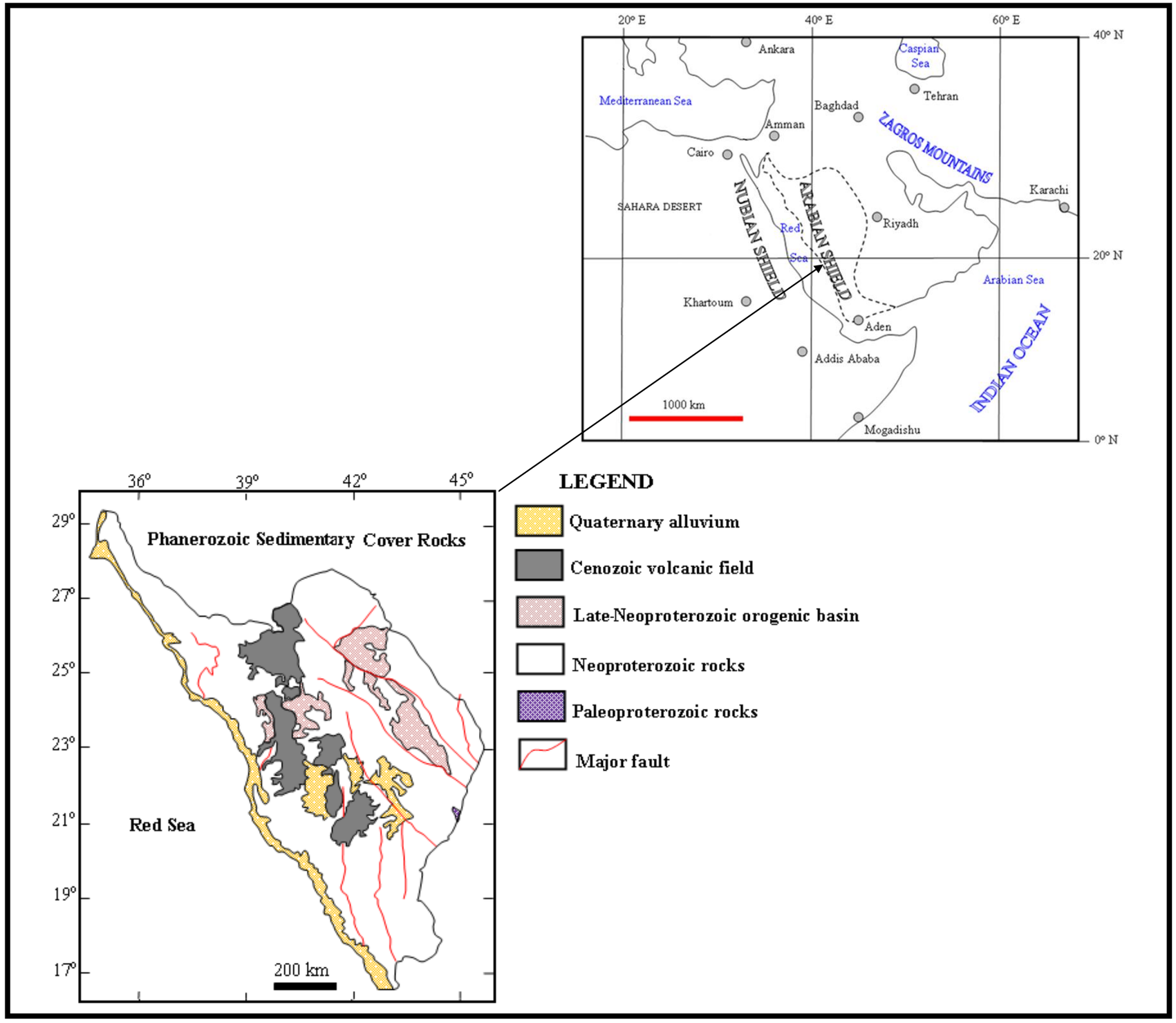

Figure 2.2: The geology of the Arabian Shield (after Saudi Geological Survey, 2012)

II.2. Classification of the Arabian Shield and history of research

For a long time there was no definite system for the nomenclature of the Arabian Shield rocks (groups and formations). For example, different names were given to very similar formations that are located far from each other. Also, the same name was given to formations that are distinctly different.

Comprehensive research work in the Arabian Shield was started when the Ministry of Petroleum and Mineral Resources ordered the Saudi geological research sector to carry out systematic mapping and mineral exploration on the Shield. Mineral exploration and reconnaissance geologic mapping was carried out by the USGS mission, mainly in the southern part of the Shield, by the Directorate General of Mineral Resources in the central and northwestern parts of the Shield and by the BRGM mission in the northern part of the Shield. The earliest work was published by Brown and Jackson (1960) who studied the sedimentary and volcanic rocks. They particularly highlighted the presence of large belts of gneiss (composed of granite or diorite and surrounded by schist) in the Shield.

Geochronological studies have been carried out in the southern part of the Shield by Cooper *et al.* (1979), Fleck *et al*. (1979) and Schmidt *et al*. (1973, 1979) and in the central region of the Shield by Jackson and Ramsay (1980), Ramsay *et al.* (1979), Delfour (1979, 1981) and Kemp *et al.* (1982). Stratigraphic and geochronological correlations were subsequently suggested for the whole Arabian Shield (Table 2.1).

Work by the USGS (Greenwood *et al.* 1976) started to classify the southern region of the Arabian Shield and suggested that the Arabian Shield was initially formed as oceanic crust and island arcs that consisted of basic (tholeiitic) volcanics, followed by the ‘layered strata’ (see below); finally all were metamorphosed and transformed into the Arabian Shield craton.

The BRGM (Delfour, 1983) established a classification for the middle and northern part of the Arabian Shield, suggesting that the Arabian Shield is recrystallized and deformed continental crust that now forms old basement with the younger layered rocks.

Johnson (1983) combined these two classifications of the Arabian Shield units and developed a third classification. The classification proposed three groups of lithological units of different age which formed in three stages and were each affected by successive tectonic cycles during the upper Neo-Proterozoic. Further detailed geological studies by Ramsay *et al*. (1986) demonstrated that there are common belts of gneissic rocks separated by belts of ophiolitic and layered volcano-sedimentary rocks. These deformed gneissic belts were intruded by granitic intrusives (before the Najd tectonic cycle, ~ 550 to 950 Ma, which is equivalent to the Hijaz tectonic cycle in the first classification). This means that these gneissic belts were subjected to a tectonic cycle that yielded continental crust before the beginning of the Najd fault (a major fault system, with a dominantly NW-SE direction, formed after the termination of the Hijaz tectonic cycle from 630 to 530 Ma and considered as the last tectonic event that took place in the Arabian Shield, Al-Shanti, 2003)

II.3. The terrains of the Arabian Shield

The five main terrains of the Arabian shield are termed the Midyan, Hijaz, Ar Rayn, Asir and Afif composite terrains. The Midyan terrain is the focus of this study and is described in more detail later. The evolution of the terrains was essentially due to the formation of island-arc crust or continental-marginal-arc crust above evolving subduction systems during the Late Proterozoic. It has been suggested that the Asir, Hijaz and Midyan terrains that form the western part of the Arabian Shield represent intraoceanic island arcs, whereas, the Afif (composite) and Ar Rayn terrains forming the eastern part of the shield have continental affinities (Al-Shanti, 2003). However, recent geological and geochronological information from Stoeser and Frost (2006) have reclassified the Arabian shield terrains. They added more terrains (Fig. 2.3) that are mostly hosted in the previous main ones. Three groups of terrain are indicated: 1) the western arc terrains, 2) the eastern arc terrains, and 3) the Khida terrain. The first and second groups are of Neoproterozoic oceanic affinity, while the third group is of pre-Neoproterozoic, continental crust affinity.

According to Al-Shanti (2003), the Arabian Shield is mainly composed of well preserved Neoproterozoic assemblages that have been slightly metamorphosed. These assemblages were generated between 900 Ma and 550 Ma, by successive accretion of inter-oceanic, island arcs along suture zones of serpentinized ultramafics of ophiolitic

affinity. They are partially obscured by thick Phanerozoic sedimentary formations. There are about six disconnected belts of ophiolites that make up the boundaries between the five major terrains (Asir, Afif, Ar Rayn, Al-Hijaz, Midyan, all showing similar compositions but of different ages). They are parallel to the main trend of the rock units and tectonism in the Shield; four of them (Al-Amar-Idsas, Jabal Humayyan-Jabal Sabhah, Al-Bijadiyah-Halaban and Al-Hamdah-Nabitah) show a N-S orientation and the other two (Jabal Ess-Jabal Al-Wask and Bir Umq-Jabal Thurwah) show an E-W/SW-NE orientation. Other minor belts are NE-SW or NW-SE trending. The main structural elements of the Shield are shown in Fig 2.3 and 2.4.

II.3.1. Midyan Terrain

According to the Saudi Geological Survey (2012), the Midyan terrain (Fig. 2.5) is basically composed of two deformed rock units: the Za`am Group (represented by volcano-sedimentary, chert and iron-rich formations) that is 800-725 Ma old and the Bayda and Hegaf formations (low-K basalt and andesite, intercalated with rhyolite, representing an island-arc volcanic environment), and epiclastic sedimentary rocks. They are over 710 Ma old and a continental-margin environment is indicated.

The above mentioned ‘layered’ rocks were intruded by diorite, tonalite (arc-related, 680 Ma) and youger I-type granite and granodiorite. The ophiolitic rocks in the terrain are displayed at Jabal Ess, Jabal Wask and along the Yanbu suture; they are 780-740 Ma old and were generated during back-arc extension as juvenile oceanic lithosphere (Johnson, 2006). The central and southern parts of the Midyan terrain host the Qazaz gneissic belt, the Azlam graben and the Hamadat gneissic belt, which all show a general northwest trend (Johnson, 2006). Greenwood *et al.* (1980) and Delfour (1981) agreed that the Midyan terrain is distinguished by containing the youngest intrusive rocks in the Arabian Shield. This appears to be the most important difference in terms of the temporal evolution of magmatism between the Midyan and other terrains of the shield.

The Yanbu suture zone separates the northern part of the Hijaz terrain from the southern part of the Midyan terrain.

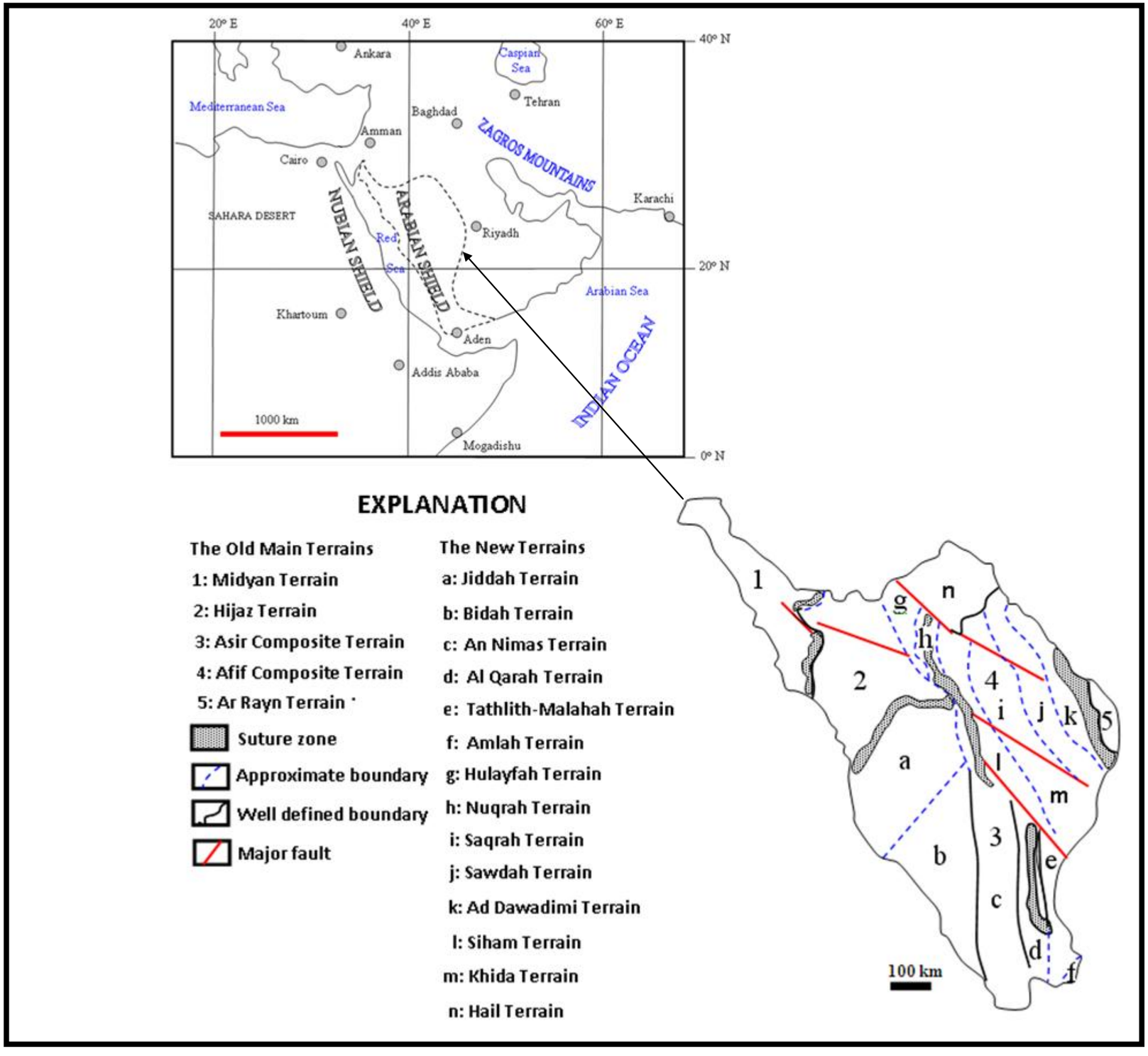

Figure 2.3: The terrains of the Arabian Shield after Stoeser and Frost (2006).

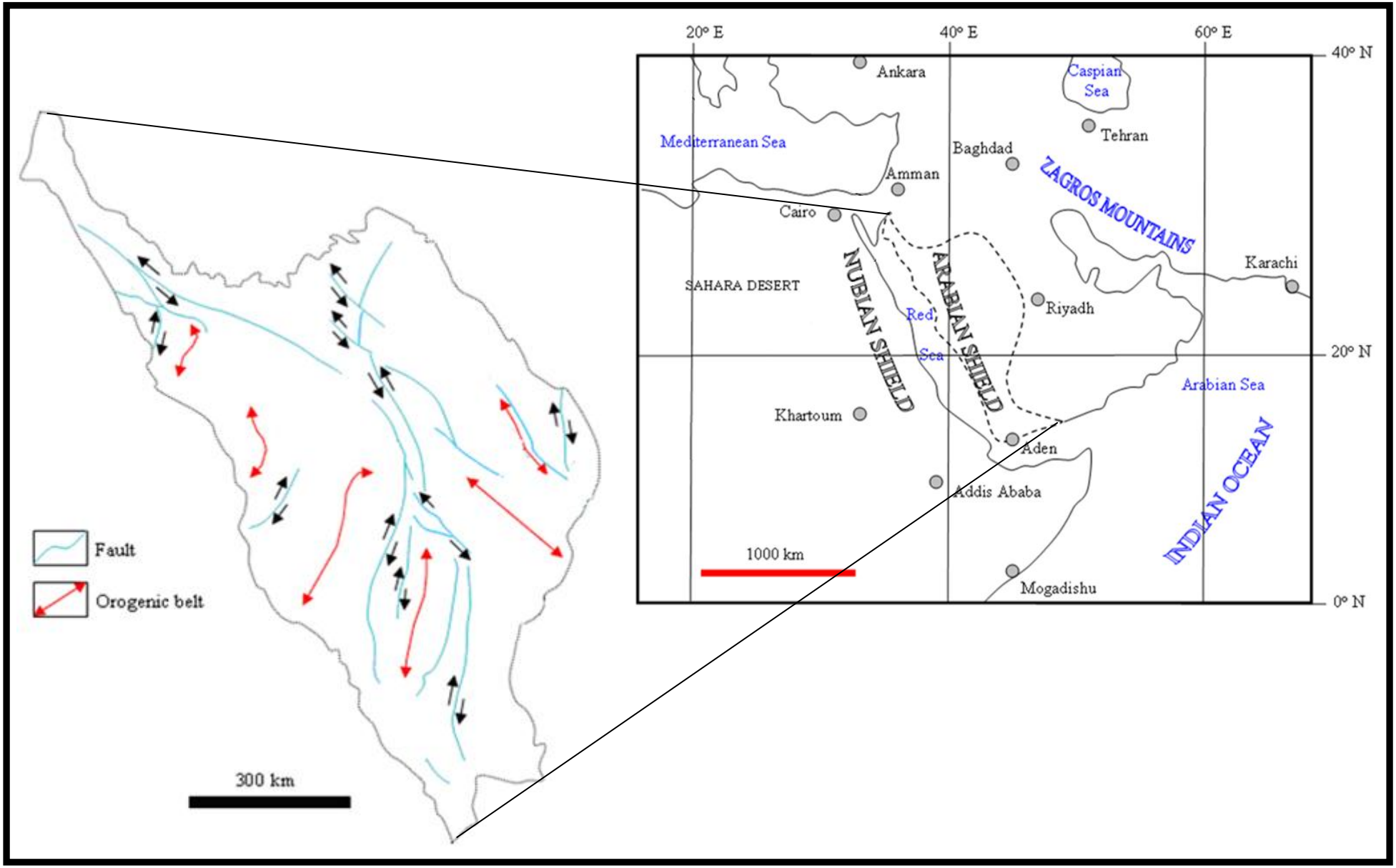

Figure 2.4: The major structural elements of the Arabian Shield (after Saudi Geological Survey, 2012). Black arrows show fault movement.

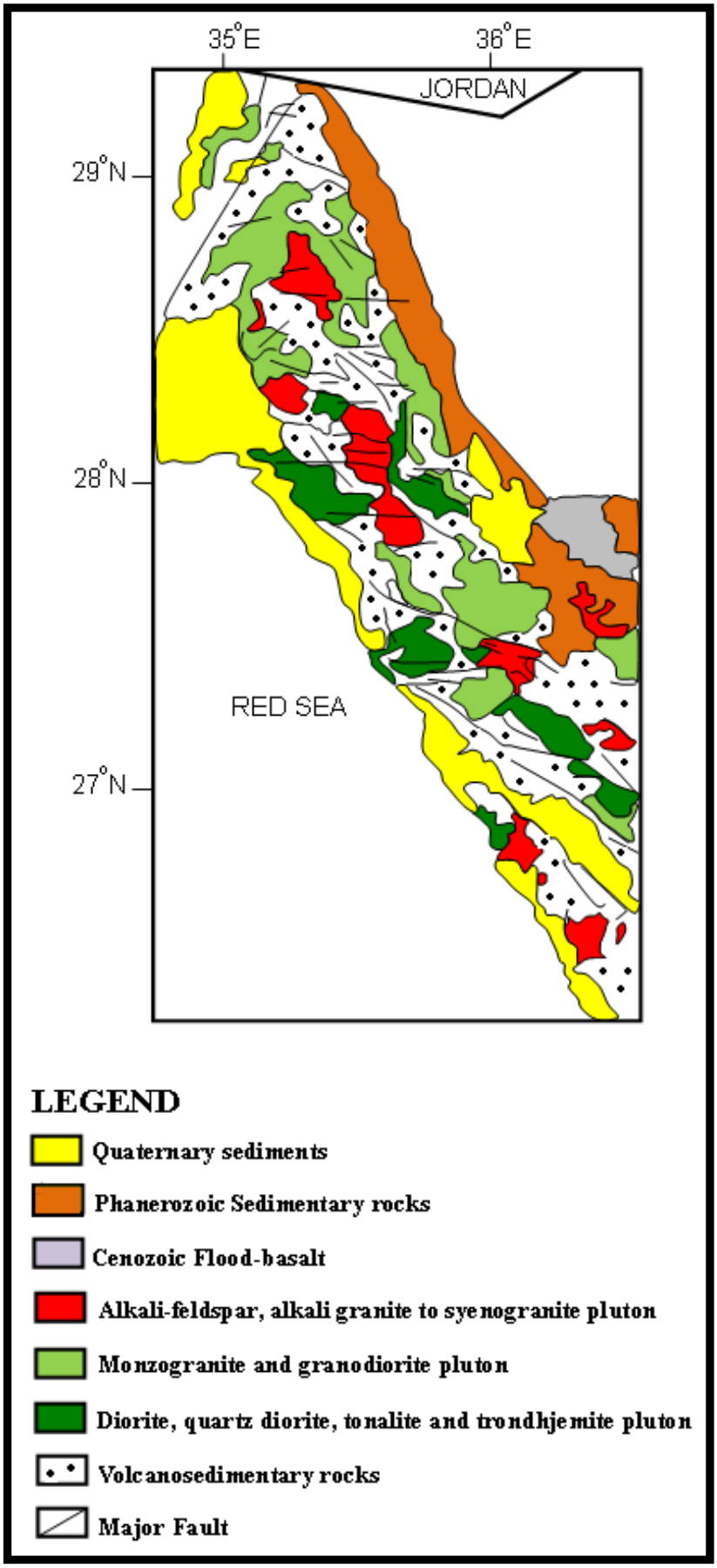

Figure 2.5: The geology of the Midyan Terrain after Stoeser *et al*. (1985).

II.4. The rock types of the Arabian Shield

According to Al-Shanti (2003), the majority of the Arabian Shield is composed of layered (see later) and plutonic, intrusive rocks. There are also lesser amounts of younger, Quaternary sediments and Cenozoic volcanic rocks. Names of groups of the Shield rocks with time and events are shown in Table 2.1.

II.4.1. Basement rocks

The basement rocks are metamorphosed, dominantly to amphibolite facies grade. Their original features have been affected by the intrusive rocks and the later orogenic activity and that makes their recognition much more difficult. Some remnants of the basement have been found in a few places like the Sawdah gneissic belts that is located in the central part of the Arabian Shield.

II.4.2. Layered rocks

The layered rocks show a distinct layered nature on a very large scale, due to depositional bedding in the sediments and volcanics. Regional metamorphism has superimposed additional layering and foliation on these units. They have an age range between 900 and 540 Ma. They are mainly composed of volcanic, volcanoclastic and sedimentary rocks. The volcanic layered rocks comprise volcanic extrusives, deposited either in basins (as molasses) or on the continent, with compositions ranging from mafic (basalt) to silicic (rhyolite). The volcano-sedimentary successions are different in nature, being composed of volcanic and plutonic fragments and sedimentary rocks. They occur as beds of conglomerate, greywacke, sandstone and chemical sediments (e.g. chert and limestone), and also as tuff and lapilli-tuff. The layered rocks are locally metamorphosed to variable degrees (e.g. gneiss and schist).

II.4.3. Plutonic rocks

Plutonic rocks occupy large areas of the Arabian Shield. Their composition ranges from ultramafic (e.g. peridotite and dunite) to mafic (e.g. gabbro) to intermediate (e.g. diorite and tonalite) to felsic (e.g. granite). They have different forms (e.g. dikes and batholiths) and the outcrop extent may reach several kilometers. Their ages range from 900 to 540 Ma.

Based on their ages and styles of emplacement (Al-Shanti, 2003), they have been classified into three distinct groups:

- Syn-kinematic intrusives: they are often deformed and sometimes contain remnants from older rock units. They occur as batholiths, are calc-alkaline in composition (dominated by diorite and trondhjemite). Their ages range between 700 to 900Ma.

- Late-kinematic intrusives: they are undeformed and are calc-alkaline in composition (dominated by monzogranite and monzonite). Their ages range from 620 to 700 Ma.

- Post- kinematic intrusives: they are the smallest and least common of the intrusives and have defined forms (e.g. circular, elliptical or ring shapes). They are undeformed and often show alkaline and per-alkaline compositions with a distinct pinkish to reddish colour. Their ages range from 620 to 540 Ma.

II.4.4. Lava fields (Harrat)

The Arabian Shield hosts some Cenozoic extrusive flood basalts which belong to two different phases of volcanism. The older phase is concurrent with the opening of the Red Sea (15 to 30 Ma) and it is represented by Tertiary alkali olivine basalt that occurs in the western part of the Shield. The younger phase (10 Ma) occurs as late Miocene alkali basaltic lava superimposed on the older phase.

II.4.5. Sedimentary rocks

The sedimentary cover rocks occupy the eastern and the northern parts of Saudi Arabia. They are exposed as arc-shaped belts of carbonate rocks which are highly-resistant to weathering. They dip toward the east and cover the empty Dahna, Nufud and Quarter deserts which occupy the central, northeast and southern parts of Saudi Arabia respectively. The age of these rocks ranges from Cambrian to Recent. Along the western coast of Saudi Arabia, the sedimentary cover occupies a narrow band up to 40 km in width and consists of rocks ranging in age from Tertiary to the present.

Table 2.1: Proposed lithostratigraphy for the Arabian shield, using different classification schemes for the groups and events.

Geo.Times		Kemp *et al*. (1982) Kemp (1981) Calvez *et al*.(1982)	Delfour (1979)	Greenwood *et al*. (1976, 1980)	Orogenic events from Gass (1981)	Depositional cycles from Jackson & Ramsay (1980)	
Paleozoic	500			JUBAYLAH			
	550		JIBALAH		UPPER PAN-AFRICAN		
	570			MURDAMA			
	600	JIBALAH?	FURAYH=MURDAMA= SHAMMAR			Sequence A	
Upper Proterozoic	650	FURAYH=GHAMR=HADIYAH		HALABAN			
	750			ABLAH			
	800	MAHD=ALAYS	HULAYFAH		MIDDLE PAN-AFRICAN	Sequence B	
	850		ABT OPHIOLITES	JEDDAH			
Middle & Lower Proterozoic	900	FARRI=ALQUNNAH=ARJ	RHARABA	BAHAH	Lower PAN-AFRICAN		
	950		OLDER BASEMENT	BAISH		Sequence C	

Najd Fault System

The Najd and the Hijaz Tectonic Cycles

II.5. Ophiolites and deformational belts

The ophiolitic rocks have been interpreted as parts of former oceanic crust that have been obducted over the continental crust at subduction zones. They are tectonically important because they define the terrain boundaries and their complete sequence is composed of serpentinized peridotite, gabbro, dike complexes, basalt and pelagic rocks. These ophiolites were subjected to folding and shearing events which have obscured many of their original features (Al-Shanti, 2003). They are mostly Mid-Neoproterozoic, with an age range between 680 to 890 Ma (Stern *et al*., 2004), were emplaced by thrusting and represent 200 Ma of oceanic magmatism in the Arabian Shield. Between 780 and 680 Ma these rocks were emplaced in suture zones (100 Ma period of terrain accretion). The major shear zones developed along suture zones hosting the ophiolites (Al-Shanti, 2003).

According to Abdelsalam and Stern (1996) the Arabian-Nubian Shield deformational belts can be classified into the following:

1- Deformational belts associated with (a) an 800-700 Ma period of arc-arc collision, (with E-NE orientation in the northern part of the Arabian-Nubian Shield and N to N-NE orientation in the southern part of the Arabian-Nubian Shield) and (b) arc-continental collision sutures (N-trending in the eastern and western boundaries of the Arabian-Nubian Shield) associated with the collision of the Arabian-Nubian Shield with east and west Gondwanaland at 750-650 Ma).

2- Deformational belts with post-accretionary structures. These are N-trending shortening zones and NW-trending strike-slip faults that offset the east to northeast oriented sutures in the north of the Arabian-Nubian Shield, but overprinted the N to NE orientation sutures in the south of the Arabian Shield.

Levin and Park (2000) suggested that the coherent fabric of the shear zone areas was initiated during late Proterozoic, continent–continent collision, contemporaneous with the northward movement of the Ar-Rayn tectonic block along the northern flank of the Najd-fault system.

II.6. Theories on the formation of the Arabian Shield

Some studies (e.g. Schmidt *et al.*, 1979 and Camp, 1984) have suggested that the Arabian Shield was formed as a result of accretion of a number of island arcs which were generated in an oceanic basin overlying oceanic crust. However, others (e.g. Kemp *et al.* 1982) have suggested that the Arabian Shield was developed and generated from magmatic activity and/or from the rifting of the silicic continental crust of an old craton.

Stoeser and Camp (1984) suggested that the Shield resulted from an accretion of microplates. Their ideas explain the divisions of the geological terrains in the Arabian shield which are delineated by tectonic suture zones that host the ophiolitic belts.

Stoeser (1986), stated that the evolution of the Arabian shield can simply explained by the classic Wilson cycle pattern of Phanerozoic plate tectonics.

The Saudi Geological Survey has summarized the geological evolution of the Arabian Shield (Fig 2.6). Be`eri-Shlevin *et al.* (2009) concluded that arc formation and accretionary processes in the Arabian Shield were still ongoing in the latest Neoproterozoic (Ediacaran), until about 620–600 Ma, and therefore that evolution of the Ar Rayn terrane (arc formation, accretion, syn- to postorogenic plutonism) defines a final stage of assembly of the Gondwana supercontinent along the northeastern margin of the East African orogen.

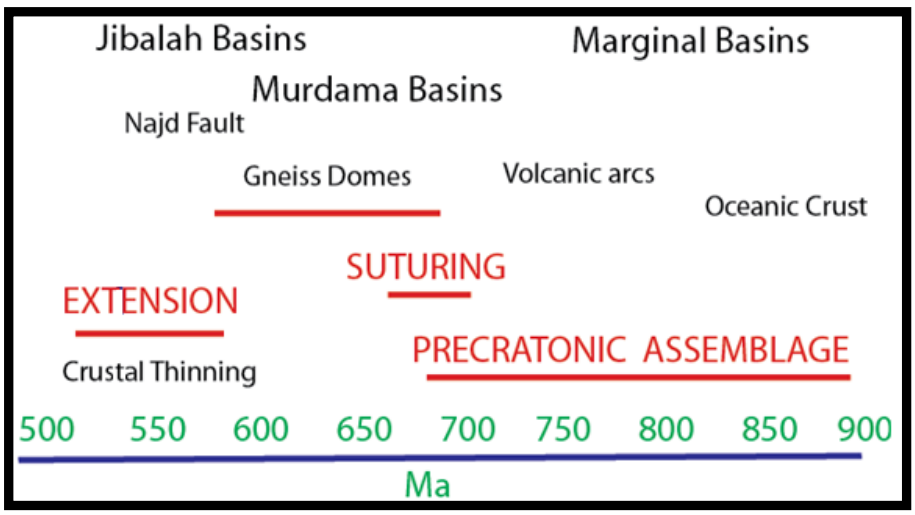

Figure 2.6: The geological-time events of the Arabian Shield (after Saudi Geological Survey, 2012).

II.6.1. Tectonic evolution of the Arabian Shield

Based on the numerous geological, geochronological, geochemical and structural studies, several plate tectonic interpretations of the Precambrian history of the Arabian-Nubian Shield in general and the Arabian Shield in particular have been carried out by many authors (e.g. Kemp, 1980; 1982, Duyverman, 1984; Al Shanti, 1993; Johnson, 2003). Several tectonic models for the evolution of the basement rocks in the Arabian Shield have been put forward. Here is a brief discussion of two examples (the most comprehensive and using the most recent data).

II.6.1.1. Duyverman (1982) Model

Figure 2.7 shows a tentative model for the evolution of the Arabian Shield in late Proterozoic times according to Duyverman (1982). According to this model, the tectonic evolution of the Shield can be classified into four stages:

Stage A: This first stage corresponds with the Baish /Bahah juvenile arc systems with submarine volcanic rocks and sediments. Three or more arcs existed during this time. Oceanic crust was originally present in the whole area and the remnants of this crust are the present- day ophiolite belts. During this stage probable eastward-dipping subduction zones generated tholeiitic to calc-alkaline volcanism and submarine erosion products.

Stage B: During this stage, further subduction caused extensive tholeiitic and calc-alkaline volcanism along with the deposition of the Hulayfah and Halaban groups.

Stage C: During this stage, the Murdama and Shammar groups were formed and the island arcs became mature with the formation of thick crust. Subduction caused the volcanic rocks to change magma type, becoming calc- alkaline in nature.

Stage D: During this stage (the Najd period) the Shield was further cratonized. Alkaline to peralkaline plutonism and volcanism occurred (e.g. the Jubalah Group).

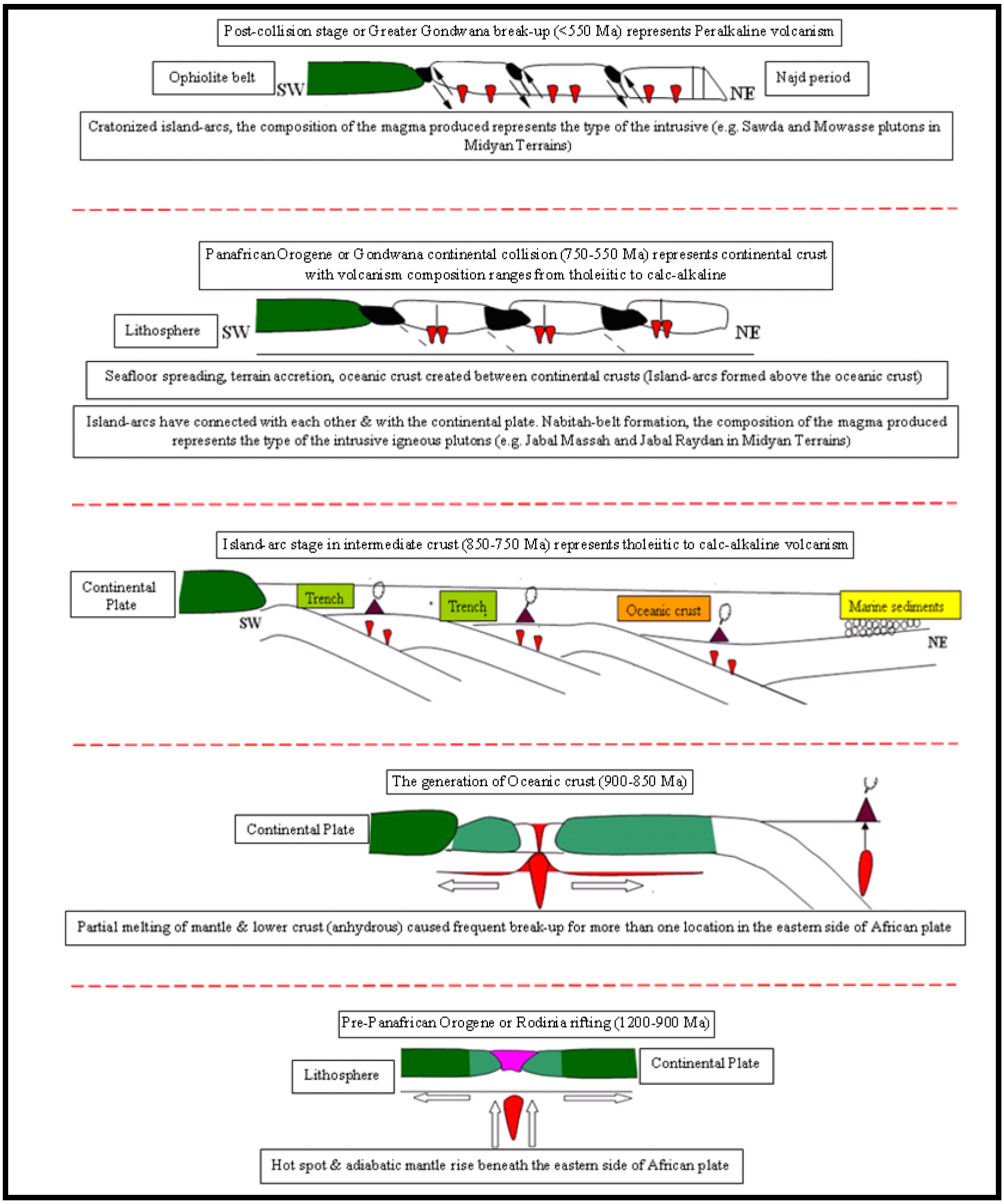

Figure 2.7: Arabian Shield evolution model (adapted after Duyverman, 1982).

II.6.1.2. Genna et al. (2002) Classification

Based on a geologic, structural, geochemical, and geochronologic synthesis, Genna *et al*. (2002) presented a new view of the anatomy and geologic history of the Arabian Shield (Table 2.2). The main geologic evolution of the Shield is limited to a period ranging from 900 to 550 Ma that led to the formation, amalgamation, and final cratonization of several tectonostratigraphic terrains. Genna *et al.* (2002) observed extensional deformation with contemporaneous bimodal magmatism in the Late Proterozoic Arabian Shield rocks, which are indicative of crustal thinning. These events were followed by a marine sedimentation event. The crustal thinning was controlled by the Najd transform fault, which also governed the Jibalah basin formation (the basal fill deposits of the Shammar group). The extrusive rocks of the Shammar group were associated with intrusive complexes and dike swarms (530-590 Ma). This extensional series was followed by a marine transgression (carbonate platforms of the Jibalah basins) and ended with the marine sediments of the Paleozoic cover.

Table 2.2: The classification of Genna *et al*. (2002) for the evolution of the Arabian Shield

Tectonic stages	**Rock units**	**Group**	**Age (Ma)**
Post-collision	-Alkaline & Peralkaline granite -Layered intrusive gabbro -Intermediate to acidic volcanics -Molasse sediments & dykes	Mardama Shammer Ablah	670-550
Collision (Pan-African)	Peralumineous granite	Nabitah belt	670
Pre-collision (island arcs)	**Island arcs** **-**Calk-alkaline granitoids -Metagabbro-diorite complexes -Volcano-sedimentrary association **Ophiolites** -Marine sediments -Massive & Pillow basalt -Sheeted dykes -Metagabbro -Metapyroxenites	Hulayfah Halaban Jiddah Baha Baish	900-670

II.6.1.3. Compatibility

These two classifications do not give an exact period of time for each tectonic event. Whereas the first classification considers an extended period of time, the second classification just considered the period between 900 Ma and 550 Ma.

However, both classifications are very similar as they propose the same tectonic stages which occurred at a similar period of time. These models will be further assessed in a later Chapter.

III. Field Observations

III.1. Introduction

Five, poorly-studied (Table 3.1) granitic plutons in the Midyan terrain, NW Arabian Shield, were selected for detailed geological study; these are (from south to north) Jabal Thalabah, Jabal Khur Dukhan, Jabal Rydan, Jabal Al-Massah and Jabal az Zuhd.

Table 3.1: Previous work on the selected plutons

Pluton	Geology	Structure	Mineralogy	Geochemistry	Economic	Geochronology
TH	Y (Mi)					
KD	Y (Mi)	Y (Mi)				
JM	Y (Mi)	Y			Y (I)	Rb-Sr
JR	Y (Mi)		Y (Mi)		Y (I)	Rb-Sr
JZ	Y (Mi)			ICP (Mi)	Y (I)	

Explanation of the abbreviations: TH, Jabal Thalabah, KD, Jabal Khur Dukhan, JM, Jabal Al-Massah, JR, Jabal Raydan, JZ, Jabal az Zuhd, Y, yes, Y(Mi), yes but minor, Y(I), yes but initial, ICP (Mi), Inductive coupled plasma but minor study.

Previous studies which focused on the economic potential of the Arabian Shield (see Chapter 1) indicated that the alkali granites are the most promising host for enrichments of REEs and RMs.

The majority of the previous work was carried out in the 1980s by the Deputy Ministry of Mineral Resources of Saudi Arabia during the production of the geological maps of the relevant quadrangles (Al Wajh, Al-Muwaylih, Shaghab, Duba and Haql) that occupy the northwestern part of the Arabian shield. The work also involved some other initial geological, structural and economic studies. The geological work was mainly based on regional mapping (simplified maps from aerial photography) and included limited sampling. The scale of the maps that were produced for these plutons was 1:250,000. Theses maps only show the main geological lithologies and do not display any detailed geological features.

This chapter will describe the major geological features of each of the plutons. These were derived by constructing geological maps which were based on the reconnaissance geological studies, recent satellite images (Google Earth) and the later more detailed fieldwork. The satellite images assisted in clarifying the extension of some major structural elements and in suggesting the approximate positions of boundaries between bodies within each pluton but were not very helpful in identifying the main rock units or the exact relationships between rock types. The initial rock names used in the field descriptions were based on the colour index and the texture of the rocks in the field, whilst the names used on the produced maps are based on subsequent petrographic analysis and are therefore more accurate (see Chapter IV).

Initial (reconnaissance) and major field trips were carried out during the summer of 2009. The first trip involved some sampling from the Jabal Thalabah and Jabal Al-Massah plutons. The second (major) trip comprised mapping the five plutons and sampling (167 representative samples were collected from all of the plutons to include the various rock varieties). The sampling method aimed to be systematic (every 5 meters along parallel traverses). However, this method did not work well because of the difficulties in finding fresh representative samples at each location. Therefore, the sampling method was changed to be stratified (each pluton was totally covered to have all the rock varieties). The study areas are located a few hundred meters east of the coastal highway that joins the cities of Al-Wajh and Duba (which were used for accommodation) and access was by four-wheel drive vehicles. The terrain is fairly rugged and mountainous and the temperatures were always high. More details of the fieldwork, including the nature of the environment and some sampling obstacles are mentioned in Appendix I.

The five plutons were selected for the following reasons:

- Jabal Thalabah: No previous, detailed geological study (only subjected to a general geological study of its host quadrangle and, based on aerial photos, an initial geological map was constructed); has not even been given a name (see later); and is close to one of the alkali granite pluton.

- Jabal Khur Dukhan: An alkali granite pluton with no economic, detailed mineralogical or detailed geological study. Only subjected to an initial structural study and general geological study of its host quadrangle and, based on aerial photos, an initial geological map was constructed.

- Jabal Al-Massah: An alkali granite pluton with no previous detailed mineralogical and geological study. Only subjected to a structural study, initial economic study and general geological study of its host quadrangle and based on aerial photos an initial geological map was constructed.

- Jabal Raydan: An alkali granite pluton with no detailed mineralogical and geological study. Only subjected to an initial economic study and general geological study of its host quadrangle and based on aerial photos an initial geological map was constructed.

- Jabal az Zuhd: An alkali granite pluton with no detailed mineralogical and geological study. Only subjected to initial economic study and general geological study (including a few geochemical analyses) of its host quadrangle and based on aerial photos an initial geological map was constructed.

III.2. Country rocks

The country rocks in the study areas are dark colored, most commonly massive, unbedded and featureless. However, the affect of regional metamorphism was reflected in the appearance of some deformational structures like folds, faults and cleavage. Basic and acidic metavolcanics are the dominant lithologies present. These include (according to Davies, 1980; Ramsay, 1983; Rowaihy, 1985; Clark, 1986; Davies and Grainger, 1985; and Grainger and Hanif, 1989):

- The **Za'am group,** consisting of metamorphosed basalt and andesite, mafic tuff and agglomerate, dacitic and rhyolitic flows and tuffs, massive to well bedded volcaniclastic sandstone or lithic arenite, siltstone, pyritic and graphitic shale and black chert.

- The **Bayda group** generally consists of andesitic tuffs, breccias, massive lavas, basaltic sills and dikes, rhyolite porphyry, dacite, trachyte flows, thickly bedded lithic, lapilli, and welded ash-flow tuffs and volcanic conglomerate and breccia.

- The **Hasha formation** is specifically characterized by basalt, andesite, andesitic tuffs and breccia.

- The **Zaytah group** generally consists of Precambrian stratiform rocks that are dominated by a succession of mafic and felsic tuffs, andesite, basalt, minor rhyolite, agglomerate, siltstone, limestone, and chert, amphibolite, mafic schist and quartz-feldspathic mica schist.

- The **Thalabah group,** consisting of an epiclastic succession, conglomerate, phyllite, lithic arenite and siltstone.

- The **Minaweh formation** generally consists of meta-volcanic (andesite to basalt) sedimentary schists.

III.3. Jabal Thalabah Complex

The Jabal Thalabah pluton belongs to some igneous intrusives that have not been assigned to any of the Midyan terrain suites and it was only described as a felsic pluton with a core of monzogranite surrounded by syenogranite (Davies, 1983; Davies and Grainger, 1985). Names were given from modal analysis (Fig. 3.3) and later geochemical classification.

III.3.1. Geology

The pluton (Fig. 3.1 and 3.2) occupies an area of 4km^2. Forty one samples were collected from the pluton. . The pluton is composed of an inner zone dominated by coarse-grained (> 5mm), grey granodiorite which grades into whitish-grey monzogranite, mostly sheared granite and an outer zone dominated by medium (1-5mm) to coarse-grained, buff-pinkish syenogranite. The contact between the inner and outer parts of the pluton is occupied by very small zones of a medium to coarse grayish

hybrid rock. At the contact with the country rocks the granite is finer grained, representing a chilled margin. The rocks are commonly altered (sericitization and chloritization) most likely due to NE-SW shear zones that have dissected the granitoids. To the south of the felsic pluton, a similar size gabbroic pluton is located. It exhibits a fresh core with slightly-highly altered margins. At the contact with the granitic pluton some weathered and carbonatized metagabbros were found as roof pendants above the Jabal Thalabah granite. These altered gabbros are part of the mafic pluton which is located just southwest of the Jabal Thalabah pluton. The relationship between the plutons indicates that the Jabal Thalabah granitoids post-dated the emplacement of the mafic pluton.

The country rocks of the Jabal Thalabah pluton are represented by the Za`am metavolcanics. Basic and felsic dykes intrude both granites and the country rocks. The dykes trend S50W, are red, black and white in colour and are mostly porphyritic. They show variable thickness, ranging from a few centimeters up to 15m in width. Faulting is visible and appears to be more prevalent away from the internal-external pluton contact.

The basic dykes are younger as they intrude the felsic dykes, but their thermal affect on the intruded rocks was limited. The pluton shows an abundance of small, rounded, mafic xenoliths which are only hosted in the granitic rocks (mostly the grey granite).

III.3.2. Form of the plutons and mode of emplacement

The Thalabah is a small, composite, oval-shaped pluton with a low topography. It is most similar to the northern Midyan granitic intrusives which were probably emplaced by cauldron-subsidence (The nature of xenoliths indicates the stoping mechanism).

III.3.3. Sequence of events

The Za'am metavolcanics were first intruded by gabbro, which was subsequently intruded by separate but contemporaneous syenogranite and monzogranite-granodiorite melts. Some assimilation and hybridization took place at the contact zones. The granitic body then fractionated. The granitoids were later intruded by felsic and basic dykes. Both the granitoids and the dykes were partially affected (foliated) by a later metamorphic event.

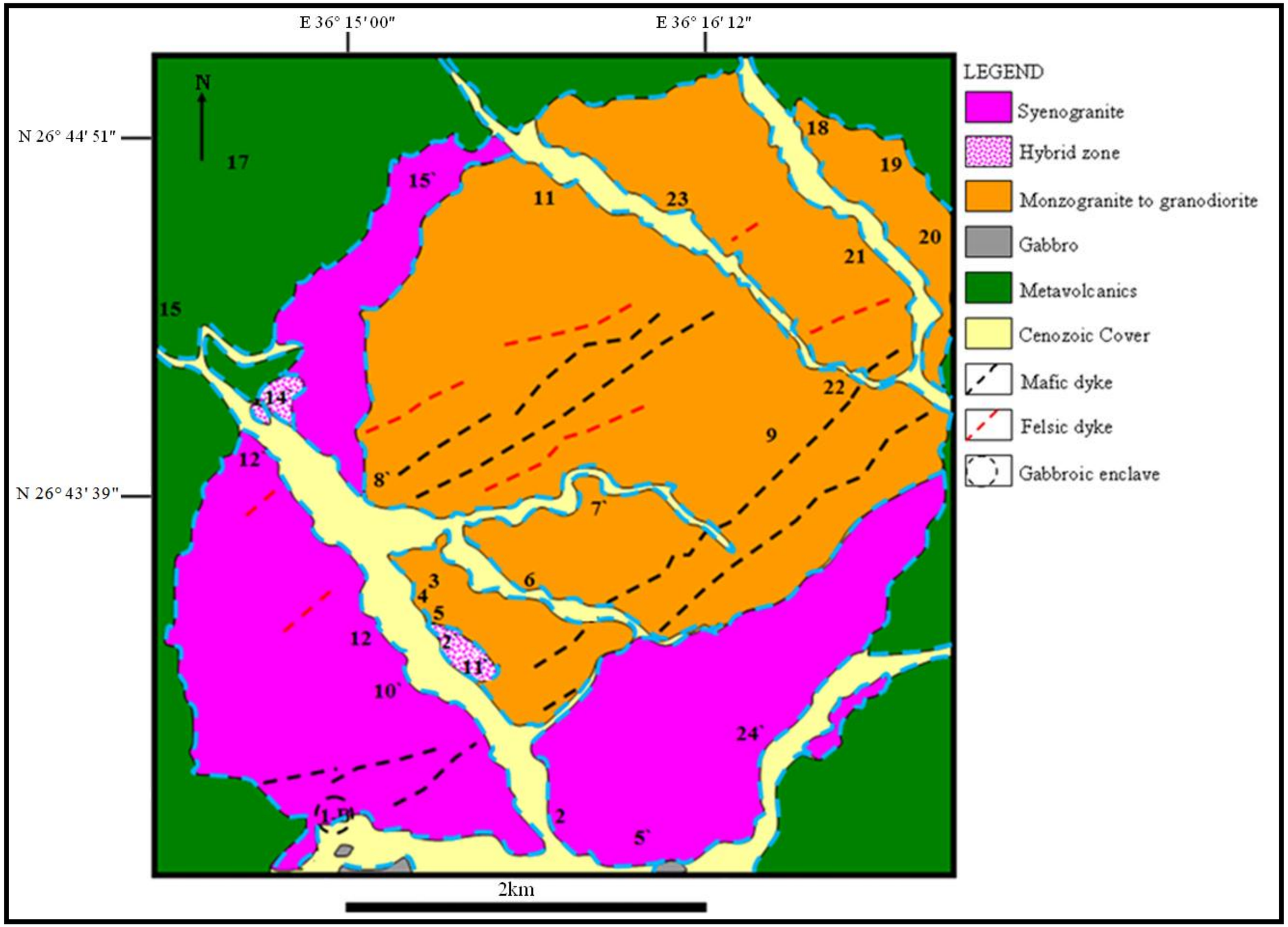

Figure 3.1: The geology of the Jabal Thalabah Complex with the sample locations (prefix JH). Rock names from later mineralogical and geochemical studies. Reconnaissance map boundaries are approximate and provided the basics for the sampling programme.

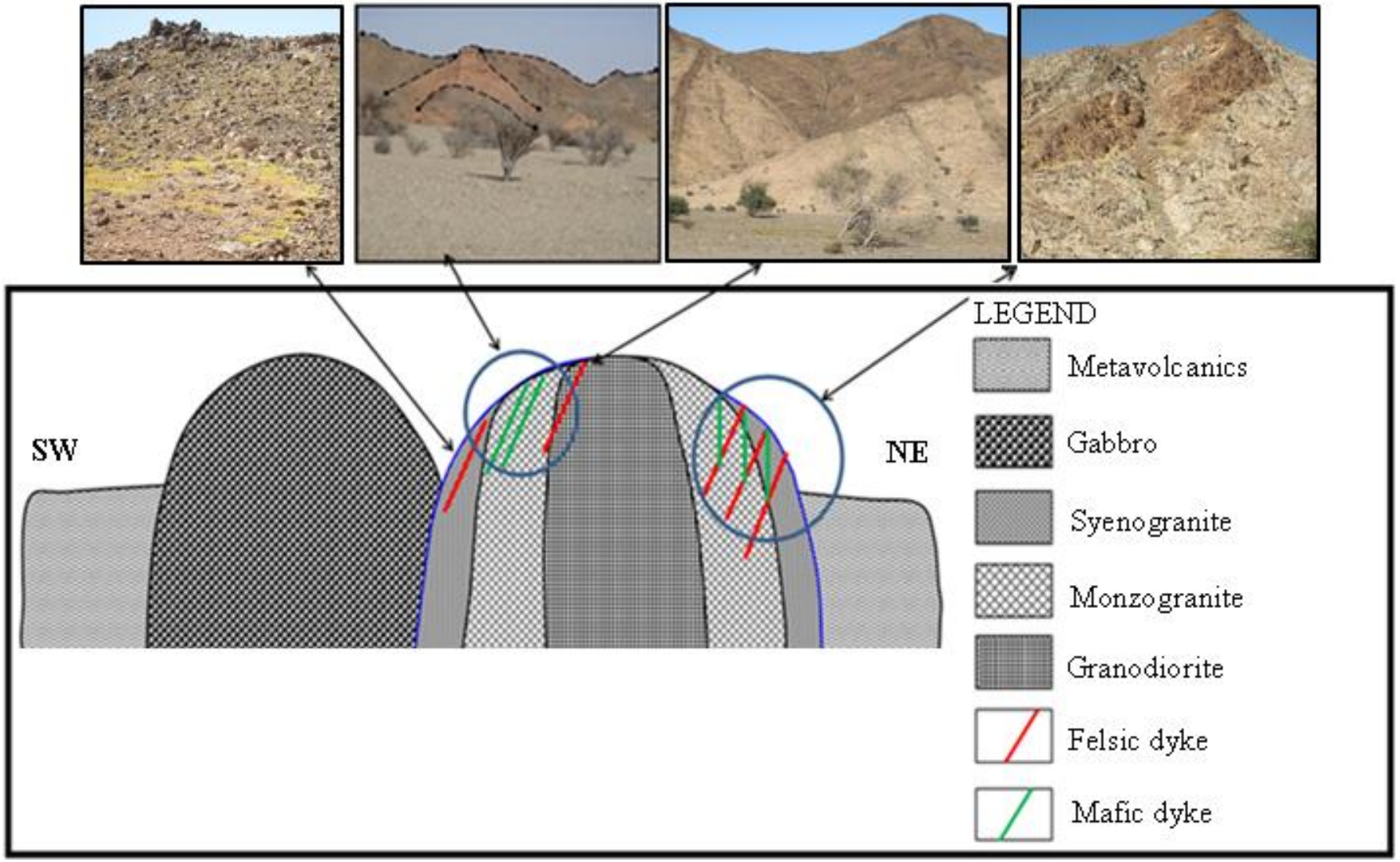

Figure 3.2: Hypothetical and idealized diagram showing lithological relationships in the Jabal Thalabah Complex.

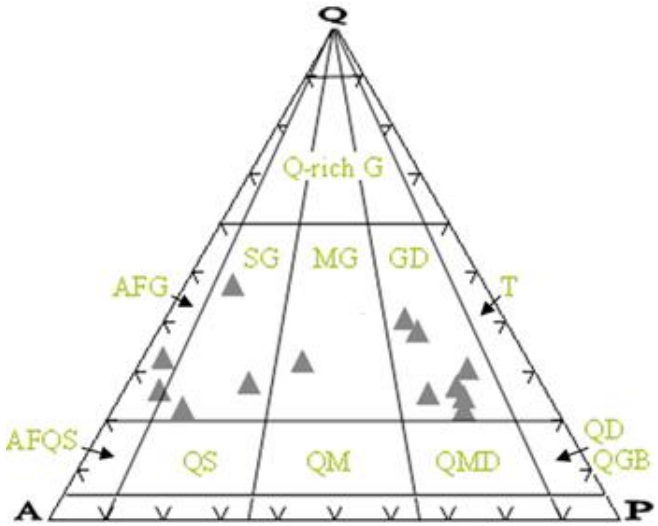

Figure 3.3: Modal composition of the Jabal Thalabah granitic rocks. Explanation of terms: Q-quartz, G-granite, AFG-alkali-feldspar granite, SG-syenogranite, MG-monzogranite, GD-granodiorite, T-tonalite, AFQS-alkali-feldspar quartz syenite, QS-quartz syenite, QM-quartz monzonite, QMD-quartz monzodiorite, QD-quartz diorite, QGB-quartz gabbro.

In summary, Jabal Thalabah is considered to be a small, composite, topographically low, oval-shaped pluton, which displays several rock varieties and contains mafic xenoliths. It is partially foliated and is intruded by numerous felsic and basic dyke swarms that may relate to NE-SW shear zones that have partially dissected the granitic rocks.

Modally, the plot (Fig 3.3) of the Jabal Thalabah granitoids displays two different groups of rocks and it is unclear whether they bear any relation to each other. The first group occupies the granodiorite field and the second one occupies the syenogranite and the alkali feldspar granite fields. Each group may represent a different magma source. The first group possibly shows a trend of fractionation, whereas the second one does not clearly show this feature. By relating the identified rocks to their field locations (Fig. 3.1) it appears that the more evolved granites occupy the outer part of the complex, while the less evolved varieties occupy the inner parts.

III.4. Jabal Khur Dukhan Complex

The pluton (Fig. 3.4 and 3.5) is exposed north of Wadi Thalabah. Forty two samples were collected from this area. Jabal Khur Dukhan has been subjected to geological studies by Davies (1980, 1983) and a structural study by Agar (1986). However, these studies were limited in their sampling and detail and it was felt that further work was justified. Names were given from modal analysis (Fig. 3.6) and later geochemical classification

III.4.1. Geology

The complex is basically composed of an inner and an outer part and each part is dominated by different granitic rocks. The inner part is mainly occupied by a coarse-grained (> 0.5cm), grey/white monzogranite and granodiorite which is porphyritic (feldspar phenocrysts), has an abundance of ferromagnesian (amphibole and biotite) minerals (~9% from modal analyses) and commonly shows a rough weathered surface texture.

The larger, surrounding part is mainly composed of medium (1-5 mm) and coarse-grained (> 5mm), reddish-pink alkali to syenogranite which becomes more reddish and more altered towards the northern and southern areas. It also forms a higher topography than that of the inner pluton. Later reddish-pink, felsic dykes of aplitic and pegmatitic character intrude most of the pluton but are particularly abundant in the monzogranite and granodiorite.

The pluton hosts xenoliths of variable shape (usually elliptical or rounded) and size (5 to 20 cm in diameter). These are mainly felsic in appearance and include some porphyritic (feldspar phyric) granites (mostly found in the inner part of the pluton).

A sharp contact between the monzogranite-granodiorite and the alkali-syenogranite was visible in the field, but the temporal relationship between these rocks is unclear as the country rocks (metavolcanics of the Za'am group) were invaded by both the monzogranite-granodiorite and the alkali-syenogranite.

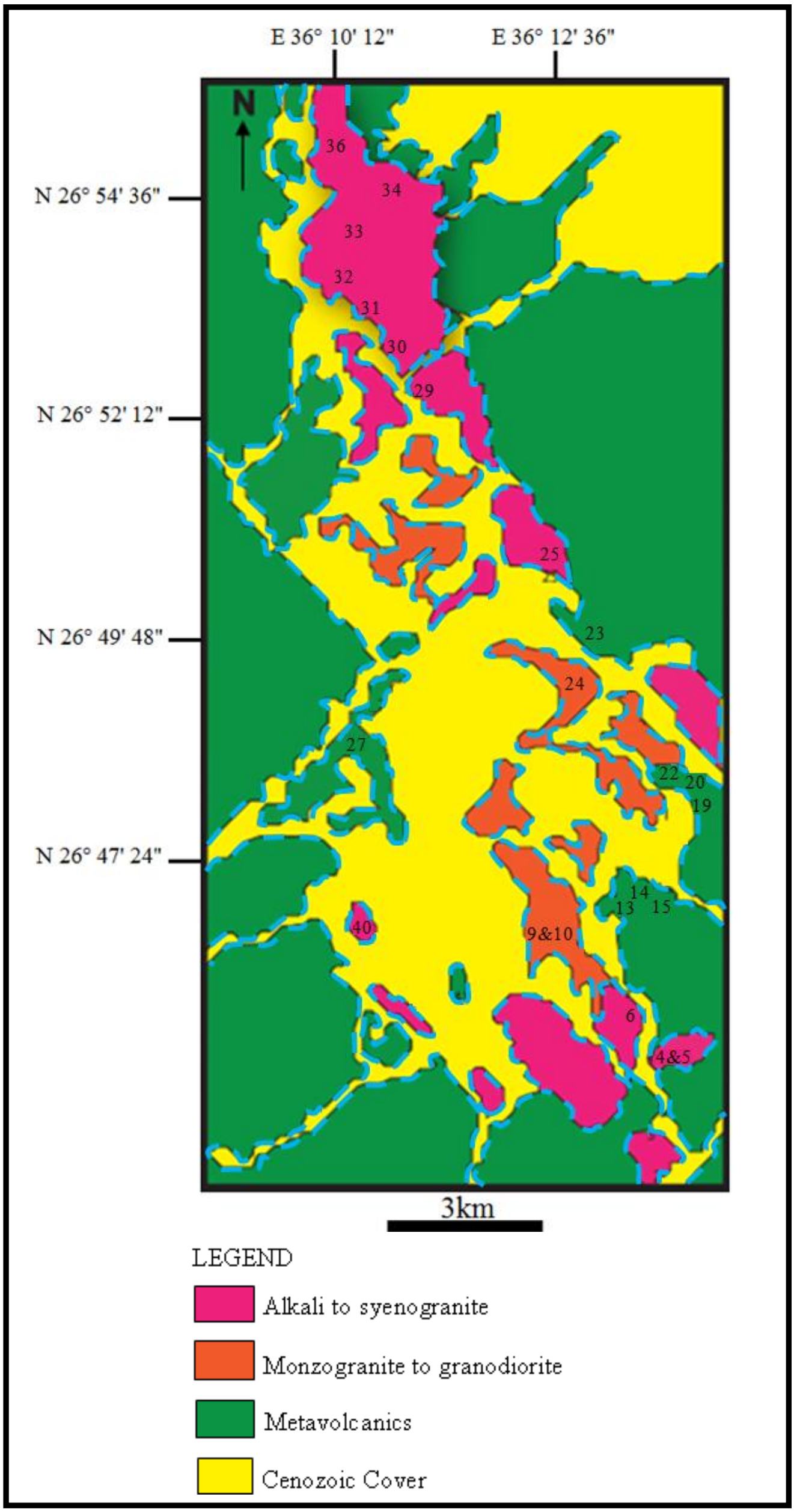

Figure 3.4: The geology of the Jabal Khur Dukhan Complex with the sample locations (prefix KD). Rock names are based on the later mineralogical and geochemical studies. Reconnaissance map boundaries are approximate and provided the basics for the sampling programme.

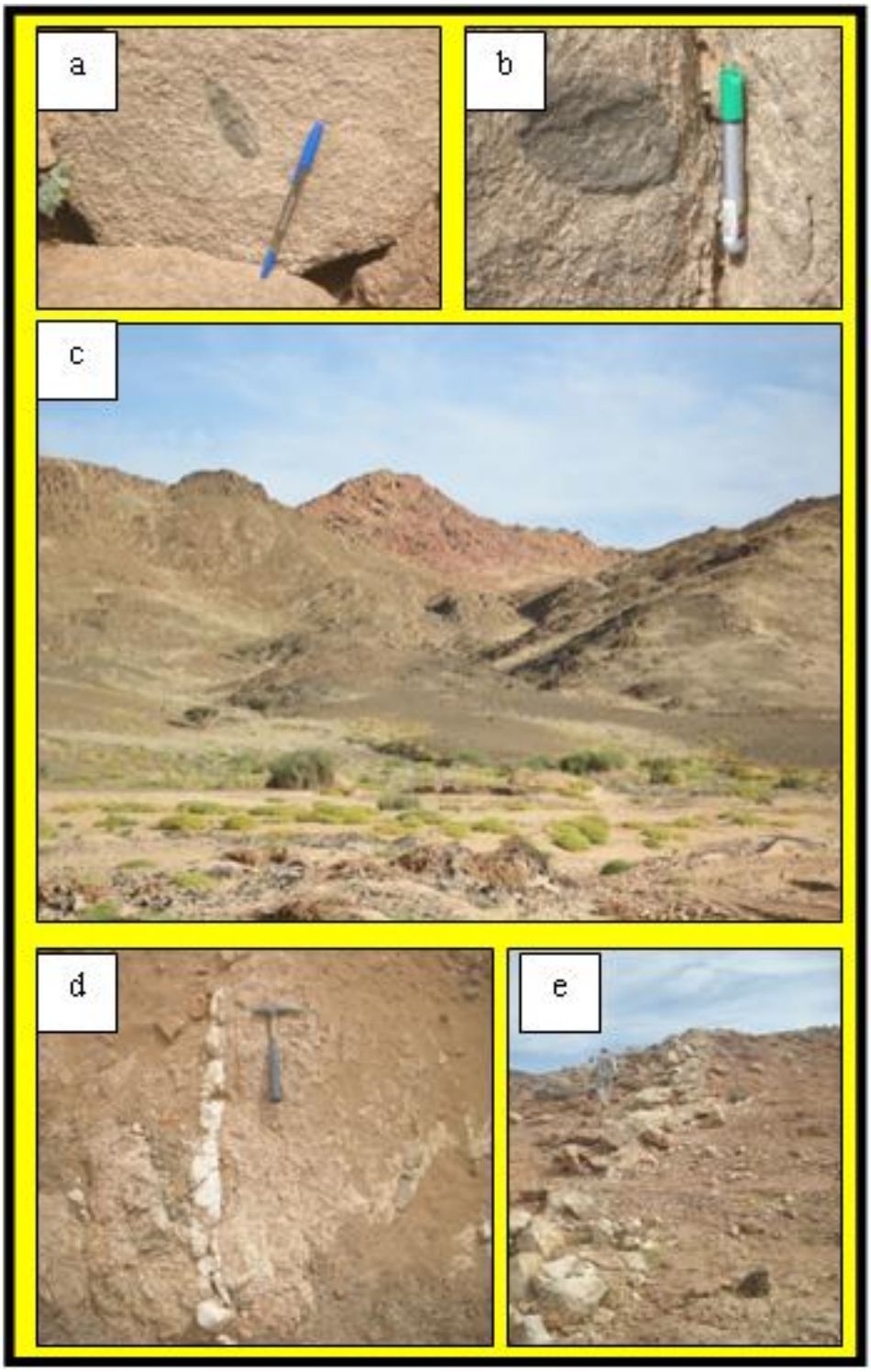

Figure 3.5: Field appearance of the Jabal Khur Dukhan Complex

a-Elliptical xenolith , b- Rounded xenolith , c- Alkali to syenogranite intrudes the country rocks of Za'am group, d- Quartz vein (late magmatic event) cutting across alkali to syenogranite, e- Large pegmatite vein cutting across alkali to syenogranite. The xenoliths represent the coutry rocks that were assimilated during the magma ascent.

III.4.2. Form of the plutons and mode of emplacement

Jabal Khur Dukhan is an irregular, epizonal, elliptical, felsic igneous pluton, with rectilinear contacts and moderate topography, which was emplaced by a passive cauldron mechanism at a depth of a few kilometers (Agar, 1986).

III.4.3. Sequence of events

The country rocks of the Za'am metavolcanics were intruded by both monzogranite-granodiorite and alkali-feldspar granite and much less syenogranite magmas which show no cross-cutting relationships. The pluton was later intruded by felsic dykes and veins (micro-granite, pegmatite and aplite) and also shows very slight alteration which may indicate a later metamorphic event.

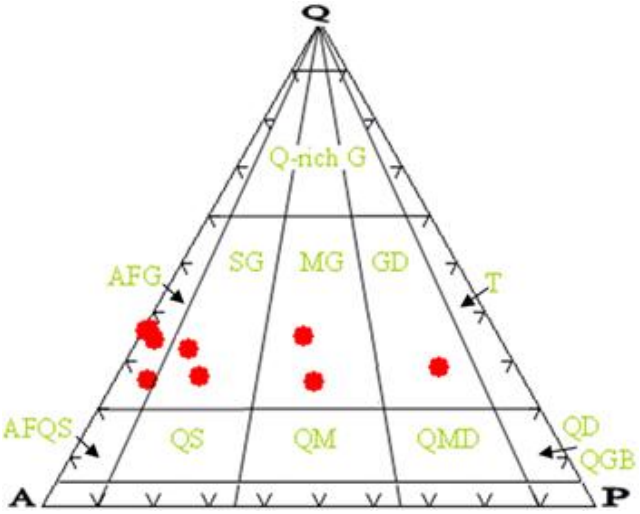

Figure 3.6: Modal compositions of the Jabal Khur Dukhan granitoids. Explanation of terms: Q-quartz, G-granite, AFG-alkali-feldspar granite, SG-syenogranite, MG-monzogranite, GD-granodiorite, T-tonalite, AFQS-alkali-feldspar quartz syenite, QS-quartz syenite, QM-quartz monzonite, QMD-quartz monzodiorite, QD-quartz diorite, QGB-quartz gabbro.

In the modal composition diagram (Fig 3.6), the granitoids show a linear array which could represent a fractionation trend from one magma source.

In summary Jabal Khur Dukhan is an elliptical-shaped pluton that hosts abundant xenoliths and consists of various types of granite. The relationship between these granitic rocks of the inner and outer parts of the complex remains unclear as there is no clear cross-cutting relationship between them. By relating the identified rocks to their

field's locations (Fig. 3.4) it appears that the more evolved granites occupy the large outer part of the complex, while the less evolved varieties occupy the inner ones.

III.5. Jabal Al-Massah Complex

The pluton (Fig. 3.7 and 3.8) occupies an area of 20 km^2. Forty samples were collected from this area. Jabal Al-Massah has been subjected to geological studies by Drysdall (1980), Davies and Grainger (1985) and Grainger and Hanif (1989) and a structural study by Agar (1986). It was also subjected to Rb-Sr age dating and chemical analysis by Stoeser and Elliott (1980) and Stoeser (1986) and an economic study has been carried out by Drysdall (1980) and Ramsay (1986). However, these studies were limited in their sampling and detail and it was felt that further work was justified. Names were given from modal analysis (Fig. 3.9) and later geochemical classification

III.5.1. Geology

The country rocks in the area are dominated by the Hasha metavolcanics as also noted by Davies and Grainger (1985). The granitic complex is mainly composed of coarse-grained (> 5mm), alkali to monzogranite (whitish), granodiorite (light grey) and porphyritic alkali to syenogranite (pinkish-red). The whitish granite mainly occupies the eastern and central part of the pluton, mostly forming isolated outcrops separated from the granodiorite. It is slightly to highly weathered, porphyritic (clearly at the northern, northwestern, and southern parts) with long K-feldspar crystals, exfoliated (due to weathering) and shows an abundance (up to 7%) of ferromagnesian (amphibole and biotite) minerals and some mafic xenoliths. The alkali to syenogranite have a higher topography, mainly covering the northeastern part of the pluton and grade from pinkish to reddish colour towards the northern and western sides, and have some felsic xenoliths (just adjacent to the country rocks that principally cover most of the southern parts). The whitish granite and the pinkish granites are possibly the younger monzogranites and older alkali-feldspar granites respectively, as described by Agar (1986).

In the southeastern and southwestern margins of the pluton the alkali to monzogranite is cut by quartz veins and by aplitic (S110°E or nearly E-W; cut by N-S trending quartz veins) and mafic dykes (N70°E). The north, northwestern and southern parts of the

alkali to monzogranite show porphyritic textures and variable granitic compositions. The pluton is cut by some major NW, N-NW and E-W trending faults.

III.5.2. Form of the plutons and mode of emplacement

The nested, circular, 'bell-jar' form of the Jabal Al-Massah pluton is typical of cauldron subsidence. According to Davies and Grainger (1985), the pluton was emplaced by the foundering of an older granite block into younger magma which moved around and above it and then continued to rise by stoping the roof. A successive upwelling magma emplacement theory of the circular structure in the homogeneous alkali granite was proposed by Drysdall (1980). It was emplaced by a passive cauldron mechanism at a depth of a few kilometers (Agar, 1986).

III.5.3. Sequence of events

The first event in the emplacement of he Jabal Al-Massah pluton was the intrusion of the pinkish-red granitoids into the metavolcanics of the Za'am, Bayda and Thalabah group. This was followed by the later, whitish granitoids and finally the pluton was intruded by felsic dykes (aplites and pegmatites), basic dykes, and some quartz veins. It is proposed that the alkali granites were post-dated by the whitish, calc-alkali granites.

Modally, although the granitic rocks of Jabal Al-Massah do not show a clear correlation, they do seem to show a trend of possible fractionation from one magma source.

As a summary it is possible to say that the nested-like Jabal Al-Massah is topographically moderate, weathered to some extent, shows different xenolith compositions (may reflect an assimilation process, which occurred between either the two plutons, as the roof of the outer pluton foundered into the inner pluton, or between the country rocks and the white, inner pluton as it was rising up and before its final solidification. This may explain the various compositions of xenoliths present in the area, different rock types, and is cut by large faults with different orientations.source). By relating the identified rocks to their field locations (Fig. 3.7) it appears that the more evolved granites occupy most of the complex, while the less evolved varieties occupy very minor parts represented by small outcrops.

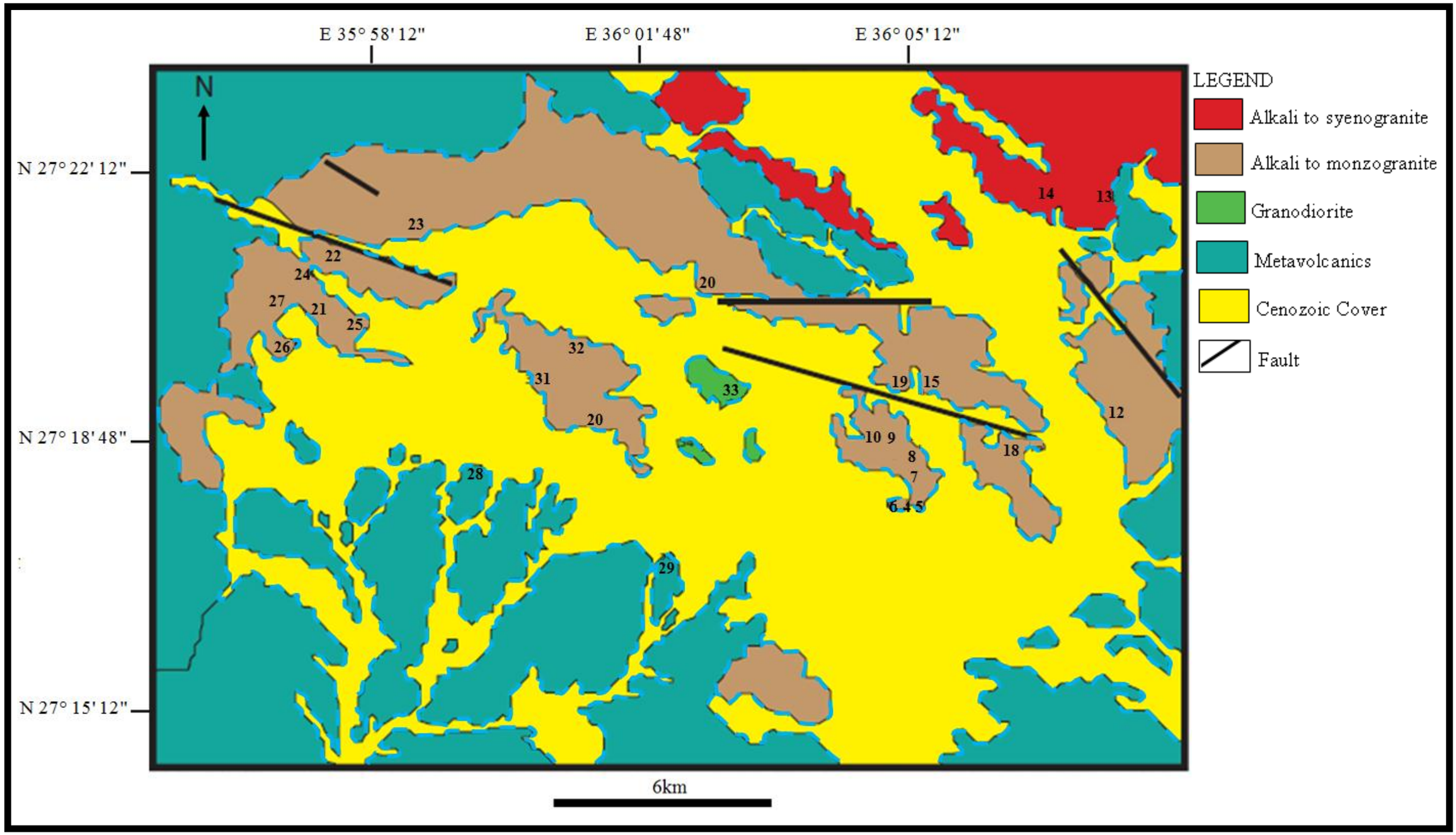

Figure 3.7: The geology of the Jabal Al-Massah Complex with sample locations (prefix JM). Rock names are from later mineralogical and geochemical studies. Reconnaissance map boundaries are approximate and provided the basics for the sampling programme.

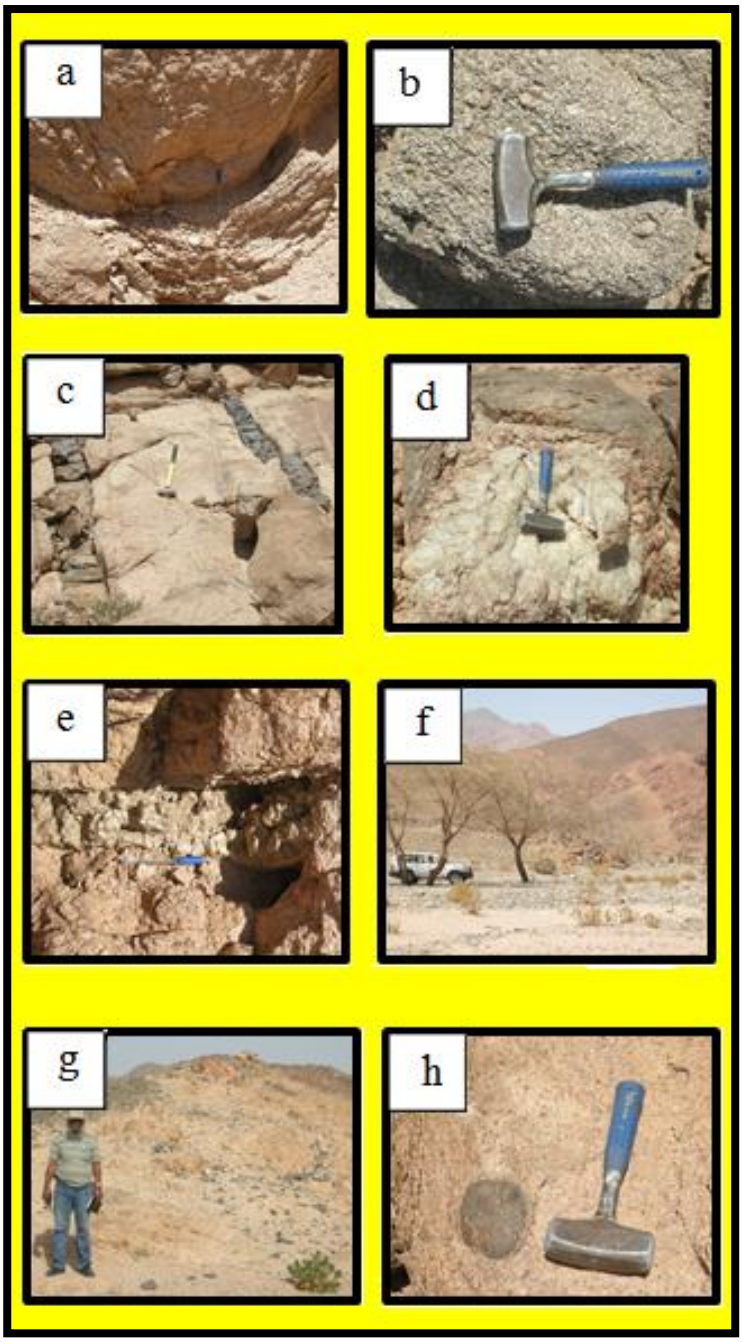

Figure 3.8: Field views of the Jabal Al-Massah Complex

a- Exfoliated (wathering) alkali to monzogranite, b- Highly weathered porphyritic granodiorite, c- Mafic dykes (late hydrothermal activity) cutting across and post-dated alkali to monzogranite, d- Quartz vein invaded alkali to syenogranite, f- Quartz vein with N-S trend cutting across a large felsic dyke, g- Alkali to syenogranite intruding the country rocks of the Hasha formation, h- Relic (mafic xenolith) of the Hasha formation in the alkali to syenogranite

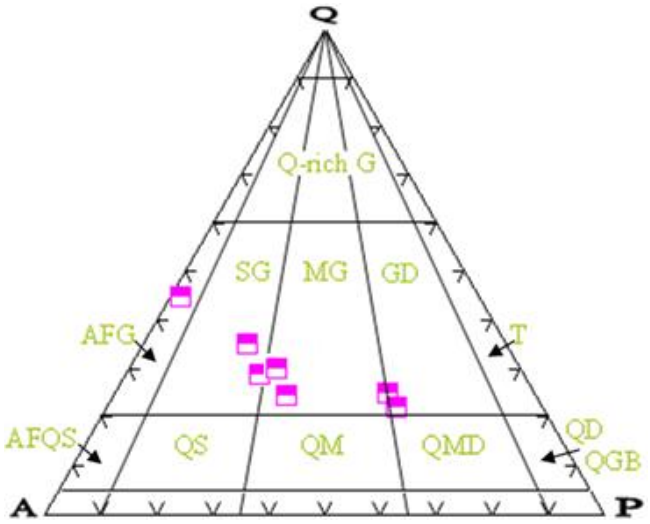

Figure 3.9: Modal composition of the Jabal Al-Massah granitoids.Explanation of terms: Q-quartz, G-granite, AFG-alkali-feldspar granite, SG-syenogranite, MG-monzogranite, GD-granodiorite, T-tonalite, AFQS-alkali-feldspar quartz syenite, QS-quartz syenite, QM-quartz monzonite, QMD-quartz monzodiorite, QD-quartz diorite, QGB-quartz gabbro.

III.6 Jabal Raydan Complex

The pluton occupies an area (Fig. 3.10 and 3.11) of almost 10 km^2. A total of thirty samples were collected from the area. Jabal Raydan was subjected to geological studies by Smith (1979), Drysdall (1980 and Grainger and Hanif (1989); age dating and chemical analysis by Stoeser and Elliott (1980), Kemp *et al*., (1980) and Stoeser (1986) and an initial economic study by Drysdall (1980) and Ramsay (1986). However, these studies were limited in their sampling and detail and it was felt that further work was justified. Names were given from modal analysis (Fig. 3.12) and later geochemical classification.

III.6.1. Geology

The pluton is composed of whitish coloured, medium-grained, arfvedsonite-bearing granite (alkali to monzogranite) and coarse to fine-grained reddish coloured granite (alkali to syenogranite), together with lesser granodiorite (Drysdall, 1980) (as small outcrops in the southern and southeastern parts of the pluton). The alkali to monzogranite represents the majority of the igneous intrusion. It is intruded by rhyolitic

dykes, which are cut in a few cases by later quartz veins. The alkali to syenogranite mostly occupies the highest part of the mountain and it is commonly foliated. In some places this foliation has been intense and equates to mylonitization, as Kemp *et al*. (1980) noticed. Along the shear zones, the quartz shows an association with possible riebeckite needles (Smith, 1979). Some of the alkali to syenogranite that occurs on the northwestern side contains pink feldspar and altered ferromagnesian minerals and could represent a contaminated phase. Some microgranitic dykes were found in the central parts of the red granite. Some mafic xenoliths were found hosted in the alkali to monzogranite on the western side of the pluton.

Some small outcrops of granodiorite were also found in the area but these show no clear cross-cutting relationship with the other granitic rocks and may in fact not be related to the main pluton. To the south of the northern margin of the pluton, there is a small, medium-grained alkali to syenogranite intrusion and further south there is another larger intrusion. The alkali to syenogranite granite is mostly weathered and intruded by quartz and pegmatite veins.

The country rocks to the medium and coarse granites are dominated by the Za`am metavolcanics. The granitic rocks are intruded by microgranite dykes which sometimes grade into pegmatite (the later often as stringers). Their strike ranges from NW to NE especially at the northeastern contact of the pluton.

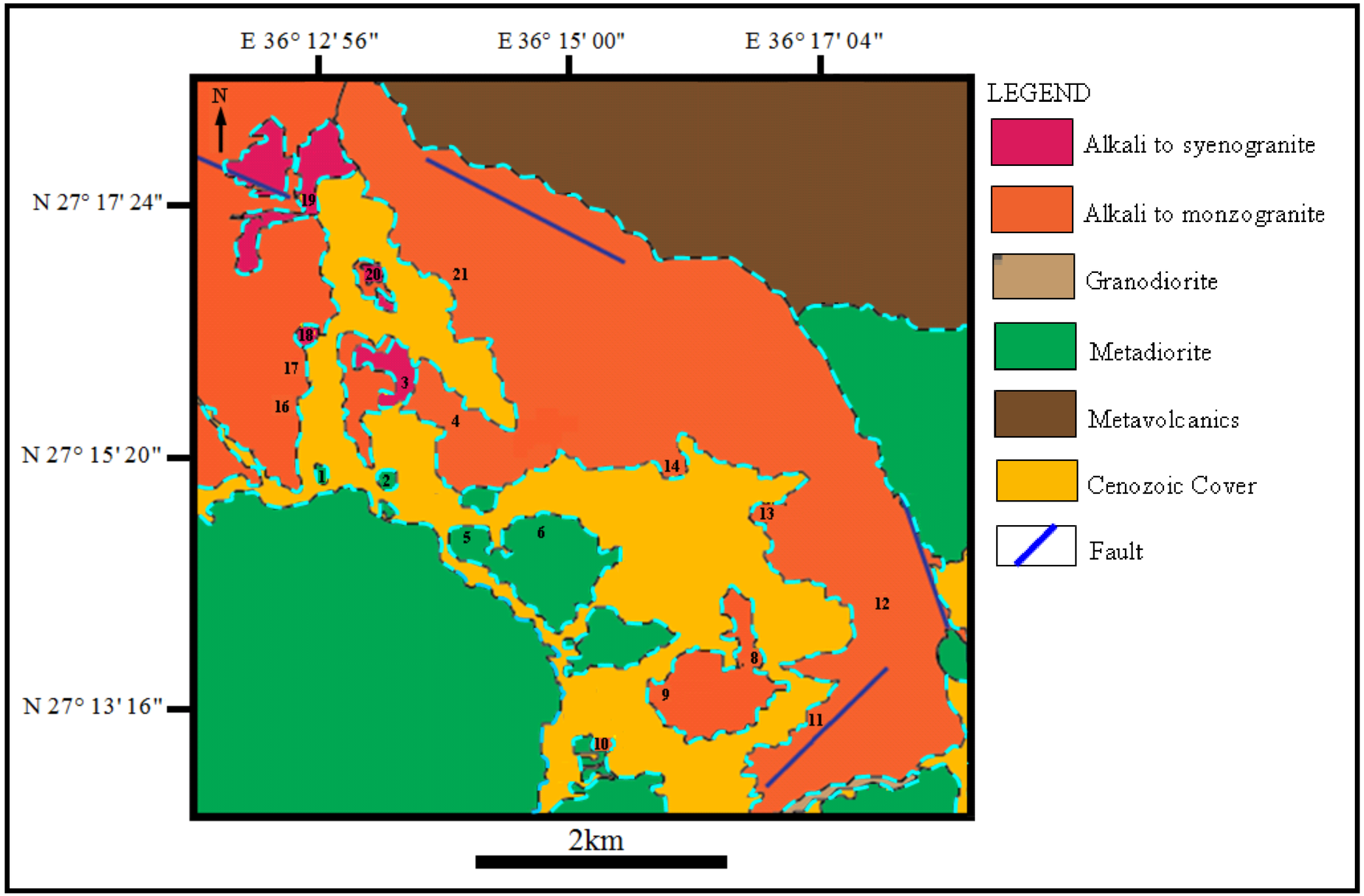

Figure 3.10: The geology of the Jabal Raydan Complex with sample locations (prefix JR). Rock names from later mineralogical and geochemical studies. Reconnaissance map boundaries are approximate and provided the basics for the sampling programme.

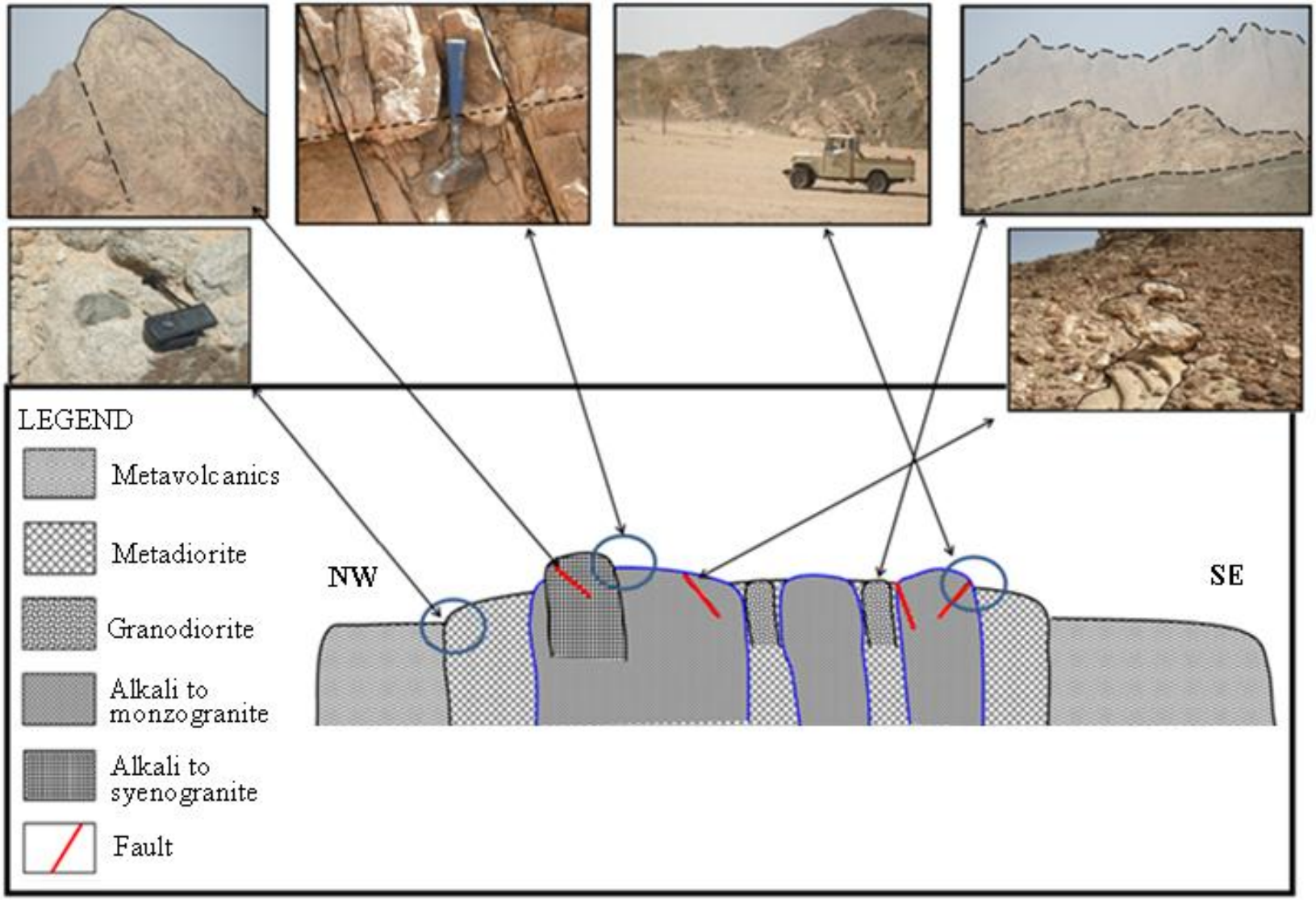

Figure 3.11: Hypothetical and idealized diagram showing lithological relationships in the Jabal Raydan Complex

The metadiorite of the Shagab complex is intruded by swarms of microgranite and pegmatitic dykes of S120°E and S155°E orientation. The intrusive rocks are foliated in the southwestern portion of the pluton and this extends along strike of a shear zone and penetrates the country rocks of the Za'am group.

III.6.2. Form of the plutons and mode of emplacement

According to Drysdall (1980), the Jabal Raydan pluton is an incomplete circular pluton which may belong to the ring complexes of the northern Midyan terrain that are of simple bell-jar type and were emplaced by cauldron- subsidence (Roobol and White, 1986).

III.6.3. Sequence of events

With the incomplete-circular pluton of Jabal Raydan (a suggested post-tectonic passive intrusion), the country rocks of the Za'am metavolcanics were first intruded by the dioritic rocks of the Shagab complex and then by small granodioritic intrusives and the –alkali to monzogranite and alkali to syenogranite intrusives. The latter rocks were then modified by fractionation and intruded by some felsic dykes (grading to pegmatites). The apices of the alkali granite intrusives were partially affected by a foliation event.

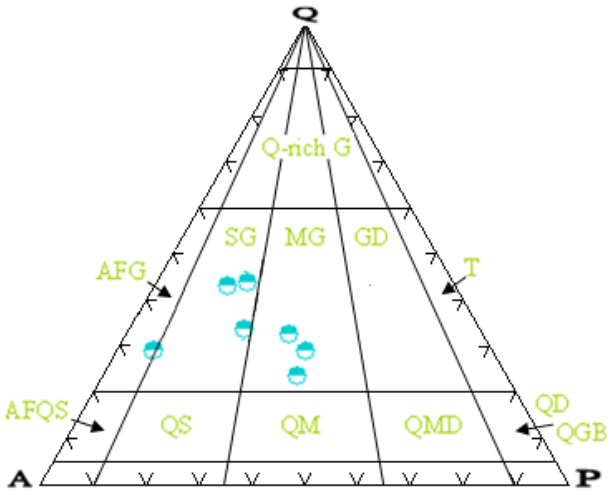

Figure 3.12: Modal composition of the Jabal Raydan granitoids. Explanation of terms: Q-quartz, G-granite, AFG-alkali-feldspar granite, SG-syenogranite, MG-monzogranite, GD-granodiorite, T-tonalite, AFQS-alkali-feldspar quartz syenite, QS-quartz syenite, QM-quartz monzonite, QMD-quartz monzodiorite, QD-quartz diorite, QGB-quartz gabbro.

The diagram showing modal compositions is similar to that of the other plutons in that it would support a fractionation from one parent granitic magma, but a clear fractionation trend is not present and sample relationships are not clear.

In summary, the Jabal Raydan pluton is topographically moderate to high but a prominent feature. It is dominated by white granites which sometimes grade into reddish coloured granites (especially in its NW part). It is foliated in some parts (the red granite roof zone), it hosts a moderate number of dykes and has very few xenoliths. It is cut by some large faults with several orientations (NW-SE, N-NW and NE-SW). By relating the identified rocks to their field locations (Fig. 3.10) it appears that the less evolved white granites occupy most of the complex, while the more evolved reddish-pinkish granite was found hosted in first type.

III.7. Jabal az Zuhd pluton

The pluton (Fig 3.13 and 3.14) occupies an area of almost 20km^2 and is located 5km northwest of the famous Tawlah prospect (Drysdall *et al*., 1986). Because of the apparent homogeneity only 14 samples were collected from the area. The Jabal az Zuhd Pluton was subjected to geological studies by Drysdall (1980), Ramsay (1982) and Drysdall *et al*. (1986) and economic studies by Drysdall (1980) and Ramsay (1986). However, these studies were limited in their sampling and detail and it was felt that further work was justified. Names were given from modal analysis (Fig. 3.15) and later geochemical classification

III.7.1. Geology

The equigranular, coarse-grained nature of this alkali granite was also noticed by Clark (1986) as the dominant lithology. Some porphyritic granite was also found along the eastern margins of the pluton. The pluton has been cut by a few pegmatite and felsic dykes and has a discordant contact with the country rocks. The country rocks of Jabal az Zuhd pluton are dominated by the Minaweh formation (explained earlier in this chapter).

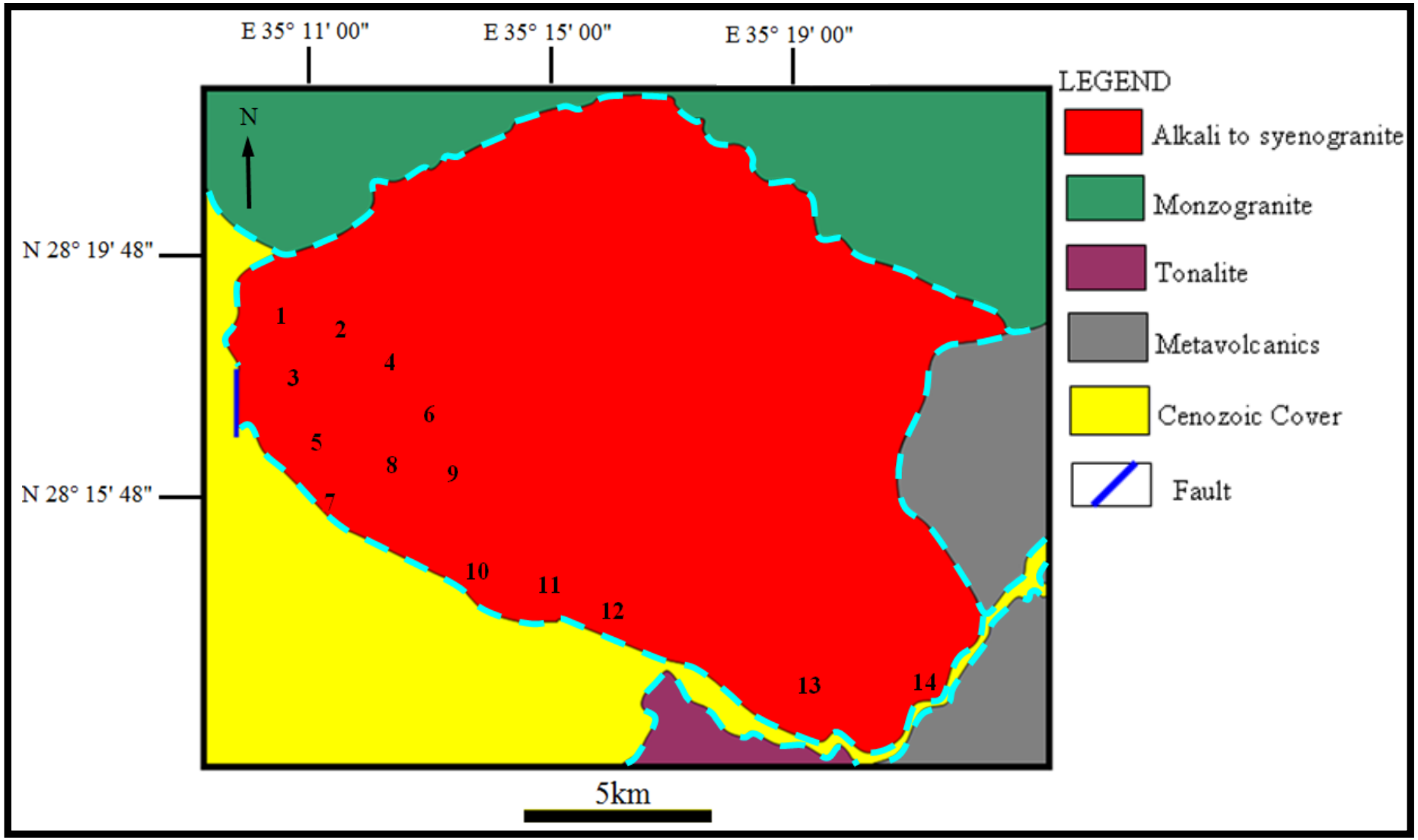

Figure 3.13: The geology of the Jabal az Zuhd Pluton with sample locations (prefix JZ). Rock names from later mineralogical and geochemical studies. Reconnaissance map boundaries are approximate and provided the basics for the sampling programme.

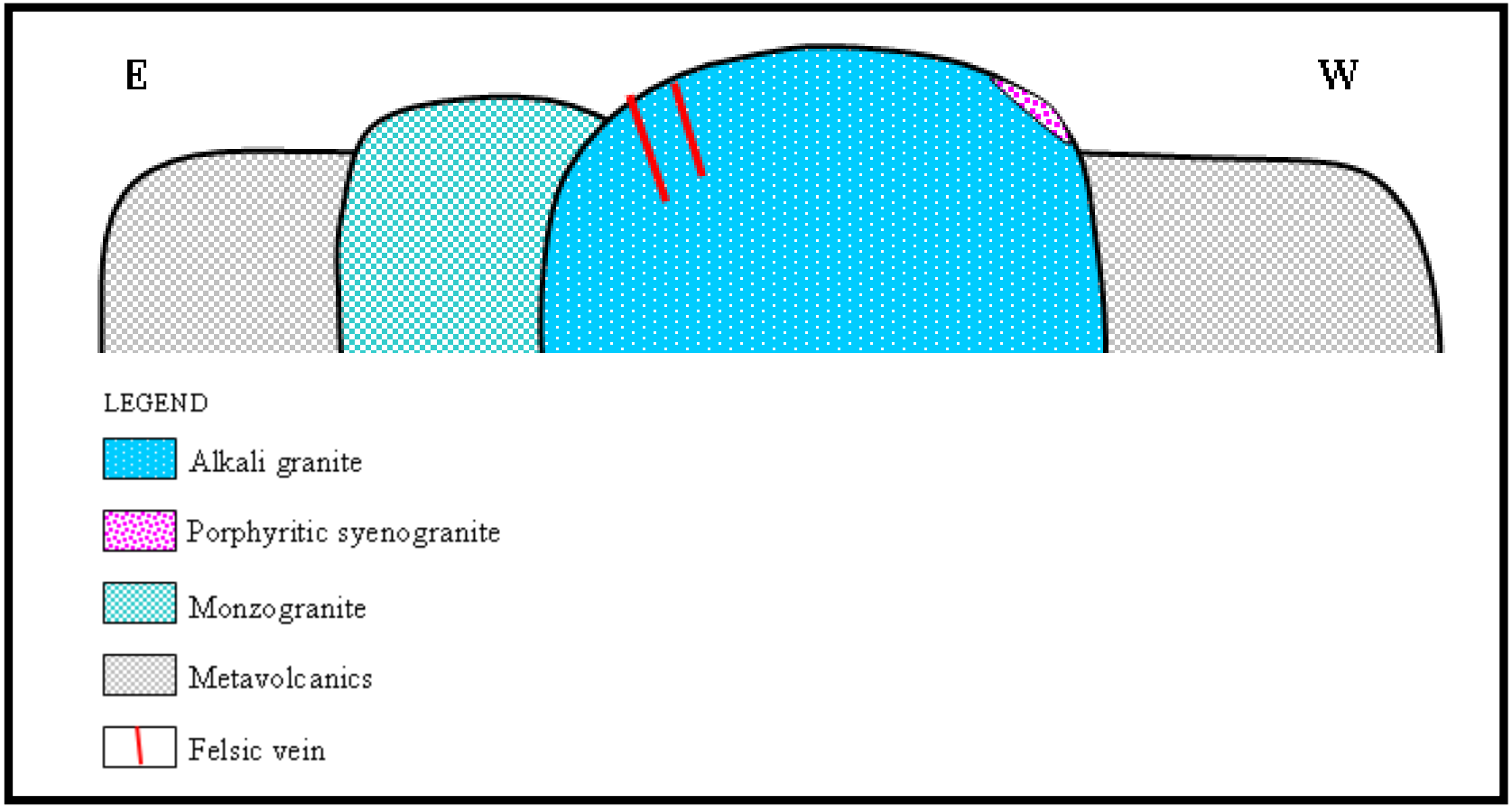

Figure 3.14: Hypothetical and idealized diagram of the Jabal az Zuhd Pluton.

III.7.2. Form of the pluton and mode of emplacement

The topographically high, sub-circular pluton of Jabal az Zuhd is a post-tectonic, massive, unfoliated body with sharp, discordant contacts against the country rocks. It is most likely related to the adjacent, forceful intrusives in the region that were emplaced during the time interval 570 to 800 Ma (Kemp et al., 1980).

III.7.3. Sequence of events

The forceful (the magma forced their way up through the denser country rocks), sub-circular, post-tectonic pluton of Jabal az Zuhd, its apparent homogeneity, indicate that the felsic intrusion was basically formed by melting of crustal material (just a suggestion based on the fact that the rocks nature and their constituents of this pluton look very different from those of the other plutons which possibly indicates magma with different chemistry and subsequently different source)

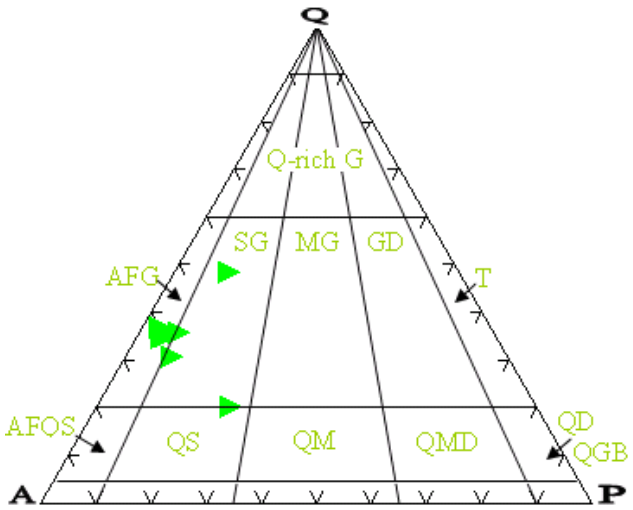

Figure 3.15: Modal compositions of the Jabal az Zuhd Pluton. Explanation of terms: Q-quartz, G-granite, AFG-alkali-feldspar granite, SG-syenogranite, MG-monzogranite, GD-granodiorite, T-tonalite, AFQS-alkali-feldspar quartz syenite, QS-quartz syenite, QM-quartz monzonite, QMD-quartz monzodiorite, QD-quartz diorite, QGB-quartz gabbro.

In the modal composition diagram (Fig. 3.15), the rocks mostly plot in the alkali-feldspar field, and they do not show a clear linear trend but plot close to each other. The abundance of allanite (especially in the syenogranites) may indicate a promising source

for some important rare metals (see later). More than one amphibole type was found (brown, green and deep blue) and this mineral is discussed further in a later chapter.

In summary, the Jabal az Zuhd pluton is a large, massive pluton with no xenoliths, very rare felsic dykes and only two types of granite, the alkali granite and the porphyritic granite. By relating the identified rocks to their field locations (Fig. 3.13) it appears that the majority of the pluton is composed of the alkali granites. The less evolved syenogranites were found in a small part of the pluton peripheries.

III.8. Comment on the presence of xenoliths

The xenoliths that were observed in most of the study areas would support the stoping magma emplacement theory. The types of xenoliths are different; some of them could represent assimilated (metavolcanic) country rocks during magma ascent, whilst others might be related to the destruction of the bell-jar plutons, where the older upper granitoids have foundered into the younger granitoids by stoping. The early stages of the enclosed xenoliths are characterized by an angular, blocky shape and as they progress through the assimilation their rims reacted and corroded, resulting in rounded-shaped xenoliths, which also become smaller and more elongate. The final stage, in the most assimilated xenoliths, show assemblages of ferromagnesian minerals. The chemistry of theses xenoliths is discussed in chapter 6.

III.9. Discussion and conclusions

Although the studied plutons were assumed to be similar in terms of their rock types and mode and age of emplacement, some major geological differences have been found (Table 3.2). The field relations between most of the studied plutons and the surrounding metamorphosed, country rocks show discordant, sharp contacts, which indicates that the plutons were emplaced post-tectonically. A sequence of age of emplacement for the studied plutons and their stratigraphical relations with their country rocks is proposed (Fig.3.16). The physical features and the formation of the studied plutons are basically related to their structural controls and mode of emplacement.

Table 3.2: Main geological features of the studied plutons

Pluton	Geology	Lithology and modal composition	Ferromagnesian minerlas (Am+Bi)
TH	Ring-complex structure and highly affected by shear zones.	MG to GD > AG to SG (7 samples plot in the GD filed, 1 plot in the MG, 3 plot in the SG and 2 plot in the AG)	All poor in Am but as a total MG to GD host up to 5%, while AG to SG do not exceed 0.8%.
KD	Heterogeneous. Comprises two plutons that show no clear relative age relationships.	AG to SG > MG to GD (3 samples plot in the AG field and 2 plot each field of MG and SG and only 1 plot in the GD of the modal composition diagram)	All poor in Am but as a total MG to GD host up to 8.7%, while AG to SG do not exceed 0.7%.
JM	Shows clear nested structure with unclear boundaries.	AG to MG > GD (2 samples plot in each field of GD, MG and SG and only 1 plot in the AG of the modal composition diagram)	All poor in Am but as a total GD host up to 6%, while AG to MG do not exceed 1.5%.
JR	Shows incomplete double ring-complex structure.	AG to MG > AG to SG (3 samples plot in the MG filed and the same number plot in the SG field and only 1 plot in the AG of the modal composition diagram)	The AG shows no presence of either Am or Bi, the SG host some (up to 2%) of them and the MG host far more (6.7%).
JZ	Large and massive; the most homogeneous pluton.	Dominated by AG with much less SG (5 samples plot in the AG filed and only 2 plot in the SG field of the modal composition diagram)	The AG host much more (up to 9.6%) Am and Bi than the SG (up to 1.2%).

Explanation: TH, Jabal Thalabah, KD, Jabal Khur Dukhan, JM, Jabal Al-Massah, JR, Jabal Raydan, JZ, Jabal az Zuhd, AG, alkali granite, SG, syenogranite, MG, monzogranite, GD, granodiorite, Am, amphibole, Bi, biotite.

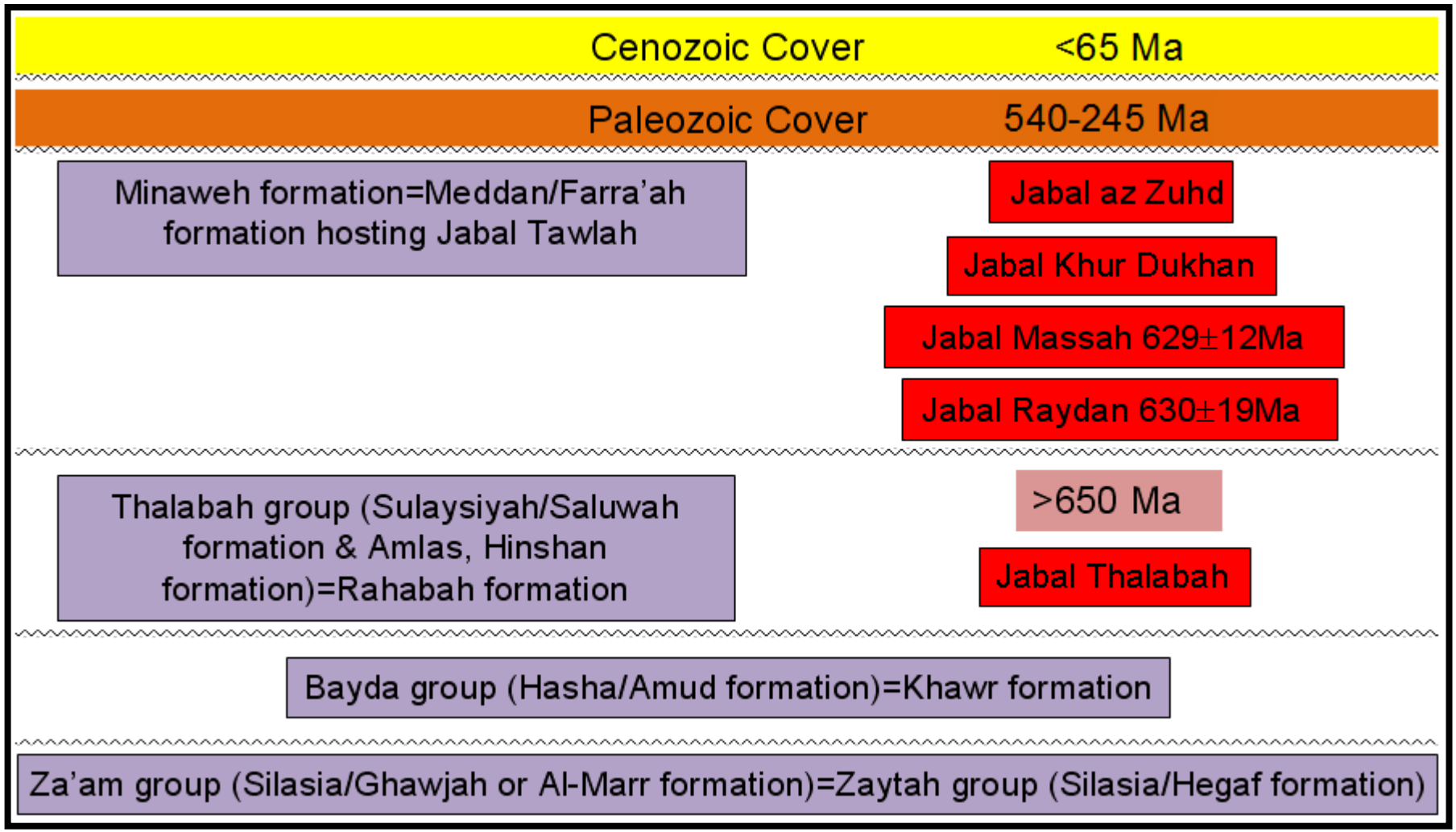

Figure 3.16: Suggested stratigraphic relationship of the studied plutons of the Precambrian layered rocks of the NW Arabian Shield after Davies and Grainger (1985), Clark (1986), Rowaihy (1986), Grainger and Hanif (1989). The suggested sequence of event is based on regional comparisons and previous classifications.

III.9.1. Regional Comparisons

Jabal Khur Dukhan, Jabal Al-Massah and Jabal Raydan resemble the youngest, cauldron type of peralkaline and younger calc-alkaline granitoids of the Arabian Shield that were classified by Drysdall and Odell (1982). These types of plutons are mostly circular, oval or rectilinear in plan and they have variable sizes, from plug to stocks. They are mainly characterized by biotite monzogranites that post-date the Thalabah group deposition (~660 Ma). These plutonic suites were episodic and the alkali granites were post-dated by calc-alkali granites. They are also very similar to the passively emplaced granites (by a cauldron stoping mechanism) bell-jar shaped plutons in the less ductile country rocks that are located in Al Wajh and Muwaylih areas (Davies, 1982).

They are more likely to have hydrothermally modified apical zones than in the larger, elongate, diapirically emplaced plutons within ductile areas of regional shear zones. The Jabal az Zuhd pluton is very similar to the homogeneous alkali granite plutons with a circular form that indicate emplacement by constantly upwelling of magma rather than a single pulse. The very low-grade contact metamorphic and metasomatic effect, pegmatite and quartz veins suggest that the granites were dead (mostly cooled and crystallised) on arrival. The final heat loss and volatiles may have been contemporary with venting. Jabal Thalabah most likely belongs to the old, small, ring structure complexes (classified by Jackson *et al*., 1984) that were partially affected by regional shear zones, contain abundant xenoliths and have common dike swarms. They pre-date the deposition of the Thalabah group and are suggested to be emplaced by a cauldron stoping mechanism. In the Arabian Shield the peralkaline granites are younger than both the Thalabah group and most of the calc-alkali granites, although there is some overlap. The overlap in time of emplacement at high levels in the crust might be due to different rates of magma upwelling that have been controlled by magma volumes and varying local temperature/pressure conditions. Further mineralogical, geochemical and geochronological studies are needed to clarify all the proposed issues raised in this chapter.

To summarize, the studied plutons exhibit subtle differences in geology and lithology and are suggested to have been emplaced at a similar time, which consequently assumes a similar tectonic setting. The major geological feature of the studied plutons indicates that biotite and amphibole are commonly found in greater abundance within the less

felsic rocks (except with Jabal az Zuhd were the majority of them are present within the alkali granite). Also, the modal composition diagrams indicate the following:

- Jabal Thalabah is composed of granitoids rocks that show a big difference in composition (may indicate magma mixing).
- Jabal Khur Dukhan is dominated by the more felsic granitoids (may indicate highly fractionated magma).
- Jabal Al-Massah shows a gradual change in compostion suggesting one magma source for the granitic rocks.
- Jabal Raydan shows a gradual change in compostion suggesting one magma source for the granitic rocks.
- Jabal az Zuhd shows that the majority of the samples are accumulated in the alkali-feldspar field (not a linear trend that may indicate fractionation) and may also indicate a different magma source from the other plutons.

IV. Petrography

IV.1. Introduction

A detailed petrographic study of the granites from the study area was deemed necessary to:

1) Identify the lithologies, confirm the field terms and assess any possible relationships between the different granitic rocks in each pluton.

2) Determine and describe the textures present, as these could help clarify the processes occurring during and after granite development.

3) Identify the minerals present, especially the potentially important accessory phases.

The petrographic and mineralogical characteristics of the studied granitic suites were obtained by optical microscopic analysis of textures, mineralogy and modal composition. These were obtained using standard petrographic thin sections and point counting a minimum of 2500 points.

In general, the samples used in the microscopic studies were relatively unaltered. If any alteration mineral was present and could clearly be seen to have derived from a primary phase then it was recorded as a primary phase. The main potential for inaccuracy in these modal analyses relates to the accurate measurement of the perthite composition and this will affect the K feldspar – plagioclase proportions. Some accessory phases could not be identified but their identity was confirmed during subsequent electron microprobe analysis (chapter 5). The main diagram used for summarizing the modal compositions is the Q-A-P (quartz-alkali feldspar-plagioclase feldspar) diagram which was originally developed by the International Union of Geological Sciences (IUGS, 1961) and later modified by Streckeisen (1967) to be utilized for plutonic igneous rocks. The nomenclature for some granitoids was slightly modified after more precise geochemical classification (see chapter VI). The modal compositions are presented in appendix II and summarized in figures in this chapter.

IV.2. Petrography of the Jabal Thalabah Complex

The macroscopic, petrographic and modal analyses of the Jabal Thalabah granitoids (Figs. 3.3 and 4.1; Table 4.1) reveal that these rocks are mainly mesocratic, coarse-medium (>5mm and 1 to 5mm) grained, grey to buff pinkish granodiorite, monzogranite and syeno- to alkali granites. Some are slightly altered. The pluton also includes some hybrid and chilled margin rocks (see later).

Plagioclase is commonly zoned and has an intermediate composition. Alkali feldspar is mostly represented by microcline perthite. The accessory phases are dominated by biotite, muscovite, hornblende and chlorite, and much less titanite, apatite and opaque minerals. Biotite occurs either as patches or elongate laths; hornblende is very rare. Some typical textures are shown in figure 4.1.

This pluton is distinguished from other plutons by the presences of some lithologies with minerals and textures which appear to represent a mixture of magma types. These include clots or assemblages of ferromagnesian minerals which commonly show an association with opaque phases, in addition to the presence of the development of myrmekites; these have been termed hybrid rocks.

Table 4.1: Lithologies and mineralogy of the Jabal Thalabah Complex

Major Rock Units	Rock-Forming Minerals	Major Accessories	General Texture	Alteration	Sample Number
SG	Qz, afs & less plg	Op and very poor altered Bi and am	Coarse & Medium-grained	Fresh	TH5`- 10` & 12`
MG	Plg, qz & kfs	Bi and am (chl) & less ms	Coarse-grained	Highly altered	TH5
Bi & Ms-GD	Plg, qz & kfs	Bi, chl, ms, op & less ap & tit.	Coarse-grained	Fresh to slightly altered	TH3-4-9-11 & 14-18-19-
HG (alkaline)	Plg, qz & kfs (showing variable ratios)	Am, Bi, chl, ms, zr, mo & tit.	Coarse-grained	Fresh to highly altered	TH13`& 14`
CMR	Qz, afs & plg	Bi, ms, chl, tit, zr & op	porphyritic	Fresh to slightly altered	TH 3`- 4` & 6`

Explanation of terms: Qz-quartz, afs-alkali feldspar, plg-plagioclase, am-amphibole, bi-biotite, ms-muscovite, chl-chlorite, ap-apatite, op-opaque minerals, zr-zircon, tit-titanite, mo-monazite, SG-syenogranite, MG-monzogranite, GD-granodiorite, HG-hybrid granite, CMR-chilled margin rocks.

IV.2.1. Syenogranite

This rock is mainly composed of quartz and alkali feldspars (perthite and micro-perthite) with much lesser amounts of plagioclase feldspar and accessory minerals, such as muscovite, apatite, zircon, titanite and some chloritized amphibole and biotite.

The plagioclase feldspar is sub- to euhedral and exhibits zoning. This zoned plagioclase hosts epidote and opaque inclusions. The perthite hosts some inclusions of finer quartz and plagioclase. The quartz occurs in two different forms. The larger variety has inclusions of muscovite apatite and biotite. The finer quartz corrodes most of the other minerals and rarely has a saccharoidal appearance.

The amphibole and biotite are rare (0 to 0.8%) and are slightly to highly altered. Chlorite corrodes plagioclase and replaces muscovite.

IV.2.2. Monzogranite

This rock is mainly composed of plagioclase, quartz and K-feldspar. The accessories are mainly highly altered biotite and much less muscovite.

Sub- to euhedral, mostly altered, twinned plagioclase (sometimes oscillatory zoned) forms much of the rock. It hosts some tabular muscovite and commonly shows sharp contacts with the quartz but unclear relations with the K-feldspar. Medium to coarse-grained quartz is the second most abundant mineral in the rock. It is commonly fractured, invaded by stringers of K-feldspar and commonly shows corrosion of the plagioclase. Fractures in the quartz are occupied by some accessory phases. This rock type is rich in accessories, especially fibrous chlorite, which replaces most of the minerals. Tabular and rarer, fan-shaped muscovite is also present but in a lower quantity than that of the chlorite. They are commonly associated with or enclosed by the plagioclase. Opaque minerals are relatively rare and often associated with chlorite and feldspar.

IV.2.3. Granodiorite

This rock is composed of plagioclase (rarely showing kinking and alignment), quartz and K-feldspar. The accessories are mainly biotite (prismatic or lath-like, brown and rarely green and reddish), variably-shaped (tabular, prismatic and fan-shaped) muscovite, fine-grained sericite, fibrous chlorite (sometimes showing anomalous purple interference color), opaque minerals and less rhombic-shaped titanite and acicular and rod-like apatite.

Subhedral plagioclase is the most dominant mineral. It shows variable sizes (up to 5mm) and types (zoned, twinned). It is commonly corroded by anhedral quartz (with rare graphic intergrowths), K-feldspar, and rarely by thin biotite and randomly oriented acicular chlorite. It hosts some inclusions of opaque minerals, muscovite and biotite. Anhedral quartz is the second most abundant mineral. It shows variable grain sizes (sometimes > 5mm) and mainly invades the K-feldspar, encloses and replaces the plagioclase and hosts fine-grained biotite, muscovite, chlorite and opaque minerals.

The K-feldspar (often perthitic) is much less abundant than quartz and plagioclase and its crystal size sometimes reaches 0.5 cm. It is often invaded by ferromagnesian minerals, especially biotite, but in a few cases there are sharp contacts between these two minerals. Biotite is replaced by fibrous chlorite and opaque minerals and mostly shows replacement of quartz and feldspar. Some muscovite is enclosed as fine tabular crystals in the feldspars and the quartz. The opaque minerals are commonly associated with the ferromagnesian minerals, especially chlorite.

IV.2.4. Chilled margin of the syenogranite

The chilled margin rocks of this complex are found at the margin of the syenogranite. They show syenogranitic composition and are mainly composed of quartz (large and small), alkali feldspar (perthite) and plagioclase (mostly zoned). Biotite, titanite, zircon, muscovite, opaque minerals, sericite and chlorite represent the accessories (some being alteration secondaries). A porphyritic texture is quite clearly seen in thin section as some of large quartz is distributed in a fine-grained matrix of the other minerals.

The quartz phenocrysts sometimes host muscovite, chlorite and opaque inclusions, and they also replace chloritized feldspars. The smaller (<1mm) quartz commonly shows a saccharoidal texture and also replaces the feldspars or occurs as inclusions in the perthite. Orthoclase perthite is represented either as patch-like or vein-like forms and it has inclusions of finer plagioclase and also replaces that mineral. The zoned feldspar hosts anhedral opaques and chlorite and replaces biotite. Chlorite and sericite show a general association with euhedral opaque minerals. Fresh biotite and amphiboles are rarely present, but red biotite is more common. Titanite, zircon, muscovite and opaque minerals are all enclosed in the larger crystals of quartz and feldspar.

IV.2.5. Hybrid rocks

The ‘hybrid’ rocks have an alkali granite composition and are characterized by the presence of abundant (~ 4%) ferromagnesian (biotite and amphibole) minerals which are associated with opaque minerals, chlorite and other fine-grained (<1mm) phases and found either as discrete assemblages or surrounding other felsic phases. Zoned plagioclase, wart-like myrmekite and slightly unclear rapakivi textures are also present (Fig 4.2). Furthermore, the quartz in the hybrid rocks is rich in trails of aqueous (vapor

and liquid) fluid inclusions. Such rock types may indicate magma mixing or assimilation process (Deer *et al*., 2001; Baxter and Feely, 2002).

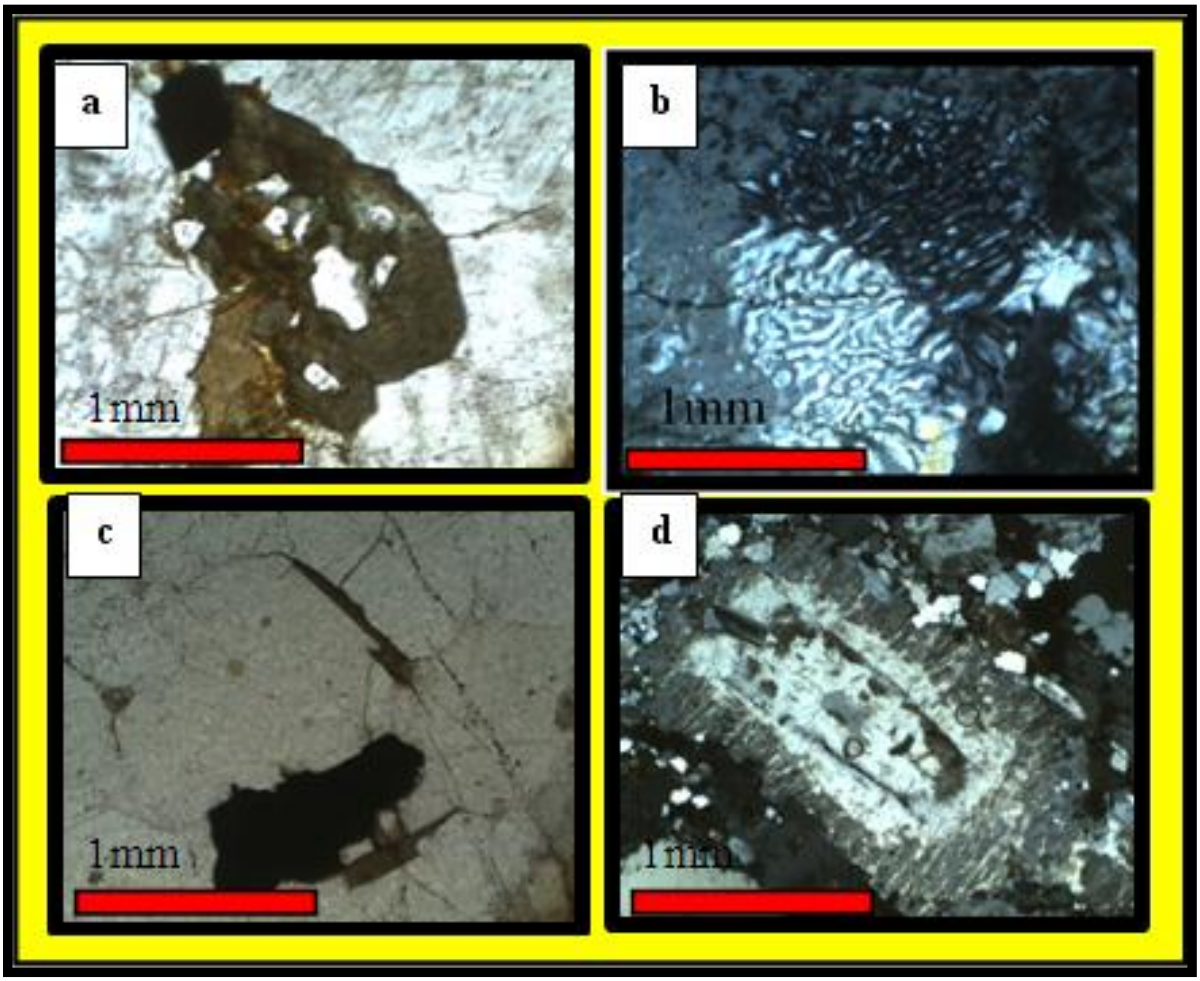

Figure 4.1: Textures in the Jabal Thalabah granitoids

a) Altered hornblende hosted in large crystal of feldspar with some quartz inclusions and associated opaque minerals (monzogranite) P.P.L.

b) Feldspar: simple twinning in irregular myrmekite (hybrid rocks) X.P.L.

c) Elongate biotite enclosed with larger irregular opaque mineral in quartz phenocryst (granodiorite) P.P.L.

d) Plagioclase showing plagioclase-alkali-feldspar reaction rim (syenogranite) X.P.L.

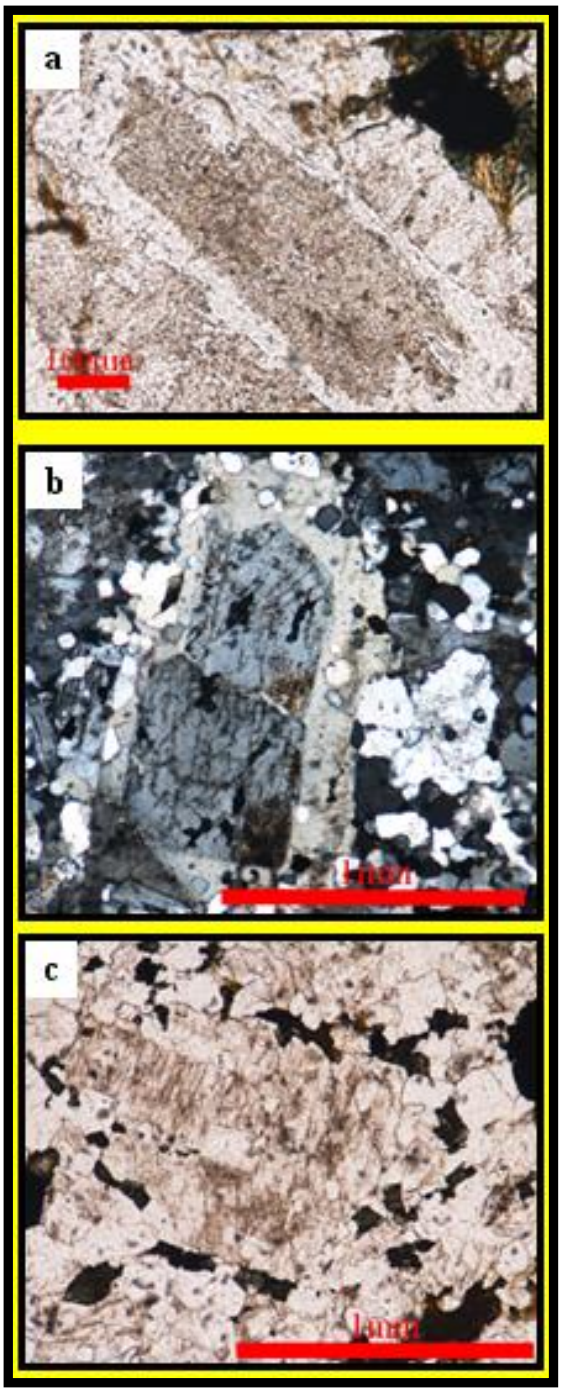

Figure 4.2: Characteristics of the Jabal Thalabah hybrid rocks

a) Rapakivi (plagioclase-mantled microcline or K-feldspar) texture, P.P.L.

b) Zoned plagioclase reflects different composition (more calcic core and more sodic rim), X.P.L.

c) Ferromagnesian (amphibole and biotite) minerals surrounding feldspar, P.P.L.

IV.2.6. Conclusions

The lithology of this complex is mainly represented by granodiorite (grading into less abundant monzogranite), syenogranite, hybrid granite (alkaline) and porphyritic chilled margin rocks. On the basis of petrography, the hybrid rocks of the Thalabah pluton are characterized by intergrowth textures (especially myrmekite and rapakivi) indicating intragranular solid-state process and abundant ferromagnesian and secondary minerals. To conclude, Jabal Thalabah is the only complex in which chilled margin facies and hybrid rocks are present. Also, it is the only pluton in which myrmekite texture reach a very advanced development stage. From the mineral relationships it is suggested that the order of mineral crystallization might be as follows:

Amphibole and biotite crystallized first, followed by plagioclase, K-feldspar and quartz; muscovite and chlorite.

IV.3. Petrography of the Jabal Khur Dukhan Complex

From the macroscopic, petrographic and modal analyses of the Jabal Khur Dukhan granitoids (Fig.3.6 and 4.3; Table 4.2), it appears that the majority of these rocks are mesocratic, coarse to medium-grained (>5mm and 1 to 5mm) and porphyritc, light grey granodiorite and monzogranite and pinkish to reddish syenogranite to alkali-feldspar granite (sometimes altered).

Plagioclase is mainly altered and rarely zoned (sometimes showing oscillatory zoning). Perthite and much lesser anti-perthite (vein-type and patch-like) are present and show reaction features with plagioclase and quartz, resulting in the development of myrmekitic intergrowths. The accessory phases are dominated by slightly to highly altered biotite (0 to 5.5%) and lesser amounts (0 to 3.2%) of amphibole. The ferromagnesian minerals, especially altered biotite, show a clear association with some opaque minerals. Fine-grained apatite and zircon are present, but quite rare. Opaque minerals and muscovite are also found in lesser quantities.

Table 4.2: Lithologies and mineralogy of the Jabal Khur Dukhan Complex

Major Rock Units	Rock-Forming Minerals	Major Accessories	General Texture	Alteration	Sample Number
AG	Afs, qz & few plg	Bi, ms & less op, hm?, mo & zr	Medium-grained	Fresh to slightly altered	KD1-4 & 41
SG	Afs, qz & plg	Am & bi (chl), less op & zr	Coarse-grained	Slightly altered	KD37 & 28
MG	Plg, afs & qz	Am & bi, less op, zr & ap	Coarse-grained & porphyritic	Fresh to slightly altered	KD11 &12
GD	Plg, afs & qz	Am & bi, less op, zr & ap	porphyritic	Highly altered	KD23

Explanation of terms: Qz-quartz, afs-alkali feldspar, plg-plagioclase, am-amphibole, bi-biotite, ms-muscovite, chl-chlorite, ap-apatite, op-opaque minerals, zr-zircon, hm-hematite, mo-monazite, AG-alkali granite, SG-syenogranite, MG-monzogranite, GD-granodiorite.

IV.3.1. Alkali granite

This rock is dominated by perthite (mostly simple-twinned), coarse to medium (-grained quartz and altered plagioclase; sub-solidus myrmekite and rare rapakivi and anti-perthite textures are also seen. It is generally rare in accessory minerals, which are mainly represented by altered biotite, fine-grained muscovite, some opaque minerals and much less, fine-grained zircon and hematite (?).

Quartz shows anhedral and subhedral (polygonal) crystal shapes. It replaces the alkali feldspar and sometimes encloses muscovite, opaque minerals and much less biotite. The plagioclase shows grain-size variability (coarse to fine-grained), oscillatory zoning and replacement by perthite. The biotite shows an association with opaque phases and is sometimes altered to chlorite. Muscovite, opaque minerals and much less fine-grained zircon and hematite (?) are enclosed in both feldspar and quartz.

IV.3.2. Syenogranite

This rock is dominated by slightly altered alkali feldspar (vein-type, flame-like, patchy perthite), less quartz and plagioclase. The accessories are represented by green ferromagnesian minerals (biotite and amphibole), opaque minerals and much less fine-grained zircon and muscovite.

The plagioclase is slightly altered and hosts some muscovite inclusions. It is enclosed in and replaces the alkali-feldspars. It is also corroded by the coarse-grained quartz, which rarely hosts fined-grained muscovite, zircon and alkali-feldspars. Altered biotite shows a clear association with opaque minerals and to a lesser extent zircon and shows some replacement of the major mineral phases.

IV.3.3. Monzogranite

This rock is dominated by coarse-grained quartz, altered alkali feldspar (vein-type, flame-like and patchy perthite), plagioclase (multiple twinned, commonly zoned with the core being sericitized) and myrmekite. The accessories are mainly biotite (mostly altered), less dark green, elongated amphibole (sometimes showing purple birefringence and simple-twinning), and fine-grained, rod like apatite and zircon.

The quartz corrodes and encloses the alkali-feldspar and the altered plagioclase. In some cases, the alkali-feldspar shows a circular arrangement, mantling the large subhedral plagioclase. It is also found as a remnant in some large quartz crystals and encloses smaller altered plagioclase. The amphibole and biotite are enclosed in the major mineral components. They sometimes show an acicular arrangement around quartz phenocrysts and a clear association with rod-like and acicular apatite and fine-grained zircon.

IV.3.4. Granodiorite

This rock is mainly composed of variable sizes (<1mm to >5mm) of altered plagioclase, quartz, altered alkali feldspar (mostly perthitic) and rare myrmekites. The rock is rich in accessories, especially, platey-like biotite, anhedral, rhombic-shaped and elongate amphibole and much less muscovite, hematite, opaque minerals, zircon and apatite.

The alkali-feldspar hosts and is corroded by most of the major phases and the accessories. The quartz is commonly coarse-grained and shows corrosion of altered plagioclase and alkali-feldspar. It also replaces some ferromagnesian minerals and hosts some fresh and altered biotite. The plagioclase is coarse-grained, highly altered and associated with inclusions of chloritized amphiboles and biotites. The amphibole and biotite sometimes show an association with fine-grained zircon and apatite.

IV.3.5. Conclusions

Lithologically and modally, the granitic units are coarse-grained monzogranites and syenogranites, porphyritic monzogranites and granodiorites, and medium-grained alkali-feldspar granite.

Petrographically, the pluton is generally rare in zircon, apatite and other accessory phases. The granitoids show different stages of myrmekitic texture development, well-developed rhombic-shaped amphibole and chloritization of biotite and amphibole. Although the minerals relationship was complicated, a suggestion for the order of mineral crystallization is given:

Amphibole, biotite and fine-grained muscovite may have crystallized first, followed by plagioclase, K-feldspar and later quartz which is post-dated by chlorite and muscovite.

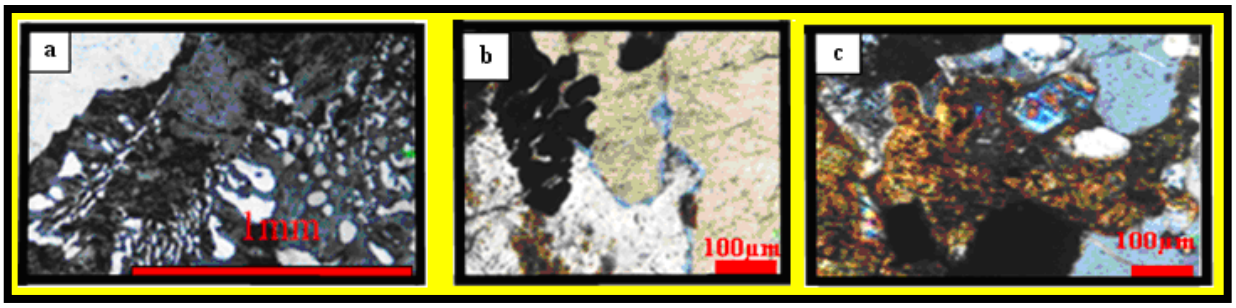

Figure 4.3: Petrographic features of the Jabal Khur Dukhan granitoids

a- Myrmekite formation along quartz-alkali-feldspar contact (alkali granite) X.P.L.

b- Quartz and alkali-feldspar corroded by 'globular' opaque minerals (granodiorite) P.P.L.

c- Fine-grained zircon enclosed in large altered alkali-feldspar (syenogranite) X.P.L.

IV.4. Petrography of the Jabal Al-Massah Complex

From the macroscopic, petrographic and modal analyses (Fig 3.9 and 4.4; Table.4.3), the Jabal Al-Massah granitoids are generally mesocratic, coarse-grained, whitish monzogranite, light grey granodiorite, reddish alkali-feldspar granite and porphyritic pinkish-red syenogranite.

The plagioclase is mostly altered and sometimes shows clear zoned and multiple (lamellar)-twinned crystals. The alkali-feldspar is dominated by perthitic textures (Fig. 4.6). Different development stages of (rim-like) myrmekites were noticed along some plagioclase crystal boundaries. The accessory phases are dominated by flaky biotite (mostly altered), which shows a clear association with globular opaque minerals. Muscovite (flaky or fan-shaped) is either associated with the biotite and the opaque minerals or found as inclusions in the larger, major components. Brown amphibole is present and together with fine-grained apatite and zircon is found as inclusions in the quartz and feldspar and associated with the opaque minerals. The alkali granites are characterized by the presence of coarse, simple-twinned perthite, while the porphyritic texture is the most notable feature of the syenogranite. The presence of fan-shaped muscovite and chloritized biotite characterizes the monzogranite and the granodiorite.

Table 4.3: Lithologies and mineralogy of the granitic rocks of the Jabal Al- Massah

Major Rock Units	Rock-Forming Minerals	Major Accessories	General Texture	Alteration	Sample Number
AG	Afs, qz & few plg	Bi (ox), ms, op & zr	Coarse-grained	Fresh	JM13
SG	afs, Plg & qz	Ms (chl & ox) & bi (chl), op ,ap & less hm	porphyritic	Fresh	JM16 &18
MG	Plg, afs & qz	Ms (chl & ox) & bi (chl), op ,ap & less hm	Coarse-grained	Fresh to slightly altered	JM7 &24
GD	Plg, afs & qz	Bi (fresh & chl), ms, chl, hm , ap & zr	Coarse-grained	Moderately to highly altered	JM4 &33

Explanation of terms: Qz-quartz, afs-alkali feldspar, plg-plagioclase, bi-biotite, ms-muscovite, chl-chlorite, ap-apatite, op-opaque minerals, zr-zircon, ox-oxidized, hm-hematite AG-alkali granite, SG-syenogranite, MG-monzogranite, GD-granodiorite.

IV.4.1. Alkali granite

This rock type is mainly composed of coarse-grained alkali-feldspar (commonly altered perthite) and quartz, very rare plagioclase and myrmekite. The accessories are dominated by fine-grained muscovite, opaque minerals and altered biotite.

The alkali-feldspar is light brown in colour, indicating the presence of hematite, possibly due to weathering or other alteration. It is perthitic and show simple twinning, and has been clearly corroded by, and enclosed in, some anhedral quartz crystals. In a few cases, small (<1mm) myrmekitic textures are traced along the edges of the altered alkali- feldspar. Fine-grained muscovite is mainly found as inclusions in the coarse-grained quartz. The opaque minerals and the oxidized biotite show an association with zircon and with a high relief creamy coloured mineral.

IV.4.2. Syenogranite

This rock is mainly composed of perthitic alkali-feldspar, euhedral zoned plagioclase, two phases of quartz (coarse and fine-grained) and rare myrmekites. The accessories are dominated by slightly altered biotite, apatite, muscovite and some opaque minerals.

Two phases of quartz are found. The quartz phenocrysts corrode the edges of the subhedral plagioclases and rarely host some fine-grained muscovite and remnants of alkali-feldspars. The fine-grained quartz phase is generally enclosed by the coarse-grained ones. Fine-grained myrmekite mainly occurs along some plagioclase crystal boundaries. The alkali-feldspar hosts some euhedral slightly altered zoned plagioclase and is partially corroded by it. The platy biotite is rich in rod-like apatite inclusions and is associated with opaque minerals. Muscovite is mostly found as inclusions in the major mineral components. Both biotite and muscovite are generally corroded by the fine-grained (<1mm) quartz.

IV.4.3. Monzogranite

The rock is mainly composed of multiple-twinned (lamellar twinning) plagioclase, alkali-feldspar (perthite, less anti-perthite and rare microcline-perthite), quartz and myrmekite. The accessories are dominated by platy biotite (sometimes chloritized), rod-like apatite, opaque minerals and muscovite (sometimes fan-shaped).

The quartz shows slight corrosion by the alkali-feldspar, slightly altered multiple-twinned plagioclase and flaky biotite. The alkali-feldspar edges are corroded by plagioclase and show some inclusions of fan-shaped muscovite and fine-grained subhedral plagioclase. The rod-like apatite is mostly found as inclusions in the large quartz grains and also shows some association with chloritized biotite. Some ‘globules’ of opaque minerals are found in association with finer muscovite and much less altered biotite. They show corrosion of the major mineral components.

IV.4.4. Granodiorite

This rock is mainly composed of altered plagioclase (sometimes showing clear zoning), quartz, alkali feldspar (poorly developed perthite) and much less myrmekite. The accessories are mainly brown and green, altered, flaky biotite, flaky and fan-shaped

muscovite, scattered opaque minerals, much less brown amphibole, fined-grained rod-like apatite and zircon.

The alkali-feldspar hosts some inclusions of muscovite and altered plagioclase and is rarely altered. The plagioclase also hosts some fine-grained muscovite and its peripheries are corroded by the alkali-feldspar. The altered plagioclase and alkali-feldspar are both invaded and corroded to some extent by coarse-grained quartz. Fine-grained myrmekite is mainly present along some feldspar crystal boundaries. Rare opaque minerals show corrosion of the main mineral components and show an association with chlorite, altered biotite and muscovite. The muscovite is mostly concentrated in the large, altered, plagioclase and alkali-feldspar crystals. Rod-like apatite and fined-grained zircon are found either as inclusions in the major mineral components or associated with the biotite. The opaque minerals commonly show an association with the amphibole and biotite and appear to replace all the other major components.

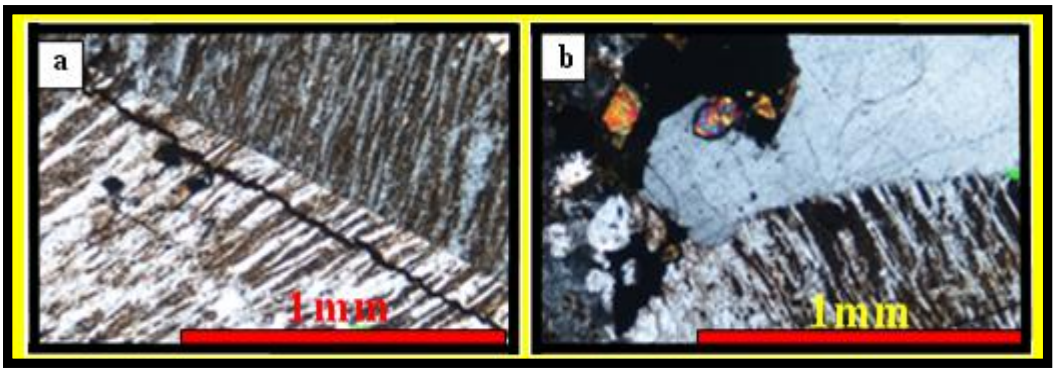

Figure 4.4: Some petrographic features of the Jabal Al-Massah granitic rocks

a- Large simple-twinned perthite (syenogranite) X.P.L.
b- General view of the relationship between quartz, alkali-feldspar, opaque minerals and zircon (alkali granite) X.P.L.

IV.4.5.Conclusions

Lithologically, the granitoids of the Jabal Al-Massah complex are represented by coarse-grained monzogranite, granodiorite and alkali-feldspar granite, and porphyritic pinkish-red syenogranite.

Petrographically, the granitoids of the Jabal Al-Massah complex are characterized by the absence or the scarcity of amphibole (0 to 1.1%) and zircon, the presence of well-developed perthitic and anti-perthitic texture (sometimes not clear due to alteration) and the existence of fine-grained myrmekite along plagioclase crystal boundaries. Determining the order of the mineral formation is difficult as this is not consistent in all granitic types, but the order of mineral formation could be as follows: Minerals like amphibole, biotite and muscovite (platy) crystallized, followed by plagioclase, quartz and muscovite (fan-shaped).

IV.5.Petrography of the Jabal Raydan Pluton

From the macroscopic, petrographic and modal analyses of Jabal Raydan granitoids (Fig.3.12 and 4.5; Table.4.4), it appears that thses rocks are mainly composed of coarse and medium-grained (>5mm and 1 to 5mm), white monzogranite and coarse to fine-grained (>5mm and < 1mm), reddish alkali-feldspar granite and pinkish syenogranite.

The alkali feldspar is generally composed of micro-perthite and microcline perthite, with minor fine granophyric texture. The plagioclase (sometimes zoned) shows a compositional range from intermediate to sodic. The accessories are represented by blue-green amphibole ± biotite, zircon, titanite, monazite, apatite, allanite, muscovite, chlorite and opaque minerals (e.g. ilmenite, hematite and magnetite).

Table 4.4: Lithologies and mineralogy of the main granite units of the Jabal Raydan Complex

Major Rock Units	Rock-Forming Minerals	Major Accessories	General Texture	Alteration	Sample Number
AG to SG	Afs, qz & less plg	Am, bi, chl, op & few ms	Coarse, medium & fine-grained	Fresh to slightly altered	JR3C-9-19 & 20
AG to MG	Plg (ser), afs & qz	Am, bi (chl), op, ms, zr, tit, mo (?), fl & ap	Coarse & Medium-grained	Fresh to slightly altered	JR3E-12 & 13

Explanation of terms: Qz-quartz, afs-alkali feldspar, plg-plagioclase, am-amphibole, bi-biotite, ms-muscovite, chl-chlorite, ap-apatite, op-opaque minerals, zr-zircon, tit-titanite, fl-fluorite, mo-monazite, AFG-alkali granite, SG-syenogranite, MG-monzogranite.

IV.5.1. Alkali to syenogranite

This rock type is basically composed of different sizes (fine to coarse-grained) and forms of alkali-feldspar (mottled, vein-like, patch-like and microcline perthite), quartz and plagioclase (rarely zoned) and shows a variable grain size. Accessories are not common, but are dominated by opaque minerals, biotite (slightly altered), chlorite, muscovite, amphibole and other (as yet) unidentified phases.

Slightly altered alkali feldspar is the most abundant mineral in the rock. It hosts muscovite and other unknown, fine-grained minerals, is corroded by quartz but sometimes shows corrosion of the plagioclase and commonly is accompanied by some opaque minerals. The plagioclase is corroded by most of the mineral present. Quartz occurs in variable (fine to coarse-grained) sizes. It replaces alkali feldspar and plagioclase and encloses them. Other inclusions of opaque minerals and fine mineral phases of muscovite and undistinguished minerals are also hosted in the larger quartz grains. Opaque minerals show a clear association with the ferromagnesian minerals (e.g. biotite and chlorite) and less commonly the alkali-feldspars and are sometimes enclosed in some coarse-grained quartz. Biotite occurs in two different colours (green and brown). The two phases are affected to some extent by alteration. They are corroded by opaque minerals and chlorite. Some fine-grained muscovite and unidentified minerals occur as inclusions in the three most dominant minerals in the rock. Green amphibole is located along the edges of the alkali feldspar and corrodes it.

IV.5.2. Alkali to monzogranite

This rock is coarse (up to 1cm crystal size) to medium-grained and is composed of plagioclase (commonly altered and zoned), alkali-feldspar (microcline perthite, micro-perthite and less vein-like and mottled or spotted-like) and quartz. The accessories are dominated by biotite (slightly altered), amphibole, rarer chlorite, muscovite, opaque minerals, titanite, ziron, apatite and other (unidentified) phases.

The slightly to highly altered plagioclase encloses most of the accessories and is commonly corroded by quartz. Alkali feldspar corrodes plagioclase and both of them are corroded by quartz. The boundaries between the quartz and feldspar sometimes exhibit micrographic texture. Some of the finer grained perthites are enclosed in the large plagioclase grains. K-feldspar hosts fewer accessories than the plagioclase does,

but it is also affected by them (the corrosion is obvious along the alkali feldspar peripheries). Coarse-grained quartz is common. Sometimes it shows clear wavy extinction and is partially cracked, with the fractures filled with muscovite. Comparing with the other studied granitic rocks this rock seems to host more accessories. Amphibole and biotite commonly occur together, but are also found distributed and enclosed in the major minerals. They also enclose finer-grained minerals (acicular apatite, zircon and the unidentified minerals). Some of the amphiboles show blue pleochrism (indicating possible alkali varieties) and other, green amphiboles show slight replacement to either red biotite or opaque minerals. The altered biotite shows a clear association with opaque minerals, which replace most of the mineral present. In a few cases, the zircon shows an association with the ferromagnesian (amphibole and biotite) and opaque minerals. Unidentified phases show a distinct association with biotite, chlorite and opaque minerals. Fine-grained, acicular apatite and muscovite are commonly hosted in the large quartz crystals.

IV.5.3.Conclusions

Lithologically, the Jabal Raydan pluton is mainly composed of white, medium (1 to 5mm) and coarse-grained (> 5mm) alkali to monzogranite and less reddish-pinkish fine-, medium and coarse-grained alkali to syenogranite.

Petrographically, the white granite is the most interesting rock unit as it relatively contains the largest amount of accessories of potential economic significance, such as allanite, zircon and monazite. These are a potential source of some important ‘trace’ elements (see later). Although the mineral relationships are complicated, a suggestion for the order of mineral crystallization is given: Amphibole and biotite may have crystallized first, followed by titanite (well-developed), plagioclase, zircon and later quartz which is post-dated by chlorite and muscovite.

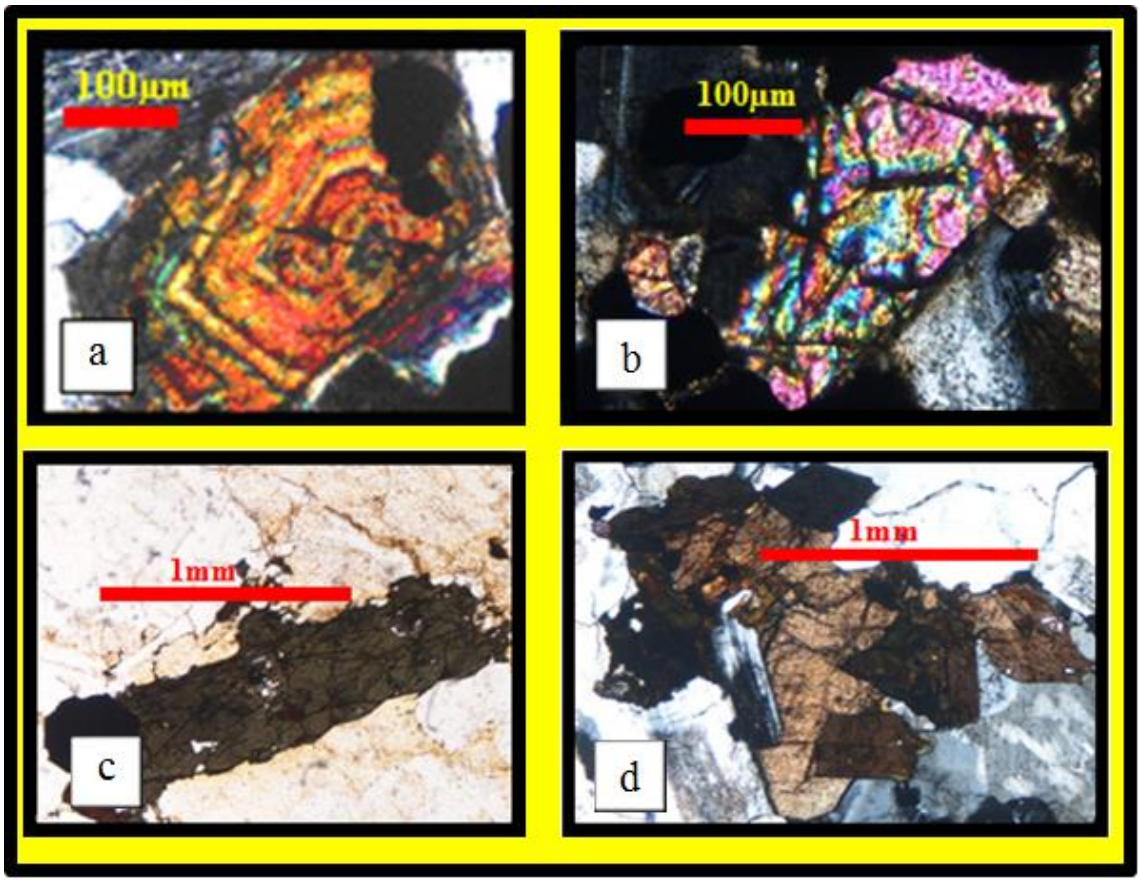

Figure 4.5: Characteristic petrographic features of the Jabal Raydan granitic rocks

a- Oscillatory, concentric zoning in zircon (alkali to monzogranite) X.P.L.

b- Association of monazite (?) with opaque minerals (alkali to monzogranite) X.P.L.

c- General relationship between large elongated brown amphibole, opaque minerals, and feldspar (alkali to syenogranite) X.P.L.

d- Brownish allanite associated with feldspar and amphibole and corroded by quartz (alkali to syenogranite) X.P.L.

IV.6. Petrography of the Jabal az Zuhd Pluton

The macroscopic, petrographic and modal analyses of the Jabal Al-Zuhd pluton (Figs. 3.15 and 4.6; Table.4.5), show that the lithology of this pluton is basically characterized by coarse-grained, grey and pink alkali granite and porphyritic syenogranite.

Feldspar is mainly striped perthite, with minor microcline perthite and plagioclase. Accessory minerals are predominantly blue-green amphibole, brown-green biotite, muscovite, zircon, monazite, apatite and opaque minerals.

Table 4.5: Lithology and mineralogy of the Jabal az Zuhd Pluton

Major Rock Units	Rock-Forming Minerals	Major Accessories	General Texture	Alteration	Sample Number
AG	Afs, qz & much less plg	Am (ox) , bi, op & few ms	Coarse-grained	Fresh to slightly altered	JZ2-5-6-8-10 & 13
SG	Afs, qz & less plg	Am, bi, ms, chl, tit, zr & op	Porphyritic and medium-grained	Slightly to moderately altered	JZ1A

Explanation of terms: Qz-quartz, afs-alkali feldspar, plg-plagioclase, am (ox)-oxidized amphibole, bi-biotite, ms-muscovite, chl-chlorite, ap-apatite, op-opaque minerals, zr-zircon, tit-titanite.

IV.6.1. Alkali granite

This rock is mainly composed of coarse (up to 1cm), alkali feldspar, which is mostly perthite, showing distinct vein-like and spotted types and simple-twinning, and hosting some prismatic biotite. Quartz and lesser amounts of plagioclase are also present. The accessories are represented by medium to coarse-grained ferromagnesian minerals (amphibole and biotite) and much less opaque minerals, chlorite, muscovite, hematite (?), allanite, zircon and other, fine-grained, unknown mineral phases.

The relationships between the feldspars and the other minerals are similar to those of the syenogranites. The majority of the quartz is intergranular (as quartz veinlets) and invades most of the feldspars. Brown and bluish amphibole and green and brown biotite are the predominant accessory phases. They are slightly to highly altered and show an association with each other and with the much less abundant opaque minerals, especially radial rutile. The accessories such as apatite and other unknown phases occure either as fine grained inclusions in coarse-grained feldspar or quartz crystals, or associated with the ferromagnesian minerals.

IV.6.2. Syenogranite

This rock is mainly composed of alkali-feldspar (perthite and microcline perthite), quartz and some (altered) plagioclase. Accessories are represented by green biotite (mostly altered) muscovite, chlorite, rhombic titanite, zircon and opaque minerals.

Variable sizes (coarse to fine-grained) of alkali-feldspars occur, but fine-grained feldspar is the most dominant and represents a large part of the groundmass. Lesser amounts of coarse-grained perthite and microcline-perthite crystals contain some inclusions of quartz, altered plagioclase and chlorite. Plagioclase is mainly euhedral and shows lamellar twinning. It is corroded by quartz, K-feldspar and chlorite. Quartz of variable size affects most of the minerals present in the section. The coarse-grained quartz grains host some K-feldspar and other accessories such as titanite and sometimes have an arrangement of fine grained muscovites along their grain boundaries. The fine-grained quartz forms the groundmass of the rock.

Altered biotit replaces most of the other minerals. Fine-grained muscovite is found either enclosed in other larger crystals (e.g. quartz, plagioclase and K-feldspar) or rarely corroding the rims of the quartz. Rhombic-shaped titanite is common as discrete crystals and also as inclusions in quartz or feldspar. Some fine-grained zircons were also noted. The opaque minerals are fine to medium-grained and rounded to subhedral in form and show a distinct association with the chlorite.

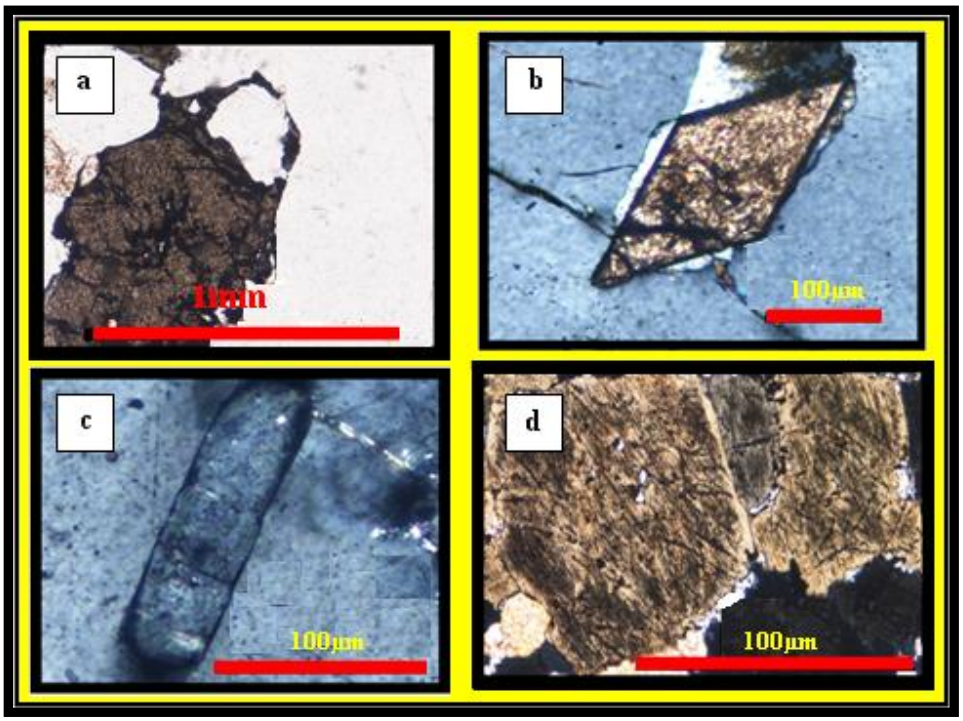

Figure 4.6: Petrographic features of the accessory minerals in the Jabal az Zuhd granitic rocks

a- General view of brown allanite associated with perthite and ferromagnesian minerals (alkali granite) P.P.L.

b- Rhombic-shaped titanite enclosed in quartz (porphyritic syenogranite) X.P.L.

c- Rod-like apatite enclosed in quartz (porphyritic syenogranite) X.P.L.

d- General view of brown and dark blue amphiboles (alkali granite) X.P.L.

IV.6.3. Conclusions

Lithologically, petrographically and modally, three different granitic units have been recognized in the field: the coarse-grained alkali-granite (comprising most of the pluton), the medium-grained syenogranite and the porphyritic micro-syenogranite. The last one is the most significant as it hosts most of the accessories, such as titanite, apatite and allanite. The pluton shows a general enrichment (up to 57%) of alkali-feldspar (striped perthite) and alkali ferromagnesian (up to 9.5%) minerals (green and brown amphibole and biotite).

Although the mineral relationships are complicated, a few clear observations suggest the order of mineral formation is as follows:

Amphibole and biotite first, then followed by titanite, plagioclase, zircon and later quartz which is post-dated by chlorite and muscovite.

IV.7. The affect of alteration in the studied plutons

Some of the studied rocks have been subjected to variable degrees of secondary alteration. Some evidence for separate thermal and regional metamorphic events (deformation and re-crystallization) has also been found (Table. 4.6). Various types of alteration have affected different minerals in different rock types (Fig.4.7; Table. 4.7). Some of the alkali-feldspar granites of the Jabal Thalabah pluton are highly altered. The majority of the altered rocks are rich in fluid inclusions (mostly multi-phase and rich in CO_2). Two-phases of secondary (vapor and liquid) fluid inclusions are found precipitated along trails and planes in the quartz. In some cases the fluids are composed of aqueous vapor and liquid and in others they show aqueous-carbonic characteristics. Most of these inclusions were too small (<10μm) to be studied in further detail.

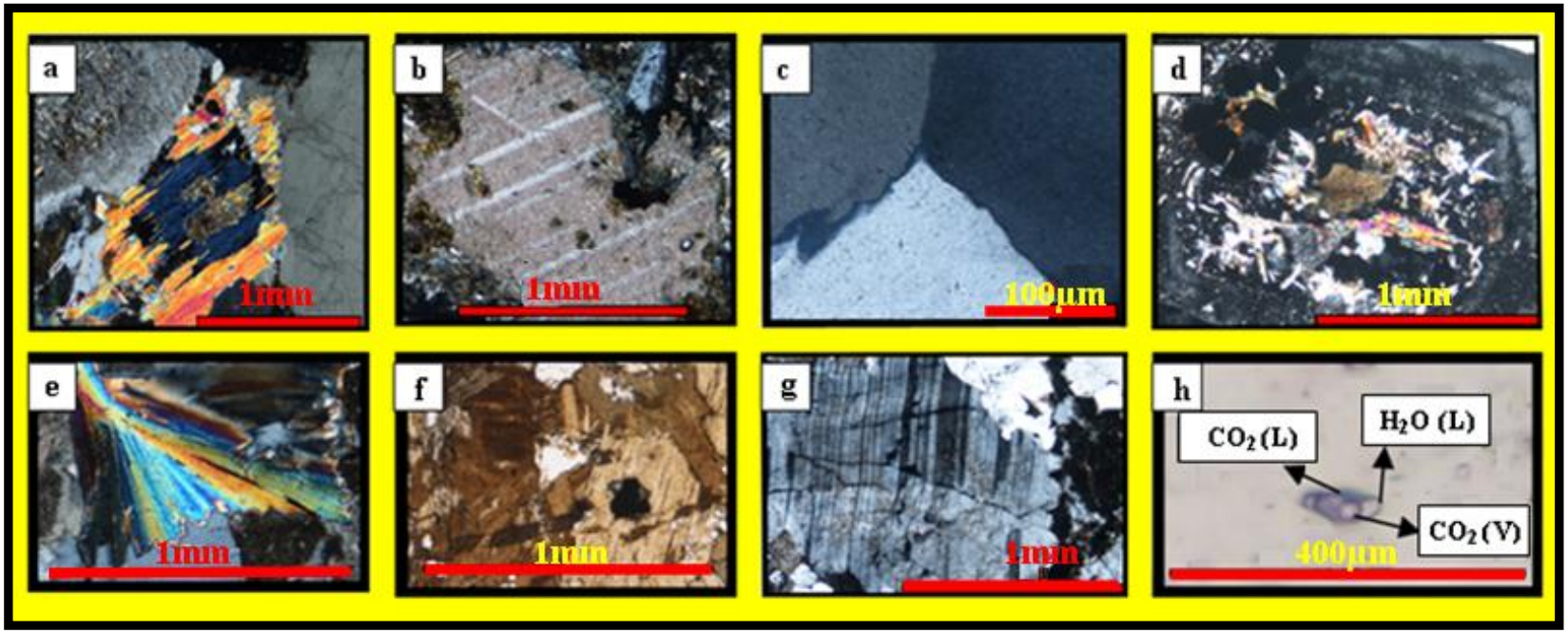

Figure 4.7: The affects of alteration in the studied rocks

a- Chloritized and oxidized muscovite in the monzogranite of Jabal Al-Massah, X.P.L.

b- Calcite in the carbonatized gabbro of the gabbroic enclave in Jabal Thalabah, X.P.L.

c- Annealing texture in quartz, possibly indicating thermal affects in the syenogranite of Jabal az Zuhd, X.P.L.

d- Large zoned-plagioclase, internally replaced by muscovite and opaque minerals in the granodiorite of Jabal Thalabah X.P.L.

e- Fan-shaped muscovite in the granodiorite of Jabal Al-Massah, X.P.L.

f- Assemblages of biotite characteristic of the hybrid rocks of Jabal Thalabah, X.P.L

g- Deformed plagioclase corroding alkali-feldspar and itself corroded by quartz in the granodiorites of Jabal Khur Dukhan, X.P.L.

h- Multi-phase aqueous-carbonic fluid inclusion in quartz, in the alkali granite of Jabal Thalabah, P.P.L.

Table 4.6: Visible affects of deformation on the studied granitoids

Name of Pluton	Indication of deformation	Rock name
Jabal Thalabah	Annealing texture	Monzogranite
Jabal Khur Dukhan	Kinked plagioclase	Syeno- and alkali granite
Jabal Raydan	Kinked plagioclase	Monzogranite
Jabal Az Zuhd	Annealing texture	Alkali granite

Three different types of alteration have been recorded:

1) Early-stage alteration. There is abundant evidence of mineral replacement by quartz and feldspar. This was most likely caused by high temperature fluids carrying Si, Na and K, which mainly interacted with the feldspars in the granitic rocks. Such processes may have changed the feldspar ratios in some of the samples plotted in the QAP ternary diagram, consequently affecting the rock classification based on the modal composition and confusing any possible identification of linear petrographic trends. These fluids are likely to have been magmatic water.

2) The second type of alteration refers to lower temperature hydrothermal fluids that mainly alter plagioclase (mostly sericitization) and biotite (chloritization), and caused some secondary minerals to form. These fluids are likely to contain a significant meteoric water component.

Fluid inclusions suggest that some of these fluids could have been CO_2-rich

3) The third type of alteration refers to weathering (externally-derived meteoric-groundwater dominated fluid) that oxidized the iron in the rocks. Such alteration is exemplified by hematized biotite and the altered, brownish, alkali-feldspars and was clearly noticed in the alkali-feldspars of the Jabal Al-Massah and Jabal Khur Dukhan plutons.

Table 4.7: The affect of alteration on the studied granitoids

Name of Pluton	Type of alteration	Evidence for alteration
Jabal Thalabah	Chloritization	Chloritized plagioclase and amphibole in AG, chloritized muscovite in GD and chloritized biotite in all rock types except AG
	Carbonitization	Calcite in the enclosed gabbro
	Sericitization	Sericitized plagioclase in all rock types
Jabal Khur Dukhan	Chloritization	Chloritized amphibole in SG and chloritized biotite in all rock types except AG
	Sericitization	Sericitized plagioclase in all rock types
	Weathering	Hematitized biotite of AG and (Fe) oxidized plagioclase in SG
Jabal Al-Massah	Chloritization	Chloritized biotite in all rock types except AG
	Sericitization	Sericitized plagioclase in all rock types
	Weathering	(Fe) Oxidized perthite in AG
Jabal Raydan	Chloritization	Chloritized biotite in all rock types except AG
	Sericitization	Sericitized plagioclase in all rock types
	Weathering	Hematitized biotite in SG
Jabal Az Zuhd	Chloritization	Chloritized biotite in SG
	Sericitization	Sericitized plagioclase in SG
	Weathering	Hematitized biotite in AG and (Fe) oxidized alkali amphibole in AG

Explanation of terms: AG-alkali granite, SG-syenogranite, GD-granodiorite

IV.8. Discussion and conclusions

Table 4.8 summarizes the main petrographic and mineralogical differences and similarities between the studied plutons.

Table 4.8: Petrographic and mineralogical characteristics of the studied plutons

Pluton	Lithology	Accessories	Modal Composition	Texture	Remarks
TH	Coarse-medium-grained, whitish grey GD & MG and buff pinkish SG & AG	Am & Bi, ms, am (chl), ap, tit, zr, op	Selected rocks plot in the GD & SG fields (no correlation may indicate two different magma sources - the GD shows a linear/fractionation trend but the SG does not)	Dominated by perthitic & less myrmekitic textures	Chilled margins. Hybrid rocks. Ferro-magnesian minerals abundant in hybrid rocks.
KD	Coarse-medium-grained, porphyritic, light grey GD & MG and pinkish to reddish SG & AFG	Am & bi (chl), op, zr, ap & hm	Selected rocks plot in the GD, MG, SG & AFG fields, and show a linear/fractionation trend (possibly one magma source?)	Show well-developed perthitic & less myrmekitic textures	Scarcity of amphibole, zircon and apatite.
JM	Coarse-grained whitish MG, light grey GD and reddish AFG, and porphyritic pinkish-reddish SG	Bi , ms, chl, op, ap, zr, mo (?) & hm	Selected rocks plot in the GD, MG & AFG fields, and do not show clear linear trend, but could possibly have one parental magma source	Show well-developed perthitic & less myrmekitic textures	Scarcity of zircon & amphibole.
JR	Coarse & medium-grained white MG and reddish AFG and less porphyritic pinkish SG	Am, bi (chl), op, ms, zr, tit, mo (?) fl & ap	Selected rocks plot in the GD, MG, SG & AFG fields, and show a possible linear/fractionation trend and possibly one magma source	Show some perthitic and much myrmekitic textures	Quite rich in accessories (presence of fl), and possible presence of alkali amphibole.
JZ	Coarse-grained, gray and pink AFG, and some porphyritic and medium-grained SG	Am (mostly ox), bi, op & some ms, chl, ap, zr, mo (?) & tit	Selected rocks only plot in the SG & AFG fields, and do not show clear linear trend	Dominated by perthitc textures	Dark blue alkali am (riebeckite or arvfedsonite), radial op (rutile?). Poor plg

Explanation of terms: Qz-quartz, afs-alkali feldspar, plg-plagioclase, kfs-k-feldspar, am-amphibole, bi-biotite, ms-muscovite, chl-chlorite, ap-apatite, op-opaque minerals, zr-zircon, tit-titanite, hm-hematite, fl-fluorite, mo-monazite, AFG-alkali-feldspar granite, SG-syenogranite, MG-monzogranite. Explanation of abbreviations: TH, Jabal Thalabah, KD, Jabal Khur Dukhan, JM, Jabal Raydan, JZ, Jabal az Zuhd.

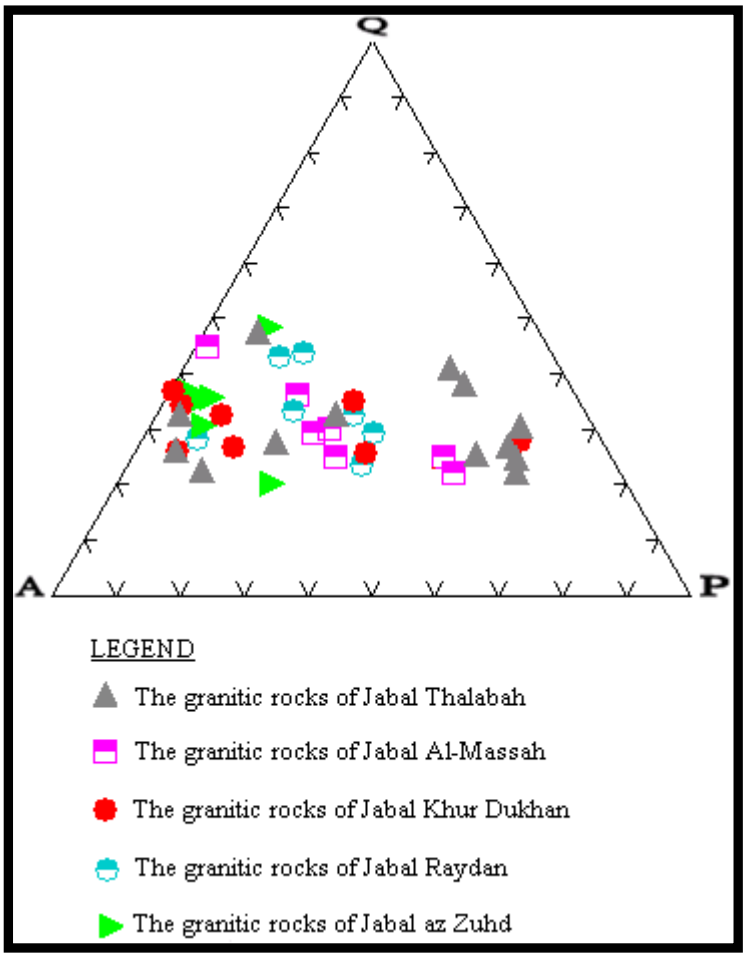

Figure 4.8: The modal composition of all of the studied granitoids

Overall, the igneous rocks show a variable compositional range within the granite field (from granodiorite to alkali-feldspar granite) and show a variable grain-size (coarse-medium and porphyritic texture). Additionally, the Jabal Thalabah pluton is noteworthy because it shows unique hybrid and chilled margin rocks.

Overall, these plutons exhibit a broad linear petrographic trend from the plagioclase apex towards the quartz-alkali feldspar tie line (Fig.4.8). This could represent a fractionation trend in which plagioclase feldspar has crystallized and been removed

from the magma; this would therefore indicate a similar parental magma source (tonalite?) for these suites. It is of course also possible that a linear trend is due to mixing between two end-members. Variations away from a suggested line of fractionation could also be derived from the affect of other processes, such as assimilation, magma mixing and alteration. There are some 'gaps'in these linear trends (e.g. the Jabal Thalabah suite) or no trend at all (Jabal az Zuhd) and it is not clear whether this is because these lithologies occur but have not been sampled or that they do not occur and thus these suites have a separate source. Chemical analysis (see later) should help to resolve some of these issues.

Mineralogically, although the major phases present are generally similar, some subtle differences (especially in accessory mineral contents) were noticed between the studied plutons. For instance, the Jabal Khur Dukhan and Jabal Al-Massah alkali granites contain less (up to 1.1%) amphibole than that of the Jabal Thalabah (.up to 2%) In addition, the Jabal Jabal Raydan and the Jabal az Zuhd plutons have amphiboles with different colours (e.g. dark blue) from those of the other plutons, which indicates a different (alkali?) amphibole composition.

Subsolidus textures (particularly perthites and myrmekites) are quite common in several of these plutons. The well-developed brownish-red perthite distinguish the Jabal Al-Massah and Jabal Khur Dukhan plutons from the others. The myrmekite texture of the Jabal Thalabah pluton is almost restricted to the altered alkali-feldspars but is less abundant than in the Jabal Raydan pluton, which dominates and characterizes its alkali-feldspar granites.

IV.8.1. Comparisons

Lithologically similar granitoids have been found elsewhere in the Arabian Shield (AS), and Stoeser and Elliott (1980) presented a map (Fig. 4.9) showing all the Neoproterozoic alkali granites in the AS. The Jabal Raydan, Jabal Al-Massah, and Jabal az Zuhd plutons are included in this map as they are assumed to be alkali plutons as classified (based on mineralogical and chemical studies) by Harris and Marriner (1980), Radain (1980) and Stoeser and Elliott (1980).

According to the map, some examples of similar granitoids to those of Jabal Rydan, Jabal Al-Massah, and Jabal az Zuhd are also found in:

1) The Midyan terrain: Jabal Murab, Jabal Dabbagh, Jabal Shar, Jabal Nurman, Jabal Qaraqir and Jaydah.
2) The Al-Hijaz terrain: Jabal Radwa, Jabal Subh and Jabal Sa`id.
3) The Asir terrain: Kwar and Najran.
4) The Afif terrain: Jabal Bidayah and Jabal as Silsilah.
5) The Ha`il terrain: Jabal Aja, Jabal Ar Rumman and Samirah.

Thus, for instance, the modal composition of the Ratamah specialized granite (in the Midyan terrain and studied by Douch in 1986) and that of the Jabal Umm Al-Suqian albitized apogranite (located in southern Najd region and studied by Bokhari *et al.* in 1986) are quite similar to the modal compositions of Jabal az Zuhd. However, there is a slight difference between their lithologies as the Ratamah granite shows more varieties of alkali granites and Jabal Umm Al-Suqian is dominated by microgranite. The petrography of the latter granitoids is almost the same as those of Jabal Sa`id (located in the Hijaz region and studied by Hackett, 1986), the Jabal Silsilah tin prospect (located in the Najd region or more specifically in Hail terrain and studied by Bary in 1986) and Jabal Hamrah (located in the Hijaz region and studied by Jackson and Douch in 1986). However Jabal Hamrah is more alkaline which may indicate a similar magma source but a more evolved magma. The lithology and the modal composition of the Akash granite (located in the Hail terrain and studied by Kellogg and Smith in 1986) and the Jabalat alkali-feldspar granite (located in Asir terrain and studied by Al-Tayyar *et al.* in 1986) also resemble the Jabal Raydan pluton in its modal composition, but show a slightly different lithology. Furthermore, the Dabbagh complex (located in the north of the shield and studied by Harris, 1985, and Davies and Grainger, 1982) shows almost identical lithology and petrography to the Jabal Raydan pluton, while Jabal Al-Hassir (located in the middle of the Asir terrain and studied by Stoeser and Elliott, 1980) shows a very similar lithology to that of the Jabal Thalabah pluton. The modal composition of the Sidarah monzogranite (from the Hijaz terrain and studied by Jackson in 1986) is quite similar to that of the Jabal Al-Massah complex.

On a global scale, some granitic intrusions exhibit some lithological and mineralogical similarities to the studied intrusions. For example, the Late-stage, Pan-African, alkali granites intrusions at Wadi Lithi and Wadi Seih in Sinai contain the accessory minerals allanite, zircon and various opaque phasess, and alteration to secondary chlorite and sericite (Ali *et al*., 2009) and the medium- to coarse-grained, subduction-related A-type alkali-feldspar granite of Daxiangling (China) that shows common perthitic texture, Fe–Ti oxides and titanite accessories (Zhao *et al*., 2008). The Homrit Waggat Complex from Egypt (A-type post-collisional intrusion studied by Hassanen, 1997) shows almost identical granitic units to those of the Al-Massah and Jabal Khur Dukhan plutons. The syn- to post-collisional Singo granite (Uganda) consists of coarse-medium grained biotite granites which plot in the monzogranite and syenogranite fields. Its accessories are zircon, apatite, titanite, monazite, xenotime and opaque phases, and its secondaries are chlorite, epidote and fluorite (Nagudi *et al*., 2003). The late Precambrian Hasan Robat Granite (Iran) is composed of syenogranite, alkali-feldspar granite, and minor monzogranite with perthitic, rapakivi textures (Esfahani *et al*. 2010). Both of these occurrences also appear to contain many similar characteristics to the granites studied here.

All the above mentioned examples indicate that many plutons from the Arabian Shield and other parts of the world show a similar lithology and mineralogy to the studied granites. However, in terms of lithology and petrography, similar or identical felsic intrusives to those in the studied areas are not particularly abundant on a global scale. Most granitic intrusives do not exhibit such a large variability in their lithology and mostly are made up of only one or two different granitic types. Good examples of such igneous plutons with a limited range of composition are presented by the late-Variscan Cornubian Land's End granite in Cornwall that is dominated by biotite granite (Muller *et al*., 2006), the Sierra Nevada batholith of California that mostly consists of either quartz monzonite or granodiorite (Barbarin, 2005) and the long-lived granite in the western Irish Caledonides which is mostly composed of granite and granodiorite (Feely *et al*., 2010).

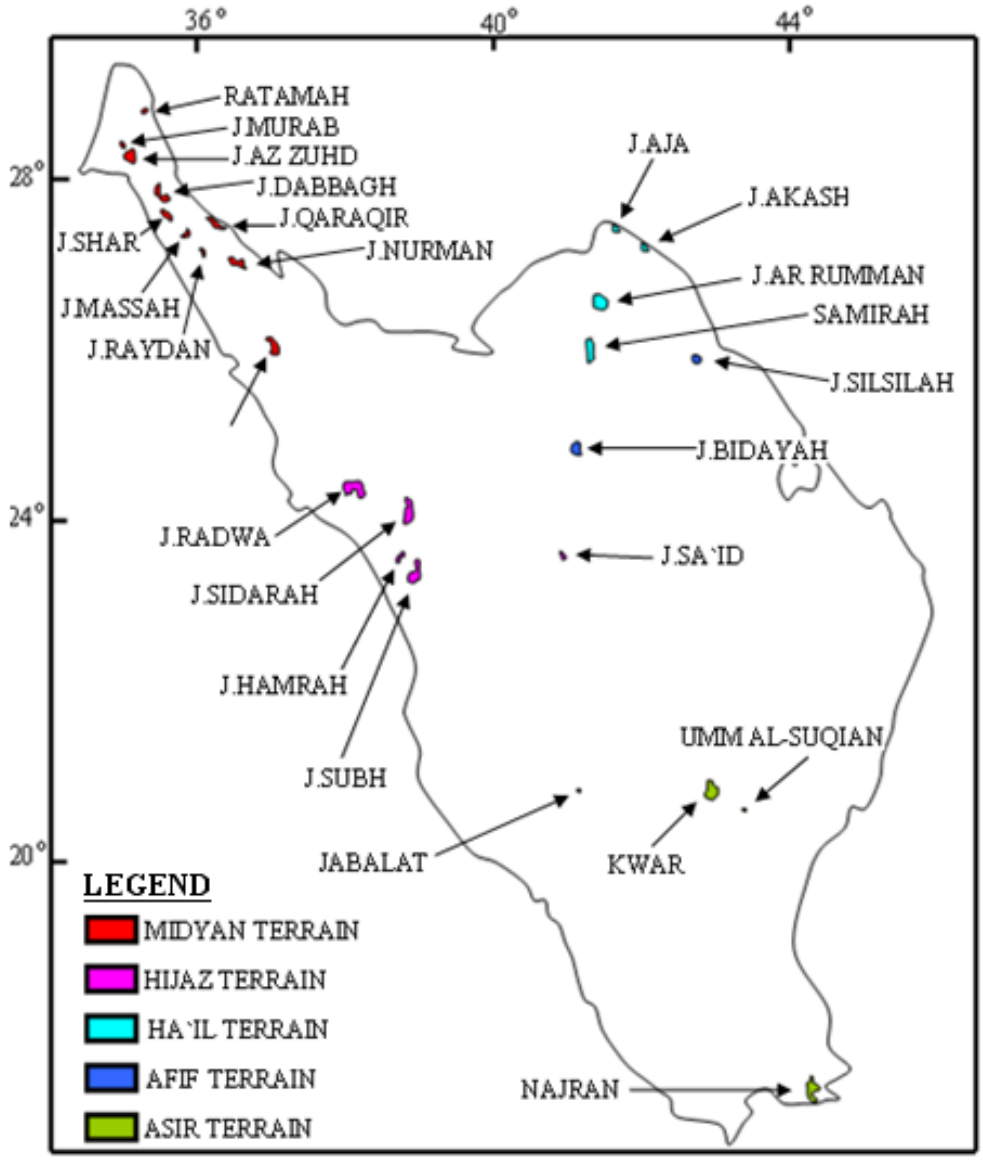

Figure 4.9: Locations of some Arabian Shield alkali granites (after Stoeser and Elliott, 1980).

In fact, most of the examples of similar granites to those studied here were found in the Arabian and the Nubian shields and these are mostly Precambrian anorogenic plutons. The more common, orogenic plutons (e.g. Land's End granite in Cornwall) are mainly characterized by a limited range of granitic varieties. This indicates that the studied plutons have experienced a more complex evolution process than that which produced more common orogenic plutons.

IV.8.2. Feldspar textures

Subsolidus feldspar textures (e.g. perthite, myrmekite, rapakivi, graphic intergrowths) are particularly common in some of the studied rocks so it is important to know how they formed and what information they can provide as regards the genesis and evolution of the granites.

Mineralogical, chemical and experimental studies over several decades have demonstrated that post-solidification exsolution textures result from deuteric/low temperature (<400°C) processes, after the cessation of crystallization and the influx into the rock mass of hydrothermal fluids (Vernon, 2004). The presence of post-magmatic hydrothermal fluids has been suggested as a cause of coarsening of textures in several studies (e.g. the A-type granite of Suzhou, eastern China, Barbarin and Stephens, 2001, and the alkali feldspars of the Ballachulish igneous complex in Scotland, Deer *et al.*, 2001).

The shape, distribution and types of perthites are important indicators of the rock evolution (Fig. 4.10). In particular they can provide important information about the stages of development of the igneous pluton (Figure 4.11) and their rate of cooling (Figure 4.12, Putnis and McConnell, 1980).
According to Smith (1974), perthite can be developed mainly by three processes:

1- Exsolution (intra-crystalline replacement)
2- Replacement (change of the bulk composition of the grain)
3- Simultaneous crystallization

Replacement as a process of formation for perthites was supported by Deer *et al*., 2001). According to Sasaki *et al*. (2003), perthitic texture is a re-crystallization texture which develops when a high-temperature granite is emplaced at a shallow depth and cools to 410-500^{o}C. Its presence may indicate fluid-rock interaction (Liu, 2002). Flame perthite can also be used as an indicator of the palaeo-stress direction because flame growth is controlled by the imposed differential stress and not by strain in the host rock (Pryer and Robin, 1996). Furthermore, the presence of flame perthite and the development of coarse lamellae may characterize the less evolved part of the pluton as found in the high level poly-phase granite of southwestern Newfoundland (Deer *et al*., 2001).

Smith (1974) stated that exsolution is the most common process responsible for the formation of myrmekite, but it can be also subjected to partial or total re-crystallization or metsomatization during its development. Yuguchi and Nishiyama (2008) have suggested that myrmekitic texture forms by an exsolution or unmixing process, as a sub-solidus reaction during the deuteric stage, together with other sub-solidus textures. Myrmekite texture may also indicate a deformational event, as the myrmekite lobes are often seen to pass into and occupy areas of polygonal re-crystallized plagioclase (Vernon, 2004). Such metamorphic events have been recorded during the formation of mylonites along the Hatagawa Shear Zone of NE Japan, where myrmekite has started to replace K-feldspar (deformation-induced replacement); with more replacement, the deformation was more enhanced (Tsurumi *et al*., 2003). However, according to Deer *et al*. (2001), myrmekites of un-deformed porphyritic felsic rocks can be distinguished from those of deformed ones, as they show different morphologies and spatial distributions within their crystals. Furthermore, in the un-deformed felsic rocks, the alkali-feldspar may be subject to some strain-energy at the boundaries of semi-coherent lamellae of exsolved albite and deformation twins (Vernon, 2004). With the un-deformed rocks, the margin between the alkali-feldspar and the plagioclase is relatively straight and runs sub-parallel to the myrmekite-free edge (Deer *et al*., 2001), similar to most of the myrmekites observed in the studied rocks. The randomly oriented lamellae of albite noticed in graphic and myrmekite textures are basically related to a rapid cooling process (Vernon, 2004). So, the presence of more ordered albite lamellae indicates a slower rate of cooling. The existence of isolated albite lozenges indicates a further coarsening process that breaks up the zig-zag albite lamealle and causes lozenge shapes to be present (Deer *et al*., 2001). Regarding graphic texture, Vernon (2004), stated that the rapid simultaneous crystallization of alkali feldspar and quartz is the main process causing the development of many granophyric textures.

Rapakivi granites can be developed by several processes such as slow cooling of deep-seated granite (Dempster *et al*., 1994) and pressure quench mechanisms (Deer *et al*., 2001). Under certain constraints, the decompression process can account for the formation of rapakivi texture in within-plate setting granite (Dempster *et al*., 1994). Rapakivi texture can also be formed by dissolution-recrystallization processes in environments involving magma mixing and mingling (Deer *et al*., 2001). So the presence of this texture could indicate a magma mixing process, as suggested for the Galway granite, Ireland (Baxter and Feely, 2002).

Willaime and Brown (in Deer *et al*., 2001) have classified perthitic intergrowths into four groups:

1- Normal perthites with fine-scale lamination of albite and K-rich feldspar

2- Braid perthite with zig-zag lamellae of Na-feldspar in a microcline matrix

3- Diagonal form containing zig-zag twins of K-rich domain and albite-twinned Na-rich domains

4- Plate perthites

All the studied granites seem to contain the third type (the diagonal form) of perthitic intergrowth.

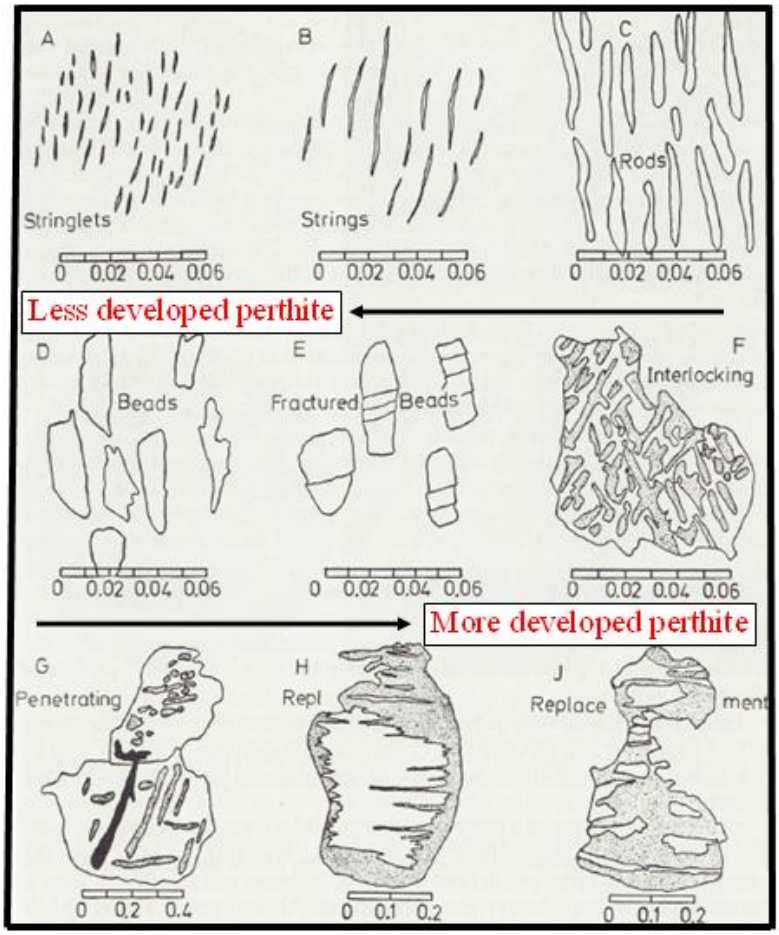

Figure 4.10: The types of perthites classified by Alling (in Smith, 1974). The scales are in centimeters. The stringlet lamellae of type A represent the quickest cooled perthite and as the temperature goes down the other perthite types form, until the last developed.

The studied perthites mostly resemble types D, E, F and G. The perthites of the Jabal Raydan alkali-granite are dominated by type C. These suggest and interim stage of development.

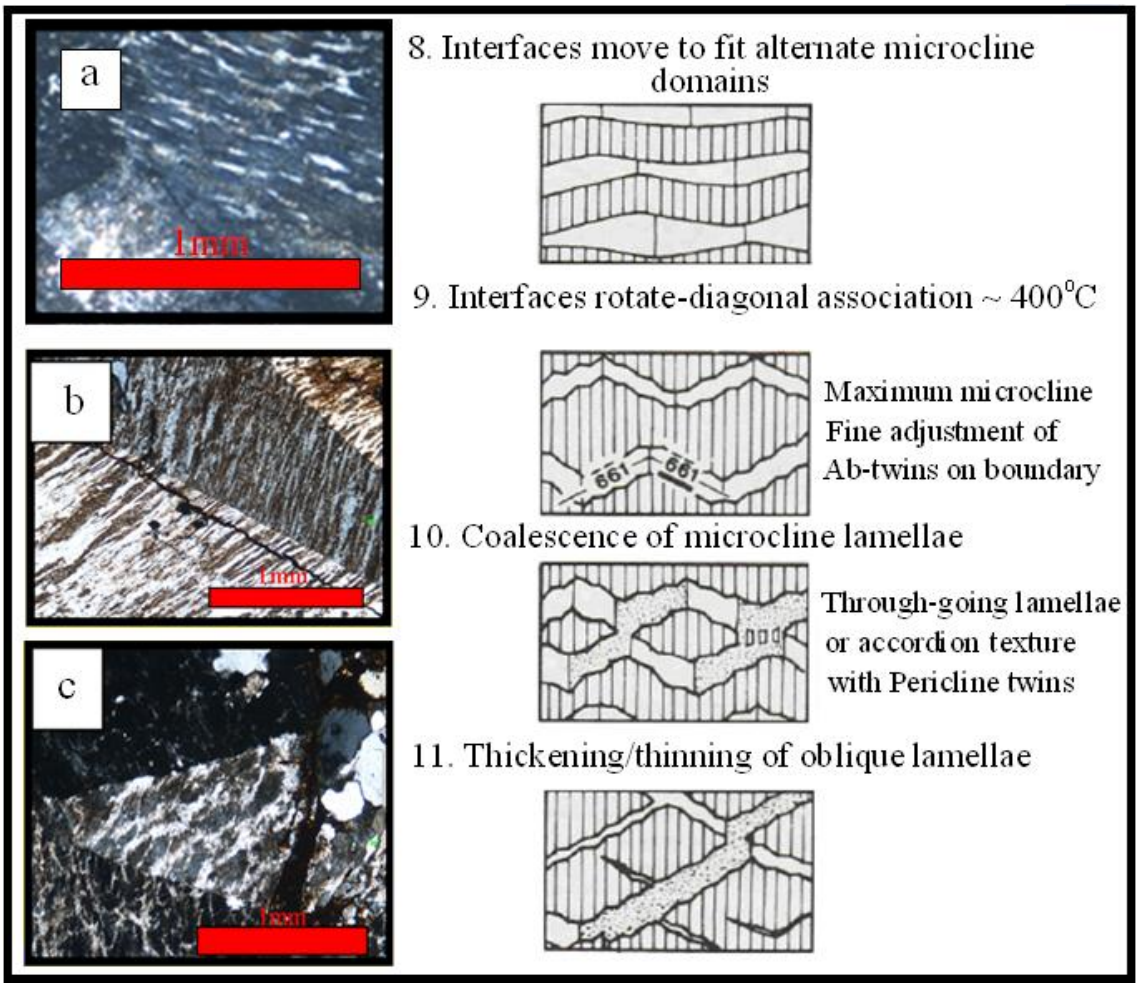

Figure 4.11: The last stages of braid microperthite development after Brown and Parsons (in Brown, 1984).

Stages number 8, 9 and 10 of the microperthite development are quite similar to the studied perthites. . Stage number 11 was noticed in the alkali-feldspar granites of Jabal Al-Massah, Jabal Khur Dukhan and Jabal az Zuhd plutons. Photos a, b and c were selected from the studied plutons for correlation purposes and suggest that they were formed at relatively low temperatures and after a fairly protracted period of cooling.

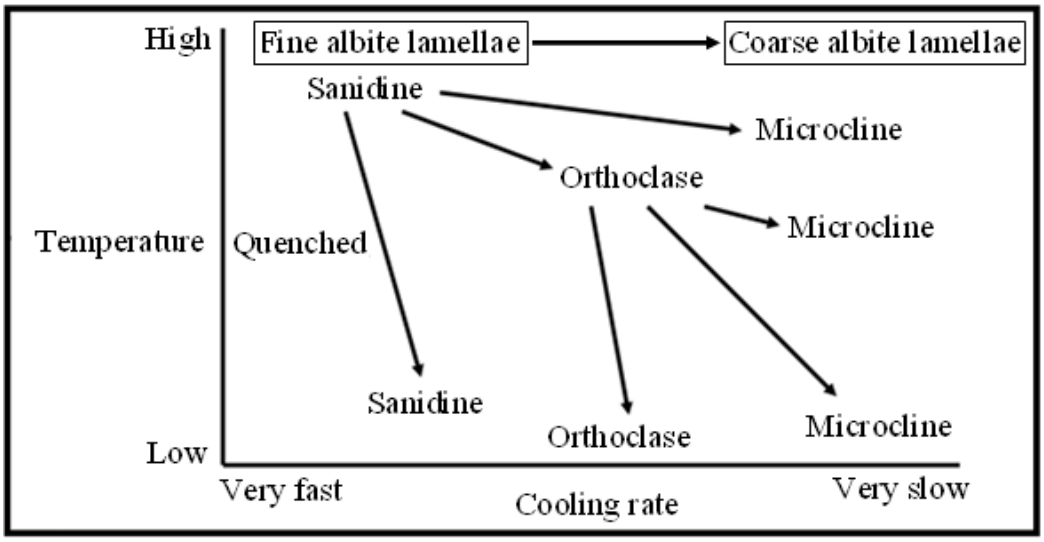

Figure 4.12: Various temperature-cooling rate paths (modified after Putnis and McConnell (1980).

Orthoclase and microcline were both found in all of the studied granites with different proportions and ratios. From the subsolidus textures, it is proposed that:

1- The alkali-feldspar granites of Jabal Thalabah and Jabal Raydan underwent faster cooling than occurred in the other plutons, as they show more myrmekite textures, and the later pluton also shows smaller, thinner albite lamellae and some clear cross-hatched twinned feldspars. Jabal Al-Massah, Jabal Khur Dukhan and Jabal az Zuhd plutons show more ordered albite lamellae and well developed perthitic texture (especially for the first two plutons), thus indicating a slower cooling rate (Jabal az Zuhd may have experienced a slightly shorter time of cooling rate than the other two plutons). It is proposed that they were subjected to further coarsening as they start to show some diamond-shaped, isolated albite.

2- Only one sample in Jabal Khur Dukhan (albite granite from an isolated body) contains abundant myrmekites, which would be indicative of a stage of rapid cooling.

3- The formation of subsolidus textures occurred in the presence of post-soldification, hydrothermal fluids that carried volatiles and enriched the rocks in alkalis (possibly also changing the rock composition). The high quantity and

types of fluid inclusions characterize the highly altered rocks and caused coarsening (mostly accompanied by turbidity) of the textures.

To summarize, the studied rocks are lithologically and mineralogically subtly different, and some are distinctly enriched in minor accessory phases. From a comparison with other plutons (locally and internationally) it seems that all these igneous intrusives occur in a similar tectonic environment. The subsolidus textures (especially perthite) provide initial evidence for the rock genesis (slow cooling at relatively low temperatures). Post-solidification alteration has contributed to the inter-growth texture development and in changing the rocks composition. The rate of cooling and volatiles (mostly likely brought by hydrothermal fluids) account for the textural variability. Such conclusions await additional support in the future using several techniques, e.g. trace element geochemistry, fluid inclusions and stable and radiogenic isotopes analysis. The petrography and field observations show that the more fractionated granites occupy the outer part of Jabal Thalabah, Jabal Khur Dukhan and Jabal Al-Massah and small portions of the inner parts of the Jabal Raydan and most of the Jabal Az Zuhd plutons.

Although the order of mineral crystallization in most of the plutons is complex and difficult to define, a few clear observations of the order of formation can be given as follows: amphibole, biotite, titanite, plagioclase, K-feldspar, quartz, chlorite and muscovite.

V. Mineralogy

V.1. Introduction

The previous chapter focused primarily on the major mineral phases present in the granitic rocks, but did indicate the following:

a. The abundance of accessory phases in some samples. Some of those accessories (e.g. monazite) are economically important minerals so their presence justifies further mineralogical study.

b. The exact identity of the opaque phases could not be established during the petrographic study as it only used transmitted light microscopy on thin sections. Reflected light microscopy using polished sections was necessary for accurate identification and description.

c. The different optical properties of the amphiboles indicate that different types, with differing chemical composition, are present. Identifying these types will assist in characterizing and differentiating the studied plutons.

This chapter is therefore a detailed mineralogical study, which is primarily concerned with identifying the types of amphibole and the other, fine-grained accessory/opaque phases.

V.2. Methodology

Six samples were selected for detailed mineralogical analysis. They were carefully chosen as the most promising host for rare earth and rare metal phases, as well as containing different types of amphiboles and opaque minerals. The samples are listed in Table 5.2. They were processed in several ways. The minor phases were liberated from the host rocks by crushing and then separated using a magnetic separator and heavy liquids; they were then mounted on stubs for semi-quantitative chemical analysis using scanning electron microscopy (SEM). Polished-thin sections were also made and these

were used for studying the opaque phases in reflected light and for quantitative microprobe analysis of the amphiboles and other accessory phases. Further details can be found in appendix II.

V.3. Mineralogical study

Reflected light microscopy and SEM (Fig 5.1) confirmed the presence of magnetite, ilmenite, hematite, zircon and other phases such as monazite-Ce, fergusonite-Y, xenotime, fluorite and thorite. Suggestions for the identity of some of the additional minor phases are given in Table 5.1.

V.3.1. Opaque phases

Most of the opaque minerals that were identified during the microscopic studies are oxides, which are characterized by some intergrowth textures which suggest secondary exsolution.

Magnetite (Fe_3O_4) in reflected light it is pale brown with a pinkish tint, isotropic and has a low reflectivity. It is present in euhedral to subhedral forms with a size range between < 100µm to approximately 0.8 mm. It mostly shows euhedral crystals. Magnetite is associated with and hosted by green amphibole, green and brown biotite, chlorite, zircon and titanite, but is also present as isolated, hexagonal crystals. An exsolution texture was identified between magnetite and ilmenite, as some euhedral magnetite has exsolved ilmenite (as small rod-like crystals) forming an ilmeno-magnetite intergrowth and in rare cases, fine exsolved skeletal ilmenite, which sometimes displays lamellar twining. Magnetite replaces the edges of some large feldspar and replaces the ferromagnesian minerals (especially the chloritized amphibole). It is sometimes replaced by martite (lamellar hematite forming along the cleavage planes; (see Fig. 5.1c) which is mostly present in the ‘oxidized’ biotite and amphibole.

Ilmenite ($FeTiO_3$**)** in reflected light the ilmenite is brownish gray to pinkish-brownish with weak anisortopism and low reflectivity. It is present in subhedral to anhedral forms with an approximate maximum size of 0.3 mm. It mostly shows a massive form and

much less as small lamella. It shows an association with slightly altered amphibole, in a few cases replaces magnetite, and is enclosed in and corrodes the cores of sericitized feldspar; it also shows partial alteration to titanite. A titanite-ilmenite reaction rim was only traced in the Jabal az Zuhd alkali granite. The chemical analyses of ilmenite reveal the presence of small amounts of Nb and Mn, possibly indicating solid-solution between Mn and Fe.

Hematite (Fe_2O_3) in reflected light the hematite is white with weak anisotropy and high reflectivity. It is present in euhedral to subhedral forms with an approximate maximum size of 0.5 mm. It shows patch-like, well and randomly oriented prismatic and elongated crystals. It commonly occurs as needle-like crystals forming along the cleavage planes of either altered biotite or amphibole.

Rutile (TiO_2) in reflected light it is found as long, thin, light grey crystals with a bluish tint and weak anistropism. It exists in variable sizes (< 100 µm to ~ 0.8 mm). Chemical analysis reveals enrichments in Nb and Ca. The latter may relate to reaction rims (titanite).

Xenotime (YPO_4) in reflected light it occurs as a very small (<100µm), irregular, slightly to highly altered, brownish-grey mineral. The chemical analyses of xenotime show the presence of enrichments in La and Nd, and lesser amounts of Pr, Sm, Gd and Ca.

V.3.2. Other accessory phases

Allanite $(Ca, Fe^{+2})_2(Al, Ce, Fe^{+3})_3(OH)(SiO_4)_3$ has a low abundance. It displays brown to reddish brown colours, the reddish colour possibly due to slight alteration. It has acute terminations and is often zoned (Fig. 5.1e). It has a limited range of sizes (0.5 to 0.1mm), and is mostly found as inclusions in large crystals of quartz and feldspar. The chemistry of the allanite reveals enrichments in La, Ce, Nd and lesser Ti.

Titanite ($CaTiSiO_5$) has high to medium abundance. It appears in two different shapes, the first is dark brown, distinctly rhombic with weak peleochroism and unclear

interference colours, while the second is yellowish to light brownish with no definite shape and high interference colours. It has various sizes (up to 1mm). The analyses reveal the presence of some REE (mostly La and Ce).

Monazite (Ce, La, Nd, Pr) PO_4 appears as small (100 to 300µm), colorless crystals with imperfect cleavage and small fractures. The analysis of the monazite indicates the presence of additional, small amounts of Si, Ca, and Fe.

Some of these rare metal-bearing minerals were found to be restricted to some plutons, while others were relatively common in all plutons. Other phases (Table 5.1) were identified during the SEM study but could not be located and characterized in the thin or polished sections of particular intereset is the presence of some phases containing Au, Ag and Pt. These observations, together with the abundance and nature of of these phases, have helped in characterizing each pluton (Table. 5.2). The interpretation of the above mentioned textures will be given later.

V.3.4. Summary

A large number of accessory phases have been found in these granites. They are relatively abundant in the studied plutons and Jabal Khur Dukhan is characterized by the most varied rare metal bearing accessories, while Jabal az Zuhd appears to contain the largest volume. Some evidence for both magmatic and late stage subsolidus and hydrothermal processes was found (see later).

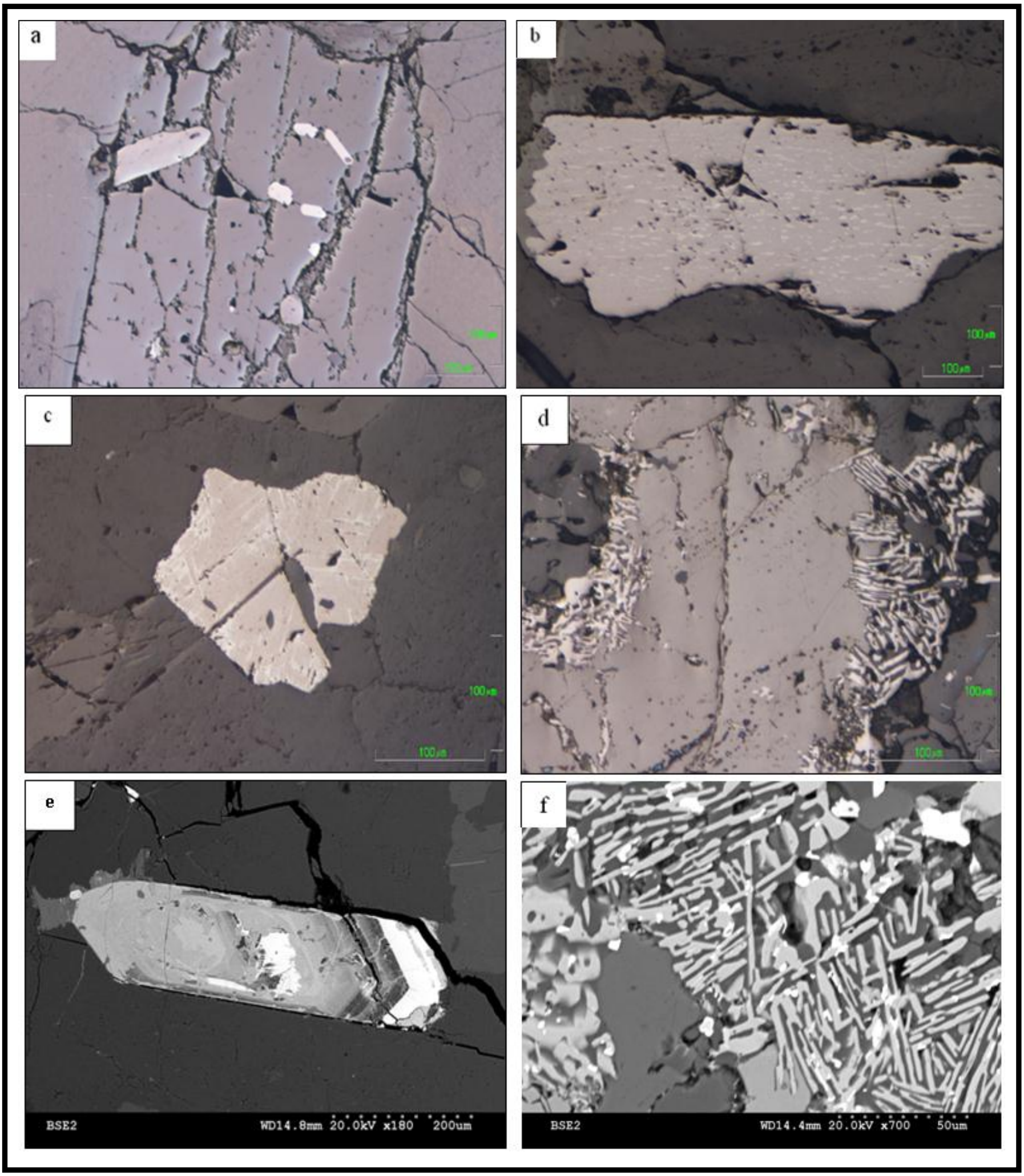

Figure 5.1: Some textures in accessory phases from the studied granitoids

a) Homogeneous, elongate crystals of magnetite (bright with a pinkish tint), in reflected light, P.P.L

b) Ilmenite (bright) exsolution in magnetite (pale brown), in reflected light, P.P.L

c) Martitized (fine bright lammalle of martite) magnetite, in reflected light, P.P.L

d) Reaction-rim between titanite (mid grey) and acicular ilmenite (pinkish-brownish), in reflected light, P.P.L.

e) Hexagonal-zoned allanite; bright zones are rich in REE (back scattered electron image)

f) Close view of titanite-ilmenite reaction-rim which also hosts some fine (white) fergusonite (back scattered electron image)

Table 5.1: Accessory phases

Qualitative chemistry from scanning electron microscope	Pluton	Mineral	Formula
Zr SiO (Hf)	All	Zircon	$ZrSiO_4$
Ca Ti (Fe,Al) SiO + REE	TH, JR & JZ	Titanite	$CaTiSiO_5$
Ca PO + REE	All except TH	Apatite	$Ca_5(PO_4)_3(OH,F,Cl)$.
Ca F (Y)	KD	Fluorite	CaF_2
Ca Al Fe SiO + REE (Ti, La, Ce, Nd)	All except JZ	Allanite	$(Ca,Fe^{+2})_2(Al,Ce,Fe^{+3})_3(OH)(SiO_4)_3$
(Ce, La, Nd) PO + Si, Ca, Fe	JZ and JM	Monazite	(Ce, La, Nd, Pr) PO_4
Y Nb O or Y Nb (Si, Fe) O	KD and JZ	Fergusonite	$YNbO_4$
(La, Pr, Nd, Sm, Gd, Ca) Y PO	KD and JZ	Xenotime	YPO_4
REE (Y, Ce, La, Nd) FeO	KD	unknown phase	(hosted by magnetite)
Au-Pt & Ag	KD	Au-Pt alloy and free Ag	(hosted by magnetite)
FeTi (Mn, Nb) O	JZ and KD	Ilmenite	$FeTiO_3$
Th SiO	JR	Thorite	$ThSiO_4$
REE (Ce, La) CaO	KD	Synchysite?	Ca (Ce, La) $[F(CO_3)_2]$
(Ca) Ti (Nb) O	JZ	Rutile	TiO_2

Table 5.2: Distribution of rare metal minerals in the plutons

Name of Pluton and sample number	Characterization	Association
Jabal Thalabah (TH13)	Low rare metal mineral abundance	Associated with zircon, apatite and titanite.
Jabal Khur Dukhan (KD28)	Shows various types of rare metal mineral and shows gold-platinum and free silver phases hosted in magnetite.	Associated with zircon, allanite and apatite, and also represented by fergusonite, xenotime and synchysite (?)
Jabal Al-Massah (JM31)	Contains largest amount of monazite	Associated with zircon, allanite and apatite, and also represented by monazite
Jabal Raydan (JR8, JR12)	Presence of thorite	Mostly restricted to allanite
Jabal Az Zuhd (JZ6)	Fergusonite and xenotime most abundant	Associated with Mn-rich ilmenite and zircon, and also represented by fergusonite and xenotime

V.3.5. Amphiboles

The petrographic study has indicated that amphiboles are generally rare in most of these granites. However, various types of amphiboles with differing optical properties have been recognized in some of the granitic units:

- Jabal Thalabah: Mostly irregular, short prisms and rarely elongated. Sub- to anhedral, yellowish, light green to dark green, with brownish to dark purple interference colours.

- Jabal Khur Dukhan: Slightly to highly altered, prismatic, rarely simple-twinned subhedral, yellowish to dark green with grayish green to orangy, pinkish purple interference colours.

- Jabal Al-Massah: Prismatic, eu- to subhedral, yellowish to green with bluish purple to orangey purple interference colours.

- Jabal Raydan : Contains more than one type of amphibole, as follows:

1- Irregular, prismatic and rhombic-shaped, light green to dark green with greenish to dark greyish interference colours.

2- Elongated and prismatic, light to dark green, simple twinned, with brownish to dark purple interference colours.

3- Slightly to highly altered, prismatic, semi-equant, subhedral, green to brownish green with greenish grey to dark interference colours.

Jabal az Zuhd: Shows the highest abundance (up to 4.5%)of amphibole among the studied granites. Large, elongated, prismatic and semi-equant, sub to anhedral, bluish and brownish in colour with dark blue to dark purple and yellowish green to purple interference colours, respectively.

Generally speaking, the amphiboles found in Jabal Khur Dukhan and Jabal Al-Massah are much less abundant and slightly smaller in size (most do not exceed 1mm) than those found in the other plutons which reach up to 1.2mm.

Electron microprobe analysis was used to chemically analyse the amphiboles as presented in appendix II. Mineral formulae derived from these analyses (recalculation based on 23 Oxygen) were used for classification using the amphibole classification schemes of Leake (1978), Leake *et al.* (1997) and Hawthorne (2007) and displayed in diagrams (Fig.5.2a to 5.2e). This system of classification is only applicable to calcic amphiboles (Hamidullah and Bowes, 1986). The diagrams used depend on the type of amphibole (e.g. Ca, Na-Ca or Ca), as each amphibole type has its own classification diagrams. Various types of amphibole are present (see also Table. 5.3). One type of amphibole was found in each pluton, except Jabal Raydan pluton that appears to contain 4 different types: dominated by the presence of Na-Ca, less Mg-Fe and much less Ca amphiboles. The chemical analyses of the amphiboles indicate that some amphiboles do not show good totals (see appendix II), and this may reflect an alteration state in some phases.

Table 5.3: Summary of amphibole varieties present

Name of Pluton	Leake (1978)	Hawthorne & Oberti (2007)	Abundance	
TH	Na-Ca	Katophorite	Low to medium (0 to 2%)	
JM	Mg-Fe	Gedrite	Low (0 to 1%)	
JR	Mg-Fe	Ferrogedrite	2 analyses out of 36	Generaly low to medium (0 to 3.5%)
	Na-Ca	Katophorite	29 analyses out of 36	
	Ca	Ferrohornblende/ferroactinolite	3 analyses out of 36	
	Ca	Ferroedenite	2 analyses out of 36	
JZ	Na	Arfvedsonite	Low to relatively high (0 to 4.5%)	

One limitation from the above mentioned comparisons is that some of the identified amphiboles show either slightly higher or slightly lower values of certain elements from the ideal types. For example, the katophorite shows higher Al and Fe, and lower Mg, Na and Si, the arfvedsonite has minor Mg, the ferroedenite show higher Al, presence of minor Mg, lower Fe and Na, and ferrohornblede show lower Al, Fe and Si, and small presence of Mg.

The Na type of amphibole that is only present in the Jabal Az Zuhd pluton indicating that the magma that formed Jabal Az Zuhd is more alkaline (possibly peralkaline) than the ones that formed the other pluton is (see chapter 6).

According to Hammarstrom and Zen (1986) a shallow level of emplacement is indicated if the Al total (number of atoms in amphibole formulae) of the amphibole is < 2; this was found to be the case in the Jabal az Zuhd, Jabal Thalabah and Jabal Raydan plutons. The Jabal Al-Massah amphiboles show > 2 Al total which possibly indicates a deeper level of emplacement.

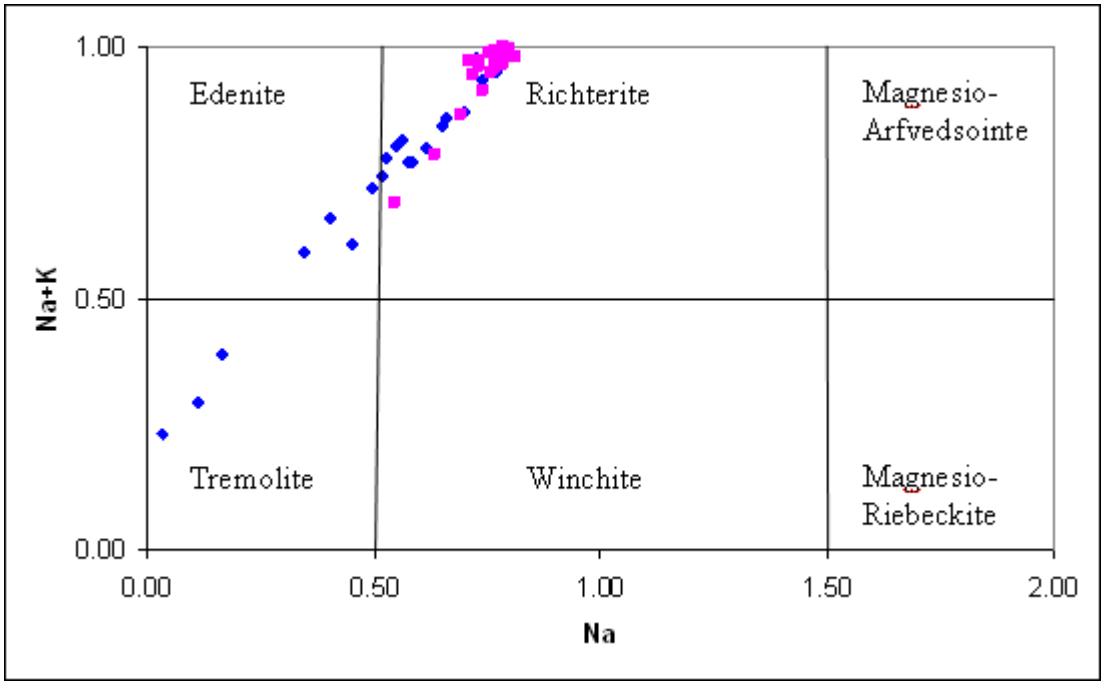

Figure 5.2a: The general amphibole classification from Leake *et al*. (1997) (pink squares = Jabal Thalabah, blue rhombohedra = Jabal Raydan)

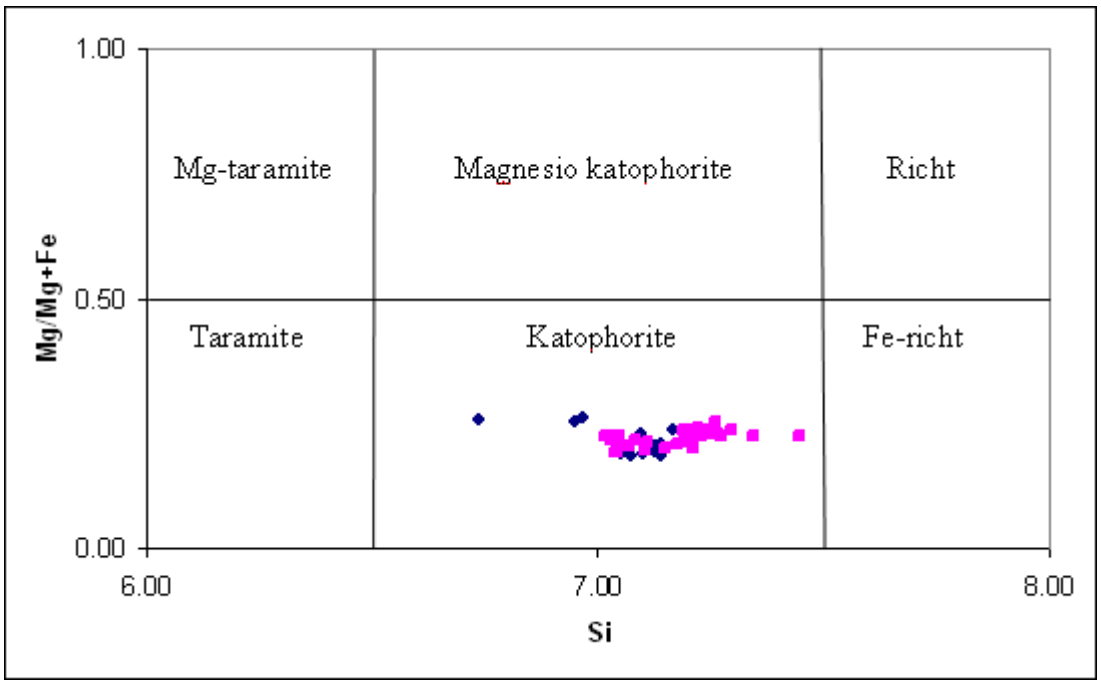

Figure 5.2b: The sodic-calcic amphibole classification from Hawthorne and Oberti (2007) (pink squares = Jabal Thalabah, blue rhombohedra = Jabal Raydan).

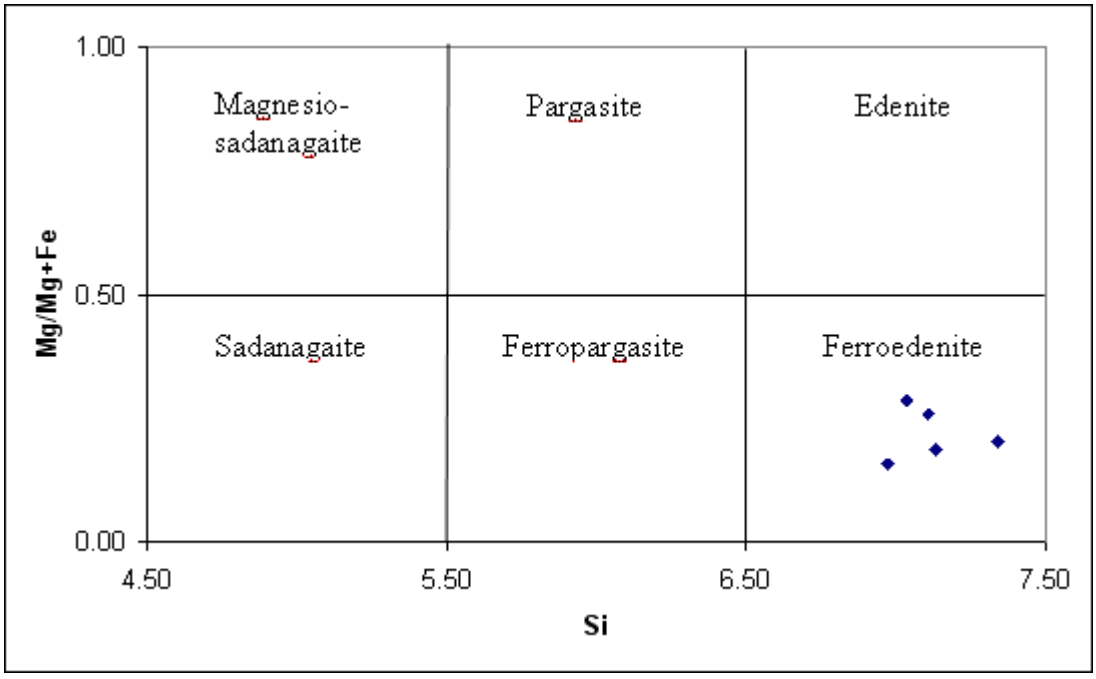

Figure 5.2c: The calcic amphibole classification from Hawthorne and Oberti (2007) (blue rhombohedra = Jabal Raydan).

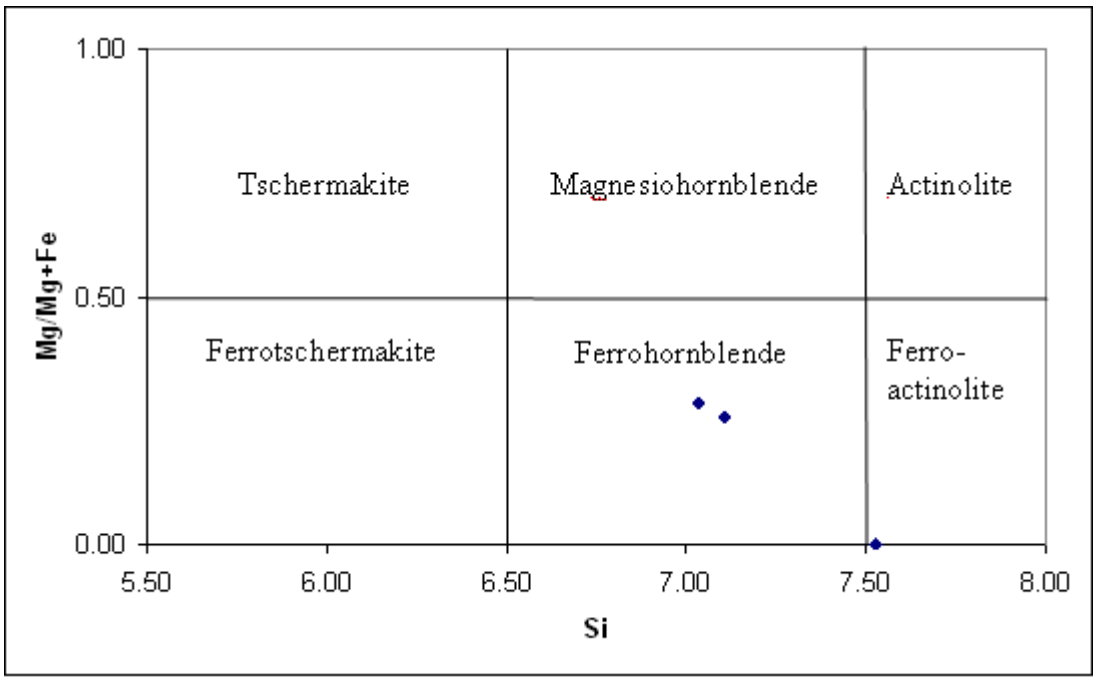

Figure 5.2d: The calcic amphibole classification from Hawthorne and Oberti (2007) (blue rhombohedra = Jabal Raydan).

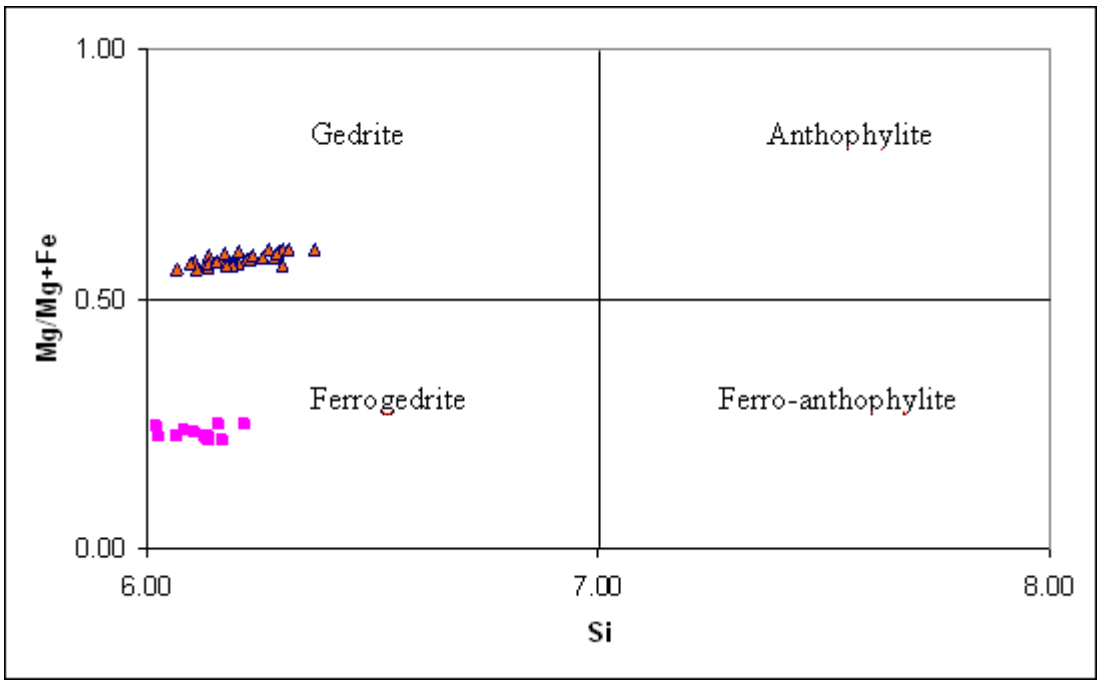

Figure 5.2e: The Mg-Fe-Mn-Li amphibole classification from Hawthorne and Oberti (2007) (pink squares = Jabal Raydan, orange triangles = Jabal Al-Massah).

V.3.6. Summary

Different types of amphiboles are present in these plutons and they provide more evidence for the differences between the studied plutons. Jabal Thalabah, Jabal Al-Massah and Jabal az Zuhd only contain one type of amphibole, Jabal Raydan has 4 types of amphibole and Jabal Khur Dukhan contains no amphibole. The difference in appearance or character could relate to alteration and/or to a mafic magma influx (amphibole associated with mixing processes), while the difference in grain size may reflect the cooling rate of the developing magma (slower rate of cooling for the coarser amphiboles).

V.3.7. Geobarometry

A method for estimating the crystallization pressure of amphibole was empirically proposed by Hammarstrom and Zen (1986). It is based on the total Al content per 23 oxygen atoms of calcic hornblende in the pressure range from <1 to 8 kbar and has a ±3 kbar uncertainty. The rocks should include the mineral assemblage of quartz, plagioclase, orthoclase, biotite, hornblende, magnetite, titanite ± epidote. The calibration has been refined several times, reducing the error to ±1 kbar (Hollister et. al. 1987), ±0.5 kbar (Johnson and Rutherford, 1989) and ±0.6 kbar (Schmidt, 1992).

Crystallization pressures, based on the compositions of amphiboles in two plutons (Jabal Thalabah and Jabal Raydan), have been calculated from the electron microprobe analysis by using these barometers and the results are summarized in tables 5.4 and 5.5. (The amphiboles in Jabal az Zuhd and Jabal Al-Massah were excluded as they do not have a calc-alkalic composition).

The average pressures range from 1.2 to 2.3kbar for Jabal Thalabah and 2.2 to 3.4kbar for Jabal Raydan; these equate to approximate depths of 4.3 to 7.9 km for Jabal Thalabah and 7.8 to 11.9 km for Jabal Raydan. Several studies have attempted to calculate the pressure of calc-alkaline plutons and then convert the crystallization pressure to depth. Conversion factors used have been 3.8 (e.g. the calc-alkaline batholith southwestern Mexico, Zenteno *et al.*, 1996), 3.7 (the North Patagonian batholith in Chile, Herve *et al.*, 1996), 3.6 (Median batholith western New Zealand, Tulloch and Challis, 2000) or 3.5 (the Manaslu granite in Central Nepal, Guillot *et al.*, 1994).

Table 5.4: Crystalliation pressure (kb) for amphibole and suggested depth (km) of emplacement for the Jabal Thalabah Pluton.

Al (T)	TH (T)	Hammarstrom and Zen 1986	Depth	Hollister et al 1987	Depth	Johnson and Rutherford 1989	Depth	Schmidt 1992	Depth
1.1	95.51	1.4	5.0	1.2	4.4	1.0	3.7	2.1	7.2
1.0	95.37	0.9	3.0	0.6	2.1	0.6	2.0	1.5	5.3
1.1	95.13	1.4	5.0	1.2	4.4	1.0	3.7	2.1	7.2
1.0	95.06	1.2	4.1	0.9	3.3	0.8	2.9	1.8	6.3
1.1	94.99	1.5	5.3	1.3	4.6	1.1	3.9	2.1	7.4
1.0	96.62	1.3	4.5	1.1	3.8	0.9	3.2	1.9	6.7
1.0	94.35	1.3	4.4	1.0	3.7	0.9	3.1	1.9	6.6
1.1	94.22	1.7	5.9	1.5	5.3	1.3	4.4	2.3	8.0
1.1	97.28	1.7	5.9	1.5	5.3	1.2	4.4	2.3	8.0
1.0	95.81	1.2	4.2	1.0	3.4	0.8	2.9	1.8	6.4
1.1	93.21	1.8	6.4	1.7	5.9	1.4	4.8	2.4	8.5
1.2	90.44	2.0	7.1	1.9	6.7	1.5	5.4	2.6	9.2
1.0	97.50	0.9	3.2	0.7	2.3	0.6	2.1	1.6	5.5
1.1	94.53	1.4	4.8	1.2	4.1	1.0	3.5	2.0	7.0
1.1	93.13	1.5	5.4	1.4	4.8	1.1	4.0	2.2	7.6
1.3	94.36	2.5	8.6	2.4	8.4	1.9	6.6	3.0	10.6
1.3	95.38	2.4	8.4	2.3	8.1	1.8	6.5	3.0	10.4
1.2	91.42	2.1	7.5	2.0	7.1	1.6	5.7	2.7	9.5
1.1	96.67	1.5	5.3	1.3	4.7	1.1	3.9	2.1	7.5
1.1	93.21	1.4	4.8	1.2	4.1	1.0	3.5	2.0	7.0
1.2	95.88	2.0	7.1	1.9	6.7	1.5	5.4	2.6	9.1
1.2	94.26	2.1	7.5	2.0	7.1	1.6	5.7	2.7	9.5
1.2	95.87	2.1	7.3	2.0	6.9	1.6	5.6	2.7	9.4
1.2	95.68	2.2	7.7	2.1	7.4	1.7	5.9	2.8	9.8
1.2	94.60	2.2	7.6	2.1	7.2	1.7	5.8	2.7	9.6
1.3	94.55	2.4	8.5	2.4	8.2	1.9	6.6	3.0	10.5
1.2	92.08	2.1	7.5	2.0	7.1	1.6	5.7	2.7	9.6
0.7	95.60	-0.4	-1.6	-0.9	-3.0	-0.5	-1.9	0.3	1.0
1.3	95.68	2.4	8.5	2.4	8.3	1.9	6.6	3.0	10.5
1.1	93.50	1.6	5.5	1.4	4.9	1.2	4.0	2.2	7.6
1.1	95.82	1.4	4.9	1.2	4.2	1.0	3.5	2.0	7.1
1.3	97.52	2.5	8.7	2.4	8.5	1.9	6.8	3.1	10.7
1.0	94.94	1.3	4.7	1.1	4.0	1.0	3.4	2.0	6.9
0.9	96.24	0.8	2.7	0.5	1.8	0.5	1.7	1.4	5.0
1.2	92.81	2.2	7.5	2.1	7.2	1.6	5.8	2.7	9.6
1.2	94.17	2.1	7.2	2.0	6.9	1.6	5.5	2.7	9.3
1.1	95.48	1.4	5.0	1.3	4.4	1.0	3.7	2.1	7.2
1.2	96.99	2.2	7.8	2.1	7.4	1.7	6.0	2.8	9.8
1.3	95.50	2.7	9.5	2.7	9.4	2.1	7.4	3.3	11.5
1.1	97.19	1.5	5.4	1.4	4.8	1.1	4.0	2.2	7.6
1.1	93.92	1.6	5.5	1.4	4.9	1.2	4.0	2.2	7.6
1.0	95.60	1.3	4.6	1.1	3.9	1.0	3.3	2.0	6.8
0.8	97.00	0.3	1.1	0.0	-0.1	0.1	0.3	1.0	3.4
1.0	97.95	1.3	4.7	1.1	4.0	1.0	3.4	2.0	6.9
1.1	96.15	1.7	5.8	1.5	5.3	1.2	4.3	2.3	8.0
1.1	97.56	1.4	4.8	1.2	4.2	1.0	3.5	2.0	7.0
1.1	97.65	1.4	4.8	1.2	4.1	1.0	3.4	2.0	7.0
1.2	97.42	2.3	8.0	2.2	7.7	1.8	6.2	2.9	10.1
1.1	95.2	1.7	5.8	1.5	5.2	1.2	4.3	2.3	7.9

Explanation: The last row represents the average values

Table 5.5: Crystallisation pressure (kb) for amphibole and suggested depth (km) of emplacement for the Jabal Raydan Pluton.

Al(T)	JR total	Hammarstrom and Zen 1986	Depth	Hollister *et al* 1987	Depth	Johnson and Rutherford 1989	Depth	Schmidt 1992	Depth
1.31	95.18	2.7	9.4	2.6	9.2	2.1	7.3	3.2	11.3
1.31	95.58	2.7	9.3	2.6	9.2	2.1	7.3	3.2	11.3
1.26	95.04	2.4	8.4	2.3	8.2	1.9	6.5	3.0	10.4
1.30	96.31	2.6	9.2	2.6	9.0	2.0	7.2	3.2	11.2
1.30	95.59	2.6	9.2	2.6	9.0	2.0	7.2	3.2	11.1
1.26	96.58	2.4	8.4	2.3	8.2	1.9	6.5	3.0	10.4
2.60	95.18	9.1	32.0	9.9	34.6	7.5	26.3	9.4	32.7
2.54	95.53	8.8	30.9	9.5	33.4	7.3	25.4	9.1	31.7
1.33	95.93	2.7	9.6	2.7	9.5	2.1	7.5	3.3	11.5
1.33	96.44	2.8	9.7	2.7	9.6	2.2	7.6	3.3	11.6
1.68	97.37	4.5	15.8	4.7	16.5	3.6	12.7	5.0	17.4
1.46	96.13	3.4	11.9	3.4	12.1	2.7	9.4	3.9	13.7
1.57	96.31	4.0	13.9	4.1	14.4	3.2	11.2	4.5	15.6
1.27	96.80	2.5	8.6	2.4	8.4	1.9	6.6	3.0	10.6
1.25	96.78	2.4	8.4	2.3	8.1	1.8	6.5	3.0	10.4
1.36	96.01	2.9	10.2	2.9	10.1	2.3	8.0	3.5	12.1
1.29	95.67	2.6	9.0	2.5	8.9	2.0	7.0	3.1	11.0
1.27	95.36	2.4	8.6	2.4	8.3	1.9	6.6	3.0	10.5
1.28	95.50	2.5	8.8	2.4	8.5	1.9	6.8	3.1	10.7
1.03	96.29	1.3	4.4	1.0	3.6	0.9	3.1	1.9	6.6
1.27	96.19	2.5	8.7	2.4	8.5	1.9	6.8	3.1	10.7
1.74	95.82	4.8	16.9	5.1	17.7	3.9	13.7	5.3	18.5
1.45	97.42	3.4	11.9	3.4	12.0	2.7	9.4	3.9	13.7
1.38	95.32	3.0	10.6	3.0	10.6	2.4	8.3	3.6	12.5
1.31	96.59	2.7	9.3	2.6	9.2	2.1	7.3	3.2	11.3
1.65	97.42	4.4	15.3	4.5	15.8	3.5	12.3	4.8	16.9
1.59	97.48	4.1	14.3	4.2	14.8	3.3	11.5	4.6	16.0
1.55	95.92	3.9	13.6	4.0	14.0	3.1	10.8	4.4	15.3
1.15	97.16	1.8	6.5	1.7	6.0	1.4	4.9	2.4	8.6
1.20	97.34	2.1	7.5	2.0	7.1	1.6	5.7	2.7	9.5
1.19	95.91	2.1	7.3	2.0	6.9	1.6	5.6	2.7	9.4
1.26	98.42	2.4	8.5	2.4	8.2	1.9	6.6	3.0	10.5
1.28	98.57	2.5	8.8	2.5	8.6	2.0	6.9	3.1	10.8
2.78	95.26	10.1	35.2	10.9	38.2	8.3	29.1	10.2	35.8
1.25	98.86	2.3	8.2	2.3	7.9	1.8	6.3	2.9	10.2
1.27	98.00	2.5	8.7	2.4	8.5	1.9	6.8	3.1	10.7
1.5	96.4	3.4	11.9	3.4	12.0	2.7	9.4	3.9	13.7
1.3	96.5	2.8	10.0	2.8	9.9	2.2	7.8	3.4	11.9

Explanation: Dark green cells represent Fe-Mg types while the light blue and orange cells represent the calcic types (the ferroedenite and the ferrohornblende). The last two rows respectively represent the average values with and without the Fe-Mg types

For the studied rocks the depth of emplacement was estimated by multiplying the crystallization pressure by 3.5 with ±0.5 km limitation. Differences in Al content of calcic amphiboles are therefore directly related to the depth of emplacement of the plutons.

V.3.8. Summary

The geobarometry study has suggested a depth of emplacement for some of the studied plutons and this will subsequently help in the tectonic reconstructions.

V.4. Discussion and Conclusions

V.4.1. Significance of textures and alteration

The textures of the opaque phases suggest that both primary magmatic and secondary, late stage, subsolidus and hydrothermal processes have been operative. These are indicated by the presence of euhedral cubes of magnetite, exsolution and replacement textures, respectively.

The ilmeno-magnetite exsolution could have resulted either from cooling (Craig and Vaughan, 1981, Vernon, 2004) due to subsolidus recrystalization (Himmelberg, 1977) or from late metamorphism (Karkkainen and Appelqvist, 1999) (which is not likely to in this situation). The idomorphic homogenous magnetite is magmatic (Himmelberg, 1977) mineral that reflect slow rate of growth (Henriquez and Martin, 1978). The titanite-ilmenite reaction rim is possibly developed due to re-crystalization decompression reaction (Mengel and Rivers, 1991), with decreasing pressure and temperature (Rumble and Finnerty, 1974) and influx of Al-rich (Frost *et al*., 2001) late-stage fluid activity accompanied by high oxygen fugacity during the subsolidus cooling (Broska *et al.,* 2007). The presence of magnetite and ilmenite indicates a relatively deep magma source, and the later mineral which was found much more with the Jabal az Zuhd than the other plutons indicate late-stage processes (Conrad *et al*., 1988, Clemens and Bea, 2012). The REE enriched zone of allanite is most likely related to hydrothermal, metasomatic process (Sorensen, 1991) or could be related to metamorphic processes which may also account for the observed growth zoning (Janots *et al.,* 2009). The presence of some Ce-dominant REE minerals in some Ca-bearing

minerals was not unexpected, as this can be interpreted by the fact that from crystal structure sense the Ce-group rare earths show similar coordination number to those of calcium (Jones *et al*., 1996) and therefore, an isomorphous substitution was more likely occurred in responding to the newly developed solid solution.

V.4.2. Rare metal - bearing phases

Generally speaking, REE-bearing minerals are formed from highly fractionated magmatic systems (Bortnikov *et al*., (2007). They can form by both magmatic and/or metasomatic process (e.g. the Palung granite in Himalaya, Scharer and Allegre, 1983, the Igralishte granite pluton, Southwestern Bulgaria, Tarassov *et al*., 2008, the Ireteba granite, Sothern Nevada, Townsend *et al*., 2000, the peraluminous Melechov granite massif, Czech Republic, Harlov *et al*., 2008, the Nizke Tarty Mountains, Western Carpathians, Slovakia, Petrik and Konecny, 2009). In addition, monazite and xenotime may result from late magmatic replacement by re-crystallization of former or inherited phases which have a restitic origin (Petrik and Konecny, 2009). The presence of monazite may also indicate slightly alkaline crystallization conditions (Popova and Churin, 2010) and it can also form by high- temperature alkaline metasomatism which results in secondary minerals like thorite and apatite (Tarassov *et al*., 2008). The presence of the Mn-poor Y-Nb-oxide may also support the late alteration process as it can be related to rapid emplacement and cooling of mantle-derived magma (Nakashima and Imaoka, 1998). The presence of magmatic REE-bearing minerals could be related to high-temperature magmatic saline solutions that are in fact very effective in carrying and transporting them (Jones *et al*., 1996). From the mineralogical study monazite appeared to be slightly altered; although it can be a weathering product of other rare earth minerals like apatite (Chang *et al*., 1996) its chemical analyses (appendix II) indicate that some at least is a primary phase as ThO_2 contents are close to the average (~ 5wt %) of primary monazite. Some idiomorphic or subidiomorphic large isolated grains of allanite are expected to be magmatic, however, primary allanite typically contains some Th, Zr and P (Bea, 1996, Clemens and Bea, 2012) and such elements did not appear in the allanite chemical analyses (appendix II). Because of its rarity and lack of chemical analyses for xenotime it was difficult to suggest wither it is a magmatic or a hydrothermal mineral. However, primary xenotime contains some UO_2, ThO_2 and appreciable amount of FeO (Bea, 1996, Clemens and Bea, 2012), and these were not present in the semi-quantitative analyses; therefore, xenotime was suggested to be of

hydrothermal origin. The relationship variation diagrams in the following chapter and in chapter eight support these suggestions for the origin of the economically important minerals.

Monazite and xenotime (phosphorous species) are crucial in transporting the REE in certain hydrothermal fluids, and may indicate the presence of REE-phosphate complexes at high temperatures (Jones *et al*., 1996). Other than PO_4^{-3} ligands like F^- and OH^- are also possible to occur at elevated temperatures, representing REE-bearing complexes, and lately all those would most likely be representing minerals like fluorite and apatite (Jones *et al*., 1996). Monazite can be related to low pressure-temperature conditions in the later magmatic differentiates (Chang *et al*., 1996). The presence of Au-Pt alloy and free silver were only found in two locations suggesting a presence of separate mineral phase.

V.4.3. Amphibole

The composition of the amphiboles can vary with bulk magma composition, pressure, temperature and oxygen fugacity. These factors will be discussed bellow.

The formation of Jabal az Zuhd arfvedsonite might be attributed to sodic metasomatism and higher oxygen fugacity condition (Mucke, 2003), more evolved earlier granites or by re-melting of earlier granite and hybridization with a more mafic magma (Pe-Piper, 2007). The presence of arfvedsonite and other iron-rich phases of magnetite and ilmenite in alkaline granites of Jabal az Zuhd indicates a higher degree of oxidation (Buddington *et al*., 1963) than the granitic rocks from the other four plutons.

Anorogenic tectonic environment is indicated if there is intergrowth between pairs of ferroan and magnesiohornblende amphibole (Yamaguchi, 1985). This is observed in Jabal Al-Massah and partially in Jabal Raydan. The katophorite that represents the Jabal Thalabah and most of the Jabal Raydan amphibole commonly occurs in the later formed granites, as it results from the development of the primary sodic-calcic amphiboles (Pe-Piper, 2007). The presence of a wide range of amphibole compositions in Jabal Raydan and its calcic amphiboles (ferrohornblende and ferro-edenite) may indicate a SiO_2-oversaturated anorogenic granite (Martin, 2007).

However, the presence of a wide range of calcic amphiboles from edenite to pargasite to magnesiohornblende and ferrohornblende can also be present in an arc-related granite (Martin, 2007). The major and minor element composition of the primary amphiboles that shows a compositional range from calcic amphiboles through sodic-calcic to alkali amphiboles relate to the stage of magmatic evolution attained by the parental mantle-derived magma as it fractionates once in the crust (Mitchel, 1990) and/or the sequence of crystallization of the Fe-rich amphiboles that range from Ca-rich to Na-rich compositions. These features be inferred by tracking the composition of the primary amphibole (Martin, 2007) but have not been prooved in any of the studied granitiods.

An extensive search was not successful in finding zoned calcic amphibole crystals, for the purpose of tracking any increment or decrease in Si and Na + K contents with time. This could be due to replacement process that affected most of the calcic amphiboles, either with decreasing temperature from 850 to 600 °C, by minerals of sub-solidus origin and/or lower temperature minerals like titanite and chlorite (just like in the younger granites of Nigeria; Mucke, 2003). This may indicate a formation temperature of < 600 °C, but this could also suggest that no progressive oxidation occurred in the calc-alkaline magmas as if so then strongly zoned crystals of clinoamphibole should be formed (Kawakatsu and Yamaguchi, 1987). All these indications for the formation conditions of the amphiboles are related to the fact that those variables associated with the bulk magma composition significantly control amphibole composition (Hammarstrom and Zen, 1986).

Regarding the level of emplacement of the studied pluton, values >2 for the Al total might not be the only reason for inferring deeper emplacement. For instance, the Barberton greenstone belt and the Manaslu granite are metamorphosed granites which commonly show Fe-Mg hornblendes are a strong indication of emplacement level. Other metamorphosed granites also show a deeper emplacement level than the studied granitoids, like in the amphibolite facies, southern Karnataka granite, India (Janardhan *et al*., 1982) that shows a range of 5-7 kbar for its pressure of crystallization. The indicated shallow emplacement might not only refer to the low value (<2) of the Al total but it can be also be accounted for by the alkalinity of the amphibole. This suggestion is also supported by the existence of other alkaline plutons from South Greenland that

suggest 1 kbar crystallization pressure (Marks and Markl, 2001). Therefore, amphibole composition also appears to influence the pressure estimation.

V.4.4. Geobarometry

Although the geobarometers used here do not seem to provide highly accurate results (large range of values), the average values probably give a good indication of the depths of emplacement. Unfortunately the method could only be applied to two of the plutons because of the limitations in using particular varieties of amphibole.

Although this method for calculating the crystallizing pressure and hence the depth of formation was not applicable for some of the granitoids, Hammarstrom and Zen (1986) suggest a shallow level of emplacement is probable if the Al total of the amphibole in granitoids is < 2 and this is seen in the Jabal Az Zuhd, Jabal Thalabah and Jabal Raydan plutons (their Al total averages are respectively 0.2, 1.1 and 1.3), while the Jabal Al-Massah pluton shows 2.5 Al total which indicates a deeper level of emplacement. Similar granitoids with amphibole Al total > 2, like the calc-alkaline batholith, southwestern Mexico (Zenteno *et al*., 1996), the metamorphosed granite, south of the Barberton greenstone belt, South Africa (Dziggel *et al*., 2001), the metamorphosed Manaslu granite, Central Nepal, (Guillot *et al*., 1994) and the amphibolite facies granite of southern Karnataka, India (Janardhan *et al*., 1982) that all show a range of 3.4 - 11 kbar for their pressure of crystallization and consequently a deeper level of emplacement. It is perhaps also important that the amphibole in these other examples of granites is a Fe-Mg variety as this seems also to be an indicator of deeper levels.

Similarly the alkaline nature of the amphibole in Jabal az Zuhd might also indicate shallower emplacement. This suggestion is supported by the existence of other alkaline plutons that have low crystallization pressures, like the alkaline granites of southern Greenland (Marks and Markl, 2001) (1 kbar).

The lack of amphibole in Jabal Khur Dukhan hinders a calculation of the crystallizing pressure and the depth of emplacement. However, a low pressure of crystallization and a shallow emplacement might be suggested based on the alkaline nature of the pluton.

To summarize, the detailed mineralogical study has indicated a low crystallization pressure (~1 to 3 kbar) and shallow emplacement depth (~4 to 12 km) and has highlighted more differences between these intrusive rocks.

V.4.5. Summary

The mineralogical study has confirmed the existence of minerals of potential economic importance such as monazite, fergusonite, xenotime and thorite, as well as other unknown REE-bearing phases. Some important textures have provided information about the formation conditions (slow cooling rates supported by ilmeno-magnetite exsolution, medium to low temperature of formation supported by the presence of calcic amphibole and titanite) and processes (magmatic fractionation supported by the formation of REE-bearing minerals, hydrothermal alteration supported by the martitization and reaction-rim textures). Various types of amphibole have also been identified (Ca, Na-Ca, Na, Mg-Fe). This has further highlighted the differences between the intrusive bodies. As the previous chapters indicates differences in the plutons shapes (e.g. nested-like form of Jabal Al-Massah), lithological homogeneity and diversity (e.g. Jabal az Zuhd is the most homogeneous pluton and the presence of the hybrid rocks in Jabal Thalabah), granitic units relative ratios (e.g. the granodirite constitutes larger area than the syenogranite in Jabal Thalabah opposite to appears in Jabal Khur Dukhan) , amphibole (rare in Jabal Khur Dukhan and Jabal Al-Massah and show distinct type in Jabal az Zuhd) and plagioclase abundancy (rare in Jabal az Zuhd).

The significance of the rare earth and rare metal phases will be discussed further in a later chapter 8 assessing the economical potential of these granites.

VI. Geochemistry

VI.1. Introduction

The aim of this chapter is to chemically characterize and classify the studied granites and compare them with other granite, both regional and global. This will help in understanding the nature of these granites and their environment of formation. However, trace elements which could have economic importance will be considered in chapter 8 (Economic potential). Therefore, this chapter will focus more on the major elements, but will also use some trace elements in certain applications.

VI.2. Methodology

The geochemical analyses of the granitic rocks were mainly obtained using Inductively Coupled Plasma Mass Spectrometry and Atomic Emission Spectrometry (ICP-MS and AES). X-ray Fluorescence (XRF) was also used to repeat some major element analyses. ICP-AES was used for analyzing major elements (presented as oxides: SiO_2, Al_2O_3, FeO, MgO, CaO, Na_2O, K_2O, TiO_2, P_2O_5 and MnO) and some trace elements (Ba, Cu, Li, Ni, Sr, Y, Zn, Rb, Zr, Nb, Mo, Sn, Hf, Ta, Pb, Th and U) while ICP-MS was used to analyze for rare earth elements (REE: La, Ce, Pr, Nd, Sm, Eu, Gd, Tb, Dy, Ho, Er, Tm, Yb, and Lu). There were some issues with the accuracy of the chemical analyses as some totals occurred outside the acceptable range of 99-101%. Those analyses that do not show good totals were checked by XRF (see appendix III) and it was found that the major component of the error is in the silica values. Some of theses analyses were retained because a relatively small change in silica value would not affect any of the classifications that have been utilised. The full methodology of the chemical analysis is presented in Appendix III. Major and trace element contents of the studied plutons are shown in tables 6.2 to 6.5 and 6.14 to 6.17, respectively. The chemistry of the granites has then been plotted in a series of diagrams for classification and to aid an understanding of their genesis and environment of formation. A summary of the diagrams used in this chapter is presented in table 6.1.

Table 6.1: Major and trace element geochemical diagrams used in this study

Type of diagrams	Elements used	Aims	References
Variation diagram for major elements	Si plotted against major elements	Tracing differentiation	Rollinson (1993)
Variation diagram for trace elements	Si plotted against trace and rare earth elements	Tracing differentiation	
Variation diagram for alteration affects	Major and trace elements plotted against loss on ignition values	To assess the affects of alteration	
R1-R2 rock classification	R1= 4Si-11(Na+K)-2(Fe+Ti) against R2= 6Ca+ 2Mg+Al. calculated from millication proportions	Detailed classification for granites and other rock types	De La Roche *et al*. (1980)
TAS	(Na_2O+K_2O) against SiO_2	To distinguish alkalic from subalkalic plutonic rocks and provide information about magmatic series	Wilson (1989)
Subalkalic subdivision	K_2O against SiO_2	Tracing K enrichmentand to provide information about magmatic series	Le Maitre *et al*. (1989)
Aluminum saturation index (ASI)	(Al_2O_3)/ (Na_2O+K_2O) against (Al_2O_3)/ ($CaO+Na_2O+K_2O$). Plot the molar ratios	Provide information about magmatic affinity	Rollinson (1993)
Granite classification	(Al_2O_3+CaO)/($FeO^*+Na_2O+K_2O$) against 100 ($MgO+FeO^*+TiO_2$)/SiO_2	Characterize granitic rocks and provide information about the degree of fractionation	Sylvester (1989)
Modified alkali lime index diagram	Na_2O+K_2O-CaO against SiO_2	Characterize/classify granitic rocks	Frost *et al*. (2001)
Fe-number diagram	FeO/(FeO+MgO) against SiO2		
Normative composition diagram using the haplogranite system	Bulk compositions of the granites are plotted in a quartz-albite-orthoclase-H_2O-fluorine ternary diagram	To identify the minimum melt composition, the approximate pressure and the possible affect of volatiles on granite formation	Moghazi *et al.* (2011) Ebadi and Johannes (1991)
Diagram for rare earth diagrams	Normalized rare earth elements plotted in a logarithmic diagram	To use the REE pattern to explain processes of formation	Boynton in Rollinson (1993)
Tectonic discrimination diagram	Rb against (Nb+Y)	To indicate tectonic environment	Pearce *et al.* (1984)
	Hf-Rb/30-Ta*3 ternary diagram		Harris et al. (1986)
	Fields of different tectonic environment are drawn on the R1-R2 diagram		Bachelor and Bowden (1985)
Rock genesis	(Na_2O+K_2O)/($FeO^*+MgO+TiO_2$) against $Na_2O+K_2O+FeO^*+MgO+TiO_2$	Indicated magma source by partial melting	Douce (1999)
	Nb/La against SiO_2	Suggest assimilation-combined fractional crystallization trend	Wang *et al*. (2005)
	Nb/Th against Nb	Indicate the composition of the magma source	Hofmann (1988), Schmidberger and Hegner (1999)
	Rb/Y against Nb/Y	Indicate the composition of the magma source and possible crustal contamination	Pearce *et al.* (1990), Taylor and McLennan (1985)

Table 6.2: Major and trace element geochemistry of the Jabal Thalabah Complex

Lithology	SG	SG	SG	SG	MG	GD	GD	GD	GD	GD	HR	HR	HR	HR	CHM	GB	GB	GB	Si	Si	Si	Si	CR
Sample Number	TH5`	TH10`	TH12`	TH12	TH5	TH3	TH7`	TH9	TH18	TH19	TH2`	TH11`	TH13`	TH14`	TH6`	TH1A	TH8	TH17	TH7	TH10	TH13	TH9`	TH15
Majors (wt %)																							
SiO_2	75.39	75.72	74.09	75.17	71.57	76.78	70.55	72.71	70.43	71.2	72.85		68.36	71.42	70.7	52.77	62.89	52.1	75.68	50.71	74.17	75.19	62.3
Al_2O_3	13.21	14.19	12.45	14.55	16.69	13.68	15.53	16.22	16.41	15.89	12.48		12.91	13.55	15.95	18	15.47	17.47	13.77	16.05	14.3	13.32	17.45
Total Fe as FeO	1.28	0.36	2.72	0.73	1.53	1.02	1.98	1.59	1.73	1.46	3.55		4.32	3.93	1.46	10.17	8.00	11.25	1.31	13.5	1.49	1.24	5.76
MgO	0.13	0.04	0.04	0.07	0.79	0.18	0.82	0.73	0.74	0.64	0.3		0.44	0.38	0.09	3.16	1.14	2.84	0.06	3.63	0.1	0.17	3.25
CaO	0.83	0.19	0.86	0.5	1.56	0.84	2.51	2.3	2.43	2.07	0.91		1.22	1.13	1.04	7.56	2.8	7.33	0.21	6.57	0.48	0.35	1.62
Na_2O	4.82	4.45	3.98	4.45	4.35	4.54	4.85	4.46	4.49	4.46	3.28		4.54	4.47	4.7	3.94	4.96	3.42	4.2	3.6	3.42	3.69	5.08
K_2O	3.13	3.51	4.44	3.86	2.74	3.22	2.33	2.37	2.36	2.68	5.09		4.22	4.32	5.42	1.65	2.93	1.78	4.42	1.2	5.17	4.73	1.03
TiO_2	0.09	0.03	0.16	0.04	0.21	0.09	0.22	0.19	0.2	0.17	0.21		0.43	0.39	0.15	2.95	0.88	2.34	0.05	2.93	0.1	0.08	0.65
P_2O_5	0.02	0.01	0.01	0.03	0.06	0.03	0.07	0.06	0.06	0.06	0.03		0.08	0.06	0.02	0.5	0.28	0.38	<0.01	0.8	0.01	<0.01	0.13
MnO	0.03	0.01	0.03	0.01	0.03	0.02	0.03	0.03	0.03	0.03	0.02		0.06	0.05	0.01	0.12	0.13	0.15	0.01	0.14	0.02	0.02	0.06
LOI	0.58	0.74	0.3	0.58	1.18	0.43	0.75	0.7	2.27	2.21	0.73		0.48	0.39	0.27	0.43	0.94	2.12	0.77	1.49	0.91	0.79	2.87
Total	99.51	99.25	99.08	99.99	100.71	100.83	99.64	101.36	101.15	100.87	99.45		97.06	100.09	99.81	101.25	100.42	101.18	100.48	100.62	100.17	99.58	100.2
Traces (ppm)																							
Ba	606	551	74	636	420	525	413	491	548	570	1025	428	431	460	833	472	677	460	94	651	750	400	153
Cu	5	1	2	1	25	5	15	14	13	15	3	5	2	3	1	55	14	65	4	54	11	2	24
Li	12	15	4	11	38	32	40	31	32	31	11	11	14	14	5	84	16	14	14	31	28	25	25
Ni	<1	11	41	<1	4	1	<1	4	3	3	5	48	22	7	<1	31	<1	10	1	21	<1	3	32
Sr	190	59	8	74	273	168	288	341	319	278	204	122	131	127	145	814	420	511	38	901	64	46	173
Y	13	20	18	5	8	4	8	8	8	6	11	47	53	50	8	26	54	41	48	32	44	28	19
Zn	11	<1	45	26	43	28	22	42	39	36	2	54	77	63	7	116	110	128	45	156	141	16	70
Rb	52	73	85	58	48	44	45	41	40	46	117	92	83	88	79	21	45	31	154	19	118	126	19
Zr	97	32	366	57	80	63	76	84	79	75	161	620	782	773	67	304	613	316	235	347	228	150	105
Nb	8	3	20	7	4	7	2	5	4	3	13	47	56	54	4	49	67	33	133	55	34	25	3
Mo	<1	<1	<1	1	1	1	<1	1	1	1	<1	1	2	1	<1	2	3	2	1	3	1	1	1
Sn	1	2	3	2	1	1	<1	1	1	1	1	4	4	4	1	1	3	2	9	2	26	4	1
Hf	3	2	7	2	2	2	2	2	2	2	5	14	18	18	3	6	12	6	9	7	6	6	2
Ta	1	1	1	<1	<1	1	<1	1	<1	<1	1	4	4	4	<1	3	5	2	9	3	3	3	<1
Pb	8	4	<1	18	25	21	6	21	19	18	9	9	9	7	9	10	13	16	20	12	28	12	11
Th	6	3	4	4	3	6	2	3	3	3	15	14	10	13	3	3	8	5	22	4	15	19	2
U	2	1	1	2	1	1	1	1	1	1	3	3	3	3	1	1	2	1	7	1	4	6	1

Explanation of abbreviations: SG, syenogranite, MG, monzogranite, GD, granodiorite, GB, gabbro, CHM, chilled margin, HR, hybrid rock, CR, country rock, Si, silica dyke/vein, F, felsic, M, mafic

Table 6.3: Major and trace elements geochemical analyses of the Jabal Khur Dukhan Complex

Lithology	MiG	AG	AG	MiG	A-SG	A-SG	A-SG	A-SG	A-SG	A-SG	A-SG	A-SG	A-SG	MG	MG	MG	MG	GD	GD	GD	GD	GD	CR
Sample Number	KD1	KD4	KD41	KD2	KD15	KD17	KD21	KD28	KD29	KD34	KD36	KD37	KD38	KD9	KD11	KD12	KD13	KD10A	KD10B	KD14	KD22	KD23	KD19
Majors (wt %)																							
SiO_2	76.93	73.11	74.00	77.90	76.75	75.02	76.12	69.95	74.55	74.80	76.67	76.00	71.51	75.90	72.88	76.15	73.37	69.37		69.90	70.12		49.23
Al_2O_3	13.18	13.47	16.18	12.08	12.13	13.55	12.82	15.89	13.70	13.24	12.62	12.78	14.91	12.43	14.27	12.85	13.25	14.18		15.83	14.66		14.87
Total Fe as FeO	0.51	1.39	1.30	0.94	1.00	1.79	1.40	3.14	1.43	1.21	1.22	0.83	2.36	1.79	2.02	1.86	2.09	4.22		3.19	2.59		14.26
MgO	0.02	0.14	0.04	0.02	0.06	0.23	0.15	0.15	0.14	0.08	0.05	0.02	0.14	0.31	0.31	0.26	0.33	1.02		1.11	0.70		4.38
CaO	0.27	0.24	0.18	0.17	0.46	0.61	0.45	0.39	0.41	0.34	0.40	0.28	0.65	0.92	1.09	0.67	0.99	2.40		2.62	1.66		9.93
Na_2O	4.10	3.07	8.35	3.59	3.86	3.98	3.74	4.60	3.95	3.90	3.82	3.90	4.09	3.83	4.14	3.79	4.01	4.40		4.74	3.60		1.45
K_2O	4.91	6.31	0.13	4.69	4.50	4.91	4.93	6.05	4.96	5.10	4.91	5.08	5.98	3.83	4.65	4.07	4.32	2.23		2.74	4.38		2.14
TiO_2	0.13	0.40	0.19	0.06	0.10	0.17	0.11	0.25	0.11	0.09	0.08	0.06	0.19	0.18	0.20	0.18	0.20	0.50		0.40	0.28		3.84
P_2O_5	<0.01	0.02	0.03	0.01	0.01	0.03	0.01	0.03	0.01	0.01	0.01	<0.01	0.01	0.04	0.05	0.04	0.05	0.19		0.12	0.08		0.51
MnO	<0.01	0.02	<0.01	<0.01	<0.01	0.02	0.01	0.02	0.01	0.01	0.02	0.01	0.03	0.03	0.04	0.02	0.03	0.05		0.06	0.05		0.30
LOI	0.56	0.60	0.36	0.51	0.50	0.51	0.49	0.40	0.46	0.50	0.61	0.49	0.73	0.60	0.49	0.61	0.49	1.05		0.74	0.66		0.46
Total	100.61	98.77	100.76	99.97	99.37	100.82	100.23	100.87	99.73	99.28	100.41	99.45	100.60	99.86	100.14	100.50	99.13	99.61		101.45	98.78		101.37
Traces (ppm)																							
Ba	556	267	14		85	218	150	867	168	109	100	93	747	203	268	200	226	273	236	447	475	744	606
Cu	5	5	2		2	2	1	7	3	2	2	3	4	2	5	4	3	8	3	10	7	6	35
Li	<1	4	6		2	14	5	3	1	1	<1	<1	9	36	54	29	64	110	52	82	54	44	52
Ni	<1	2	<1		<1	<1	<1	<1	<1	1	<1	<1	<1	1	1	1	1	3	1	2	5	2	32
Sr	31	54	140		8	48	22	44	28	10	11	8	46	72	77	62	68	178	78	201	153	161	440
Y	18	80	37		147	64	51	62	42	71	89	43	82	75	78	78	93	49	88	33	49	57	47
Zn	7	88	14		76	95	79	65	81	113	122	59	115	69	102	84	100	166	94	68	64	75	136
Rb	58	105	3		113	105	109	55	106	104	110	123	64	90	108	94	107	91	110	55	119	102	49
Zr	313	88	239		233	210	197	475	203	204	246	175	383	135	174	184	204	223	185	146	200	253	307
Nb	67	40	36		58	35	37	39	36	38	68	43	29	30	58	32	35	19	33	16	19	26	43
Mo	3	4	1		3	1	2	3	1	2	2	2	4	2	1	1	2	1	2	1	2	2	2
Sn	2	3	5		6	6	5	3	7	6	5	6	3	15	5	6	5	1	9	2	4	4	2
Hf	11	4	8		10	7	7	11	7	7	9	7	10	5	6	7	7	5	6	4	6	6	6
Ta	6	4	2		4	3	3	3	3	2	5	3	2	2	4	3	2	1	3	2	2	4	3
Pb	10	27	19		26	18	14	26	18	14	17	10	18	34	26	18	17	15	37	16	16	17	11
Th	7	8	7		11	9	9	17	10	8	11	9	8	8	9	9	11	7	10	9	13	11	4
U	3	3	1		6	3	3	2	3	4	3	4	2	3	3	3	4	2	3	2	3	2	1

Explanation of rocks abbreviations: AG, alkali granite, A-SG, alkali to syenogranite, MG, monzogranite, GD, granodiorite, MiG, microgranite, CR, country rock

Table 6.4: Major and trace element geochemical analyses of the Jabal Al-Massah Complex

Lithology	AG	AG	A-MG	A-MG	A-MG	A-MG	A-MG	A-MG	Por-SG	Por-SG	Por-SG	MG	MG	GD	GD	Xen	Si (V)	CR
Sample Number	JM13	M5	JM7	JM18	JM20	JM24	JM27	JM31	JM4	JM16	JM17	M2	M3	JM33	M4	JM21H	JM2	JM29
Majors (wt %)																		
SiO_2	75.76	76.25	71.82	76.15	73.26	76.17	75.07	75.15	72.12	74.99	73.80	75.28		74.85	68.04		100.05	70.65
Al_2O_3	13.19	12.68	14.98	13.46	14.87	13.54	13.68	13.78	14.74	13.90	13.64	13.19		13.76	15.87		0.07	14.50
Total Fe as FeO	1.29	0.75	0.77	0.47	0.61	0.39	0.54	1.00	1.10	0.85	1.27	1.40		1.25	2.97		0.02	3.83
MgO	0.05	0.03	0.19	0.07	0.14	0.09	0.10	0.17	0.22	0.25	0.31	0.28		0.39	1.05		0.01	1.13
CaO	0.21	0.23	0.86	0.18	0.47	0.47	0.48	0.75	0.79	0.76	1.07	0.85		0.90	2.57		0.02	4.25
Na_2O	4.33	3.49	4.66	4.17	5.02	4.85	3.98	3.88	4.18	4.37	4.19	3.78		4.64	5.11		0.01	2.00
K_2O	5.28	5.77	5.25	5.25	4.94	4.52	5.39	5.21	5.68	4.41	4.42	4.44		3.26	2.51		<0.01	2.63
TiO_2	0.08	0.08	0.13	0.05	0.08	0.07	0.09	0.14	0.19	0.13	0.20	0.16		0.19	0.49		0.01	0.39
P_2O_5	0.01	0.01	0.02	0.01	0.01	<0.01	<0.01	0.03	0.03	0.03	0.04	0.03		0.05	0.18		<0.01	0.05
MnO	0.01	0.04	0.03	0.04	0.04	0.04	0.03	0.03	0.03	0.06	0.07	0.04		0.06	0.05		<0.01	0.08
LOI	0.29	0.28	0.44	0.38	0.40	0.29	0.29	0.20	0.30	0.20	0.56	0.25		0.51	0.67		0.10	1.18
Total	100.50	99.61	99.15	100.23	99.84	100.43	99.65	100.34	99.38	99.95	99.57	99.70		99.86	99.51		100.29	100.69
Traces (ppm)																		
Ba	60	46	423	123	203	73	115	801	908	430	556	580	869	850	1128	94	1	626
Cu	1	1	1	<1	<1	<1	<1	1	1	1	2	1	<1	1	5	123	<1	5
Li	<1	15	20	5	9	3	5	15	7	51	36	19	17	23	19	<1	1	8
Ni	<1	2	<1	<1	<1	<1	<1	1	1	1	1	<1	13	1	7	13	<1	3
Sr	9	689	135	21	63	19	37	185	191	169	217	159	1109	314	800	98	1	187
Y	35	4	8	7	10	4	4	13	4	12	12	6	4	9	3	18	<1	21
Zn	34	4	31	25	31	23	19	26	27	37	39	6	4	29	25	129	2	54
Rb	104	53	78	158	116		63	64	49	104	87	55	60	90	44	1	<1	44
Zr	241	173	78	38	64		50	122	114	71	128	144	97	91	278	42	3	146
Nb	27	2	4	6	9		4	5	4	11	9	3	2	7	1	1	1	3
Mo	2	<1	1	1	1		1	1	1	1	1	<1	<1	1	<1	1	1	2
Sn	7	<1	1	1	1		<1	1	<1	1	1	1	<1	<1	<1	<1	1	2
Hf	7	4	2	1	2		1	3	3	2	3	4	3	2	6	1	<1	3
Ta	2	<1	<1	<1	1		<1	<1	<1	1	<1	<1	<1	1	<1	<1	<1	<1
Pb	21	14	24	18	21		21	22	22	23	22	14	18	24	11	8	11	14
Th	10	7	9	3	6		5	11	6	6	5	6	9	5	5	1	1	4
U	3	2	2	1	3		1	2	1	6	2	2	2	1	2	<1	<1	1

Explanation of abbreviations: AG, alkali granite, A-MG, alkali to monzogranite, Por-SG, porphyritic syenogranite, MG, monzogranite, GD, granodiorite, Xen, xenolith, MiG, microgranite, Si, dyke/vein, CR, country rock.

Table 6.5: Major and trace element geochemical analyses of the Jabal Raydan and the Jabal az Zuhd Plutons

Lithology	A-SG	A-SG	A-SG	A-SG	A-MG	A-MG	A-MG	MiG	Si (F)	Si (F)	CR	AG	AG	AG	AG	AG	AG	AG	AG	Por-MG	Por-MG
Sample Number	JR3C	JR9	JR19	JR20	JR12	JR13	JR3E	JR3D	JR1A	JR6	JR2B	JZ2	JZ4	JZ6	JZ8	JZ10	JZ12	JZ14	JZ5	JZ1A	JZ1B
Majors (wt %)																					
SiO_2	77.64	71.87		78.23	72.54	71.43	76.58			91.18	48.36	72.33	72.11	74.63	74.28	73.31	72.85	71.25	73.94	73.91	
Al_2O_3	13.16	12.44		12.52	13.25	13.45	13.1			4.74	16.7	11.47	10.46	10.95	10.27	11.58	10.15	14.86	10.7	13.49	
Total Fe as FeO	0.49	3.3		0.79	2.26	3.3	0.53			0.32	9.23	6.04	5.91	3.69	6.48	3.59	6.04	0.82	4.61	1.62	
MgO	0.05	0.32		0.03	0.28	0.4	0.04			0.06	9.73	0.37	0.23	0.05	0.11	0.09	0.06	0.19	0.09	0.55	
CaO	0.58	0.73		0.5	1.1	1.48	0.79			0.18	9.7	1.05	0.59	0.22	0.38	0.5	0.35	0.86	0.61	1.4	
Na_2O	4.85	4.42		4.94	4.58	3.97	4.04			1.37	2.1	4.55	4.4	3.84	3.12	4.3	4.26	4.64	3.75	4.2	
K_2O	3.98	4.79		3.69	4.54	4.09	4.37			1.53	1.32	4.38	4.64	5.24	4.7	5.16	4.69	5.2	4.72	3.99	
TiO_2	0.03	0.35		0.04	0.25	0.42	0.05			0.04	0.84	0.5	0.43	0.12	0.12	0.19	0.56	0.13	0.43	0.22	
P_2O_5	0.01	0.01		0.01	0.04	0.05	0.01			0.08	0.11	0.1	0.07	0.01	<0.01	0.03	0.02	0.02	0.04	0.05	
MnO	0.01	0.02		0.01	0.04	0.04	0.01			0.01	0.15	0.13	0.14	0.05	0.03	0.06	0.11	0.04	0.09	0.07	
LOI	0.50	0.28		0.48	0.43	0.41	0.37			0.39	1.94	0.21	0.11	0.4	0.3	0.11	0.3	0.45	0.22	0.69	
Total	101.30	98.53		101.24	99.31	99.04	99.89			99.90	100.18	101.13	99.09	99.27	99.79	98.92	99.39	98.46	99.20	100.19	
Traces (ppm)																					
Ba	17	4	211	173	260	401	352	1077	114	121	148	78	53	75	92	87	75	45	60	305	330
Cu	<1	<1	3	<1	4	6	<1	1	<1	117	87	8	3	6	5	2	5	2	5	6	6
Li	<1	<1	<1	<1	14	63	<1	6	<1	<1	8	73	32	54	23	6	27	13	<1	13	41
Ni	<1	<1	1	<1	1	1	<1	<1	<1	<1	177	<1	<1	1	<1	<1	<1	<1	<1	2	3
Sr	7	3	66	63	76	126	81	300	38	60	241	30	8	21	31	5	6	6	12	183	236
Y	3	16	24	5	57	72	10	18	11	21	17	72	11	160	48	63	37	77	12	41	47
Zn	19	41	94	37	75	98	20	53	12	18	70	201	147	272	155	96	181	151	76	48	83
Rb	32	41	56	57	79	121	58	70	84	33	39	97	117	138	69	81	80	97	89	107	
Zr	9	22	331	130	291	354	25	193	64	203	77	99	57	345	248	470	410	1017	235	188	
Nb	6	7	26	11	33	43	19	10	20	15	3	54	10	100	25	38	33	65	2	42	
Mo	1	1	3	1	1	1	1	1	1	1	1	1	2	1	4	1	1	2	2	1	
Sn	<1	1	3	12	8	4	<1	1	1	<1	1	7	1	19	3	3	12	3	25	4	
Hf	<1	1	7	4	7	10	1	4	3	6	1	3	1	13	5	10	9	19	9	6	
Ta	<1	<1	1	1	3	4	2	1	2	1	<1	4	<1	12	1	3	2	5	<1	4	
Pb	20	11	14	13	14	19	15	17	17	11	9	14	14	10	8	14	16	16	10	21	
Th	2	3	5	3	7	11	4	9	8	4	1	7	1	7	2	5	4	10	<1	14	
U	1	1	2	1	2	4	2	3	3	2	1	1	1	2	1	2	1	3	1	3	

Explanation of rocks abbreviations: AG, alkali granite, A-SG, alkali to syenogranite, A-MG, alkali to monzogranite, Por-MG, porphyritic monzogranite, Si, silica dyke/vein, CR, country rock.

VI.3. The use of geochemical classifications for granitic rocks

Various geochemical classification diagrams were used in this chapter for the purpose of characterizing the studied plutons. These diagrams were carefully selected, as some commonly used genetic and tectonic diagrams can produce uncertain and confusing results.

Frost and Frost (2010) clarified why there is no one specific geochemical classification scheme for granitic rocks in widespread use, because the main mineral constituents of the granitoids (quartz, feldspars and ferromagnesian minerals) can be produced by several processes and in different tectonic regimes. Maniar and Piccoli (1989) further highlighted the limitations of some of these diagrams. They said firstly, that the data used were gathered from well-characterized Phanerozoic granitoids and not from Proterozoic rocks. Secondly, the classification diagrams have been established empirically and have used granitic suites which are presumed to be representative for that tectonic environment. Thirdly, applying different classification schemes to one granite can show different results. A good example of a granitic classification scheme that shows uncertain results is the so-called alphabetic (A1 and A2-I-S-C-M) classification of granitic rocks (Frost *et al.* 2001). It has resulted in some confusion in the definition of granite type and characteristics (Maniar and Piccoli, 1989), as there are some overlaps between them. For instance, the anorogenic A1-type that relates to hotspots or plumes can be considered as a subtype of the M-type that has a mantle origin, while the post-orogenic, A2-type that is generated from crustal melting from extended subduction collision cycles can also be considered as a subtype of the I-type that has a crustal source (Eby, 1992). Furthermore, both the A-type granites derived from recycled, dehydrated continental crust and the M-type granites that are derived from melting of subducted oceanic crust can be considered as subgroups of the I-type granites. In addition, there is an overlap between the A1 and A2 types, as some of the A2 granites can have a mantle origin, as do the A1 granites.

Frost *et al.* (2001) have established the foundation of a new geochemical classification scheme for granitic rocks, trying to avoid the misleading results delivered from many other granite classifications. Their classification is based on three variables: the Fe-number, which is expressed as $FeO^{tot}/ (FeO^{tot} + MgO)$, the MALI, or modified alkali-lime index (Na_2O+K_2O-CaO) and the aluminum saturation index (ASI) = [(Al/Ca-

1.67+Na+K)]. The Fe-number is used to distinguish Fe-enriched granitoids from the magnesian types and both can be further classified by using the MALI diagram into alkali, alkali-calcic, calcic-alkalic and calcic and/or using the ASI into peraluminous, metaluminous or peralkaline. This scheme and some other diagrams (primarily using trace element compositions to derive information about the nature of the source rock and the melt development history, and secondarily for the tectonic environment) have provided consistent results and have been used in this chapter for granite classification.

To summarize, it was decided to choose those diagrams and schemes that do not show contradictions or overlaps (the indicated source region can be represented by more than one magma type) and are mostly recommended and used by Frost *et al.* (2001) and by Frost and Frost (2010).

VI.4. Major and Trace Elements Characteristics

The major oxides have been used for classifying the studied rocks, determining their magma series, magmatic affinity and normative composition, while the trace elements were mainly used for identifying the geological setting. The major and trace elements were also used in other applications: to initially define the magmatic processes (majors and traces vs. SiO_2 and using normalized REE diagrams) and to assess the possibility of any alteration and/or mineralization that may have affected the granitic suites (majors and traces vs. loss on ignition values).

VI.4.1. Major and trace element variation diagrams

The major and trace element variation (Harker) diagrams are not a very helpful tool in distinguishing clear relationships, as many of the diagrams do not show any clear trend. Only a few examples are given to clarify the relationship between silica and some other major and traces elements, and to indicate the affect of alteration on some elements from different plutons (Fig 6.1).

VI.4.1.1. Majors and traces versus SiO_2

The major and trace element variation diagrams indicate the following:

- Jabal Thalabah: The alkali and syenogranites display an increase in Al and K with increasing Si; the granodiorites show the opposite relationship. The granitoids in general display a decrease in FeO* and Rb/K with increasing Si.

- Jabal Khur Dukan: The alkali-syenogranites and the monzogranite display a decrease in Al, Na and Fe, and an increase in K, with increasing Si.

- Jabal Al-Massah: the granitoids display a general increase in K and a general decrease in Al, Na and Fe with increasing Si.

- Jabal Raydan: the alkali-granites and monzogranites mostly display a decrease in Al, K, and Rb/K, and an increase in Na, with increasing Si.

- Jabal az Zuhd: the alkali granite displays a general increase in K and Fe, and a general decrease in Na and Rb/K with increasing Si.

Fractionation in granites is normally expected to increase Si, K and Na and decrease Ti, Mn, Ca and P. The other major elements (Al, Fe and Mg) do not usually show a constant and consistent trend of fractionation, as they can increase up to a certain point and then start to decrease (a concave-shaped trend).

To summarize, in comparison with the other plutons, Jabal Khur Dukhan and Jabal Al-Massah seem to be more dominated by fractional crystallization trends as the Al and Fe contents seem to follow the trend of a fractionating magma. However, the plutons of Jabal Khur Dukhan and Jabal Al-Massah do not show such clear fractionation trends and other processes are probably also involved. They could have been affected by post-magmatic fluids (subsolidus) as the behavior of the alkali elements (Na and K) do not always show the clear increment which is expected to be present with normal fractionation.

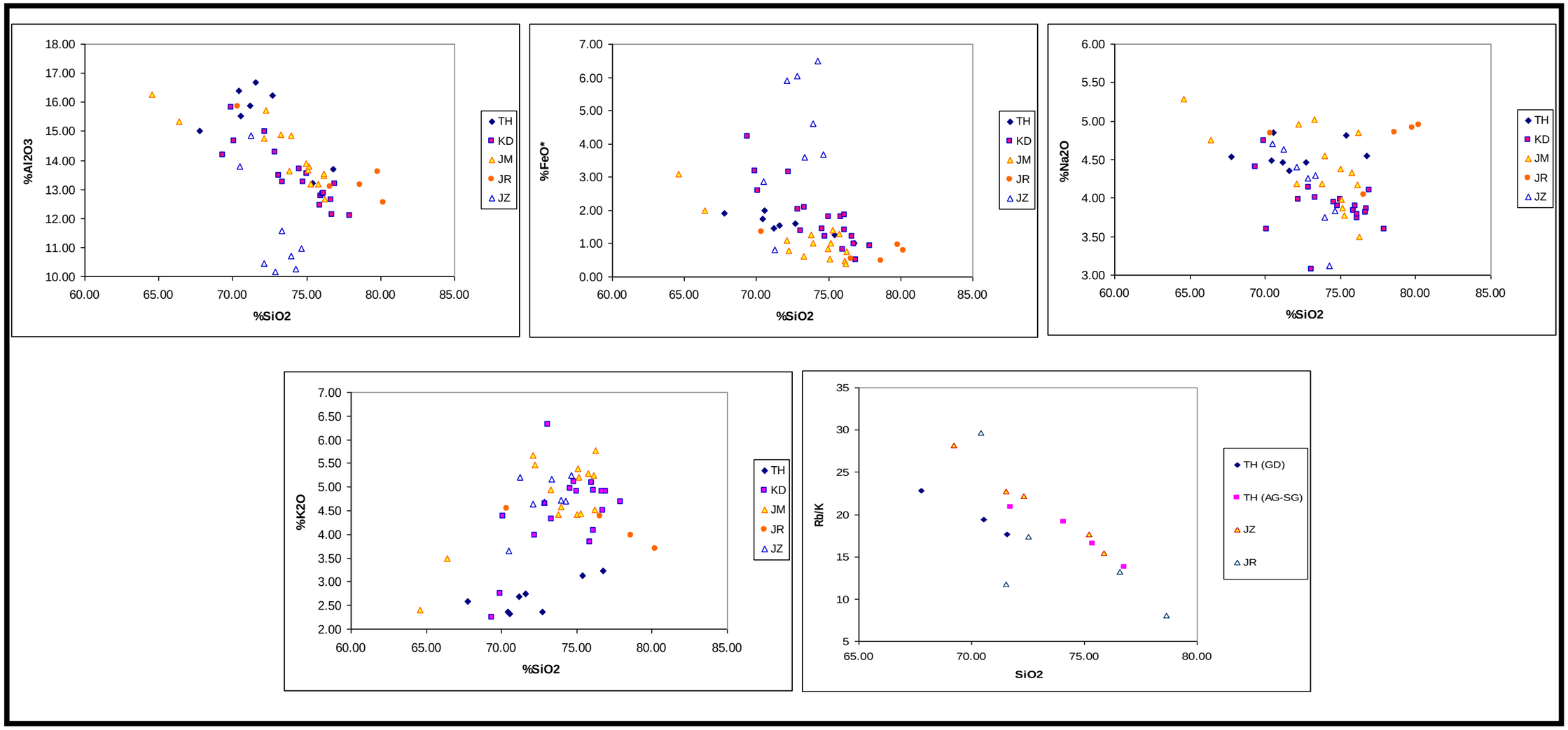

Figure 6.1: Selected variation diagrams for the studied rocks to illustrate possible trends of fractionation

VI.4.1.2. The affect of alteration

Certain elements were plotted against the loss on ignition (LOI) values (Fig. 6.2), the latter representing the content of volatiles (e.g. H_2O, CO_2, S) and therefore a possible indicator of the affect of fluids on the chemical composition. Obviously LOI alone can not represent just alteration as volatile content may also increase with the fractionation (or maybe even assimilation). Although there is no definite LOI value which would indicate an altered granite, a content of <0.5% of LOI is typical for fresh granite and therefore in these diagrams values exceeding this limit are likely to be related to alteration rather than other process.

Indication for alteration:

- Jabal Thalabah: As LOI increases the granodiorites show a slight enrichment in K (supported by the presence of muscovite) and the alkali granites show and increase in Na (secondary albite?). The alkaline hybrid rocks show a slight depletion in Na and K. These elements are the main constituents of feldspars and their depletion was possibly compensated by the presence ferromagnesian minerals (e.g. amphibole, biotite and chlorite).

- Jabal Khur Dukhan: As LOI increases, the granodiorites show a clear enrichment in Na. Again, this could relate to secondary albite formation associated with hydrothermal alteration. Some of the alkali to syenogranites show a depletion in their Si content which may relate to the development of secondary ferromagnesian minerals (e.g. chlorite) (also supported by the high Fe content of KD28). The presence of fluorite also supports the presence of late-stage, hydrothermal fluids.

- Jabal Al-Massah: As LOI increases the granitoids show a slight enrichment in Na. This could be due to normal fractionation but the presence of some hydrothermal minerals (e.g. chlorite and muscovite) and slightly altered perthites suggest a slight alteration affect.

- Jabal Raydan: As LOI increases, the granites show a slight enrichment in Na and a slight depletion in K. With normal fractionation both elements might be expected to increase. It is possible that the Na enrichment and K depletion

represent subsolidus alteration and feldspar replacement. The action of late hydrothermal fluids is also supported by the presence of fluorite in the alkali to monzogranites.

- Jabal az Zuhd: As LOI increases the alkali granites show a slight enrichment in Al and slight depletion in the K which is not compatible with normal fractionation. This might equate to the presence of some secondary minerals like muscovite and chlorite.

It is difficult to distinguish the LOI related to the magma and that due to secondary alteration. However, by using both the mineralogy and the geochemistry an alteration impact is indicated. The stronger affect of hydrothermal alteration is supported by the presence of secondary minerals and by the fact that some of the altered granites plot away from the minimum melt compositions in the haplogranite system, either indicating the presence of other elements (e.g. F) or the affects of alkali metasomatism (Fig. 6.5).

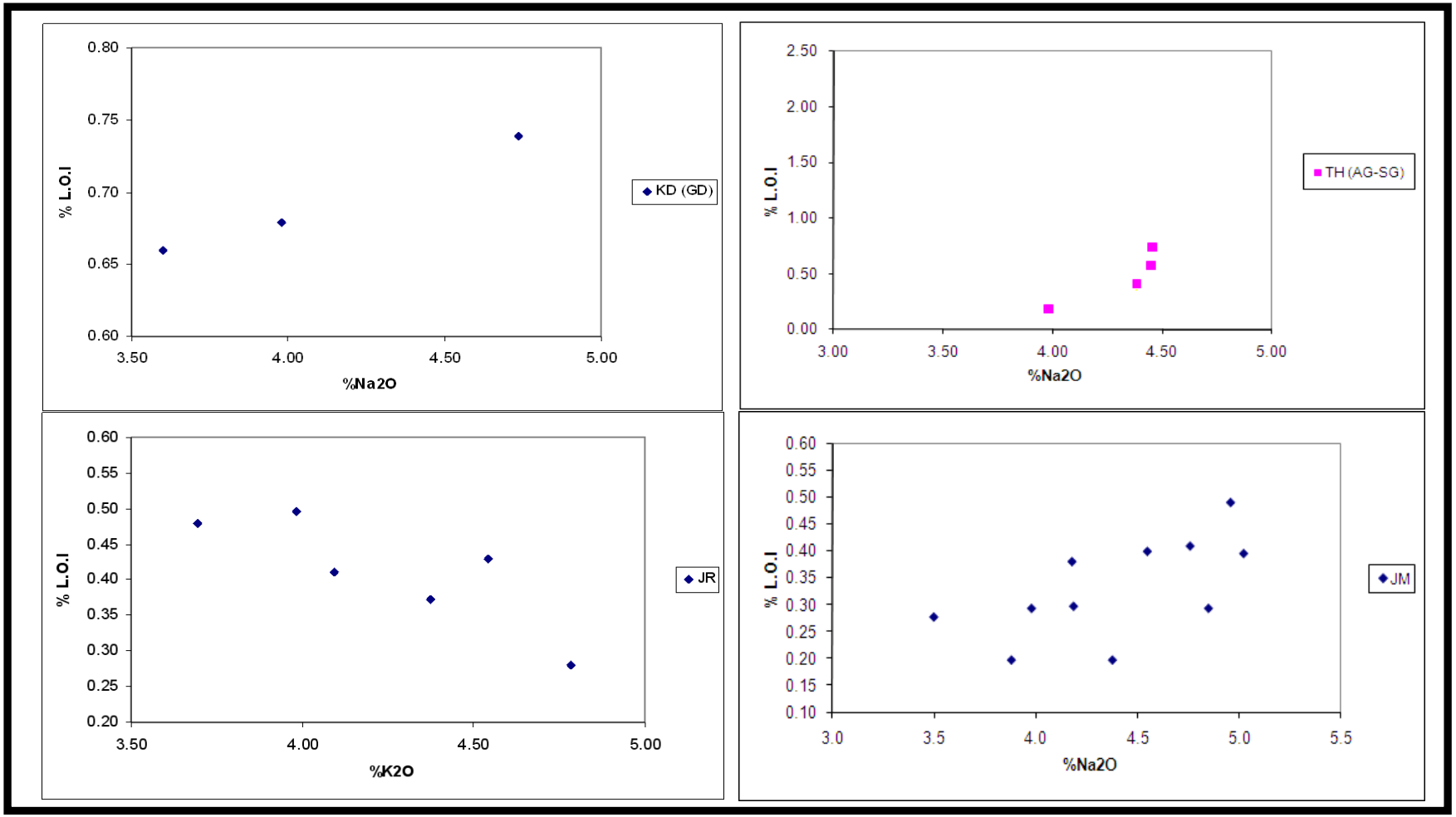

Figure 6.2: Affect of alteration on element content in selected granitoids. Explanation: TH, Jabal Thalabah, JM, Jabal Al-Massah, KD, Jabal Khur Dukhan, JR, Jabal Raydan, AG, alkali granite, SG, syenogranite, GD, granodiorite.

VI.4.2. Comparison with 'average' granites

The range in major element chemistry of the different plutons is summarized in Table 6.6 and compared with some world average granite values in Table 6.7. Over the last few decades various ranges of averages from different tectonic settings have been proposed. This may increase the uncertainty of ideal or typical ranges of averages of granitic rocks. Although, the studied granites in some cases do not match the composition of average granites that does not necessarily mean that they are abnormal; such differences can be accommodated either by some global plutons with known tectonic setting (Table 6.8 to 6.12) or by others plutons (Table 6.13) from the Arabian Shield. Comparing the studied granites with those from a known tectonic setting may give an indication for the most likely tectonic environment for the studied pluton.

To summarize, yes the studied granite are typical granites in terms of their composition but some elements plot outside the range (e.g. Si in some of the alkali to syenogranites of Jabal Khur Dukhan and Raydan, table 6.17) and this might in some cases be related to alteration and redistribution of elements due to the fluid activity.

VI.4.3. Geochemical classification, magmatic series and magmatic affinity

The TAS diagram of Wilson (1989) and the subalkalic subdivision diagram of Le Maitre *et al.* (1989) were originally used for volcanic rocks but are now also used to display the overall magmatic series. The first diagram was derived from the TAS diagram that was used to name volcanic rocks as well as discriminate between rocks of the alkaline and sub-alkaline series, while the second diagram was used to assess the K-enrichment within the magmatic series. Based on the TAS diagram (Fig.6.3a) it appears that most of the samples from the Jabal Al-Massah, Jabal Raydan and Jabal az Zuhd plutons plot in the alkaline field, below the alkaline line for the Jabal Thalabah pluton, and equally in both fields for the Jabal Khur Dukhan pluton. In the Jabal az Zuhd, Jabal Raydan and Jabal Khur Dukhan (outer part) plutons, the general trend is that the total alkalis slightly decrease with increasing silica.

Table 6.6: Major oxide ranges (wt %) for the studied plutons.

Name of pluton / Major elements	Jabal Thalabah	Jabal Khur Dukhan	Jabal Al-Massah	Jabal Raydan	Jabal az Zuhd
SiO_2	68.36-75.39	69.95-77.90	71.82-76.25	70.43-80.23	71.25-74.63
Al_2O_3	11.45-14.55	12.08-16.98	12.68-14.98	12.44-13.45	10.15-14.86
K_2O	3.13-5.09	0.13-6.05	4.41-5.77	3.69-4.79	4.38-5.24
Na_2O	3.28-4.82	3.07-8.35	3.49-5.02	3.97-4.94	3.12-4.64
CaO	0.06-1.22	0.17-1.15	0.18-0.86	0.23-1.48	0.22- 1.05
FeO	0.36-4.32	0.51-3.14	0.39-1.40	0.49-2.30	0.82-6.48
MgO	0.04-0.44	0.02-0.40	0.03-0.28	0.02-0.40	0.05-0.37
TiO_2	0.03-0.43	0.06-0.23	0.05-0.19	0.03-0.25	0.12-0.56
P_2O_5	0.01-0.08	0.00-0.06	0.00-0.03	0.01-.0.05	0.00-0.07
MnO	0.01-0.06	0.00-0.04	0.01-0.06	0.01-0.04	0.03-0.14

Table 6.7: Major oxides values (wt %) for average granites and for granites with known tectonic environments.

Major oxides	Krauskopf (1967)	Cox *et al.* (1979)	Krauskopf and Bird (1985)	Pearce *et al.* (1984) VAG	Pearce *et al.* (1984) WPG	Pearce *et al.* (1984) CCG
SiO_2	69.21	71.3	72.77	68.43-74.50	70.41-76.02	70.69-76.20
Al_2O_3	14.55	14.32	14.04	12-14.60	11.68-13.01	13.34-15.80
K_2O	3.86	4.07	5.42	0.28-5.51	4.40-5.46	3.38-5.83
Na_2O	3.78	3.68	3.32	3.56-5.33	2.90-6.14	2.52-4.37
CaO	2.24	1.84	1.39	0.29-3.06	0.06-1.34	0.69-2.76
FeO	3.47	1.21	1.80	1-4.85	1.95-4.48	0.26-4.73
MgO	0.66	0.71	0.40	0.07-1.35	0.08-0.17	0.11-2.40
TiO_2	0.35	0.31	0.25	0.16-0.53	0.19-0.33	0.07-0.66
P_2O_5	0.16	0.12	0.09	0.01-0.12	0.03-0.06	0.01-0.23
MnO	0.06	0.05	0.03	0.01-0.13	0.02-0.20	0.00-0.10

Explanation: the first three columns represent world average granites, while the next three represent the range of element contents in volcanic-arc granites, VAG, within-plate granites, WPG and continental-collision granites, CCG, respectively.

Table 6.8: Comparison of the major oxide content (wt %) of Jabal Thalabah with that of Table 6.7

Name of pluton / Major elements	Jabal Thalabah	Comment
SiO_2	Varies	Mostly accommodated by VAG and CCG.
Al_2O_3	Mostly BAV	Mostly accommodated by VAG and CCG).
K_2O	Mostly WTR	Some typical VAG accommodate the full range.
Na_2O	Mostly AAV	This range is not accommodated by specific tectonic setting.
CaO	BAV	This range is not accommodated by specific tectonic setting.
FeO	Varies	Some typical CCG accommodate the full range.
MgO	Mostly BAV	Mostly accommodated by VAG. Still shows few low values. (see table 6.13)
TiO_2	Mostly BAV	Mostly accommodated by VAG and CCG. Still shows few low values. (see table 6.13)
P_2O_5	BAV	Some typical VAG and CCG accommodate the full range.
MnO	Some are BAV	Some typical VAG and CCG accommodate the full range.

Table 6.9: Comparison of the major oxides content (wt %) of Jabal Khur Dukhan with that of Table 6.7

Name of pluton / Major elements	Jabal Khur Dukhan	Exception	Comment
SiO_2	Mostly AAV		Mostly accommodated by CCG. Still shows few high values (See table 6.13).
Al_2O_3	Varies		Mostly accommodated by CCG and VAG. Still shows few high values (See table 6.13).
K_2O	Varies		Mostly accommodated by CCG.
Na_2O	Some are AAV	KD41 is very high	Some typical WPG accommodate most of the range.
CaO	BAV		Some typical WPG accommodate the full range.
FeO	Mostly WTR		Some typical CCG accommodate the full range.
MgO	BAV		See table 6.13.
TiO_2	BAV		Some typical CCG accommodate the full range.
P_2O_5	BAV		Mostly accommodated by CCG. Still shows few low values. (See table 6.13).
MnO	BAV		Some typical CCG accommodate the full range.

Table 6.10: Comparison of the major oxide content (wt %) of Jabal Al-Massah with that of Table 6.7

Name of pluton / Major elements	Jabal Al-Massah	Comment
SiO_2	Mostly AAV	Some typical CCG accommodate the full range. Most of the value can be also found with WPG.
Al_2O_3	Varies	Found in different (not restricted) tectonic setting.
K_2O	Some are AAV	Some typical CCG accommodate the full range. Most of the value can be also found with WPG.
Na_2O	Mostly AAV	Found in different (not restricted) tectonic setting.
CaO	BAV	Some typical WPG accommodate the full range. However, some can be found with typical CCG and VAG.
FeO	Mostly BAV	Some typical CCG accommodate the full range.
MgO	BAV	Mostly accommodated by VAG. Still shows few low values (See table 6.13).
TiO_2	BAV	Mostly accommodated by CCG.
P_2O_5	BAV	Mostly accommodated by VAG and CCG. Still shows few low values (See table 6.13).
MnO	Mostly WTR	

Table 6.11: Comparison of the major oxide content (wt %) of Jabal Raydan with that of Table 6.7

Name of pluton / Major elements	Jabal Raydan	Exception	Comment
SiO_2	Some are AAV		See table 6.13
Al_2O_3	BAV		Some typical VAG accommodate the full range. However, some can be also found with some typical CCG
K_2O	Mostly are WTR	JR20 is BAV	Some typical VAG and CCG accommodate JR20
Na_2O	AAV		Some typical VAG and WPG accommodate the full range
CaO	Mostly are BAV	JR13 is WTR	This range is not accommodated by specific tectonic setting
FeO	Some are BAV		The BAV can be found with CCG
MgO	Mostly are BAV	JR13 is WTR	See table 6.13
TiO_2	Mostly are BAV	JR12 is WTR	See table 6.13
P_2O_5	BAV		Some typical VAG and CCG accommodate the full range. Most of the value can be also found with WPG
MnO	BAV		Some typical VAG and CCG accommodate the full range. Most of the value can be also found with WPG

Table 6.12: Comparison of the major oxide content (wt %) of Jabal az Zuhd with that of Table 6.7

Name of pluton / Major elements	Jabal az Zuhd	Comment
SiO_2	Mostly AAV	The AAV is accommodated by some typical WPG.
Al_2O_3	Mostly BAV	See table 6.13.
K_2O	WTR	
Na_2O	Mostly AAV	Some typical WPG accommodate the full range.
CaO	BAV	Some typical WPG accommodate the full range.
FeO	Mostly AAV	See table 6.13.
MgO	Mostly BAV	Some typical VAG accommodate most of the range.
TiO_2	Varies	Some typical CCG accommodate the full range.
P_2O_5	Mostly BAV	Some are accommodated by typical WPG and others by typical VAG.
MnO	Some are AAV	Some typical WPG accommodate the full range.

Table 6.13: Examples for some out of range values from the studied plutons

Element, case and pluton	Examples from the Arabian Shield
Si, enrichment, JR and KD	Huqban AFG (Du Bray, 1986) located northeastern Arabian Shield.
Al, enrichment , KD	Some Sy (Ramsay, 1986), located in Midyan and Central Hijaz regions.
Al, depletion, TH and JZ	Low-Ca AG (Ramsay, 1986), located in Midyan and Central Hijaz regions.
Fe, enrichment , JZ	Jabal Hamra and Jabal Abu-ad Dud AFG (Jackson and Douch, 1986), located in Hijaz region.
Mg, depletion, All	Umm Al-Suqian MiG (Bokhari *et al*., 1986), located in southern Najd region.
Ti, depletion, TH and JR	Sitarah AFG (Du Bray, 1986) located northeastern Arabian Shield.
P, depletion, JM and KD	Jabal Sa'id AMiG (Hackett, 1986), located in Hijaz region.

Explanation of abbreviations: VAG, volcanic arc granite, WPG, within-plate granite, CCG, continental collision granite TH, Jabal Thalabah, KD, Jabal Khur Dukhan, JM or M, Jabal Al-Massah, JR, Jabal Raydan, JZ, Jabal Az Zuhd, within-plate granite, CG, continental collision granite, AAV, above the average granite, WTR, within the range of the average granites, BAV, below the range of the average granites, AFG, alkali-feldspar granite, Sy, syenotoid, AG, alkali granite, MiG, micro-granite, AMiG, alkali micro-granite.

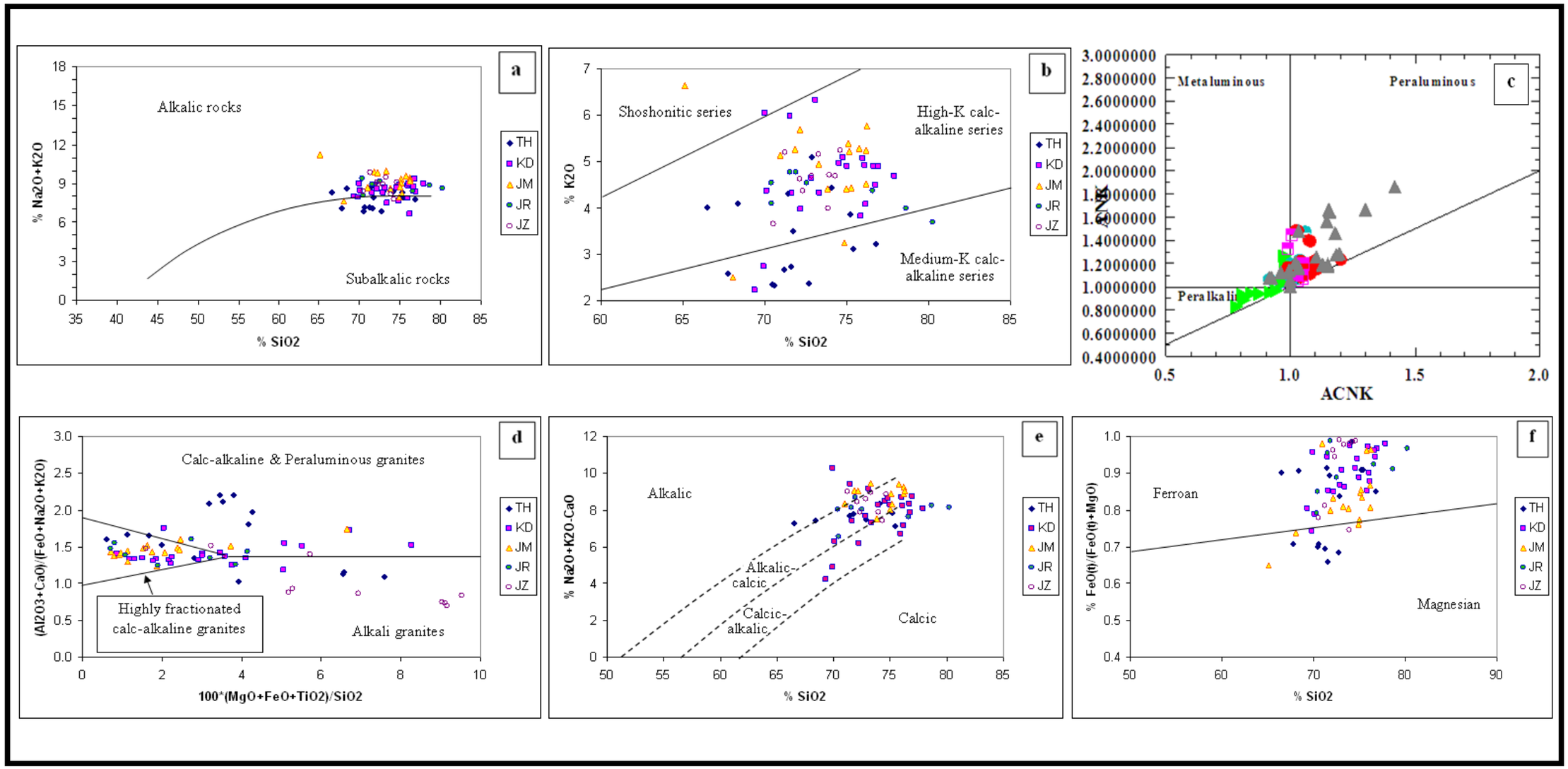

Figure 6.3:Plots for the studied granitoids using geochemical classification diagrams of (a) TAS of Wilson (1989), (b) subalkalic subdivision of Le Maitre *et al*. (1989), (c) Alumina saturation index diagram Rollinson (1993) , (d) 100 $(MgO+FeO^*+TiO_2)/SiO_2$ vs. $(Al_2O_3+CaO)/(FeO^*+Na_2O+K_2O)$ of (Sylvester, 1989), (e) Na_2O+K_2O-CaO vs. SiO_2 of Frost *et a*l. (2001) and (f) FeO/(FeO+MgO) vs. SiO2 of Frost *et al*. (2001). Explanation of the symbols in the diagram (c): Jabal Thalabah granitoids, grey triangle, Jabal Khur Dukhan granitoids, red circle, Jabal Al-Massah granitoids, half-filled pink square, Jabal Raydan granitoids, half-filled blue circle, Jabal az Zuhd granitoids, bright green triangle. Explanation of terms for the other diagrams: TH, Jabal Thalabah, KD, Jabal Khur Dukhan, JM, Jabal Al-Massah, JR, Jabal Raydan, JZ, Jabal az Zuhd.

The magmatic series for the studied granitoids were identified by using the TAS and the subalkalic subdivision (Fig. 6.3b) diagrams:

1- Jabal az Zuhd: alkaline, high-K, calc-alkaline.

2- Jabal Raydan: alkaline, medium to high-K, calc-alkaline for alkali and syenogranites and high-K, calc-alkaline for monzogranites.

3- Jabal Al-Massah: alkaline, high-K, calk-alkaline for the alkali-syeno and monzogranites and subalkaline, medium-K, calk-alkaline for the granodiorites.

4- Jabal Khur Dukhan: alkaline, high-K, calk-alkaline for alkali granites, sub-alkaline, high-K calk-alkaline for syenogranites and sub-alkaline, medium to high-K calk-alkaline for monzo and granodiorites.

5- Jabal Thalabah: alkaline, high-K, calc-alkaline for the alkali granites and subalkaline, medium-K, calk-alkaline for the syeno, monzo and granodiorites.

Based on the A/CNK diagram (Fig. 6.3c) of Pearce *et al.* (1984), the rocks are low-metaluminous to variable peraluminous for the Jabal Thalabah pluton, low peraluminous for the Jabal Khur Dukhan pluton and the Jabal Al-Massah pluton, low-metaluminous to peraluminous for the Jabal Raydan pluton and finally the fresh alkaline rocks of Jabal az Zuhd pluton are variably per-alkaline, while the slightly altered porphyritic syenogranite shows metaluminous characteristics.

Based on the 100 $(MgO+FeO^*+TiO_2)/SiO_2$ vs. $(Al_2O_3+CaO)/(FeO^*+Na_2O+K_2O)$ diagram (Fig. 6.3d) of Sylvester (1989), the porphyritic syenogranites of Jabal az Zuhd and the granodiorites of Jabal Thalabah, Jabal Khur Dukhan and Jabal Al-Massah are un-fractionated and calc-alkaline, while most of the other granites are highly fractionated calcic-alkaline. Only the Jabal az Zuhd and Jabal Thalabah alkali granites plot entirely in the alkaline field, while the other alkali granites are distributed between the alkaline and the highly fractionated, calcic-alkaline fields.

Based on the Na_2O+K_2O-CaO vs. SiO_2 and the FeO/(FeO+MgO) vs. SiO2 diagrams (Fig. 6.3e and f) of Frost *et al*. (2001), it appears that the granodiorites of Jabal Thalabah and Jabal Al-Massah are magnesian, the Jabal Khur Dukhan granodiorites and the porphyritic syenogranites of Jabal az Zuhd granodiorites lie along the discrimination line (magnesian to ferroan) , while the other granitoids are ferroan. Most of the ferroan granitoids are alkalic-calcic to calcic-alkalic and only a few granites of Jabal az Zuhd, Jabal Al-Massah and Jabal Raydan plot in the alkalic field.

To conclude, the studied granitoids show characteristics which are alkalic to subalkalic and medium to high K calc-alkaline series; they are mostly highly fractionated, ferroan, alkalic-calcic to calcic alkalic granitoids and magmatic affinity ranges from peralkaline to mildly metaluminous to peraluminous. The subalkalic, magnesian, peraluminous varieties are mostly represented by the granodiorites which fit into the medium K calc-alkaline series. Jabal az Zuhd appears to have the most alkaline granites, as it is the only pluton that shows a peralkaline magmatic affinity. In addition to the above applications, the geochemical classifications can also be used to throw light on the alkaline nature, source region and tectonic environment. The implications of these observations are further discussed in Chapter 9.

VI.5. Rock Classification using the R1-R2 diagram

The R1-R2 multi-cationic diagram (Fig. 6.4) uses some major oxides to provide more precise names for the studied rocks. The diagram is based on the cation proportions of the plutonic rocks, to include all of the major cations, normative mineralogy, the degree of silica saturation and the combined changes in Fe/ (Fe+Mg) and (Ab+Or)/An ratios. The R 1 and R 2 parameters were calculated from the chemical analyses (oxide percentages converted to millications).

For the Jabal Thalabah pluton, most of the samples from the outer part of the pluton plot in the field of syenogranite and less plot in the alkaline field; the samples that represent the inner part of the pluton (the main body) plot in the granodiorite field, with less in the monzogranite field. For the Jabal Khur Dukhan pluton, most of the investigated samples from the outer pluton, which represents the main body, plot in the field of alkali granite and less plot in the syenogranite field; the samples that represent the inner pluton plot in both the monzogranite and the granodiorite fields.

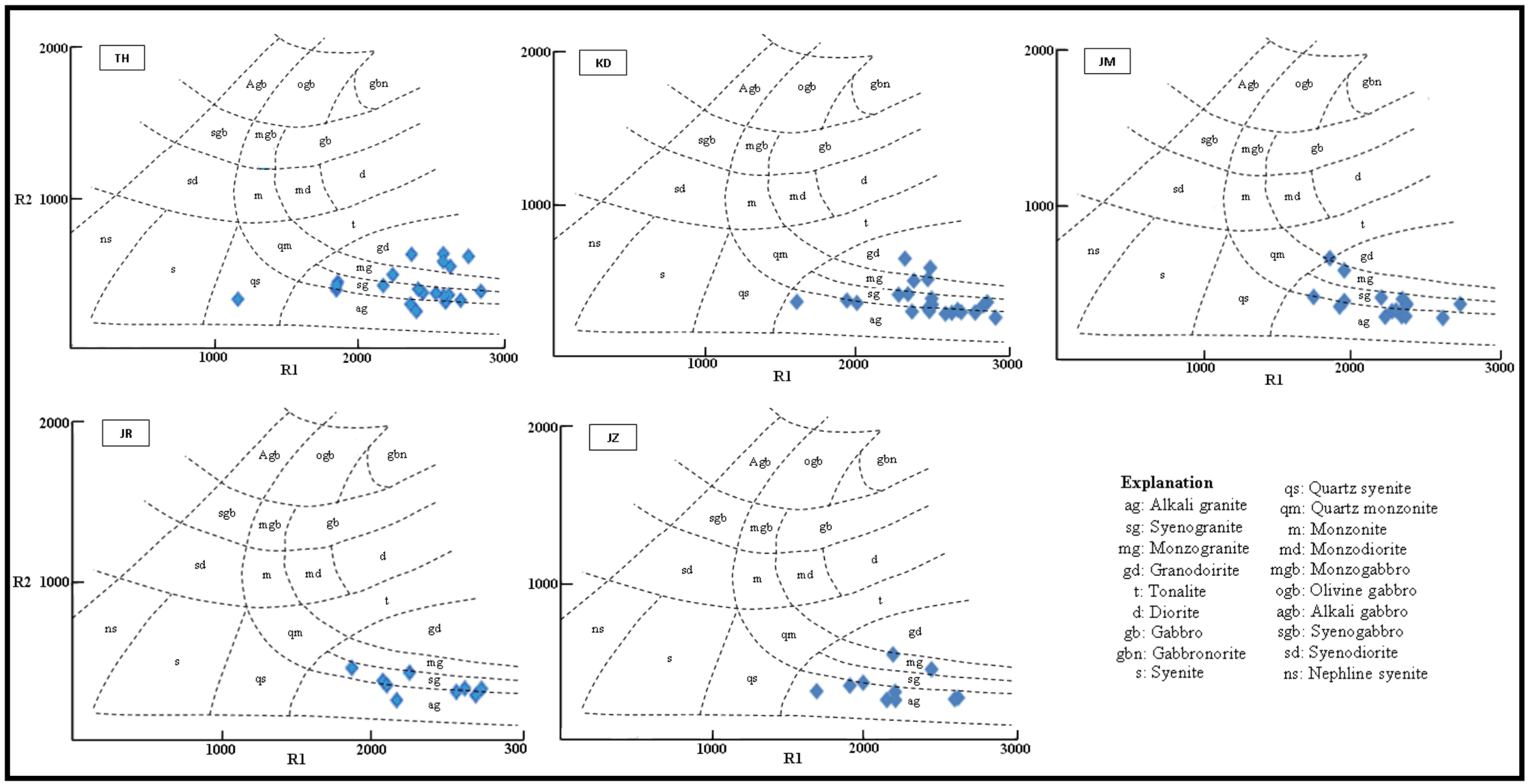

Figure 6.4: Plot of the studied granites in the R1-R2 rock classification diagram of De La Roche et al. (1980). Symbols in boxes: TH, Jabal Thalabah, KD, Jabal Khur Dukhan, JM, Jabal Al-Massah, JR, Jabal Raydan, JZ, Jabal az Zuhd

For the Jabal Al-Massah pluton, most of the investigated samples plot in the field of alkali granite and less plot in the syenogranite and monzogranite fields. For the Jabal Raydan pluton most of the investigated samples plot in both the alkali and the syenogranite fields. For the Jabal az Zuhd pluton almost all of the investigated samples plot in the field of alkali granites and a few plot in the monzogranite field

The R1-R2 rock classification diagram of De La Roche *et al.* (1980), has confirmed the previous classifications based on mineralogy and has also given more precise names to the granitic rocks.

VI.6. Normative composition diagrams

The bulk compositions of the studied granites are plotted in a normative quartz-albite-orthoclase-H_2O-fluorine (Qz-Ab-Or-H_2O-F) haplogranite system (Fig. 6.5). These plots show the composition of the first material to melt or the last material to crystallize in a granitic system. Some samples plot close to the minimum melt compositions and some do not and one reason for the latter observation might be the presence of additional volatiles such as fluorine or subsolidus fluids. Such post-magmatic affects could have played a major role in displacing the plots of the samples away from the minimum melt by either varying the temperature of crystallisation or redistributing alkalis, or it could indicate the impact of fluctuations in volatile pressure.

The granitoids plot in various positions on these ternary diagrams. The granitoids of Jabal Thalabah, Jabal Khur Dukhan, Jabal Al-Massah and Jabal Raydan and the porphyritic syenogranites of Jabal az Zuhd plot in similar fields on the ternary diagrams. Only the Jabal az Zuhd alkali granites plot far from the other granitoids, near the quartz-orthoclase line.

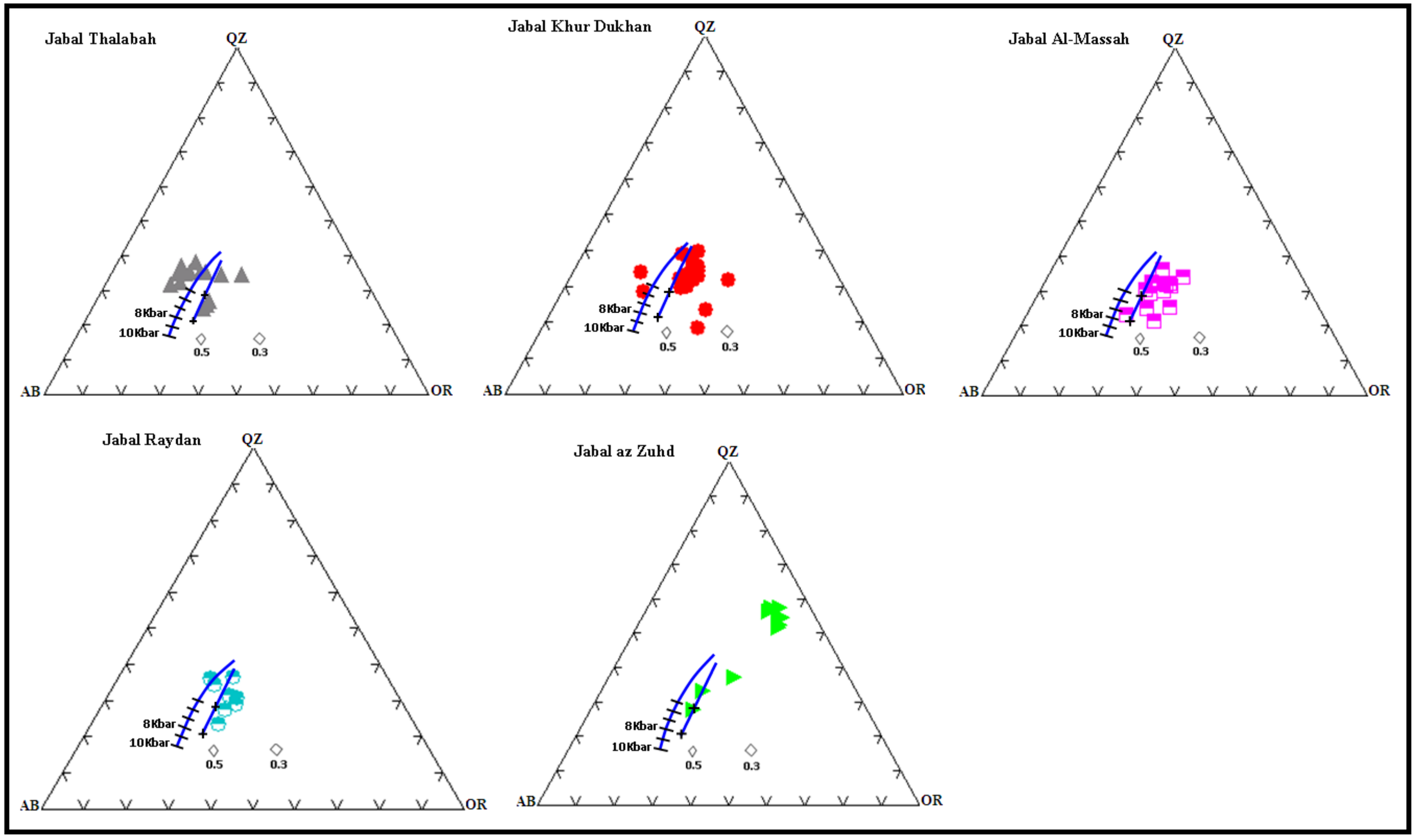

Figure 6.5: Normative composition of the studied granites plotted in the haplogranite system Qz-Ab-Or+H_20+F. The blue solid lines show the locations of minimum melt compositions at saturated water pressures ranging from 0.5 kbar to 10 kbar and 2 and 4% F (represented by crosses) (after Moghazi *et al.*, 2011), while the rhombs represent minimum melt compositions in water under-saturated systems at a H_2O = 0.5 and 0.3 kbar after Ebadi and Johannes (1991).

There is a possible contribution of additional volatiles on some of the Jabal Al-Massah, Jabal Raydan and Jabal Khur Dukhan granitoids and on the Jabal Thalabah alkali granite. This suggestion is supported by the presence of fluorite (see chapter 6) although the amounts are probably not sufficient to have a major influence here. Some of the less acidic granitoids (mostly granodiorites) from Jababal Khur Dukhan and Jabal Thalabah are clustered to the left of the minimum melt at low Or/Ab ratios and other rocks from both Jabal Khur Dukhan and Jabal Al-Massah granitoids plot close to the minimum composition at 2-4 kbar, aH_20 ~ 0.5-0.3 kb and show an elongate cluster defined by variable quartz/orthoclase ratios. For the Jabal Thalabah samples, the 3 clustered samples (11`, 13`, 14`) are alkali granites which lie close to the F trend line, while the granodiorites and syenogranites plot close to the minimum composition at 2-7 kbar (mostly between 3 and 4 kbar), and some of them show an elongate cluster defined by variable albite/orthoclase ratios at almost constant quartz content. The syenogranites plot close to the minimum composition at 1-3 kbar, aH20 ~ 0.5-0.3 and show an elongate cluster defined by variable quartz/orthoclase ratios at roughly constant albite content. Jabal az Zuhd granitoids differ from the other alkali granites in that they are enriched in normative quartz (they show the highest Qz/Or and Qz/Ab ratios) and are depleted in albite (showing the lowest Ab/Or ratio). The normative composition of Jabal az Zuhd alkali granites plot off the line joining the minimum melt compositions for different PH_2O and H_2O saturated conditions. Hyper and the subsolvus granites are both suggested to be present in the studied granites, as the first ones are most likely represented by the highly fractionated, calc-alkaline granites (Fig. 6.3 d) that are depleted in TiO_2 and FeO relative to the second type which are dominated by the alkali metaluminous and peralkaline granites and contain abundant perthites. For these plutons, the samples that plot a way from the crystallization trend or the minimum melt composition may indicate a different formation process (e.g. assimilation, metasomatic alteration).

To summarize, the normative composition diagrams do not indicate simple differentiation, as such process should show a trend towards the minima. Most of the samples plot either close to or on the fluorine addition line. Some plot at nearly constant quartz (mostly unfractionated) and others plot far from the minimum melt and could be related to subsolidus fluids. So, it can be said that the sample trends could be related to some extent by changes of water pressure or fluorine or both.

VI.6.1. Suggested depth of emplacement

In the normative composition diagrams, the compositions of many of the granites which lay close to the minimum composition, plot at 2-7 kbar water pressure. Converting these values to depth has resulted in a range of 7 to 24.5 ±0.5 km. This range appears to be rather high (compared to the depth estimated during the mineralogical study), no doubt because alkali redistribution has affected the positions of the plots in the normative diagrams.

VI.7. Rare Earth Element (REE) Geochemistry

The rare earth element contents of rocks from the five plutons are shown in tables 6.14 to 6.17 and presented in chondrite-normalized diagrams (Figs 6.6 and 6.7).

VI.7.1. Rare Earth Diagrams

The samples plot in normalized diagrams using the chondrite data of Boynton (in Rollinson, 1993). The diagrams suggest fractionation patterns in which REE profiles display an overall increase of REE concentration towards the more felsic granites (from granodiorite to alkali granites). There is also a slight decrease in light rare earth elements (LREEs) relative to the heavy rare earth elements (HREEs), a Eu depletion (which may indicate feldspar fractionation) and Eu/Eu* values increase.

Table 6.14: Rare earth element analyses of the Jabal Thalabah Pluton (ppm)

Lithology	SG	SG	SG	SG	MG	GD	GD	GD	GD	GD	GD	CHM	HR	HR	HR	HR	GB	GB	GB	Si	Si	Si	Si	CR
Sample Number	TH5`	TH10`	TH12`	TH12	TH5	TH3	TH7`	TH8`	TH9	TH18	TH19	TH6`	TH2`	TH11`	TH13`	TH14`	TH1A	TH8	TH17	TH7	TH10	TH13	TH9`	TH15
La	23	18	24	11	14	21	10	12	13	15	15	17	36	55	57	76	34	66	34	4	47	53	40	11
Ce	49	51	79	20	25	38	22	23	24	28	28	30	66	131	125	162	71	139	71	37	102	97	79	22
Pr	5	4	6	3	3	4	2	3	3	3	3	3	6	14	15	18	9	16	9	2	13	11	8	3
Nd	21	15	25	10	12	16	10	10	12	13	13	11	24	58	63	73	40	69	40	9	58	46	33	14
Sm	4	4	6	2	2	3	2	2	2	2	2	2	4	13	14	15	8	14	10	5	12	9	7	3
Eu	1	1	<1	1	1	1	1	1	1	1	1	1	1	1	1	1	3	3	3	<1	3	1	1	1
Gd	3	3	4	2	2	2	2	1	2	2	2	2	3	9	10	11	6	10	8	5	9	7	5	2
Tb	<1	1	1	<1	<1	<1	<1	<1	<1	<1	<1	<1	<1	2	2	2	1	2	1	1	1	1	1	1
Dy	2	3	4	2	1	2	1	1	1	1	1	1	2	8	9	9	4	8	7	8	6	5	5	3
Ho	<1	1	1	<1	<1	<1	<1	<1	<1	<1	<1	<1	<1	1	2	2	1	1	1	1	1	1	1	1
Er	1	1	2	1	1	1	1	<1	1	1	1	<1	1	4	4	4	2	4	3	4	2	3	3	1
Tm	<1	<1	<1	<1	<1	<1	<1	<1	<1	<1	<1	<1	<1	1	1	1	<1	1	1	1	<1	<1	<1	<1
Yb	1	1	2	1	1	1	1	1	1	1	<1	1	1	4	5	4	2	4	4	4	2	3	3	1
Lu	<1	<1	<1	<1	<1	<1	<1	<1	<1	<1	<1	<1	<1	1	1	1	<1	1	1	1	<1	<1	<1	<1

Table 6.15: Rare earth element analyses of the Jabal Khur Dukhan Pluton (ppm)

Lithology	MiG	AG	AG	A-SG	A-SG	A-SG	A-SG	A-SG	A-SG	A-SG	A-SG	A-SG	MG	MG	MG	MG	MG	GD	GD	GD	GD	CR
Sample Number	KD1	KD4	KD41	KD15	KD17	KD21	KD28	KD29	KD34	KD36	KD37	KD38	KD9	KD11	KD12	KD13	KD10B	KD10A	KD14	KD22	KD23	KD19
La	11	17	26	124	30	29	254	35	38	39	26	74	43	32	35	34	26	45	19	22	45	37
Ce	22	58	66	182	65	65	384	76	86	83	29	159	88	71	73	73	54	94	38	51	77	79
Pr	3	6	6	34	8	8	50	9	11	10	6	19	10	8	9	9	7	11	5	6	10	10
Nd	13	31	27	155	37	38	215	41	47	44	27	80	44	36	39	40	29	47	20	25	43	46
Sm	4	11	8	45	11	11	40	11	13	12	7	18	11	9	10	11	7	12	5	6	9	11
Eu	1	1	1	1	1	1	3	1	1	<1	<1	2	1	1	1	1	1	1	1	1	2	3
Gd	5	10	10	36	9	10	29	9	11	11	5	13	9	8	8	9	6	10	4	5	7	9
Tb	2	2	3	6	2	2	4	2	3	2	1	2	2	2	2	2	1	2	1	1	1	2
Dy	9	14	16	26	11	12	16	12	14	14	9	11	10	10	10	11	7	12	4	6	7	9
Ho	2	3	3	4	2	2	3	2	3	3	2	2	2	2	2	2	1	2	1	1	1	1
Er	5	7	8	10	6	7	6	6	7	7	6	5	5	5	5	6	3	6	2	3	4	4
Tm	1	1	1	2	1	1	1	1	1	1	1	1	1	1	1	1	1	1	<1	1	1	1
Yb	7	8	7	11	7	8	6	7	8	10	7	6	6	6	7	7	4	8	2	4	4	4
Lu	1	1	1	2	1	1	1	1	1	1	1	1	1	1	1	1	1	1	<1	1	1	1

Table 6.16: Rare earth element analyses of the Jabal Al-Massah Pluton (ppm)

Lithology	AG	AG	A-MG	A-MG	A-MG	A-MG	A-MG	MiG	Por-SG	Por-SG	PoR-SG	MG	MG	GD	GD	Xen	Xen	Si	CR
Sample Number	JM13	M5	JM7	JM18	JM20	JM24	JM31	M1	JM4	JM16	JM17	M2	M3	JM33	M4	JM21H	JM21B	JM2	JM29
La	37	21	46	13	18	16	115	9	36	18	19	21	18	17	24	6	7	3	12
Ce	74	36	83	23	34	30	210	23	61	34	35	41	35	31	32	12	6	2	22
Pr	9	4	9	3	4	3	20	3	6	4	4	4	4	3	3	2	1	<1	3
Nd	39	14	33	10	15	13	66	10	22	14	15	16	15	13	12	9	5	2	13
Sm	9	2	5	2	3	2	8	2	3	3	3	3	2	2	2	2	1	<1	3
Eu	<1	1	1	<1	<1	<1	1	<1	1	<1	1	1	1	1	1	1	<1	<1	1
Gd	7	2	3	2	2	1	6	2	2	2	2	2	2	2	1	2	1	<1	3
Tb	1	<1	<1	<1	<1	<1	1	<1	<1	<1	<1	<1	<1	<1	<1	<1	<1	<1	1
Dy	8	1	1	2	2	1	2	2	1	2	2	1	1	2	<1	3	1	<1	3
Ho	1	<1	<1	<1	<1	<1	<1	<1	<1	<1	<1	<1	<1	<1	<1	1	<1	<1	1
Er	4	<1	1	1	1	1	1	1	1	1	1	1	<1	1	<1	2	1	<1	2
Tm	1	<1	<1	<1	<1	<1	<1	<1	<1	<1	<1	<1	<1	<1	<1	<1	<1	<1	<1
Yb	5	1	1	1	1	1	1	1	<1	1	1	1	<1	1	<1	2	1	<1	2
Lu	1	<1	<1	<1	<1	<1	<1	<1	<1	<1	<1	<1	<1	<1	<1	<1	<1	<1	<1

Table 6.17: Rare earth element analyses of the Jabal Raydan and the Jabal az Zuhd Pluton (ppm)

Lithology	A-SG	A-SG	A-SG	A-SG	MiG	A-MG	A-MG	A-MG	AG	AG	AG	AG	AG	AG	AG	SG	Por-SG
Sample Number	JR3C	JR9	JR19	JR20	JR3D	JR3E	JR12	JR13	JZ2	JZ4	JZ6	JZ8	JZ10	JZ12	JZ14	JZ5	JZ1A
La	4	37	42	4	63	5	58	35	203	35	64	60	47	79	58	4	33
Ce	5	87	86	6	120	13	120	72	400	64	169	147	107	157	167	10	64
Pr	1	11	11	1	13	1	14	9	45	7	23	19	14	20	16	2	7
Nd	4	49	50	4	50	6	59	38	187	30	112	85	62	85	71	12	26
Sm	1	10	15	1	7	1	12	10	35	5	33	18	14	17	17	4	5
Eu	<1	<1	1	<1	2	1	1	1	3	1	4	2	2	2	2	<1	1
Gd	1	6	13	1	5	1	9	8	25	3	26	12	10	12	15	3	4
Tb	<1	1	2	<1	1	<1	2	2	4	1	5	2	2	2	3	1	1
Dy	1	3	10	1	3	2	8	9	14	2	27	8	9	8	20	3	5
Ho	<1	1	2	<1	<1	<1	1	2	2	<1	5	1	2	2	4	1	1
Er	1	2	4	1	1	1	4	5	6	1	12	4	5	4	11	2	3
Tm	<1	<1	1	<1	<1	<1	1	1	1	<1	2	1	1	1	2	<1	1
Yb	1	2	4	1	1	1	5	6	8	3	15	6	6	5	11	3	4
Lu	<1	<1	1	<1	<1	<1	1	1	2	1	2	1	1	1	1	1	1

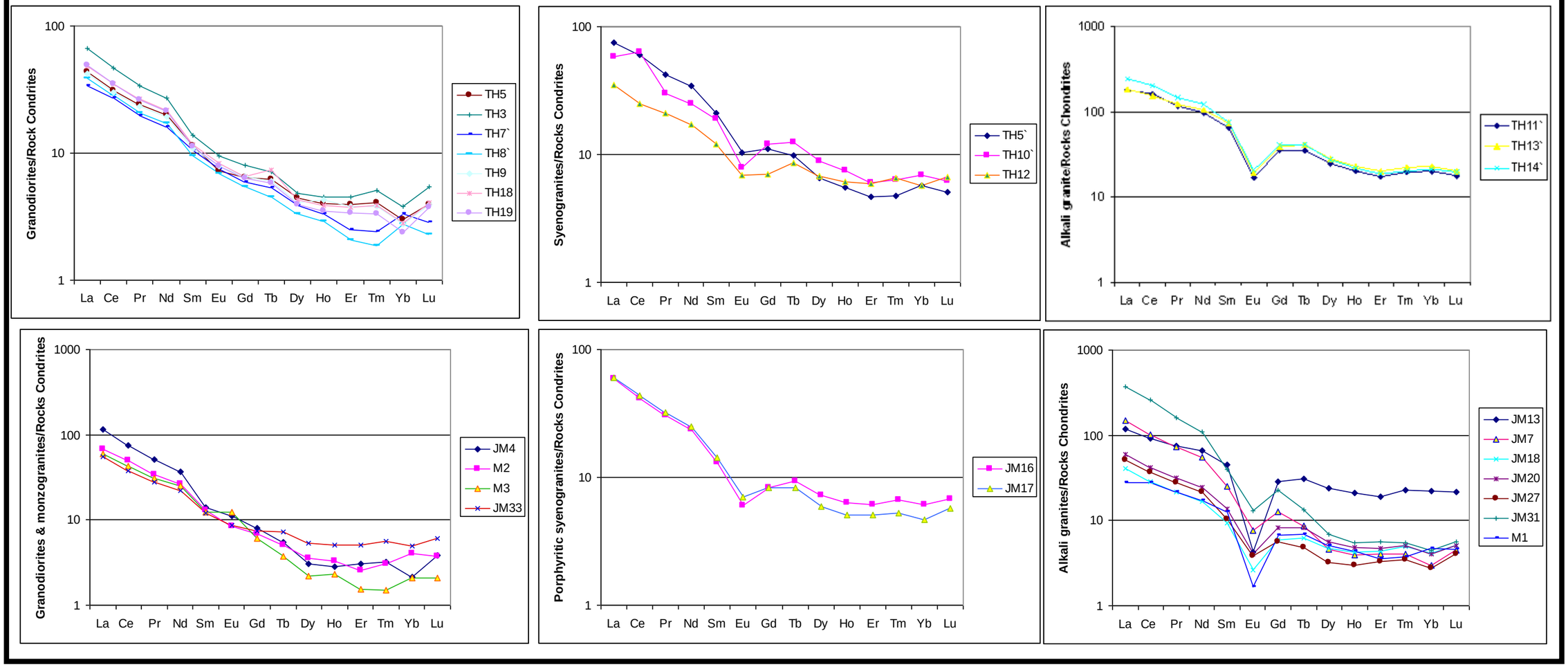

Figure 6.6: Chondrite-normalized rare earth element diagrams for the Jabal Thalabah (TH) and Jabal Al-Massah (JM) granites.

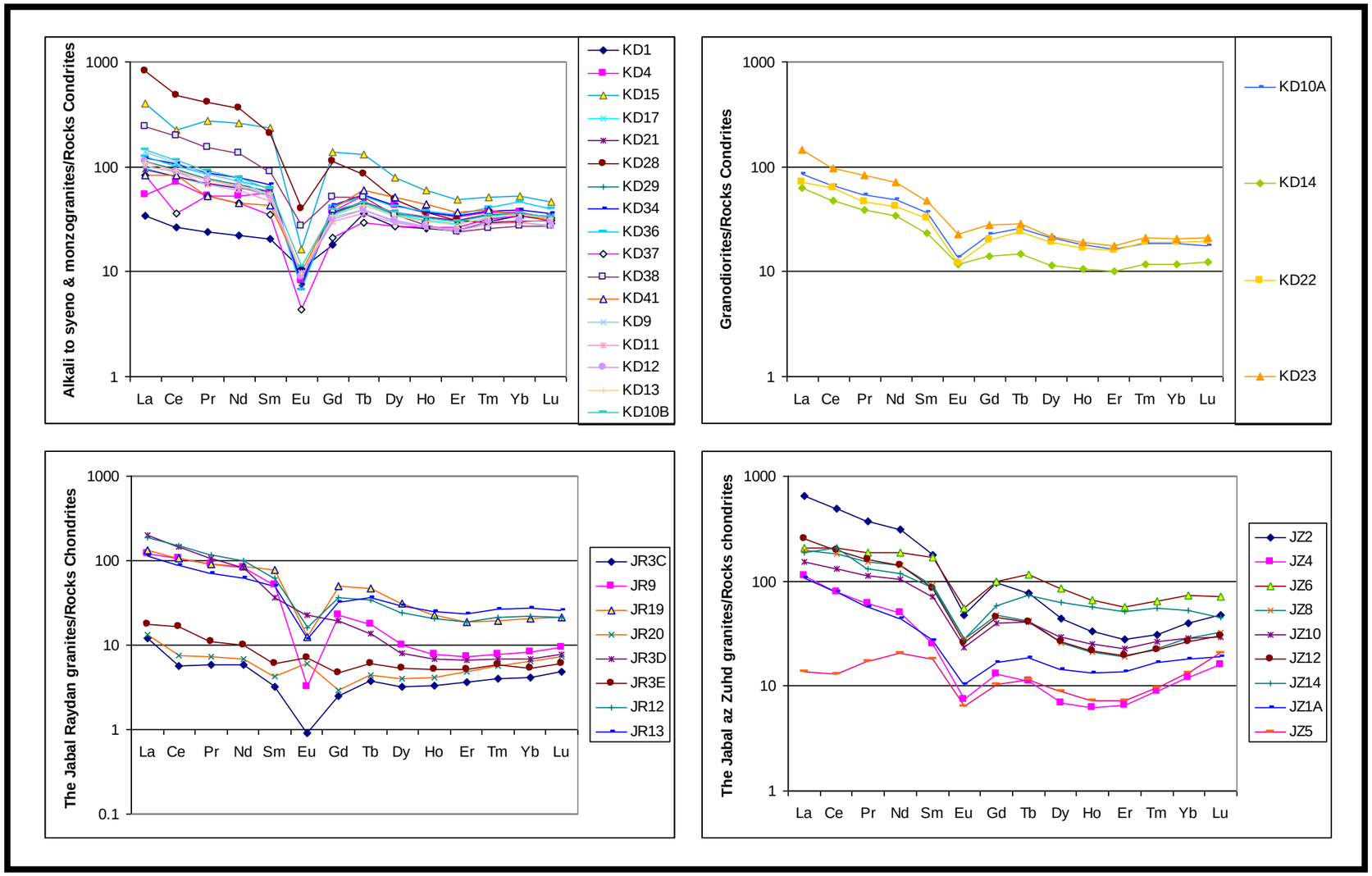

Figure 6.7: Chondrite-normalized rare earth element diagrams for the Jabal Khur Dukhan (KD), Jabal Raydan (JR) and Jabal az Zuhd (JZ) granites.

Jabal Thalabah pluton (Fig 6.6): the granodiorites are characterized by a smooth negative slope with LREE enrichment (Lan= 34-67 chondrite value), fractionated REE patterns (La/Ybn= 10.2-20.6; La/Smn= 3.2-4.9), weak negative Eu anomalies (Eu/Eu*= 0.03 to 0.04) and total REE (52-68 or 89ppm). The syenogranites display similar characteristics (Lan= 35-75 chondrite value, La/Ybn= 6.1-13.1 and La/Smn= 2.9-3.5) to those of the granodiorites, but with slightly stronger negative Eu anomalies (Eu/Eu*= 0.04 to 0.06) and higher total REE (54-111ppm). In contrast, the alkali-granites can be easily distinguished as they show more fractionated patterns (La/Ybn= 8.1-11.5; La/Smn= 2.5-3.2), stronger Eu anomalies (0.11) and total REE (153-377ppm). One, altered sample (TH2) shows a positive Eu anomaly.

Jabal Khur Dukan pluton (Fig. 6.7): the alkali-feldspar granites are characterized by smooth negative slopes with LREE enrichment (Lan= 34-399 chondrite value), fractionated REE patterns (La/Ybn= 1-8.8 or 27.2; La/Smn= 1-4), weak to strong negative Eu anomalies (Eu/Eu*= 0.09 to 0.36, on average) and a wide range of total REE (84-1013ppm). Two weak negative Ce anomalies were found in KD15 and KD37. The white monzogranites-granodiorites are also characterized by smooth negative slopes but with less LREE enrichment (Lan= 102-147 chondrite value), less fractionated REE patterns (La/Ybn= 3.2-7.2; La/Smn= 2-3.1), less strong negative Eu anomalies (Eu/Eu*= 0.09 to 0.17, on average) and lower total REE (102-253ppm).

Jabal Al-Massah pluton (Fig 6.6): the alkali-feldspar granites are characterized by smooth negative slopes with LREE enrichment (Lan= 28-371 chondrite value), fractionated REE patterns (La/Ybn= 5.3-82; La/Smn= 2.7-9.3), weak to strong negative Eu anomalies (Eu/Eu*= 0.04 to 0.01) and a wide range of total REE (53-197ppm). The porphyritic syenogranites are also characterized by smooth negative slopes but with less LREE enrichment (Lan= 59-60 chondrite value), less fractionated REE patterns (La/Ybn= 9.7-12.7; La/Smn= 4.2-4.5), less strong negative Eu anomalies (Eu/Eu*= 0.03 to 0.04) and lower total REE (81-83ppm). The white monzogranites-granodiorites are also characterized by smooth negative slopes but with less LREE enrichment (Lan= 55-117 chondrite value), less fractionated REE patterns (La/Ybn= 11.3-54.1; La/Smn= 4.6-8.3), less strong negative Eu anomalies (Eu/Eu*= 0.02 to 0.04) and lower total REE (75-134ppm).

Jabal Rydan pluton (Fig 6.7): all the alkali-feldspar granites and the syenogranites are characterized by smooth negative slopes, with LREE enrichment (Lan= 12-202 chondrite value), fractionated REE patterns (La/Ybn= 2-29.3; La/Smn= 2.3-5.5), weak to strong negative Eu anomalies (Eu/Eu*= 0.01 to 0.12) and total REE (17-266ppm). A weak negative Ce anomaly was traced in JR3C and JR20 shows a positive Eu anomaly. The white monzogranites also show smooth negative slopes, but with slightly less LREE enrichment, less fractionated REE patterns and higher total REE (Lan= 18-187 chondrite value, La/Ybn= 3.3-8.5; La/Smn= 2.3-3, Eu/Eu*= 0.09 to 0.1, and total REE ranges from 34 to 295ppm). They also display one sample (JR3E) that shows a positive Eu anomaly.

Jabal az Zuhd Pluton (Fig. 6.7): the alkali-feldspar granites of the studied pluton plus one porphyritic syenogranite are characterized by a smooth negative slope with LREE enrichment (Lan= 14-656 chondrite value), fractionated REE patterns (La/Ybn= 1-16.7; La/Smn= 0.8-4.5), moderate negative Eu anomalies (Eu/Eu*= 0.08 to 0.65, on average) and total REE (45-936ppm).

The REE values and profiles are typical of granites, but some (see chapter 8) show values (e.g. MREE, HREE and Nd of the Jabal az Zuhd alkali granite) higher than in average granites. The high values observed in the REE diagrams do not seem to be related to higher LOI and in most cases appear more related to higher contents of Fe. The REE plots indicate that fractionation processes could have played an important role in the REE content of the granitoids. The development of the process has coupled with suggested feldspar fractionation in the more alkali grantoids. The increasing of fractionation showed no relation with LOI. The presence of Eu anomaly is most likely indicates fractionation process while the Ce anomaly is possibly indicates other processes (see later). From the diagrams it seems that the more fractionated granite may be derived from the unfractionated granodiorites. The absence or the positive Eu anomaly suggests that some of the granites did not experience feldspar fractionation.

VI.8. Comment on the Chemical analysis

The data from the chemical analyses indicate that some plutons are enriched in Si, Al, and Fe and depleted in Ti and Mg. This could be related to various factors such as later sodium rich-fluid (e.g. subsolidus alteration), high oxygen fugacity (see below), fractionation and later hydrothermal alteration processes. The total alkali contents (Na_2O+K_2O) are high and nearly constant. A clear depletion in K_2O was traced in all of the alkali granites of Jabal Thalabah and some of the peraluminous calc-alkaline granodiorites of Jabal Khur Dukhan pluton, while the alkali-metaluminous granites of Jabal Khur Dukhan pluton have high K_2O values, possibly from K-rich fluids. The concentrations of MgO are regularly low.

The chemical analyses of the xenoliths are presented in Table III.4 of the appendix. These demonstrate the felsic nature of the xenoliths from the Jabal Khur Dukhan pluton suuport the assimilation of felsic material, as suggested by Drysdall (1980). The mafic xenoliths found in the Jabal Al-Massah pluton may indicate an earlier stage of assimilation that took place before the stoping of the granites as suggested by Davies (1983). (Mafic xenoliths were also found in the Jabal Thalabah pluton but were not analyzed). The absence of the xenoliths in both Jabal Raydan and Jabal az Zuhd may indicate a different development process from the other plutons (e.g. not involving assimilation processes, specifically in the later stage of formation).

From the above-mentioned observations, it seems that fluid/rock interaction and fractionation could both be important. The hydrothermal alteration and the large number of dykes (felsic and mafic) that intruded the Jabal Thalabah Complex could have transported high concentrations of many elements, changing the rock composition and possibly giving some misleading ideas about the genetic types and the tectonic setting. Among the studied plutons, the Jabal az Zuhd alkali granite appears to be the most evolved.

To conclude, various process of formation (e.g. contamination, fractionation, subsolidus alteration) are suggested but there is also the possibility of more than one magma being present in some of the plutons.

VI.9. Tectonic Environment

Tectonic discrimination diagrams use the concentrations of various chemical components to suggest environments for granite formation. These have been used on the studied plutions and are presented in Figs. 6.8 and 6.9. The discrimination boundaries in the Rb vs Y+Nb tectonic diagrams of Pearce *et al.* (1984) and Harris *et al*. (1986) were empirically drawn but based on petrographic, bulk chemistry and isotopic constraints.

1) Based on the tectonic discrimination diagrams devised by Pearce *et al.* (1984):

- Jabal Thalabah pluton: all the granitoids plot in the volcanic-arc and within-plate fields.

- Jabal Khur Dukhan pluton: all the granitoids plot in the within-plate field, except for one sample which plots in the volcanic-arc field.

- Jabal Al-Massah pluton: most of the granitoids plot in the volcanic-arc field and only a few samples plot in the within-plate field.

- Jabal Raydan pluton: many of the granitoids plot in the volcanic-arc field and a few samples plot in the within-plate field.

- Jabal az Zuhd pluton: the alkali-granites plot in the within-plate field, while the syenogranites plot in the volcanic-arc field.

2) Based on the tectonic discrimination diagrams devised by Harris *et al.* (1986):

- Jabal Thalabah pluton: the granodiorites plot in the volcanic-arc granite field, the syenogranites lie along the post-collision - volcanic arc boundary line, while the alkali granites plot in the within-plate field.

- Jabal Khur Dukhan pluton: almost all the granitoids plot in the within-plate field. Some granitoids lie along the post-collision - within-plate boundary line.

- Jabal Al-Massah pluton: almost all the granitoids plot in the volcanic-arc field. One sample lies on the volcanic arc - syn-collision field boundary.

- Jabal Raydan granitoids are scattered in 4 different fields. They plot in the volcanic-arc, post-collision and within-plate fields, while one sample plots in the syn-collision field.

- Jabal az Zuhd pluton: the alkali granitess plot in the within-plate field and the syenogranites plot in the syn-collision field.

3) Based on the tectonic discrimination diagrams devised by Pitcher (1982):

- Jabal Thalabah pluton: the alkali granites mostly plot in the anorogenic field, the syenogranites and monzogranites extend from the late orogenic to the syn-collision fields and the granodiorites lies between the pre-plate collision and the syn-collision field, but they fit better into the latter field.

- Jabal Khur Dukhan pluton: the alkali granites extend from the anorogenic field to the post-orogenic field, while the other granitoids (the syeno, monzo and granodiorites) are fit into the syn-collision field.

- Jabal Al-Massah pluton: the alkali granites plot in the anorogenic field, while the syenogranites and monzogranites extend from the late orogenic to the syn-collision fields.

- Jabal Raydan pluton: the alkali granites mostly plot in the anorogenic field and partially extend to the post orogenic field, while the syenogranites extend from the late orogenic to the syn-collision fields.

- Jabal az Zuhd pluton: the alkali granites plot in the anorogenic field, while the monzogranites plots into the syn-collision field.

To summarize, it is concluded that the five plutons were emplaced in a very similar tectonic environment, that spans the Panafrican orogeny and implies late stage of island-arc accretion to post-collision events, followed by the waning (relaxation) of the orogeny. This suggestion is supported by the chemical characteristics of the studied

granitoids and by comparison with other chemically similar granitoids in the Arabian Shield (see later).

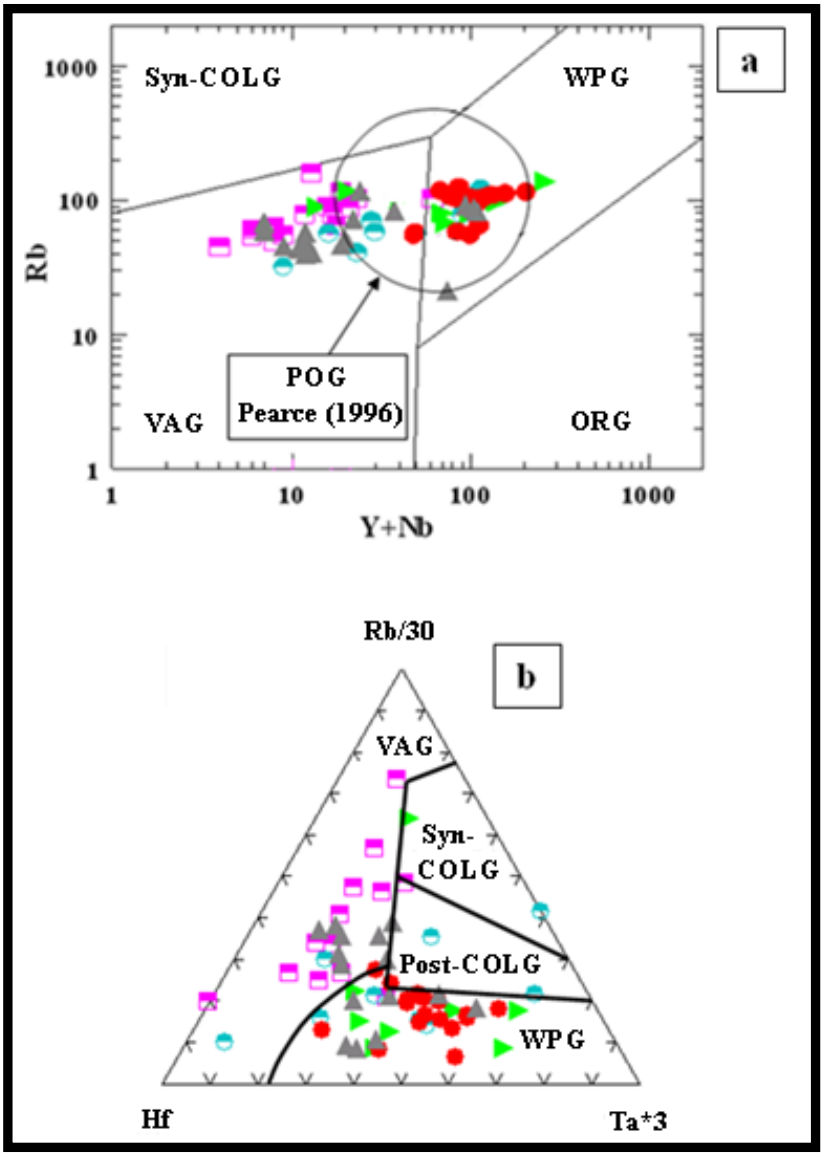

Figure 6.8: Tectonic discrimination diagrams for the granites: (a) Rb vs. (Nb+Y) of Pearce *et al.* (1984) and (b) Hf-Rb/30-Ta*3 of Harris *et al.* (1986). Abbreviations: WPG, within-plate granite, Post-COLG, post-collision granite, Syn-COLG, syn-collision granite, VAG, volcanic-arc granite, ORG, orogenic granite, POG, post-orogenic granite. Symbols as in Fig. 6.12.

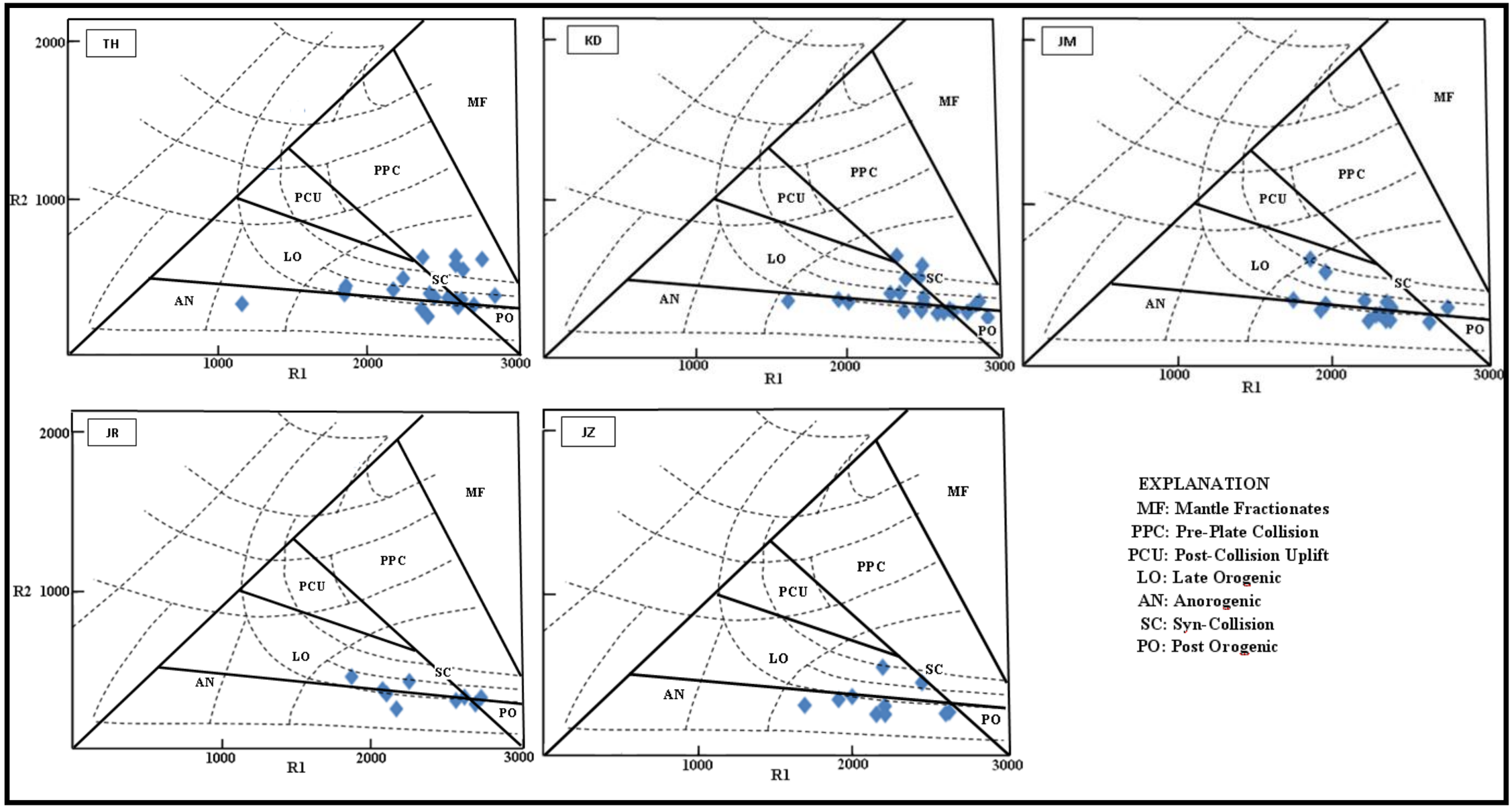

Figure 6.9: Plots of the studied granites on a major granitic classification diagram (fields after Pitcher, 1982). Abbreviation: TH, Jabal Thalabah, KD, Jabal Khur Dukhan, JM, Jabal Al-Massah, JR, Jabal Raydan, JZ, Jabal az Zuhd.

VI.10. Economic Potential

The aim of this part is to evaluate the potential of the studied granites as a resource for rare elements. This will be based upon: 1) The outcome of the previous mineralogical and geochemical studies; 2) Comparisons with average world granites and 3) Comparisons with some other local and global deposits. Therefore, this must only be considered as a pilot study that can help in finding evidence for the possible presence of rare metal deposit within the areas of interest.

The earlier mineralogical study indicated the presence of some economically important minerals like monazite, xenotime, fergusonite, synchysite, Au-Pt alloy and Ag. This was also demonstrated during the chemical studies that determined their chemical compositions. To see how unusual these granites are from a geochemical view (especially as regards REE and other selected traces: Nb, Y and Zr) samples from the most promising granites (based on mineralogy or chemistry) were compared (Table 6.18) with the average granite from Krauskopf (1979) and Krauskopf and Bird (1995). The selected granites were also compared with other global rare metal deposits (Table 6.21) that show the percentage of the total rare earth oxides and individual values for some rare metals.

VI.10.1. Comparisons

For comparison with global deposits, the sum of the rare earths is a better indicator of potential rather than simply looking at individual values. The enriched granites show a total range from 197.4 (~0.02%) to 1012.7 (~0.1%) ppm REE. These are not as high as those found in working deposits but the highest value (0.10%) almost matches that of the Dubbo, New South Wales deposit (0.12%; Alkane Resources Ltd., 2010) although this deposit is not currently working. Regarding the rare metals, the enriched granites show ranges from 47 to 160 ppm for Y, 233 to 1017 ppm for Zr and 25 to 100 ppm for Nb. Thus the highest values are almost 0.02% for Y, 0.01% for Nb and 0.1% for Zr. The required minimum values for Y and Nb should be almost 0.14% and 0.13% (1400 and 1300 ppm) respectively, to match the values of Dubbo deposit for Y and the value of Bayan Obo deposits for Nb, while Zr need to reach 0.8% to resemble the Hastings deposit(AustralianMinesAtlas,2011).

Table 6.18: Content of selected elements in the enriched granites and world averages (ppm)

Elements		TH11` (AM)	TH13` (AM)	TH14` (AM)	KD15 (HFCA)	KD28 (APL)	KD36 (HFCA)	KD38 (APL)	JM31 (HFCA)	JR19 (HFCA)	JR12 (AM)	JR13 (AM)	JZ2 (APK)	JZ6 (APK)	JZ8 (APK)	JZ10 (APK)	JZ12 (APK)	JZ14 (APK)	World average granites
RMs	Y	47	53.2	50	147	62	89	82	13	24	57	72	72	160	48	63	37	77	13-40
	Zr	620	782	773	233	475	246	383	122	331	291	354	99	345	248	470	410	1017	180-210
	Nb	47	56	54	58	39	68	29	5	27	33	43	54	100	25	38	33	65	20.24
LREEs	La	55	57	76	124	254	39	74	115	42	58	35	203	64	60	47	79	58	55-101
	Ce	131	125	162	182	384	83	159	210	86	120	72	400	169	147	107	157	167	90-170
	Pr	14	15	18	34	50	10	19	20	11	14	9	45	23	19	14	20	16	10-19
	Nd	58	63	73	155	215	44	80	66	51	59	38	187	112	85	62	85	72	35-55
MREEs	Sm	12.6	14.1	14.7	45.5	40.3	12.1	17.6	7.8	15.3	12.3	9.7	34.6	33.3	17.8	14.0	16.5	17.1	8.3-9
	Eu	1.2	1.4	1.5	1.2	2.9	0.5	2.0	0.9	0.9	1.2	0.9	3.5	4.1	2.1	1.7	1.9	2.1	1-1.3
	Gd	9.1	10.1	10.7	35.5	29.1	10.9	13.2	5.8	13.0	9.4	8.2	24.7	25.7	12.2	10.4	11.8	14.9	5-8
	Tb	1.7	1.9	1.9	6.2	4.1	2.5	2.4	0.6	2.3	1.6	1.7	3.7	5.5	2.0	2.0	1.9	3.5	0.5-1.5
	Dy	7.9	9.0	8.7	25.5	15.9	13.5	11.2	2.2	9.9	7.7	9.3	14.3	27.3	8.3	9.3	8.5	20.1	2.4-6.5
	Ho	1.4	1.6	1.6	4.2	2.7	2.7	2.0	0.4	1.6	1.5	1.8	2.4	4.8	1.5	1.8	1.5	4.1	0.35-2
HREEs	Er	3.6	4.2	3.9	10.1	6.4	7.3	5.0	1.2	3.9	3.9	4.9	5.9	12.0	4.0	4.8	4.1	10.8	1.2-4.5
	Tm	0.6	0.7	0.7	1.6	1.0	1.3	0.8	0.2	0.6	0.7	0.9	1.0	2.1	0.7	0.9	0.7	1.8	0.15-0.6
	Yb	4.2	4.7	4.4	11.1	6.3	9.6	5.7	0.9	4.3	4.6	5.8	8.2	15.3	6.0	6.0	5.5	11.0	1.1-4
	Lu	0.6	0.6	0.6	1.5	1.0	1.3	0.9	0.2	0.7	0.7	0.8	1.5	2.3	1.1	0.9	1.0	1.4	0.2-0.7
	REEs` total	301.5	307.3	376.9	636.3	1012.7	238.1	392.9	430.9	241.9	295.2	197.4	936.2	500.9	365.9	281.4	394.3	399.8	

Explanation for abbreviations: TH, Jabal Thalabah, KD, Jabal Khur Dukhan, JM, Jabal Al-Massah, JR, Jabal Raydan, JZ, Jabal az Zuhd, AM, alkali metaluminous, APL, alkali peraluminous, APK, alkali peralkaline, HFCA, highly fractionated calc-alkaline, RMs, rare metals, LREEs, light rare earths elements, MREEs, middle rare earth elements snd HREEs, high rare earth elements. The chemical values: black: below or mostly within the world average range; pink: above the world average; blue: twice the world average; red: three to four times the world average granite from from Krauskopf (1979) and Krauskopf and Bird (1995).

Table 6.19: Rare metal content of dykes (ppm)

Elements		JR1C (PD)	TH7 (FD)
RMs	Y	49	48
	Zr	<210	235
	Nb	69	133

Abbreviations: JR, Jabal Raydan, TH, Jabal Thalabah, PD, Pegmatitic dyke, FD, Felsic dyke

Table 6.20: Rare earth content of mafic dyke

Elements		TH10 (MD)
LREEs	La	47
	Ce	102
	Pr	13
	Nd	58
MREEs	Sm	12
	Eu	3
	Gd	9
	Tb	1
	Dy	6
	Ho	1
HREEs	Er	2
	Tm	0
	Yb	2
	Lu	0
	REEs total	256.5

Abbreviations: TH, Jabal Thalabah, MD, Mafic dyke

Table 6.21: Characteristics of some rare earth and rare metal world class deposits

Locations of deposits	Host rock	Ore minerals	grades of ore or resource (weight % element or oxides)	References
Bayan Obo in Mongolia (mined for REE)	Carbonatite dikes in gabbro and alkali gabrro	Monazite, bastnasite, huanghoite, parasite, cebaite and columbite	0.13% Nb and 6% REOs	(USGS, 2010), (BGS, 2011) (Yang *et al.*, 2011)
Mountain Pass in California, USA (mined for REE)	Carbonatite	Dominant bastnasite	8.9% REOs	(Castor and Nason 2004) (Castor, 2008)
Jabai Tawlah in Saudi Arabia (resource, Nb-Th-Zr mineralization)	Microgranite and microsyenite	Gagarinite, fergusonite, xenotime, yttrian fluorite, yttrian-REE zircon, columbite and thorite	0.34% Nb, 0.52% Y, and 0.47% Zr	(Drysdall *et al*., 1984, Drysdall and Douch, 1986, and Kuster, 2009)
Ghurayyah in Saudi Arabia (resource, Nb-Th-Zr mineralization)	Porphyritic microgranite	Xenotime, monazite, samarskite, pyrochlore, columbite-tantalite, uraninite, aeschynite and zircon	1.8% Nb, 0.75% Y, 0.35% Th and 6% Zr	(Drysdall *et al*., 1984, Kuster, 2009 and Elliott *et al*., 2001).
Toongi in New South Wales, Australia (resource, Nb-Y-Zr and REE mineralization)	Intrusive trachyte	Dominant columbite	0.46% Nb, 0.14% Y, 1.93% Zr and 0.74% REOs	(Australian Mines Atlas, 2011) and (Alkane Resources Ltd., 2012).
Dubbo, New South Wales, Australia (resource, Ta-Y-Zr and REE mineralization)	Trachyte plug	Calcium and REE-rich zirconosilicates (similar to eudialyite or armstrongite) natroniobite and calcian bastnasite	0.14% Y, 1.9% Zr and 0.12% REOs	(Alkane Resources Ltd., 2010).
Thor Lake, Canada (resource, Ta-Nb-Y-Zr and REE mineralization)	Peralkaline syenites, granites and gabbros	Eudialyite, fergusonite and zircon, bastnaesite, synchysite, allanite and monazite.	1.64% REOs	(BGS, 2011) and (Avalon rare metals, 2012)

Thus the rare metals in these granites are much lower than those of economic deposits. The ratio of the mineral presence sometimes considered during the deposit assessment, and this of course reflects the chemical content of the constituting elements of such mineral. To summarize, it is possible to say that not all of the enriched granites show both rare earth and rare metal contents of significance. For instance, JM31 shows only REE enrichment and other samples like KD36 are more enriched in HREE. The chemical analysis of felsic and mafic dykes (Tables 8.3 and 8.4) show that the pegmatitic dyke in Jabal Raydan and the felsic dyke in Jabal Thalabah may have potential for some rare-metal-bearing minerals, while the mafic dyke in the latter pluton could have potential for elevated Nd and some MREE

VI.10.2. Industrial applications

The studied alkali granites, especially those of Jabal az Zuhd and Jabal Khur Dukhan, have relatively high values of LREE (specifically La, Ce, Pr, Nd), which are either hosted in minerals like titanite, apatite, allanite, rutile and ilmenite, or form their own minerals, such as monazite, fergusonite xenotime and synchysite. The form of the minerals is important as it relates to ease of processing and REE extraction. These elements are of increasing importance for metallurgy, magnets, electronics and the optics. However, for their commercial use, it is crucial that either the other REEs should not cause any detrimental affects or all of the REEs should show a similar behaviour in their applications. In modern day applications the MREE and HREE are the most desirable elements and thus the most valuable.

VI.10.3. Cause of enrichment

The enrichment in the elements Nb, Zr, Y and the rare earths in the studied granites is the focus of this study. This enrichment is associated with the formation of some economically important minerals (e.g. fergusonite, monazite, xenotime and possibly synchesite) and other minerals which can concentrate these rarer elements (e.g. zircon, titanite, apatite, allanite, rutile).

Several variation diagrams (Fig. 6.10 to 6.12) have been plotted to find out possible elemental relationships. From these diagrams it is suggested that the cause of enrichment is related to more than one process, as the increase in the enriched element contents are not consistent and no clear pattern is apparent. Overall, the increase in REE contents is mostly associated with increasing Zr, Nb, Y, K, Na and Fe. This possibly means that the concentrations of REE, Zr, Nb and Y were increased together in the melt by fractionation and are most concentrated in the Fe- and alkali-rich granites (see tables 6.2 to 6.5 and 6.14 to 6.17). However, an increase of the REE with alkalis does not necessarily mean that enrichment is only related to the most evolved alkaline varieties, as it has been found that Si (the fractionation index) has not shown a clear proportional correlation with the REE. This could indicate that the enrichment is more likely related to late-stage, alkaline, subsolidus fluids. However, it appears that most commercial REE deposits are mainly associated with magmatic processes related to alkaline igneous rocks(BGS,2011).

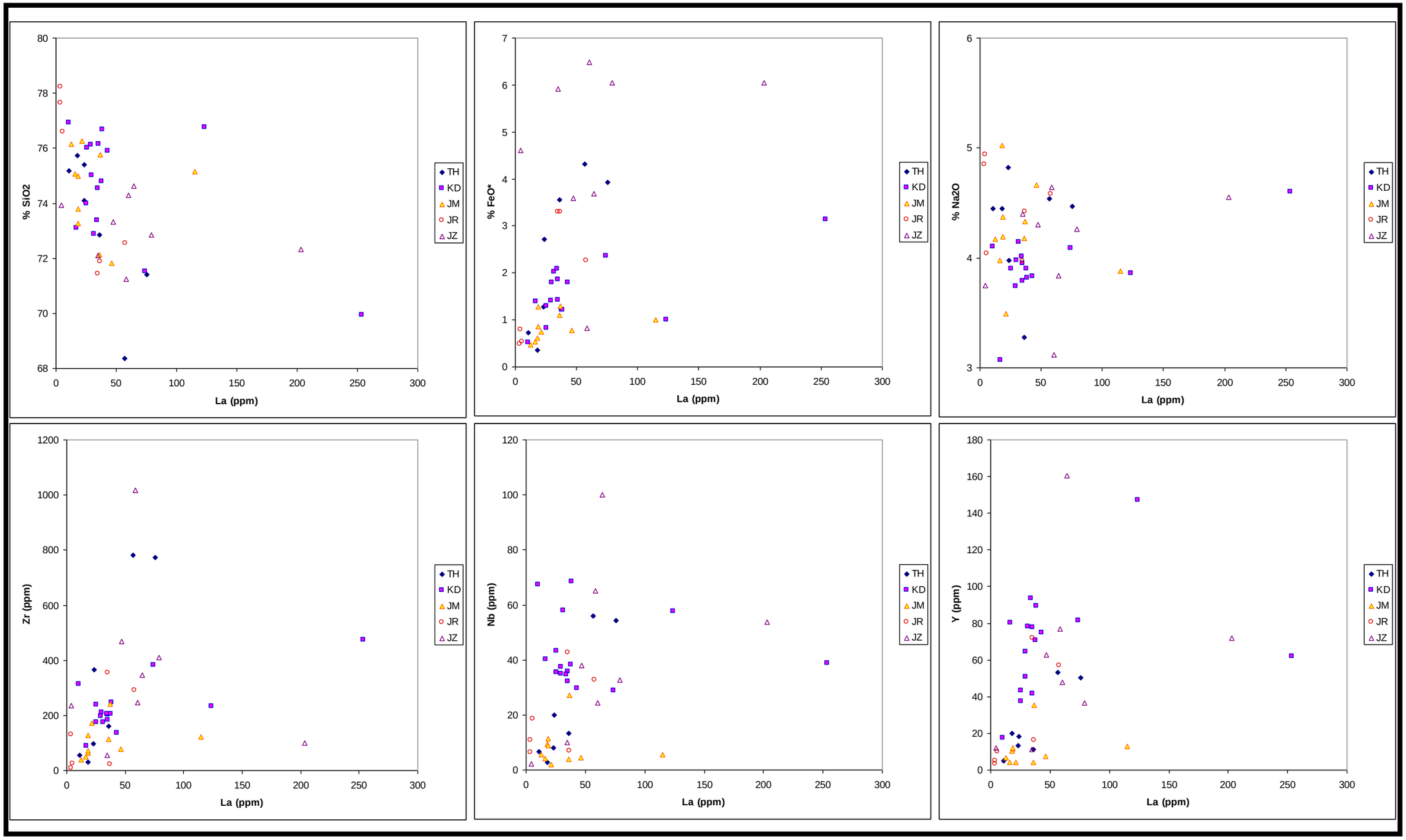

Figure 6.10: Relationships between certain elements Explanation: TH, Jabal Thalabah, KD, Jabal Khur Dukhan, JM, Jabal Al-Massah, JR, Jabal Raydan, JZ, Jabal az Zuhd.

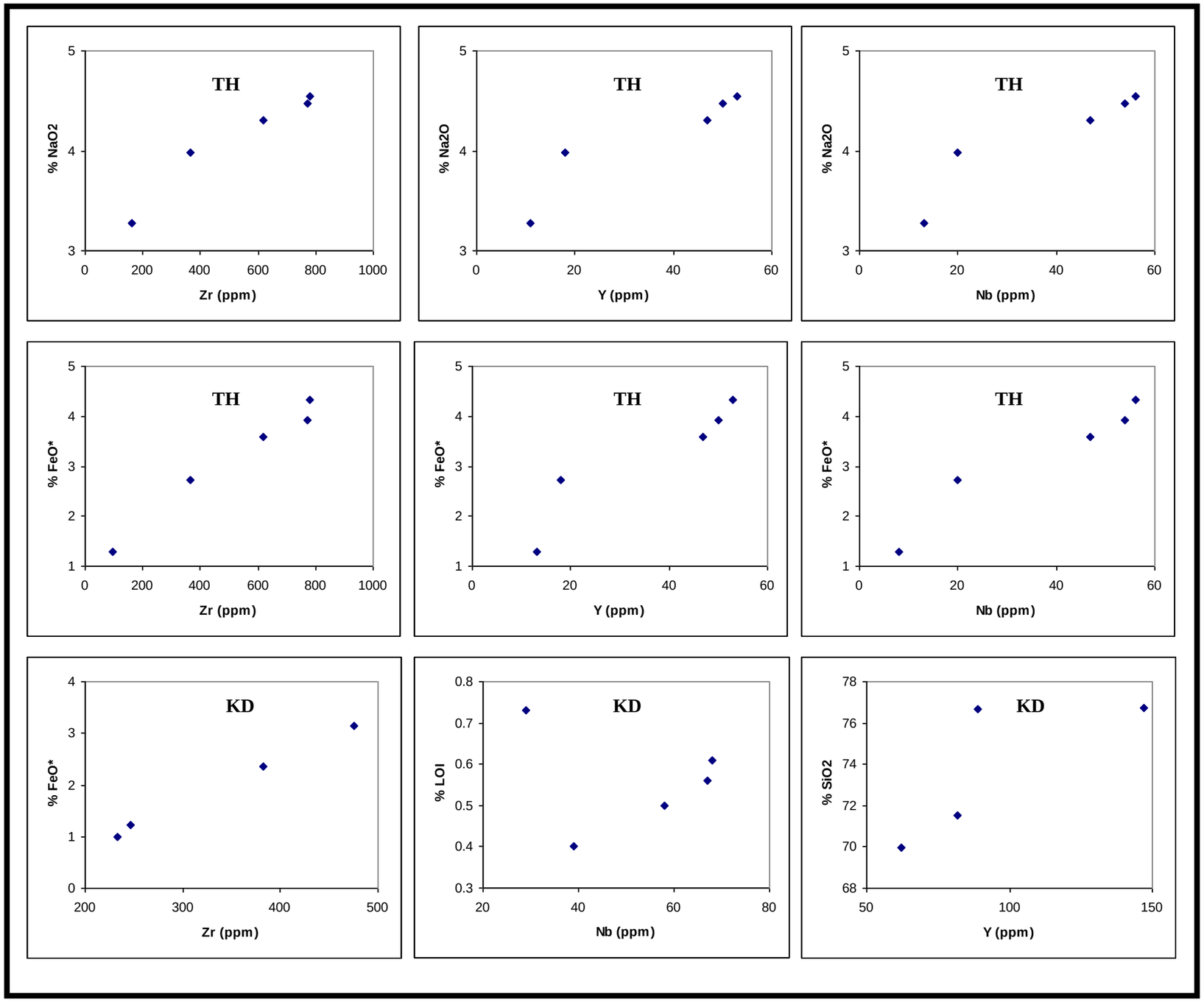

Figure 6.11: Relationships between certain elements. Explanation: TH, Jabal Thalabah, KD, Jabal Khur Dukhan.

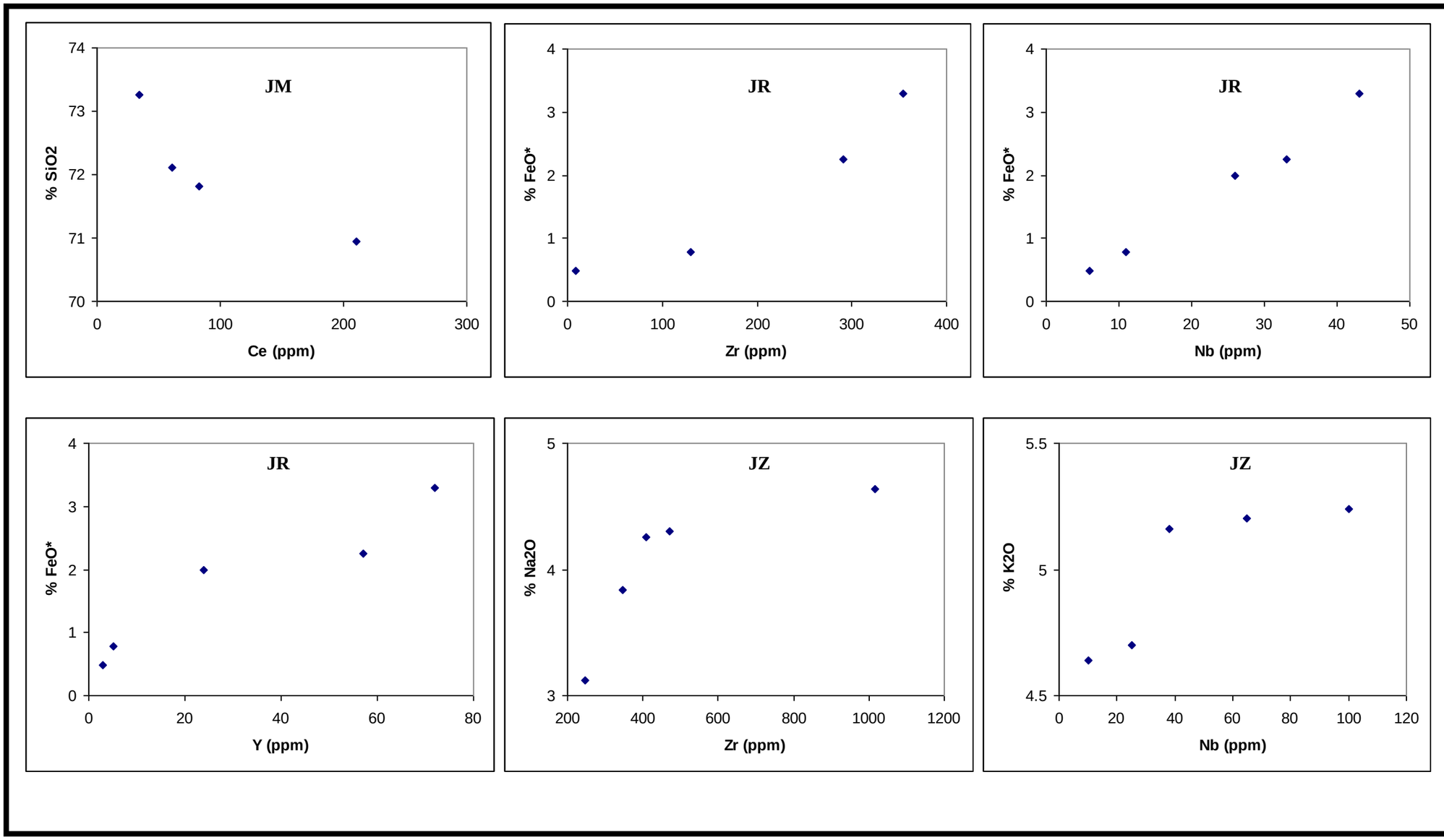

Figure 6.12: Relationships between certain elements. Explanation: JM, Jabal Al-Massah, JR, Jabal Raydan, JZ, Jabal az Zuhd.

To summarize, it is possible to say that not all of the enriched granites show both rare earth and rare metal contents of significance. For instance, JM31 shows only REE enrichment and other samples like KD36 are more enriched in HREE. The chemical analysis of felsic and mafic dykes (Tables 8.3 and 8.4) show that the pegmatitic dyke in Jabal Raydan and the felsic dyke in Jabal Thalabah may have potential for some rare-metal-bearing minerals, while the mafic dyke in the latter pluton could have potential for elevated Nd and some MREE.

VI.11. Discussion and conclusions

Based on the geochemical analyses of major and trace elements, significant information has been obtained to explain the magmatic affinity, the granitic types, the tectonic environment, the major and trace element behaviour, the nature of the parental magma and the processes involved in yielding the final granitoids. The studied granites show similar geochemical characteristics to world average granites and others granites that from similar tectonic regimes.

VI.11.1. Comment on the normative study

Many of the granites are compositionally close to anatectic melts. A general constant orthoclase content for most of the samples in the plots may be attributed to a decrease of pressure in water-undersaturated melts (Johannes and Holtz, 1990), while variable albite/orthoclase ratios at almost constant quartz content may indicate undifferentiated rocks. The affect of late stage fluids on the normative diagram may be due to the development of fluoride complexes to element mobility in peralkaline magmas (Harris, 1981). This can be exemplified by the alkali granites of Jabal Thalabah that lie on the F trend line The low Or/Ab ratios of the less acidic granitoids of Jababal Khur Dukhan and Jabal Thalabah may directly relate to lower water activities (Ebadi and Johannes, 1991). The presence of perthite that distinguishes the hypersolvus granites from the subsolvus may reflect insufficient H_2O contents or low water pressure that is required for the formation of two-feldspar granite (Charoy and Raimbault, 1994; Johannes and Holtz, 1996). This can be exemplified by the normative composition of Jabal az Zuhd alkali granites that plot off the minimum melt compositions. At high water contents, the melt shows a notable increase in the Ab/Or ratio which is the reverse of what is expected (Clemens and Bea, 2012; Conrad et al., 1988). It is unlikely that granitic magmas, specifically those melted from a crustal source, started as water under-

saturated melt but even the water-undersaturated melts would evolve towards water saturation in the late crystallization stages (Clemens and Bea, 2012; Maaloe and Wyllie, 1975). This may explain the variation in the Ab/Or ratio (see Fig. 6.5) for the studied granitoids in the triangular haplogranite system. The water undersaturated nature of some of the magmas is also supported by the rare presence of water-bearing minerals (e.g. amphibole and biotite).

VI.11.2. Comment on granite classification

The studied granites are mostly metaluminous to mildly peraluminous. Such a magmatic affinity is likely to be derived from either a metaluminous or moderately peraluminous metaigneous source (Clemens and Bea, 2012; Conrad *et al.*, 1988), while a strongly peraluminous metasedimentary protolith can be a source rock for peraluminous granitoids (e.g. the Jabal Thalabah granodiorites) (Clemens and Bea, 2012; Conrad *et al.*, 1988). The peralkaline nature of the Jabal az Zuhd granitoids indicates A-type (anorogenic/anhydrous) granitoids that were generated along rift zones and within stable continental blocks.

The ferroan nature of most of the studied granitoids reflects crystallization of relatively anhydrous silicates (that drives a melt to higher Fe/(Fe+Mg) ratios) from reduced magmas and source regions. Such conditions are common in extensional environments (Frost *et al.*, 2001). In contrast the magnesian nature that characterizes the un-fractionated granodiorites reflects a close affinity to relatively hydrous, oxidizing magmas and source regions which is consistent with origins that are broadly subduction related (Frost and Lindsly, 1991). The high Fe-number of ferroan granites is apparent in the Jabal az Zuhd alkali granites and some other alkali granites from Jabal Raydan and Jabal Khur Dukhan. These iron-rich melts probably reflect derivation from reduced basaltic rocks (either tholeiitic or mildly alkalic), by either partial melting or fractional crystallization, as the magmas are likely to undergo extensive fractionation toward iron-rich, alkalic compositions (Frost and Frost, 1997). The TAS diagram shows that the studied granitoids are mildly alkaline and this may indicate higher melt fractions and consequently a high degree of melting. However, high melt fractions need to have high MgO and SiO_2 contents. Such characteristics were mostly noticed in the Jabal az Zuhd alkali granite which is also considered as the most alkaline pluton with the lowest contents of Si. This may indicate deeper melts for Jabal az Zuhd than the other plutons

and this is not unexpected as there has been always a link between melt fraction and melting depth.

To conclude, a relatively anhydrous, reduced silicate melt that evolved to higher Fe/Mg ratios, is suggested to account for the formation of most of the granitoids. A slight change in the tectonic environment (from subduction-related to intra-cratonic) is also proposed.

VI.11.3. Comment on REE patterns and tectonic setting

The REE patterns of the granodiorite of Jabal Thalabah and Jabal Al-Massah (Fig. 6.6) (which are classified as volcanic-arc granites) may imply a source magma that separated from a residue containing hornblende (e.g. Gromet and Silver, 1983; Rollinson, 1993). Such granitoids are most likely in late- or post-accretion emplacement that is characterized by flatter REEs pattern than the other more alkaline anorogenic granites (Rogers and Greenberg, 1990). The absence of a Eu anomaly in these granodiorites may also indicate that significant amounts of plagioclase and amphibole remained in the residue, as the effects of Eu fractionation in amphibole and plagioclase counterbalance each other and produce a rock with no significant Eu anomaly. A positive Eu anomaly in some of the Jabal Raydan pluton may indicate cumulates and unfractionated material. The negative Ce anomaly seen in a few samples may indicate the interaction with aqueous fluids during the evolution process (Jones *et al*., 1996).

Plots of the studied granites on the Rb vs Y+Nb discrimination diagrams of Pearce *et al*. (1984) and Pearce (1996) reveal the possibility for some granites to be tectonically mistaken. However, the Rb/30-Hf-Ta*3 diagram of Harris *et al*. (1986) and that of Pitcher (1982) have permitted additional separation and can clarify the misleading tectonic proposals. Therefore, some explanation for the observed shifts in position is necessary.

The Jabal Thalabah and the Jabal Raydan plutons may suggest formation in a changing tectonic environment from first anhydrous and subsequently hydrous source regions. The anorogenic, within plate, alkali granite are considered as earlier granites (650-500 Ma) in the AS which are characterized by alkali and HFS element (Nb, Ta, Zr, Hf, Y,

HREE) enrichment and a Rb and LREE depleted source region for the magmas, and is consistent with a source from crustal rocks which had an age of less than 800 Ma (Harris, 1984). Such anorogenic alkaline complexes can also be exemplified by anorogenic complexes in Egypt, NE and central Sudan, Niger, Nigeria, Cameroon, Malawi, Mozambique, Zimbabwe, Namibia and Angola that have an age range of 550 to 500 Ma (Vail, 1989). The presence of xenoliths in the Jabal Thalabah and Jabal Al-Massah granodiorites support the suggestion of crustal contamination which is also supported by the nested-like nature (stoping) of the Jabal Al-Massah pluton. Asimilation and mixing may have displaced the positions of these rocks on the classification diagrams (e.g. mixing with more mafic rocks would deplete the magma in Rb, Y and Nb and move the plots from the syn- and/or the post-collision field and put them in the volcanic-arc setting. Later igneous activity and fluid alteration may also have caused mobility of many incompatible trace elements, again displacing some of the granites from the post-collisional field.

The slight variation in the composition of the suggested post-collisional granitoids may directly relate to the fact that the chemical composition of these types of granites is due to the relative proportions of mantle and crustal-derived magmas and on the enrichment history of the mantle concerned (Pearce *et al*., 1984). Typical post-collision granites that plot in the volcanic-arc granites and (partially) the syn-collision fields (the Adamello and Querigut pluton from Pearce *et al*., 1984) show a similar general trend to that of the Jabal Raydan and Jabal Al-Massah plutons. This means these plutons do not necessarily represent volcanic-arc granites.

To conclude, it is suggested that the less evolved granitoids were emplaced in a hydrous, subduction-related environment while the more evolved granites were most likely emplaced in an anhydrous stable continental setting. Certain processes like fluid alteration and assimilation could possibly have affected the plots of the samples on the tectonic setting diagrams, as they could affect the Nb and Rb content and therefore cause displacement of the plotted samples (see Fig 6.10 d and 6.11).

VI.11.4. Comparisons

According to Drysdall *et al.* (1986) some of the plutons studied here and others in the Arabian Shield (e.g. the alkali and monzogranites of Jabal Ulub, Jabal Subh, Jabal Hamrah, Jabal Dabbagh and Jabal Said alkali) also display similar normalized REE profiles. Similar normative values (especially to the Jabal Al-Massah, Jabal Khur Dukhan and Jabal Raydan plutons) can be seen in the Jabal Silsilah complex (Du Bray, 1986), the Sidarah monzogranite (Jackson, 1986), the Jabalat alkali-feldspar granite (Al-Tayyar *et al*., 1986), and the Jabal Umm Al Suqian albitized apogranite (Bokhari *et al*., 1986). Some of these and others (e.g. the post-orogenic metaluminous Akash granite; Kellogg and Smith, 1986) also indicate a similar tectonic emplacement environment. This may indicate that these granites represent a regional event of granite formation across the Arabian Shield.

Based on the mineralogy and major, trace and RE elements, the alkali-feldspar granites of Jabal az Zuhd show the typical chemical characteristics of post-orogenic, evolved magmatism. However, the mineralogy and some element ratios (Zr/Nb, K/Ba, Rb/Sr) in addition to comparison with other chemically similar granitoids in the Arabian Shield and elsewhere suggest that the pluton developed in attenuated crust during the waning (relaxation) stage of the Pan African Orogeny. On a global scale, the Jabal az Zuhd alkali-granites show similar geochemical characteristics (variable peralkaline granites emplaced in the within-plate field) to other plutons such as the northern Daolinshan granites from China (Wang *et al*., 2010), the Homrit Mukbid pink granite from the central eastern desert of Egypt (Hassanen and Harraz, 1995), the Late Neoproterozoic granites of Jabal Kamil, NW Sudan (Kuster and Harms, 1998) and the late Precambrian Hasan Robat hypersolvus granite form Iran (Esfahani *et al*., 2010). Although the latter was assumed to be lithologically and mineralogically similar to the Jabal Raydan pluton, it shows a slightly different tectonic environment but a similar magmatic affinity for the subsolvus granites. The geochemical characteristics of the Singo granite from Uganda (Nagudi *et al*., 2003) are confirmed as similar to the Jabal Raydan pluton. A slight difference was noticed which may refer to both the emplacement span of the Jabal Raydan pluton and the evolution (more evolved) of their granites. In addition to the lithological and mineralogical similarities that been mentioned in the chapter 4 between Homrit Waggat Complex (Hassanen, 1997) from Egypt and Jabal Khur Dukhan plutons, the two plutons have also shown similarities in their geochemical characteristics

(tectonic environment and geochemical affinity). However, the Homrit Waggat Complex shows a dissimilar tectonic environment to that of the Jabal Al-Massah pluton (they were assumed to be identical in the chapter 4). Several late orogenic, subsolvus, calc-alkaline granitoids (e.g. the 830–740 Ma granites in the Yangtze Block south China that was studied by Wang *et al*., 2010 and the Madagascar granites that was studied by Kuster and Harms (1998) show similar geochemical characteristics to that of the Jabal Thalabah and Jabal Al-Massah plutons.

To summarize, various Arabian Shield and global examples of igneous plutons are similar in character and/or tectonic setting to the studied plutons. Such comparisons help in understanding the geological history of the studied plutons. The nature and tectonic setting of these plutons, coupled with further geochronological data (from chapter 7), will be integrated to see how and when the studied plutons fit into the tectonic history of the Arabian Shield. This will be done by producing a model that takes into account some previously generated Arabian Shield evolution models (see chapter 9).

VI.11.5. Suggestion for rock genesis

Several bivariate diagrams (Fig. 6.13a to d) have been used as an aid in determining magma source composition and the possible tectonic environment. The diagrams used are:

- $(Na_2O+K_2O)/(FeO^*+MgO+TiO_2)$ vs $Na_2O+K_2O+FeO^*+MgO+TiO_2$ diagram of Patino Douce (1999), who delineated fields of different melt compositions produced by experimental, dehydration melting of metasedimentary rocks.

- Nb/La vs SiO_2 diagram of Wang *et al*. (2005), who observed some geochemical signatures that indicated crustal contamination during magma ascent in the Dabie Orogen, Central China.

- Nb/Th vs Nb diagram from Hofmann (1988) who normalized the average chemical compositions of the continental crust and the oceanic crust (represented by MORB) to primitive mantle values. The compositional fields of

continental crust, mid-ocean ridge basalts, ocean island basalts and arc volcanics were derived from Schmidberger and Hegner (1999).

- Rb/Y vs Nb/Y plot of Pearce *et al.* (1990) who plotted the composition of the continental crust (from Taylor and McLennan, 1985) and suggested the possible composition for the total and lower crust and the trends that represent enrichment of within-plate and subduction zone, crustal contamination.

The studied granitoid compositions have been compared with those produced by experimental dehydration melting of metasedimentary rocks (Fig. 6.13, a). These comparisons indicate that the studied granitoids have a similar magma source and they could have been produced by partial melting of metagreywackes. Some samples also plot just inside the amphibolite field. However, this would contradict the earlier suggstion of a mafic magma source for the granites. Some samples from Jabal az Zuhd plot away from the rest of the samples, indicating a different source of magma and some samples from the other plutons extend further up the diagram, away from the felsic pelite partial melting field. These have most likely been subjected to other processes of formation, such as fractional crystallization and/or crustal contamination and/or subsolidus alteration. The magma source is discussed further later.

The Nb/Th vs Nb diagram shows a generally similar trend and composition for all of the studied granitoids. However, exceptionally Jabal az Zhud seems to have a different magma source that is close to that of primitive mantle. Jabal Thalabah shows a discontinuous trend as it seems to have two groups, possibly from two different sources (possible magma mixing or assimilation?). The granites mostly fit into the arc volcanics composition field, especially the Jabal Thalabah, Jabal Al-Massah and Jabal Raydan granitoids. These partially extend into the ocean-island basalt field (equal to within-plate) that is mostly occupied by the Jabal Khur Dukhan and Jabal az Zuhd granitoids. The general plot of the samples also indicates a transitional period of emplacement from arc-arc collision to intra-plate rifting (possibly from subduction-related to island-arc collision to within-plate) of the latter two granitoids and indicating more evolved magma emplaced in a stable craton.

The Rb/Y vs Nb/Y plot suggests that the Jabal Khur Dukhan granitoids were generated from the lower crust and were less contaminated by crust than the other plutons. A within-plate enrichment trend appears to be present. However, the other plutons seem to be evolved from the bulk crust; some follow the within-plate enrichment trend (Jabal az Zuhd and Jabal Raydan) but are partially contaminated by crust, while Jabal Al-Massah and Jabal Thalabah follow the subduction zone enrichment trend and indicate magma mixing processes for the latter. The suggested crustal contamination process is highly noticeable in the Nb/La vs SiO_2 diagram where some parts of each pluton seem to follow the assimilation-combined fractional crystallization trend.

Genetically, Harris (1985) has classified the alkaline complexes of the Arabian Shield into two types, peralkaline to non-peralkaline anorogenic (e.g. Jabal Aja: crustal derived material in the peralkaline magmas. The complex shows chemical heterogeneity with abundances of Zr, Y and Nb and genetically occurred in a relaxation event that followed a progressive collision (Radain *et al*. 1981) and non-peralkaline subduction-related (e.g. Jabal Sayid complex: source region in the mantle wedge overlying a subduction zone). Based on the geochemical study it was suggested that the Jabal az Zuhd and Jabal Khur Dukan pluton may belong to the first type while the rest of the plutons may belongs to the second type of the alkaline complexes of Harris classification.

VI.11.6. Processes of formation

Several processes appear to have been responsible for the formation of the studied granitoids and these are partial melting, fractional crystallization, rock assimilation and post-solidification alteration. Earlier, it was difficult to demonstrate fractional crystallization using the variation diagrams, possibly because of the affects of assimilation and subsolidus processes. A discrimination between various processes of formation (Fig.6.14) has indicated that the undifferentiated (mostly granodiorite) and the least evolved rocks are not arranged on a linear trend, while the highly-fractionated rocks (mostly alkali granite) are arranged on a linear trend. The affect of the assimilation process was noticed by the dislocation of the less evolved or the more evolved rocks from their expected position on a normal fractionation trend line. This process was also suggested based on the earlier modal composition diagram (Fig. 6.15) as some of the plotted samples have Rb contents which do not show a consistent

relationship of increasing Rb values towards the more evolved granitoids and indicate other processes might be operating.

VI.11.7. Comment on the economic study

The geochemical analyses have shown that some high rare metal concentrations occur in some of the alkali granites, indicating some potential for the presence of these elements in higher concentrations. The analyses of JZ2 and KD28 are particularly interesting as they display high total rare earth oxide contents and more detailed work in these areas is recommended.

Obviously, this study is not detailed enough to conclude if a rare metal deposit exists in the region as a variety of factors, including size and cut-off grade (COG) would be important. With rare metal deposits the COG always varies, because its determination is based on variable factors but especially the hydrometallurgical recovery, which is itself based on mineralogy (Avalon Rare Metals Inc., 2011). For example, the company that runs the Bull Hill deposit in the US has suggested 1 to 2.5% rare earth oxides (REOs) as a cut-off grade and considered values above 0.5% as low-grade material (Rare Element Resources Ltd., 2012). The Taseko Mines Limited Company shows ranges (0.10 to 0.30 wt%) of COG which varies with the Nb2O5 grade (Taseko Mines Ltd., 2011). Furthermore the exact elements present can be important; for instance a combined La+Ce+Y value in the Tawlah and Ghurayyah deposits is given as 0.15 to 0.50% (Kuster, 2009) and the Foxtrot Project (Minerals Announces Resource Estimates, 2011) shows 0.21% for the HREO+Y and 0.89% for the TREO+Y. It was not unexpected that these granites showed polymetallic Zr, Nb, Y and REE enrichment, as this was found to be a common feature of the specialized alkali granites in the northern part of the Arabian Shield, especially in the Midyan terrain (Jackson, 1986). This type of specialization is known as ‘agpaitic’ and has been identified in other parts of the Arabian shield (e.g. Ghurayyah, Umm al Birak, Jabal Sa`id and Jabal Hadb ad Dayahin) by Ramsay (1986) and Drysdall et al. (1984). However, agpaitic rocks also show enrichment in Th and U which was not found in these granites. This means that these rocks have not quite reached the optimum level of enrichment to be called agpaitic. These characteristics are (ppm): F>1000, Be>7, La>70, Li>40, Nb>70, Rb>200, Y>60, Ba<200, Sr<80, Rb/Sr>18, Y/Ba>4, Rb/Ba>6, Ba/Be>10 or K/Rb<200 (Ramsay; 1986).

It has been discovered that these enriched granites are possible economic targets, although there are slight differences in mineralogy between each pluton. Although the economic potential of these granites is not yet definite, because economic rare metal deposits associated with alkali granites commonly have a low-grade (e.g. 1.16wt% REOs for Strange Lake, 0.51wt% REOs for Zues in Canada and 1.07 REOs for Uvane in Greenland; British Geological Survey, 2011) the potential is clearly present. In addition, the extraction of REE is highly dependant on mineralogy. From a review of large numbers of Nb-Y-Zr-REE deposits in the world it seems that the most common rare metals-bearing minerals found are fergusonite, xenotime, monazite, synchysite, columbite, pyrochlore and samarskite. The presence of some of the above mentioned rare earth and rare metal-bearing minerals in this study indicates that these Midyan granites are unusual. More detailed sampling from the areas of the enriched rocks is justified. Very few samples were gathered from the pegmatitic and felsic veins of Jabal Thalabah and Jabal Raydan; these show high Nb and Y contents and would be worth further study. The studied granites seem to be better targets for REE than the rare metals, but new REE targets will probably also lead to the occurrence of enrichments of rare metals.

VI.11.8. Conclusion

To conclude, the geochemical study has supported the earlier petrographic and mineralogical studies, as it has confirmed the rock classification for each pluton, confirmed the differences between the studied plutons, proved the suggested REE enrichment in some plutons and the proposed similarity for the tectonic environment for the studied intrusives, clarified the strong affect of late-stage subsolidus alteration, demonstrated the affects of fractionation processes and strengthened the initial views about the rock genesis and depth of emplacement. The suggestion for the rock genesis has taken into account the proposal from Frost et al. (2001) during the classification of the studied rocks. This has indicated that the granites were most likely derived by low-pressure (shallower melting for Jabal az Zuhd) partial melting of calc-alkalic crustal rocks with possible crustal contamination, followed by fractional crystallization and later sub-solidus alteration. Crustal assimilation is indicated from the chemical composition of the granitoids and confirms observations from the mineralogical studies. It is proposed that most of the studied granites extend from a post-collision to within-plate setting. The economic study has suggested the following:

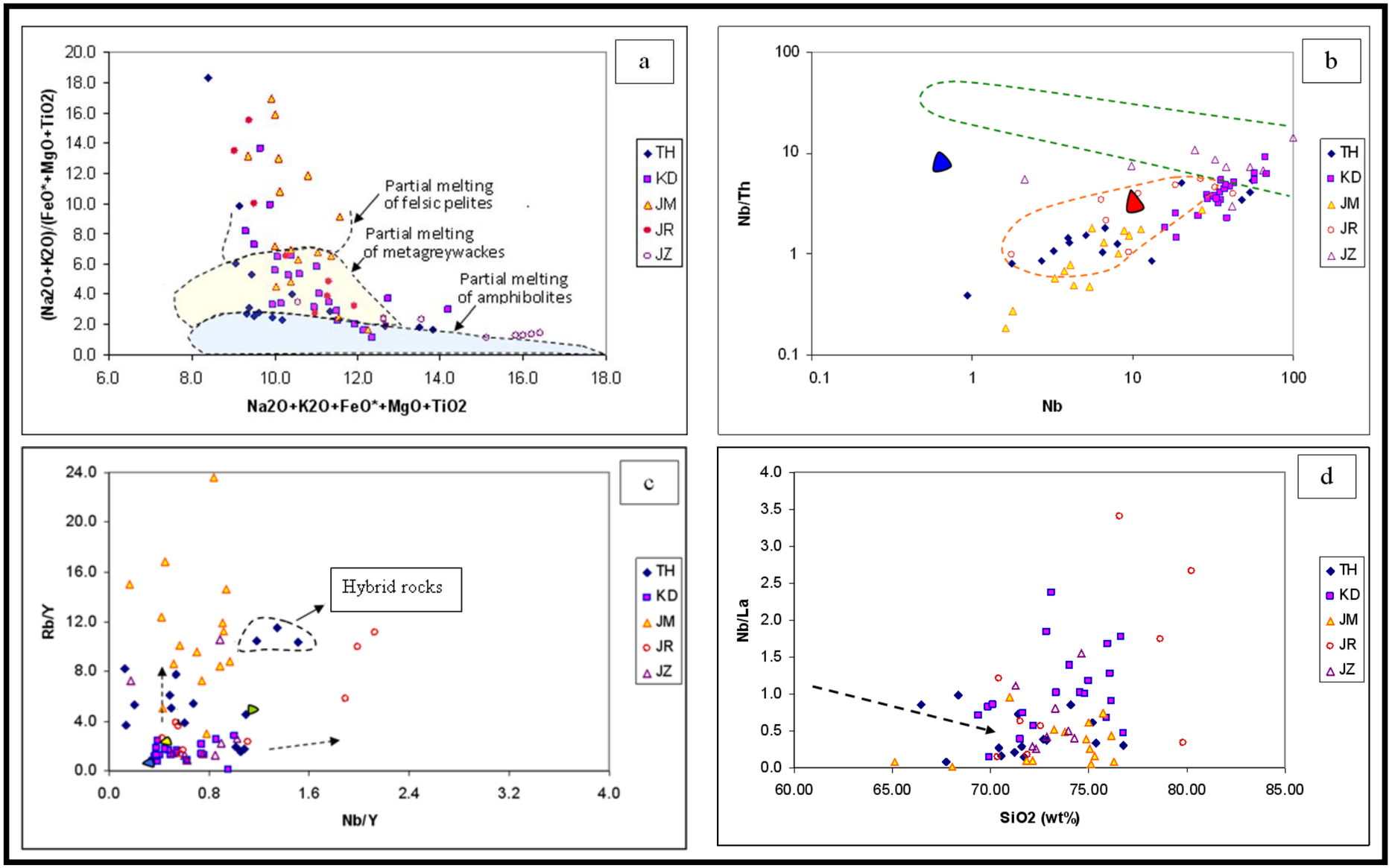

Figure 6.13: Plot of the studied granites to show suggested magma source composition and possible processes of formation (a) $(Na_2O+K_2O)/(FeO^*+MgO+TiO_2)$ vs $Na_2O+K_2O+FeO^*+MgO+TiO_2$ showing compositions of the studied granitoids compared to melts produced by experimental dehydration melting of meta-sedimentary rocks (fields of melt compositions after Douce, 1999). (b) Nb/Th vs Nb diagram. Primitive mantle (blue triangle) after Hofmann (1988); continental crust (red triangle), mid-ocean ridge basalts + ocean–island basalts (green field), and arc volcanics compositions (orange field) after Schmidberger and Hegner (1999). (c) Rb/Y vs Nb/Y plot of the studied granites after Pearce *et al*. (1990). The compositions of the lower (the blue triangle)-, bulk (the yellow triangle)-, and upper (the green triangle) crusts are after Taylor and McLennan (1985); the vectors for the subduction zone enrichment or crustal contamination (vertical arrow) and within-plate enrichment (inclined arrow) are based on the data of Pearce *et al*. (1990). (d) Nb/La vs SiO_2 diagram showing the suggested assimilation-combined fractional crystallization trend, after Wang *et al*. (2005).

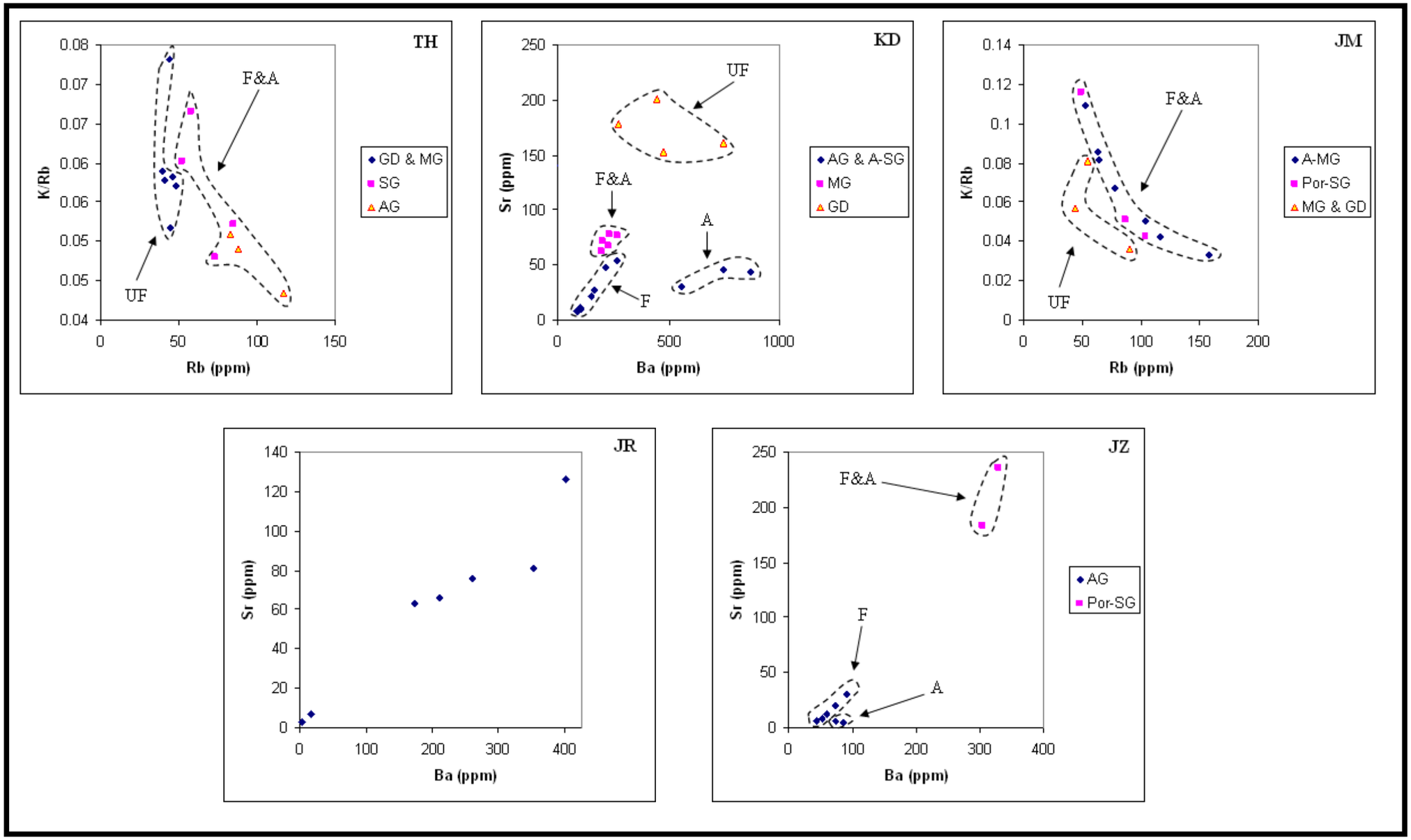

Figure 6.14: Variation diagrams showing dominant affect of fractionation (F), assimilation (A), both (F & A) and also the unfractionated (UF) rocks. Abbreviations: TH, Jabal Thalabah, KD, Jabal Khur Dukhan, JM, Jabal Al-Massah, JR, Jabal Raydan, JZ, Jabal az Zuhd, GD, granodiorite, MG, monzogranite, SG, syenogranite, Por-SG, porphyritic syenogranite, AG, alkali granite, A-SG, alkali to syenogranite, A-MG, alkali to monzogranite.

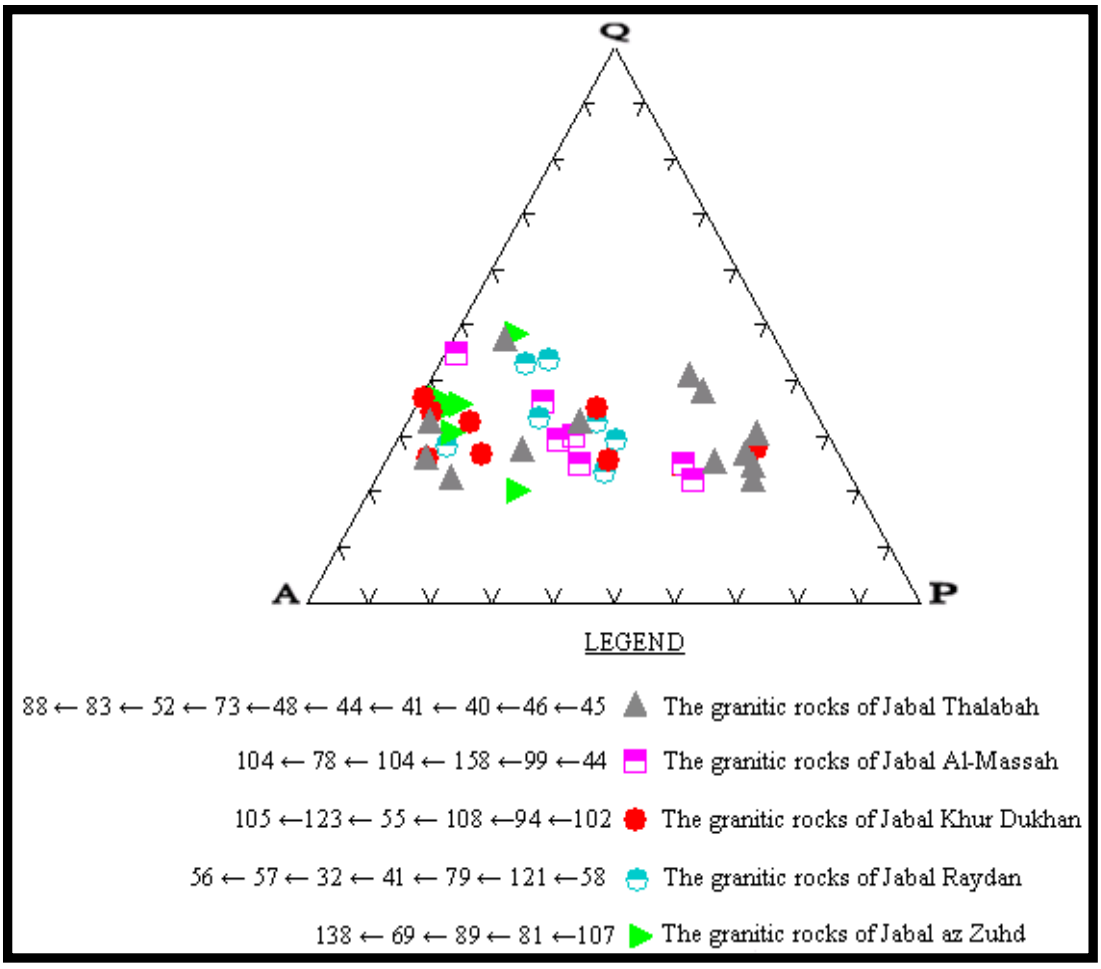

Figure 6.15: Modal composition diagram with Rb values (from the plagioclase apex to the alkali feldspar apex) for some of the granitic rocks.

1- The fractionation process (most fractionated and specifically most ferroan) and alkaline nature (late subsolidus fluids) are the main controlling factors for the enrichment. The hydrothermal alteration show minor enrichment impact.

2- Further work is recommended on the very alkaline varieties of granite at Jabal az Zuhd, Jabal Khur Dukahn and Jabal Al-Massah, the pegmatitc and porphyritic felsic dykes of Jabal Raydan and the mafic dykes of Jabal Thalabah, as these are considered to be the best targets in the study areas. The presence of Au-Pt alloy and free Ag in the Jabal Khur Dukhan pluton requires more detailed mineralogical work.

3- Although the hybrid rocks of Jabal Thalabah displayed high rare metal contents, this is not necessarily justification to do further work as the mineral hosts are silicates which consequently would make any extraction process both complicated and uneconomic. Recently, the Saudi government has signed an agreement to exploit the world's largest tantalum deposit of Ghurayyah, aiming to supply 10% of the world annual demand (Tertiary Minerals plc. 2006).

VII. Geochronology

VII.1. Introduction

This chapter is mainly concerned with defining ages and assessing the evolution and source material for the granitic rocks in the study areas. This was achieved by:

1) Rb-Sr radiogenic isotopic analysis of whole rocks, and

2) U-Pb isotopic analysis of zircons.

VII.2. Methodology

Using the mineralogical and geochemical rock classifications (and in particular the zircon abundance and Rb/Sr ratios), nineteen whole-rock samples, representing different granitic units from each of the studied plutons, were selected to be analyzed for Rb-Sr isotopic compositions and 5 samples were selected for zircon dating. Three samples were used for both dating methods and also included one hybrid sample from Jabal Thalabah, to date the local hybridization event. The samples (see appendix IV) were deliberately collected away from sites of known hydrothermal alteration. Their field locations are shown on the constructed geological maps in chapter three.

For the Rb-Sr work, the selected samples were analyzed for Sr isotopic ratios by Thermal Ionic Mass Spectrometer (TIMS), using standard methods and using the Sr analyses already presented in chapter six. The work was carried out in the Department of Earth Sciences at Royal Holloway, University of London (see appendix IV).

For the U-Pb zircon analysis, zircons were hand-picked using a binocular microscope from the heavy mineral concentrate produced by magnetic and heavy liquid separations. Zircons were separated from all of the plutons except Jabal Al-Massah which appeared to be very poor in zircon. The zircons were mounted, polished and then dated using LA-ICP-MS (Laser Ablation Inductively Coupled Plasma Mass Spectrometry) at University College of London. Concordia plots were generated using the software program "Isoplot'. Full details of the analytical methods and accuracy are presented in appendix IV.

The LA-ICP-MS zircon method is not as precise as that of the Shrimp and the latter has much better spatial resolution. While the method used here analyses relatively large areas, the Shrimp can analyse individual zones within a single grain of zircon and consequently it has been used many zircon dating studies (e.g. the Caddy Lake granites in Canada, Halden *et al*., 2007; the Neoproterozoic granitoids in south China, Wang *et al*., 2006; the A-type granites in southern India, Sato *et al*., 2010).

Because of its longer half life, the Pb^{206}/U^{238} ratio was believed to be the most appropriate one for Proterozoic rocks and therefore it was chosen to represent the ages. However, ages derived from the other isotopic ratios (Pb^{207}/U^{235}, Pb^{208}/Pb^{206}, Pb^{207}/Pb^{206}) can also be used but their accuracy is probably lower.

VII.3. Sr results

The Sr isotopic results are shown in Table 7.1. Isochrons were generated using the software program 'Isoplot' using the Sr isotopic analyses from TIMS and the Rb and Sr concentrations from the ICP analysis. The Rb-Sr whole-rock isochron plots and derived ages are given in Figs. 7.1 and 7.2.

Based on the isochron plots, the ages of the plutons span almost 200 Ma as they range from 518 to 720 Ma. Jabal Al-Massah shows the youngest age whereas Jabal Thalabah shows the oldest. The plutons show a modest age uncertainty (~ 50 to 70 Ma) except for Jabal az Zuhd that has an uncertainty of 140 Ma. The isochron for Jabal Raydan gives an age of 776± 210 Ma, which may be because it is only based on 3 points while the other plutons used 4 points. Based on the later comparison with the U-Pb analyses and some previously published dating, the Rb-Sr age for Jabal Raydan is considered unreliable and excluded. In terms of initial ratios, similar values were observed for Jabal Thalabah (0.700) and Jabal Raydan (0.698) and also between Jabal Khur Dukhan (0.7052) and Jabal Al-Massah (0.7054), while Jabal az Zuhd exceptionally shows a much higher value (0.718).

Table 7.1: Strontium isotopic data of representative samples from the studied granites

	Sample	Rb (ppm)	Sr (ppm)	$^{87}Rb/^{86}Sr$	$^{87}Sr/^{86}Sr$	$(^{87}Sr/^{86}Sr)$ i	Absolute errors	MSWD
AM	TH12`	85	8	31.69484	1.025949 ± 31	0.7000 ± 0.0027	0.0035	11.7
HFCA	TH12	58	74	2.27101	0.724225 ± 14			
	TH10`	73	59	3.58855	0.73370 ± 12			
	TH5`	52	190	0.78718	0.709644 ± 11			
APL	KD28	55	44	3.37926	0.737314 ± 17	0.7052 ± 0.0034	0.0021	3.5
HFCA	KD41	3	140	0.05380	0.704766 ± 11			
	KD37	123	8	45.77892	1.093870 ± 43			
	KD13	107	68	4.57494	0.744445 ± 10			
HFCA	JM31	64	185	1.00665	0.711789 ± 11	0.7054 ± 0.0062	0.0041	57
	JM27	63	37	4.96577	0.740275 ± 13			
	JM18	158	21	21.78070	0.866312 ± 38			
	JM16	104	169	1.78170	0.720749 ± 14			
AM	JR12	79	76	3.00384	0.729580 ± 11	0.698 ± 0.0027	0.0053	23
HFCA	JR9	41	3	41.92572	1.161624 ± 19			
	JR3E	58	81	2.07092	0.723070 ± 14			
APK	JZ10	81	5	44.05872	1.064500 ± 20	0.718 ± 0.047	0.026	14
	JZ8	69	31	6.48073	0.764212			
	JZ6	138	21	19.57569	0.890878 ± 10			
	JZ2	79	30	9.31333	0.78805 ± 3			

* Errors or uncertainties were reported as two standard errors (2 se) for samples with 95% confidence limit.

* Calculated initial ratios using ages and uncertainties in Fig. 7.1.

* Source parameters for model ages are $0.0736^{87}Rb/^{86}Sr$ and $0.7039^{87}Sr/^{86}Sr$

Explanation for abbreviations: TH, Jabal Thalabah, KD, Jabal Khur Dukhan, JM, Jabal Al-Massah, JR, Jabal Raydan, JZ, Jabal az Zuhd, AM, alkali metaluminous, APL, alkali peraluminous, APK, alkali peralkaline, HFCA, highly fractionated calc-alkaline.

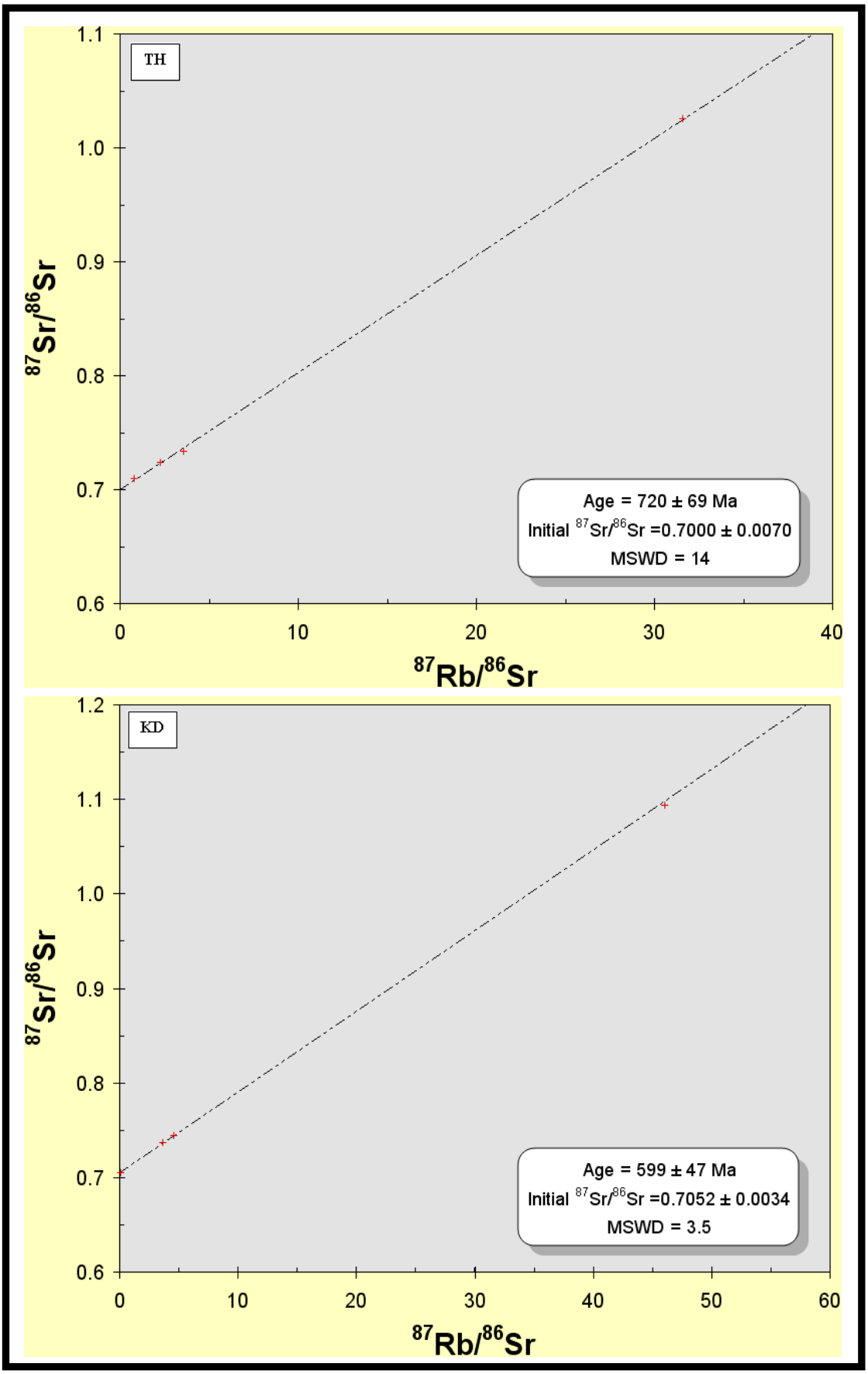

Figure 7.1: Rb-Sr whole-rock isochron plots for the studied granites. Abbreviations: TH, Jabal Thalabah, KD, Jabal Khur Dukhan.

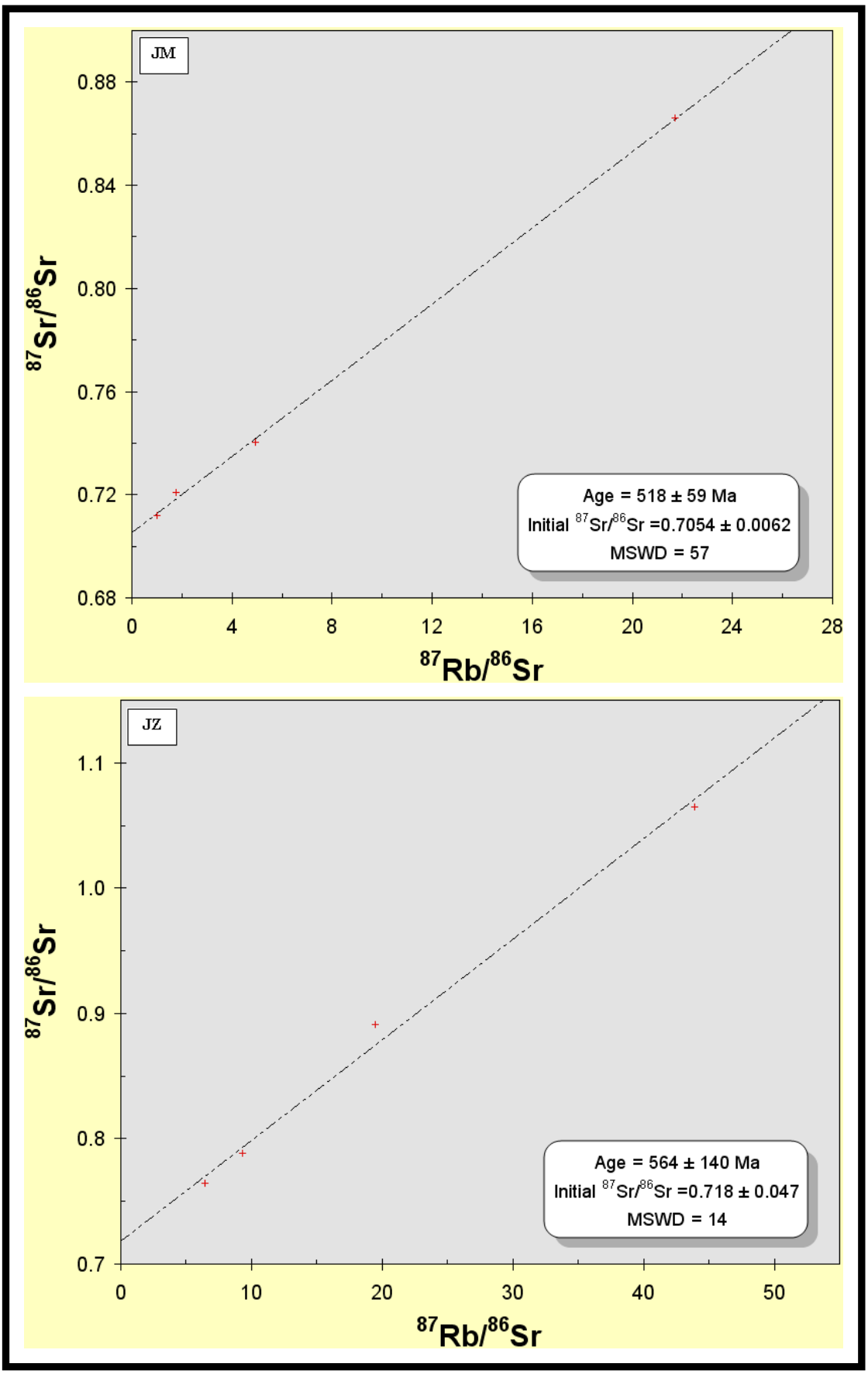

Figure 7.2: Rb-Sr whole-rock isochron plots for the studied granites. Abbreviations: JM, Jabal Al-Massah, JZ, Jabal az Zuhd.

The observed similarity in the initial $^{87}Sr/^{86}Sr$ ratios may indicate a similar magma source. Jabal az Zuhd, with a quite different initial $^{87}Sr/^{86}Sr$ ratio, presumably has a different magma source from the other plutons. Igneous source material is suggested for the studied plutons, except for Jabal az Zuhd which is suggested to have a sedimentary source.

VII.4. Results of the U-Pb analysis

The full results of the U-Pb analyses are given in appendix IV. The results from different isotopic systems are summarised in Table 7.2 and Figs 7.3 and 7.4. The LA ICP-MS $^{206}Pb/^{238}U$ ages for these zircons yield consistent ages of 554 to 634 Ma. Ages based on $^{207}Pb/^{235}U$ are very similar.

Most of the data appear to be concordant and relatively few points plot away from the concordia. Although a mixing line has been plotted in the figures and intercept ages calculated, their significance is doubtful.

Table 7.2: Ages (Ma) from the U-Pb zircon analyses (error: 1s)

	From Concordia plot		Average age	
	Upper intercept	Lower intercept	$^{206}Pb/^{238}U$	$^{207}Pb/^{235}U$
TH	4681±310	576±17	581	608
KD	2311±790	474±100	590	609
JR	3269±1700	597±42	634	637
JZ	2417±780	533±44	554	554

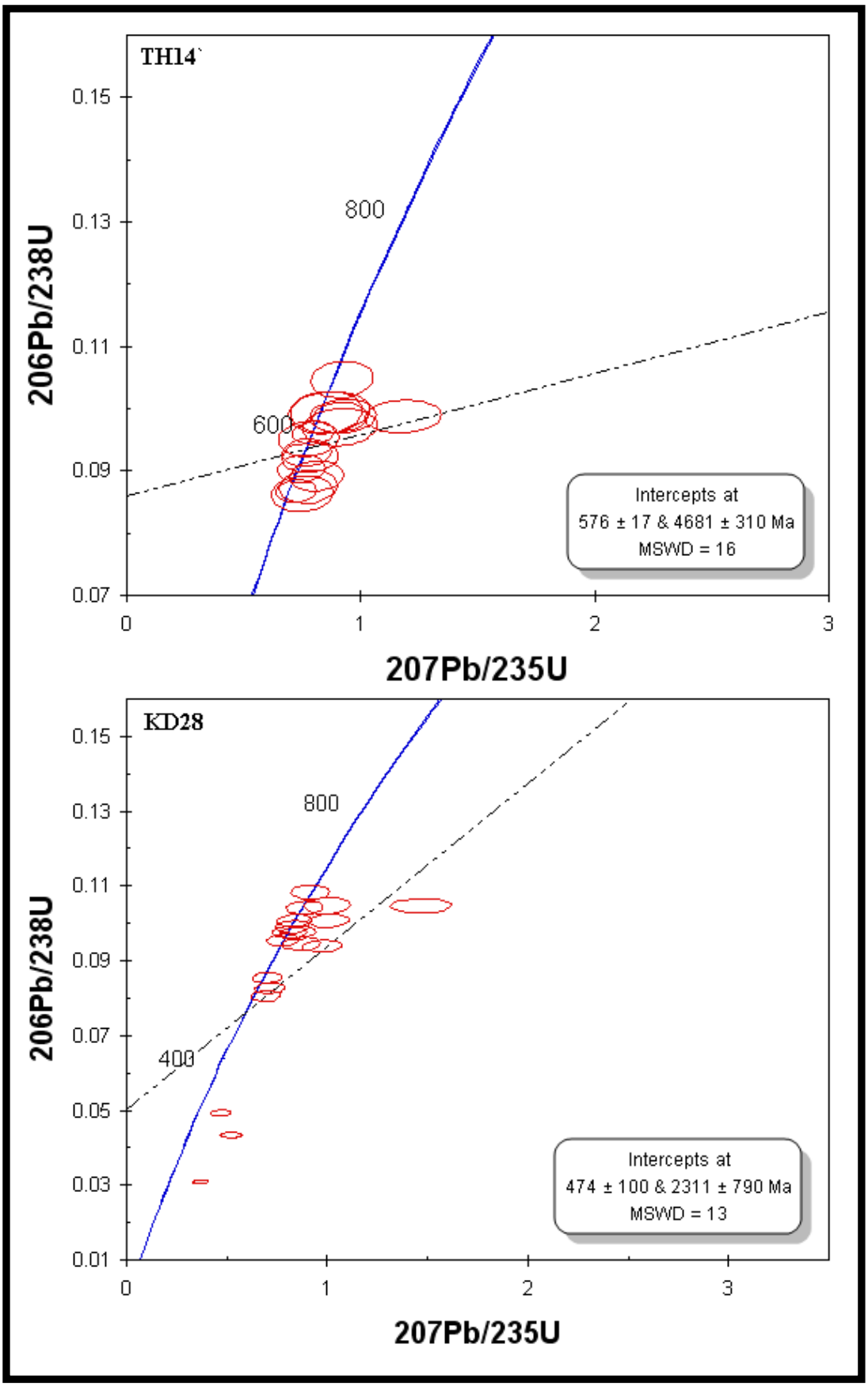

Figure 7.3: Zircon U-Pb Concordia plots for the studied plutons (error: 1s). Dashed line is the best fit line. Abbreviations: TH, Jabal Thalabah, KD, Jabal Khur Dukhan.

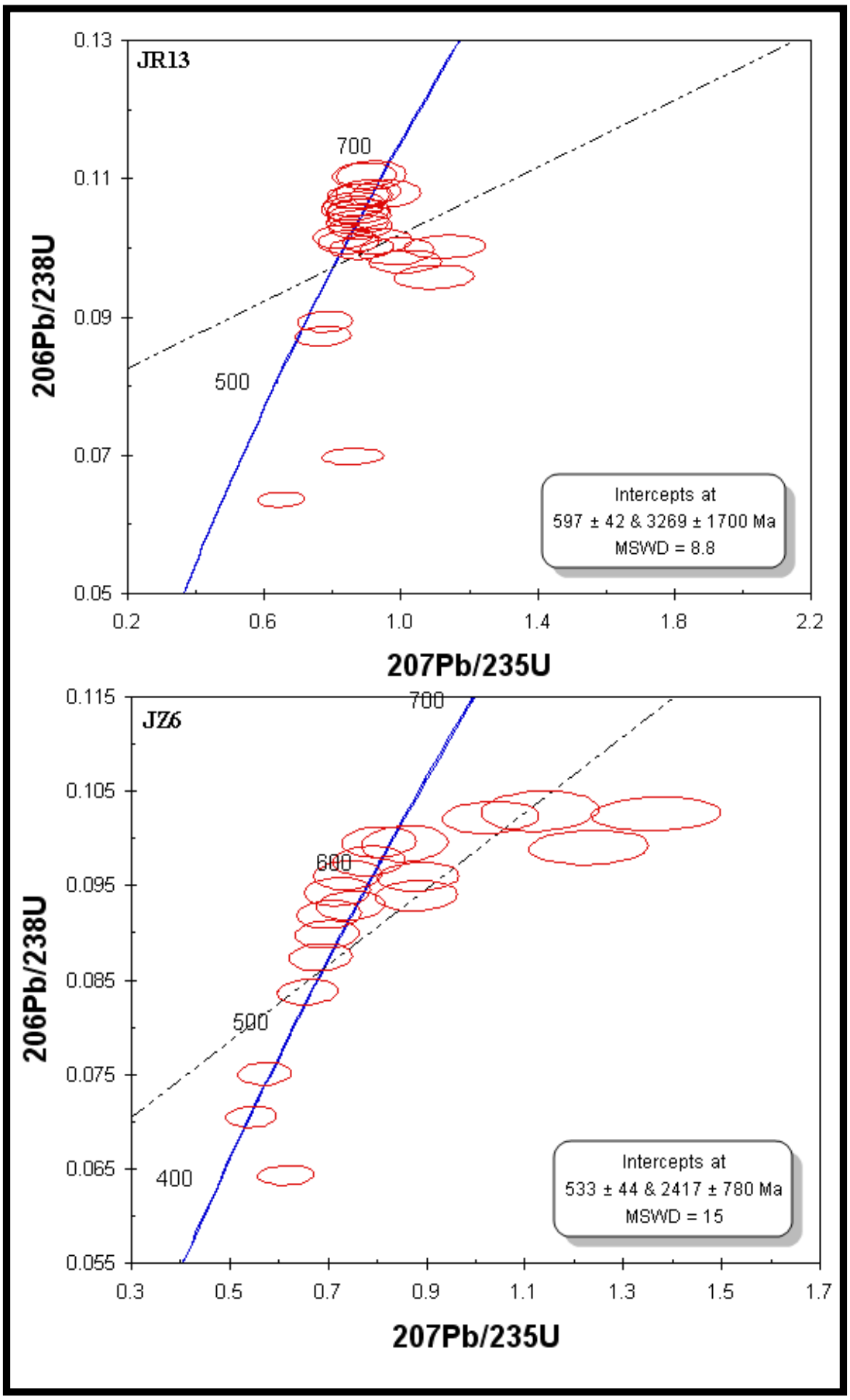

Figure 7.4: Zircon U-Pb Concordia plots for the studied plutons (error: 1s). Dashed line is the best fit line. Abbreviations: JR, Jabal Raydan, JZ, Jabal az Zuhd.

According to Koksal *et al*. (2012), if points do plot off the concordia, the older intercept ages on the concordia may reflect mixing with old material, while the younger intercept ages could mark the age of granite crystallization or the timing of a younger event (e.g. metasomatic alteration) (e.g. Wu *et al*., 2007; Harley and Kelly, 2007). However, because there is little evidence for zircon inheritance, it is probable that the discordance is likely due to Pb loss (Wang *et al*., 2006; Wu *et al*., 2007). This could be natural, but it is also possible that the laser sometimes partially ablated fractures within the zircons or the epoxy mounting material.

VII.5. Comparison of Rb-Sr and U-Pb ages

Ages derived from the two methods, together with some previous determinations, are presented in Table 7.3.

- Jabal Thalabah: The Rb-Sr rock age (720±69 Ma) is much older than the U-Pb zircon age (581 Ma). A very likely reason for this difference is that the zircon age represents the time of magma crystallization, whereas the apparent Rb-Sr isochron represents a mixing line between magma source material and older crust with higher Rb/Sr ratios.

- Jabal Khur Dukhan: The ages from both dating methods (590 and 599±47 Ma) are very similar and probably represent the emplacement age.

- Jabal Al-Massah: The Rb-Sr age (518±59 Ma) is less than the previously determined Rb-Sr age of 630 Ma.

- Jabal Raydan: The zircon age (634 Ma) is much less than the Rb-Sr age (although the latter has a large error, 210 Ma). Mixing may also be invoked here.

- Jabal az Zuhd: The age from the zircon analysis (554 Ma) is very simiar to the Rb-Sr age (564±140 Ma) and is considered as the crystallisation age of this pluton.

VII.6. Discussion

The results for the initial $^{87}Sr/^{86}Sr$ ratios at the time of crystallization of the five plutons provide information about processes of formation and magma source. The ages can be used to show how the intrusives were emplaced during the Arabian Shield evolution history and clarify the sequence of events for each pluton (see chapter 9).

VII.6.1 Comment on initial $^{87}Sr/^{86}Sr$ ratios

The initial $^{87}Sr/^{86}Sr$ ratios for the studied rocks are mostly low (except Jabal az Zuhd). Such low ratios are common in the Arabian Shield felsic plutons. These are exemplified by the Jabal Tays and Jabal Sayid granitoids (0.703) that are suggested to have an origin by partial melting of mafic material in an island-arc tectonic setting over a subduction zone (Al-Shanti *et al*., 1984) and with insignificant contribution from the crust (Harris *et al*., 1986).

On the scale of the Arabian-Nubian Shield, the Nakfa intrusive rocks, northern Eritrea, the Wallagga area and the Ganjii granitoids, western Ethiopia, also show low initial $^{87}Sr/^{86}Sr$ ratios (0.702 to 0.704, 0.703 and < 0.703, respectively) and they were all proposed to be granitoids derived from a mantle and/or juvenile crustal source with no, or only very little, contribution from the pre-Pan-African crust or an older continental component (Teklay *et al*. 2001; Kebede and Koeberl, 2003). Globally, very similar processes of formation have been also proposed for the Bulguksa granite in Korea and the Balkan Granite intrusion, western Turkey, both characterized by low $^{87}Sr/^{86}Sr$ ratios (0.705, 0.703 to 0.704, respectively) (Kim and Kim, 1997; Aydogan *et al*., 2008). A mantle-derived magma was also suggested for other granitoids from Scotland which show low $^{87}Sr/^{86}Sr$ initial ratios (Faure and Powell, 1972). Many granite plutons that show a range of initial $^{87}Sr/^{86}Sr$ ratios from 0.705 to 0.709 (e.g. the Damaran A-type granites, Namibia, the Nuweibi albite granite, the felsic rocks from the Sulu orogenic belt, eastern China, and the Pampean ranges granites, Argentina) are derived by a variety of processes, including partial melting of lower crust or upper enriched lithospheric mantle (Liu *et al.,* 2008) coupled with minimal involvement of LREE-enriched continental crust and limited crystal fractionation (Jung *et al*., 1998; Hassanen and Harraz,1996; Rapela *et al.,* 1982). Other plutons with higher initial $^{87}Sr/^{86}Sr$ ratios (above 0.709) like the Yayla granites from the Bitlis Massif, southeastern Turkey**,** the

granitoids of the Urucum suite, south eastern Brazil, the Jalama batholith granites from Spain, the Paresis ring complex, Namibia, the Carboniferous granitoids from Argentina and the Gabalat area, west-central Arabian Shield indicate major anatexis (Helvaci and Griffin, 1984), partial melting of pre-existing crustal material (Ruiz *et al*., 2008), and/or possibly upper (Jung *et al*., 1998, Rapela *et al.*, 1982) or lower crustal material (Radain *et al.*, 1987). It basically means that the magma formation processes is dominated by a large contribution of crustal material (Nalini *et al.*, 2000, Jones *et al*., 1996). Initial $^{87}Sr/^{86}Sr$ ratios of some plutons (0.705 to 0.709 from Jung *et al*., 1998 and 0.717 from Zaw, 1990) are similar to those of some of the studied granites. This suggests that a metatonalite source is possible for Jabal Khur Dukhan and Jabal Al-Massah and a possible derivation by melting of medium- to high-grade, regionally metamorphosed country rocks for Jabal az Zuhd. A metamorphic source rock for the studied rocks is possible based on other examples of metasedimentry rocks which show similar initial $^{87}Sr/^{86}Sr$ ratios (e.g. 0.709 to 0.730 from Buller Terrain in New Zealand, 0.651 to 0.728 from the Lachlan fold belt in southeastern Australia and 0.705 to 0.719 from southern Chile, Adams *et al*., 2005). Some Neoproterozoic granitoids in northeastern Africa which are characterised by low initial strontium ratios (0.703–0.707) are suggested to be derived from juvenile, Neoproterozoic crust (Kuster and Harms, 1998). The initial strontium ratios of Jabal Al-Massah and Jabal Khur Dukhan fit within this range, possibly indicating a similar source.

According to Mohamed and El-Sayed (2008) a major difference between the hypersolvus Gabal Gharib granite and the subsolvus Homer Akarem granite from Egypt is the initial strontium ratios (0.711 for the former and 0.706 for the latter). In the study area, the Jabal az Zuhd alkali granites are only hypersolvus and have a high initial strontium ratio > 0.711, while the other granites are both hyper- and subsolvus in nature with and have lower initial strontium ratios < 0.706). The much higher initial $^{87}Sr/^{86}Sr$ ratios of Jabal az Zuhd in comparison with the other studied plutons indicates a significant crustal contribution in the peralkaline magma as Radain *et al.* (1981) suggested for peralkaline granites elsewhere in the Arabian shield.

Genetically, the mantle-type igneous pluton has $^{87}Sr/^{86}Sr$ isotopic ratio < 0.706, while that of the crustal-type is > 0.710 (Fitton and Upton, 1987). This means that the Jabal az Zuhd granitoids could be of crustal-type while the other plutons are of mantle-type.

Generally speaking, intermediate to high ratios may indicate either hybridization of magmas with contrasting composition and source (Halliday *et al.,* 1980) or crustal contamination (Mackenzie, 1988; Jones *et al*., 1996). The isotopic studies show that upper mantle-related sources contaminated by crustal material represent a possible source material for the studied granites. Exceptionally, Jabal az Zuhd could represent anatectic melts of mostly lower crustal rocks which were contaminated with upper mantle-derived material and this may have led to an assimilation fractional crystallization process, as in the Neoproterozoic post-orogenic granites of Agudos Grandes in southeastern Brazil (Leite *et al.,* 2007).

VII.6.2 Comment on ages

The ages from both Rb-Sr and U–Pb zircon methods are compared with previously published values in Table 7.3.

Table 7.3: Ages of granites derived from different methods and previous studies (Stoeser, 1986).

	Rb-Sr (Ma)	U-Pb zircon (Ma)	Previous Rb-Sr (Ma)
TH	720±69	581	
KD	599±47	590	
JM	518±59		630
JR	776±210	634	629
JZ	564±140	554	

The ages for the studied intrusives indicate a broad duration of magmatic activities (~ 170 Ma) which fits into the Arabian Shield evolution models of both Genna *et al*. (2002) and Duyverman (1982) and the age range (517 to720 Ma) of the Arabian-Nubian Shield ring complexes that were given by Vail (1987). During the formation of the Arabian Shield the magmatic-arc stage was terminated by two collisions (680-630 Ma) resulting in a shift from arc magmatism dominated by intermediate plutonic rocks to collision-related granitic magmatism (660-610 Ma). The final phase of plutonism within the Shield (610-510 Ma) was the formation of widespread postorogenic, intracratonic,

evolved, peraluminous to peralkaline, alkali-feldspar granites (Stoeser, 1986). All the plutons appear to be Ediacaran in age. Jabal Al-Massah and Jabal Raydan are Ediacaran post-collision plutons but represent transitional stage of events. Jabal Khur Dukhan and Jabal az Zuhd represent the post-orogenic-intracratonic shift stage. Jabal az Zuhd more specifically correlates with the final suturing event of the Gondwana supercontinent that occurred between 480–560 Ma (Sato *et al*., 2010) and is contemporary with the final post-tectonic magmatic event in northern Ethiopia (Tadesse *et al*., 2000). On a global scale, the studied granites show contemporary emplacement with several other alkaline intrusives (Table 7.4).

VII.7. Conclusions

The earlier chapters have shown that each pluton is characterized by a certain lithology, mineralogy and geochemistry. This study has added more geochemical differences between the plutons. Jabal az Zuhd has already been distinguished from the other plutons by: having a different magma source, its hypersolvus and peralkaline nature, considered as the most evolved pluton, hosting alkaline amphibole, being the richest pluton in Fe and REE and rare metal content. This study has added significant information about the source material, age and evolution of the granites:

1- Source material: Jabal az Zuhd may have been derived from lower crustal source material (possibly metasedimentary) and contaminated with either a crustal component or upper mantle-derived magmas. An involvement of Archaean crustal components in the petrogenesis of these granitoids could also be possible (particularly for those of Jabal Thalabah and Jabal Raydan. The other plutons were possibly derived from an upper mantle, possibly metaigneous source and were also subjected to contamination.

2- Age: the granites range from early (Jabal Raydan and Jabal Al-Massah) to late (Jabal Khur Dukhan, Jabal Thalabah and Jabal az Zuhd) Ediacaran.

3- Evolution: the granites range from post-collision (Jabal Raydan and Jabal Al-Massah) to early intra-plate (Jabal Khur Dukhan, Jabal Thalabah and Jabal az Zuhd).

Table 7.4: Examples of granitoids with similar ages to the studied plutons

Name of Pluton	Plutons with contemporaneous emplacement	References
Jabal Raydan and Jabal Al-Massah	Nakfa intrusive rocks, northern Eritrea, 620-640 Ma	(Teklay *et al*., 2002)
Jabal Thalabah and Jabal Khur Dukhan	The Neoproterozic metaluminous Galiléia and peraluminous Urucum suites in SE Brazil, 594 ± 6 Ma and 582 ± 2 Ma.	(Leite *et al*., 2007)
	The post-collisional metaluminous granitoids in the Late Neoproterozoic East African Orogen, in northern Africa, 550-590 Ma and granites from Madagascar with 585 Ma old.	(Kuster and Harms, 1998)
Jabal Az Zuhd	Neoproterozoic granitoids in northern Ethiopia, 550 Ma.	(Tadesse *et al*., 2000)
	Post-collisional granitoids north central of Sudan, 549±12 Ma.	(Kuster and Harms, 1998)

VIII. Summary and conclusions

VIII.1. Introduction

This chapter focusses on the issues that are directly related to the aims of the project:

- Characterising the five studied intrusives in the study areas,
- Determining when they formed, how they formed and how they fit into the tectonic evolution of the Arabian Shield,
- Finding out if they could have any economic potential in terms of metal resources.

These aspects will be covered in three parts:

1) List the characteristics of the rocks and assess their similarities and differences.

2) Construct a model for the evolutionary history of the area and the sequence of events, using information about the tectonic setting, ages, magma source and depth of emplacement of the plutons.

3) Based on the above information, suggest why these plutons were emplaced in certain tectonic regimes and why they show such characteristics.

VIII.2. Characterization

The main characteristics of the studied plutons are summarized in table 8.1. Furthermore, geological maps of these granitoids have been produce (Chapter 3). Overall, the plutons are similar as they are all magnesian to ferroan, unfractionated calc-alkaline to highly fractionated alkaline and exhibit medium to high K characteristics. However, subtle differences (Table 8.2) have been observed, mostly between Jabal az Zuhd and the other plutons. Such differences may relate to a different magma source and different degrees of contamination and fractionation, which consequently have led to their different chemical characteristics.

Table 8.1: Characterization of the studied plutons

Pluton	Geology	Lithology	Mineralogy and textures	Geochemistry	Resources	Age and setting	Process of formation and magma source
Jabal Thalabah	Ring-complex structure and affected by shear zones.	MG to GD > AG to SG Coarse-medium-grained, whitish grey GD & MG and buff pinkish SG & AG	Am (katophorite), bi, ms, chl, ap, zr, tit, hm & mag Dominated by perthitic & less myrmekitic textures	Dominantly subsolvus, ferroan to magnesian, alkaline to calc-alkaline, medium to high K, low metaluminous to variable peraluminous	Low potential: poorest pluton in rare metals; found associated with ap, zr & tit.	Rb-Sr: 720 Ma (mixing?) U-Pb zircon: 581 Ma (crystallization age). Post-orogenic to within-plate magmatism	Partial melting, fractionation, local hybridization (late) and subsoldus alteration From an upper mantle source
Jabal Khur Dukhan	Heterogeneous. Comprises two plutons that show no clear, relative age relationships.	AG to SG > MG to GD Coarse-medium- grained, porphyritic, light grey GD & MG and pinkish to reddish SG & AFG	Am (rare, not characterised) bi, chl, ap, zr, alla, fl, hm, mag, ilm, xe, ferg, syn (?), Au-Pt alloy & free Ag. Shows well-developed perthitic & less myrmekitic textures.	Dominantly subsolvus and ferroan, alkaline to calc-alkaline, medium to very high K, mildly metaluminous to peraluminous.	Potential: the second richest pluton in rare metals and their minerals	Age of emplacement from 599 (Rb-Sr) to 590 (U-Pb zircon) Ma Post-orogenic to within-plate magmatism	Partial melting, assimilation-fractional crystallization, fractionation and subsoldus alteration From an upper mantle source
Jabal Al-Massah	Shows clear nested structure with unclear boundaries.	AG to MG > GD Coarse-grained whitish MG, light grey GD and reddish AFG, and porphyritic pinkish-reddish SG	Am (gedrite), bi , ms, chl, ap, zr, hm, mag & mo Shows well-developed perthitic & less myrmekitic textures	Dominantly subsolvus and ferroan to magnesian, alkaline to calc-alkaline, medium to high K, mildly metaluminous to peraluminous	Low potential: largest amount of monazite. Rare metals are associated with zr, apatite & mo.	Rb-Sr: 518 Ma (metasomatic age?) Previous Rb-Sr: 629 Ma (emplacement age?). Syn- to Post-orogenic magmatism	Partial melting, assimilation-fractional crystallization and subsolidus alteration. From an upper mantle source
Jabal Raydan	Shows incomplete double ring-complex structure	AG to MG > AG to SG Coarse & medium-grained white MG and reddish AFG and less porphyritic pinkish SG	Am (katophorite, low ferrogedrite and very low ferrohornblende/ferroactinolite and ferroedenite) bi, ms, chl, ap, zr, alla, tit, th. Shows some perthitic and common myrmekitic textures	Dominantly subsolvus and ferroan, alkaline to calc-alkaline, medium to high K, metaluminous to peraluminous	Low potential: presence of fl and th. Rare metals are mostly restricted to alla.	Age of emplacement from 634 (U-Pb zircon) to 630 (Previous Rb-Sr) Ma. Syn- to Post-orogenic magmatism	Partial melting, assimilation-fractional crystallization (weak), fractionation and subsolidus alteration. From an upper mantle source
Jabal az Zuhd	Large and massive; the most homogeneous pluton.	Dominated by AG with much less SG. Coarse-grained, gray and pink AFG and some porphyritic and medium-grained SG	Am (arfvedsonite), bi, ms, chl, ap, zr, tit, hm, mag, ilm, ru mo, xe & ferg. Dominated by perthitc textures	Dominantly hypersolvus and ferroan, alkaline, High-K, variable peralkaline to low metaluminous	Good potential: richest pluton in rare metals and their minerals	Age of emplacement from 564 (Rb-Sr) to 554 (U-Pb zircon) Ma. Post-orogenic to within-plate magmatism	Partial melting, assimilation-fractional crystallization, fractionation and subsoldus alteration From a lower crustal source

Explanation of terms: am-amphibole, bi-biotite, ms-muscovite, chl-chlorite, ap-apatite, zr-zircon, tit-titanite, alla-allanite, fl-fluorite, th-thorite, hm-hematite, mg-magnetite, ilm-ilmenite, ru-rutile, mo-monazite, xe-xenotime, ferg-fergusonite, syn-synchysite, AG-alkali granite, SG-syenogranite, MG-monzogranite, GD-granodiorite.

Table 8.2: Differences between the studied plutons

Differences	Jabal az Zuhd pluton	The other studied plutons	Between the other studied plutons
Liththology	More homogeneous and has no xenoliths	Heterogeneous with abundant xenoliths	JR is less heterogenous and much less xenolith. TH displays hybrid rocks and chilled margins.
Mineralogy	Richest pluton in Fe-Ti oxides (magnetite, hematite, ilmenite & rutile) and the poorest in plg	The oxides are less abundant and are dominated by magnetite and hematite.	JM and KD are poor in amphibole. JR is the only pluton that shows more than one type of amphibole
Geochemistry	Peralkaline to metaluminous Shows the highest Fe content The most alkaline (evolved)	Meta to mildy peraluminous Only the enriched phases show a high Fe content	TH shows variable peraluminous granodiorites
Resources	The richest pluton in rare earths and rare metals	Less enriched in rare earths and rare metals but show variability in their content of metals of significance.	JR presents th. JM is richest in monazite. KD contains synchysite and fluorite, Au and Ag
Formation process and magma source	The most contaminated pluton and the only one that suggests a crustal source	Less contaminated and all suggest a mantle source	JM and KD show almost the same intial Sr ratio, therefore, suggesting a similar magma source. TH and JR are less affected by contamination

Abbreviations: TH, Jabal Thalabah, KD, Jabal Khur Dukhan, JM, Jabal Al-Massah, JR, Jabal Raydan, JZ, Jabal az Zuhd.

VIII.3. Geological evolution

The previous models of Genna *et al*. (2002) and Duyverman (1982) did not give detailed information about the evolutionary history of the Arabian Shield. This study has provided more detail. New stratigraphic relationships (Table 8.3) are presented to suggest the sequences of events that occurred during the Arabian Shield formation and to clarify in which stage the studied granites were emplaced. Furthermore, the suggested ages and the source of magma have assisted in determining the granites' genesis and the tectonic regime of the plutons.

In terms of stratigraphic relationships, the Arabian Shield formation was initiated during the beginning of the NeoProterozoic (Upper Proterozoic) Era, a period that was dominated by island-arc collision and was accompanied with several depositional and tectonic cycles (Najd and the Hijaz). The tectonic and depositional cycles lasted for almost 400 Ma. Between 950 and 670 Ma deposition was dominated by the Baish, Baha, Jeddah, Halaban and Hulaysah groups (older to younger, in the south and central parts of the Shield), by the Za`am, Zaytah and younger Bayda groups (in the northwestern part of the Shield) and associated with metapyroxenites, metagabbro, sheeted dykes, massive and pillow basalt, marine sediments, volcano-sedimentary association, metagabbro-diorite complexes, calk-alkaline granitoids rock units. The last stage of these events was marked by the depositon of the Thalabah group and the initiation of the post-amalgamation period. From ~670 to 550 Ma continual depositions was dominated by the Ablah, Shammer and Mardama groups and the Minaweh formation (older to younger). These consisted of molasse sediments, dykes, intermediate to acidic volcanics, layered intrusive gabbros and alkaline and peralkaline granites together with synchronous, post-amalgamation tectonism. The early to middle stages were marked by the initiation of the Najd Fault System and by the emplacement of both the Jabal Raydan and Jabal Al-Massah plutons. The middle to late stages were marked by the end of the post-amalgamtion events and the beginning of the intra-plate (Gondwana break-up) tectonism in which the Jabal Khur Dukhan, Jabal Thalabah and Jabal az Zuhd granites respectively were emplaced.

Table 8.3: Proposed stratigraphy for the Arabian shield, combining different classification schemes for tectonic events

Geological times			Orogenic events	Depostional cycles		Groups and Formations	Rock units	Pluton
Paleozoic		542						JRA
Upper Proterozoic	Ediacaran	550	UPPER PAN-AFRICAN	Sequence A	Najd Fault System	Minaweh = Meddan/Farra`ah formations Mardama, Shammer and Ablah groups	Alkaline & Peralkaline granite Layered intrusive gabbro Intermediate to acidic volcanics Molasse sediments & dykes	JZ JD JTUK JA AAA JARR JHAS B KD JB JAW S TH ANN L JS JASH JM JR K
	Cryogenian	600 650	**Island arcs and Ophiolites**			Thalabah group (Sulaysiyah/Saluwah and Amlas, Hinshan) = Rahabah formations Hulayfah, Halaban, Jeddah, Baha and Baish groups	Peraluminous granite Calk-alkaline granitoids Metagabbro-diorite complexes Volcano-sedimentary association	H
	Tonian	800 850	MIDDLE PAN-AFRICAN	Sequence B	The Najd and the Hijaz Tectonic Cycles	Bayda group (Hasha/Amud formation) = Khawr formation	Marine sediments Massive & Pillow basalt Sheeted dykes	
		1000		Sequence C		Za`am group (Silasia/ Ghawjah or Al-Marr formation) = Zaytah group (Silasia/Hegaf formation)	Metagabbro Metapyroxenites	
Middle Proterozoic			LOWER PAN-AFRICAN					

Explanation of terms: JZ, Jabal az Zuhd, KD, Jabal Khur Dukhan, JM, Jabal Al-Massah, JR, Jabal Raydan, TH, Jabal Thalabah (black colored = studied pluton), S, Sadr, L, Liban, JS, Jabal Shar (blue colored = previous dated plutons from Midyan terrain) JRA, Jabal Radwa, JD, Jabal Dabbagh, JTUK, Jabal Tukhfah, JA, Jabal Aja , AAA, Aban Al Ahmar, JARR, Jabal Ar Rumman, JHAS, Jabal Hadb Ash Sharar, B, Badan JB, Jabal Bidayah, JAW, Jabal Awaj, ANN, An Nimar, JASH, Jabal Ashirah, K, Kwar, H, Hamra (red colored = previous dated alkali pluton from the Arabian Shield), single-pointed blue arrow, post-amalgamation event, double-pointed blue arrow, amalgamation events. Orogenic events from Gass (1981), Genna *et al*. (2002) and Johnson (2006), depositional cycles from Jackson and Ramsay (1980) and Al-Shanti (2003), groups and formations from Davies and Grainger (1985), Clark (1986), Rowaihy (1986), Grainger and Hanif (1989) and Genna *et al*. (2002), rock units from Genna *et al*. (2002), additional pluton ages from Stoeser (1986).

In terms of regional plate tectonics, two phases (Fig. 8.1) of collision (representing three tectonic environments) are proposed:

1- Syn to post-collision: this environment is exemplified by the circular, nested complex of Jabal Al-Massah and by the incomplete-circular pluton of Jabal Raydan. Both were derived by partial melting of an undersaturated to saturated, calc-alkaline, metaigneous, upper mantle source followed by assimilation-fractionation. Around 630 Ma the Jabal Al-Massah and Jabal Raydan plutons were emplaced. Jabal Al-Massah intruded the country rocks of the Za'am, Bayda and Thalabah groups and was later intruded by felsic and basic dykes, and possibly affected by a much younger (fluid-related?) event around 520 Ma. Jabal Raydan intruded the country rocks of the Za'am metavolcanics and was later intruded by felsic dykes. The apices of the alkali granite intrusives were partially affected by a later foliation event.

2- Post-collision to rift-related: this environment is exemplified by the elliptical-shaped complex of Jabal Khur Dukhan, the small ring structure complex of Jabal Thalabah and the sub-circular pluton of Jabal az Zuhd. These plutons show different magma sources and processes of formation. Jabal Khur Dukhan were derived by partial melting of undersaturated to saturated, calc-alkaline metaigneous upper mantle material followed by assimilation-fractionation at around 600 Ma. This pluton intruded the country rocks of the Za'am metavolcanics as separate, but possibly contemporaneous alkali-syenogranite and monzogranite-granodiorite. The pluton was later intruded by felsic dykes and affected by fluids, leading to the development of pegmatitic veins. During the final stages of development the plutons were affected by slight metamorphism. Jabal Thalabah was derived by partial melting of undersaturated to saturated, calc-alkaline metaigneous, upper mantle source material followed by assimilation-fractionation and some local hybridization at the contact zones of the complex shortly before solidification. At around 580 Ma the complex intruded the Za'am metavolcanics by separate but contemporaneous syenogranite and monzogranite-granodiorite melts

followed by felsic and basic dike swarms and late-satge, subsolidus fluid processes. Finally the pluton and dykes were partially affected by a NE-SW regional shear zone. Jabal az Zuhd was derived by partial melting of reduced, relatively anhydrous metasedimentary lower crustal source which was to some extent contaminated by either upper crustal material or rising upper mantle-derived melt. At around 550 Ma the pluton intruded the metavolcanics of the Zaytah group and the metasediments of the Minaewh formation. Finally it was affected by late post-solidificatioin fluids which produced pegmatite and quartz veins.

The granites range from late subduction-related Cryogenian to early intra-plate Ediacaran. All of the plutons (with the exception of Jabal az Zuhd) are suggested to be bell-jar shaped and passively emplaced into the less ductile country rocks by a cauldron stoping mechanism. (Jabal az Zuhd was probably emplaced by more constant upwelling of magma). Depths of emplacement were in the range 4-12 km. Almost all of the plutons which are considered as alkaline (whether from Midyan terrain or elsewhere) were mainly emplaced in post-orogenic to rift-related environments. The most evolved granites appear to be emplaced at the shallowest level but at the highest temperature, and in the most advanced tectonic setting.

This work suggests that the formation of the Arabian Shield was marked by the occurrence of Neoproterozic igneous plutons that were associated with complex and evolving tectonic events. The study has also assisted in constructing a new map (Fig. 8.2) containing the plutons of the Midyan terrain and their ages. The geochemical study has raised the possibility of the various types of source material, but the Sr isotopic study appears to be the most definitive and has suggested metasedimentary source material for the Jabal az Zuhd granite and metaigneous source material for the other granites (Table 8.4). In addition, the tectonic setting diagrams were found to be not particularly definitive in suggesting a precise tectonic environment, possibly because of the affect of other processes (element redistribution from hydrothermal fluids and/or assimilation); this is particularly the case with the diagrams using the Rb, Nb and Y values.

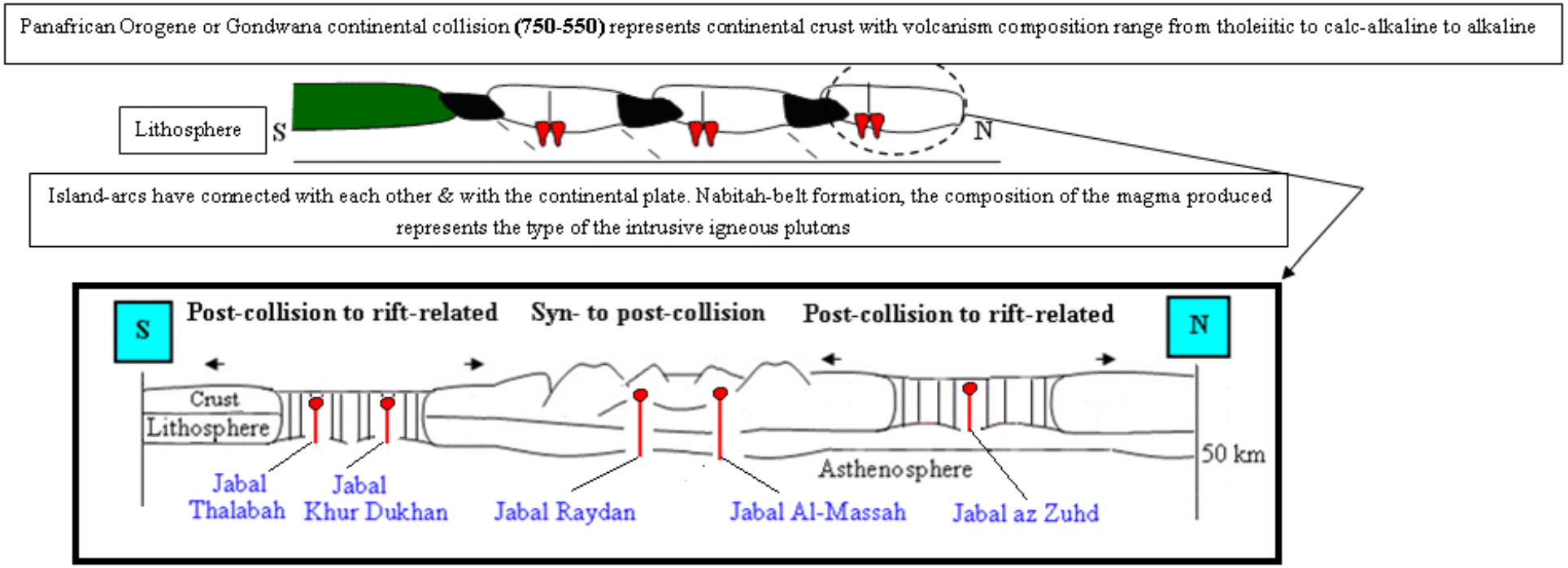

Fig.8.1: Proposed evolutionary model for the studied igneous intrusives in the Midyan terrain. (Location of Midyan terrain highlighted in upper diagram from Duyverman, 1982).

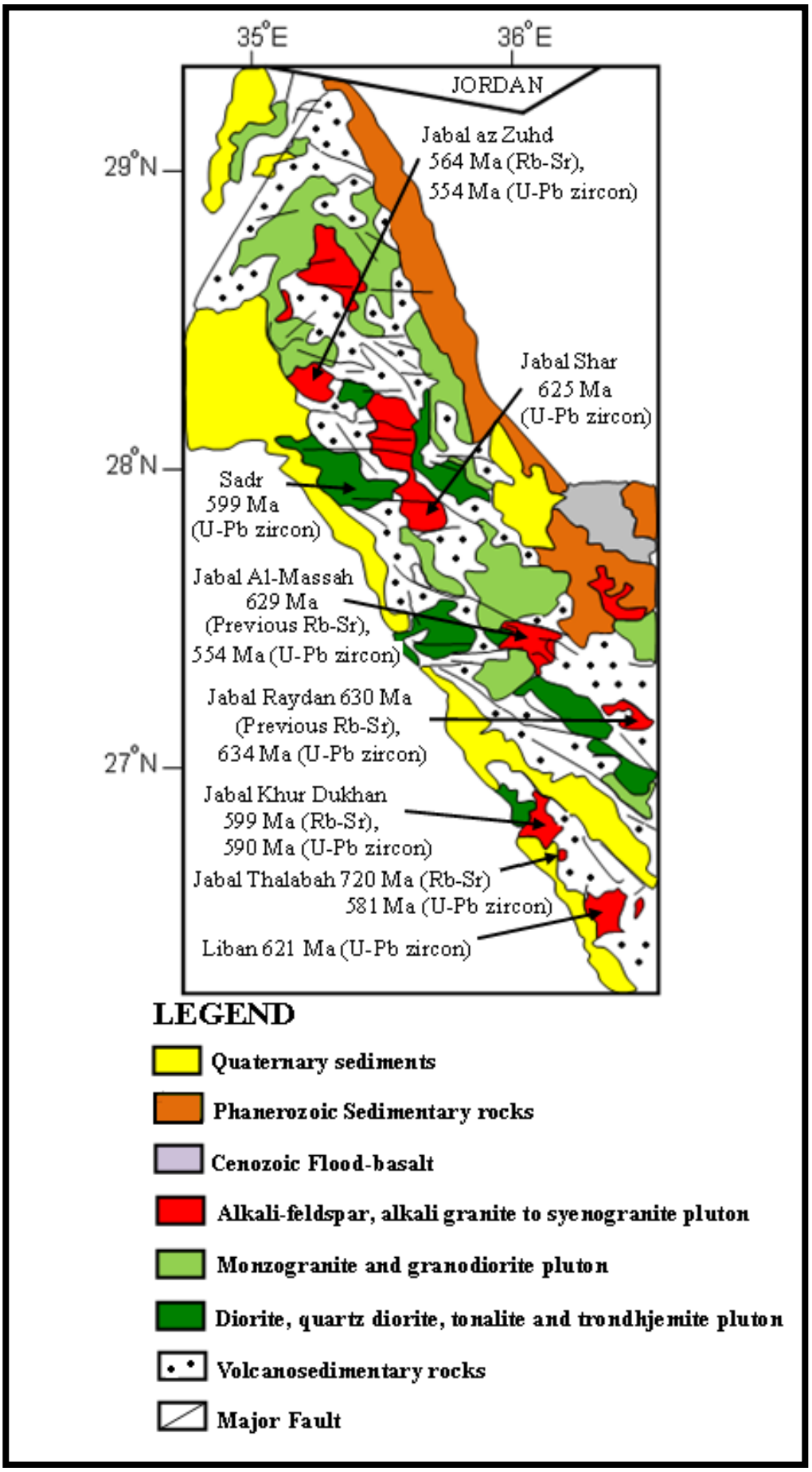

Fig.8.2: Midyan terrain geology with the dated igneous plutons (partially after Stoeser, 1986)

Referring to the Arabian Shield, this project has added some valuable information:

1- Based on fieldwork and detailed mineralogical and geochemical studies, the granites from the five areas have been mapped and characterized.

2- For the first time, the ages of the five granites have been determined using U-Pb zircon dating. This has generated more precise information about the time of formation and, coupled with the geochemical studies; it has helped to provide a model for the evolution of the Midyan terrain. There is clear evidence (Table 9.4) indicating the roles of several processes in magma development: fractional crystallization, subsolidus fluid activity and assimilation.

3- The economic study has indicated the potential of these granites for certain rare elements, but particulary the granites of Jabal az Zuhd, Jabal Khur Dukan and Jabal Al- Massah. Further work is recommended, focussing on the very alkaline varieties of these granites, together with the pegmatitc and porphyritic felsic dykes of Jabal Raydan and the mafic dykes at Jabal Thalabah. The presence of Au-Pt alloy and free Ag in the Jabal Khur Dukhan pluton requires more detailed mineralogical work.

4- It is suggested that the enrichment in rare elements is most likely controlled by fractionation and subsequent fluid processes. The rare elements seem to have been concentrated in the Na and Fe-rich granites by fractionation, but they were then probably redistributed by late-stage, alkaline, subsolidus fluids.

Table: 8.4.Evidence for magma sources and process of formation

Magma source	Fractional crystallization	Mixing or assimilation	Subsolidus alteraiton
1) Modal diagram suggests parental tonalitic composition. 2) Fe-rich melts probably reflect derivation from reduced basaltic rocks (Frost and Frost, 1997). 3) The experimental dehydration melting of metasedimentary rocks (Fig. 6.10, a) suggests metagreywacke source for some of the rocks. 4) The isotopic work suggests metaigneous source for all the plutons except Jabal az Zuhd (metsedimentary source)	1) The presence of granitoids with various composition (GD to AG) 2) The REE-bearing minerals are formed from highly fractionated magmatic systems (Bortnikov *et al*., 2007) 3) The development of the negative Eu anomaly from the less to the more felsic rocks. 4) The diagram 6.d of Sylvester (1989) shows that most of the rocks plot in the field of highly fractionated calck-alkaline granites 5) Diagram 6.11 display that the highly-fractionated rocks are arranged on a linear trend specifically on the Sr vs Ba diagram	1) The presence of xenoliths 2) The presence of rapakivi texture (re-crystallization involving magma mixing) 3) Assimilation-combined fractional crystallization trend (Fig. 6.10, a) 4) Mixing line on modal composition diagram (Fig.6.12) 5) The isotopic study indicates variable degree of contamination.	1) Altered rocks 2) Mineral replacement or the presence of secondary minerals 3) The proportional relationship between the L.O.I and K coupled with the presence of muscovite.

Appendices

I. Sampling

One hundred and sixty-seven samples (Table I.1), covering different rock varieties, were collected during a major trip which was carried out from late April until late June 2009. The trip covered 5 different igneous plutons in the Midyan terrain and from the south to the north these are: Jabal Thalabah (41 samples), Jabal Khur Dukhan (42 samples), Jabal Al-Massah (40 samples), Jabal Raydan (30 samples) and Jabal az Zuhd (14 samples).

In terms of climate, the trip began in warm, sunny and humid weather, but in late May and June, the weather became harsher and the working hours in the field had to be reduced. Another important issue was that the areas have a fairly mountainous nature with steep slopes and this caused some difficulties in reaching their upper parts. Furthermore, during the summer time, as the heat increases, various wild animals leave the valleys and seek the higher parts to find more relief. So, climbing the mountains was both difficult and potentially quite dangerous.

The felsic complexes have to some extent been affected by deformation, alteration and weathering, so collecting fresh samples was sometimes difficult.

Table I.1. Sample numbers and locations.

TH1`	N 26° 42' 50", E 36° 15' 30"	KD1	N 26° 44' 39", E 36° 13' 20"	JM1	N 27° 17' 00", E 36° 04' 24"	JR1-A	N 27° 15' 28", E 36° 13' 01"
TH2`	N 26° 43' 21", E 36° 15' 22"	KD2	N 26° 45' 09", E 36° 13' 38"	JM2	N 27° 17' 28", E 36° 04' 11"	JR1-B	N 27° 15' 28", E 36° 13' 01"
TH3`	N 26° 44' 04", E 36° 14' 45"	KD3	N 26° 45' 42", E 36° 13' 28"	JM3	N 27° 18' 15", E 36° 04' 05"	JR1-C	N 27° 15' 28", E 36° 13' 01"
TH4`	N 26° 44' 02", E 36° 14' 43"	KD4	N 26° 46' 26", E 36° 13' 29"	JM4	N 27° 18' 08", E 36° 05' 22"	JR2-A	N 27° 15' 25", E 36° 13' 30"
TH5`	N 26° 42' 53", E 36° 15' 54"	KD5	N 26° 46' 28", E 36° 13' 31"	JM5	N 27° 18' 15", E 36° 05' 56"	JR2-B	N 27° 15' 25", E 36° 13' 30"
TH6`	N 26° 44' 04", E 36° 14' 45"	KD6	N 26° 46' 53", E 36° 13' 24"	JM6	N 27° 18' 10", E 36° 05' 39"	JR3-A	N 27° 16' 01", E 36° 13' 35"
TH7`	N 26° 43' 46", E 36° 15' 50"	KD7	N 26° 46' 57", E 36° 13' 16"	JM7	N 27° 18' 29", E 36° 05' 39"	JR3-B	N 27° 16' 01", E 36° 13' 35"
TH8`	N 26° 43' 49", E36° 15' 16"	KD8	N 26° 47' 08", E 36° 13' 08"	JM8	N 27° 18' 50", E 36° 05' 47"	JR3-C	N 27° 16' 01", E 36° 13' 35"
TH9`	N 26° 43' 49", E36° 14' 46"	KD9	N 26° 47' 19", E 36° 12' 60"	JM9	N 27° 18' 60", E 36° 05' 18"	JR3-D	N 27° 16' 01", E 36° 13' 35"
TH10`	N 26° 43' 13", E 36° 15' 22"	KD10	N 26° 47' 19", E 36° 12' 60"	JM10A	N 27° 18' 60", E 36° 05' 00"	JR3-E	N 27° 16' 01", E 36° 13' 35"
TH11`	N 26° 43' 15", E 36° 15' 30"	KD11	N 26° 47' 57", E 36° 13' 12"	JM10 B	N 27° 18' 60", E 36° 05' 00"	JR4	N 27° 15' 46", E 36° 14' 01"
TH12`	N 26° 43' 57", E 36° 14' 45"	KD12	N 26° 47' 57", E 36° 13' 23"	JM11	N 27° 19' 00", E 36° 05' 00"	JR5	N 27° 15' 03", E 36° 14' 20"
TH13`	N 26° 44' 02", E 36° 14' 44"	KD13-A	N 26° 47' 57", E 36° 13' 23"	JM12	N 27° 19' 17", E 36° 08' 41"	JR6	N 27° 15' 06", E 36° 14' 57"
TH14`	N 26° 44' 04", E 36° 14' 44"	KD13-B	N 26° 47' 57", E 36° 13' 23"	JM13	N 27° 21' 60", E 36° 08' 27"	JR7	N 27° 14' 44", E 36° 15' 31"
TH15`	N 26° 42' 44", E 36° 15' 24"	KD14	N 26° 47' 60", E 36° 13' 20"	JM14	N 27° 22' 00", E 36° 07' 37"	JR8	N 27° 14' 02", E 36° 16' 16"
TH1-A	N 26° 42' 49", E 36° 15' 01"	KD15	N 26° 48' 01", E 36° 13' 42"	JM15	N 27° 19' 33", E 36° 05' 56"	JR9	N 27° 13' 48", E 36° 15' 45"
TH1-B	N 26° 42' 49", E 36° 15' 02"	KD16	N 26° 48' 18", E 36° 13' 44"	JM16	N 27° 20' 23", E 36° 04' 32"	JR10	N 27° 13' 27", E 36° 15' 24"
TH2	N 26° 42' 56", E 36° 15' 38"	KD17	N 26° 48' 26", E 36° 13' 50"	JM17	N 27° 18' 54", E 36° 02' 46"	JR11	N 27° 13' 35", E 36° 16' 59"
TH3	N 26° 43' 34", E 36° 15' 23"	KD18	N 26° 48' 44", E 36° 13' 45"	JM18	N 27° 18' 57", E 36° 07' 26"	JR12	N 27° 14' 28", E 36° 17' 21"
TH4	N 26° 43' 31", E 36° 15' 16"	KD19	N 26° 48' 54", E 36° 14' 04"	JM19	N 27° 19' 36", E 36° 05' 28"	JR13-A	N 27° 15' 05", E 36° 16' 37"
TH5	N 26° 43' 22", E 36° 15' 20"	KD20	N 26° 49' 08", E 36° 14' 01"	JM20	N 27° 20' 48", E 36° 02' 53"	JR13-B	N 27° 15' 05", E 36 16' 37"
TH6	N 26° 43' 33", E 36° 15' 38"	KD21	N 26° 49' 24", E 36° 14' 08"	JM21	N 27° 20' 30", E 35° 57' 25"	JR14	N 27° 15' 26", E 36° 16' 00"
TH7	N 26° 43' 56", E 36° 15' 40"	KD22	N 26° 49' 40", E 36° 13' 24"	JM22	N 27° 21' 23", E 35° 57' 46"	JR15	N 27° 15' 34", E 36° 14' 55"
TH8	N 26° 44' 01", E 36° 16' 03"	KD23	N 26° 49' 36", E 36° 13' 05"	JM23	N 27° 21' 29", E 35° 58' 52"	JR16	N 27° 15' 53", E 36° 12' 52"
TH9	N 26° 43' 58", E 36° 16' 21"	KD24	N 26° 49' 07", E 36° 12' 60"	JM24	N 27° 21' 06", E 35° 57' 17"	JR17	N 27° 16' 08", E 36° 12' 54"
TH10	N 26° 43' 32", E 36° 15' 31"	KD25	N 26° 50' 57", E 36° 12' 38"	JM25	N 27° 20' 26", E 35° 58' 07"	JR18	N 27° 16' 23", E 36° 12' 52"
TH11	N 26° 44' 38", E 36° 15' 38"	KD26	N 26° 50' 39", E 36° 11' 08"	JM26	N 27° 20' 13", E 35° 57' 06"	JR19	N 27° 17' 25", E 36° 12' 59"
TH12	N 26° 43' 20", E 36° 15' 14"	KD27	N 26° 49' 44", E 36° 10' 44"	JM27	N 27° 20' 40", E 35° 56' 48"	JR20	N 27° 16' 57", E 36° 13' 28"
TH13	N 26° 43' 51", E 36° 14' 49"	KD28	N 26° 49' 44", E 36° 10' 48"	JM28	N 27° 18' 39", E 35° 59' 38"	JR21	N 27° 16' 48", E 36° 14' 08"
TH14	N 26° 44' 02", E 36° 14' 43"	KD29	N 26° 52' 48", E 36° 10' 57"	JM29	N 27° 17' 30", E 36° 02' 21"	JR22	N 27° 16' 49", E 36° 14' 08"
TH15	N 26° 44' 19", E 36° 14' 17"	KD30	N 26° 53' 14", E 36° 10' 39"	JM30	N 27° 19' 11", E 36° 01' 15"	JZ1	N 28° 18' 59", E 35° 10' 26"
TH16	N 26° 44' 15", E 36° 14' 46"	KD31	N 26° 53' 26", E 36° 10' 20"	JM31	N 27° 19' 46", E 36° 00' 16"	JZ2	N 28° 18' 48", E 35° 11' 37"
TH17	N 26° 44' 47", E 36° 14' 33"	KD32	N 26° 53' 47", E 36° 10' 19"	JM32	N 27° 20' 32", E 36° 01' 14"	JZ3	N 28° 18' 04", E 35° 10' 39"
TH18	N 26° 44' 54", E 36° 16' 30"	KD33	N 26° 54' 14", E 36° 10' 25"	JM33	N 27° 19' 28", E 36° 03' 12"	JZ4	N 28° 18' 17", E 35° 12' 18"
TH19	N 26° 44' 47", E 36° 16' 45"	KD34	N 26° 54' 26", E 36° 10' 08"	JM34	N 27° 18' 57", E 36° 02' 43"	JZ5	N 28° 17' 11", E 35° 10' 58"
TH20	N 26° 44' 33", E 36° 16' 55"	KD35	N 26° 54' 28", E 36° 10' 06"	M1	N 27° 20' 28", E 36° 02' 14"	JZ6	N 28° 17' 34", E 35° 12' 54"
TH21	N 26° 44' 31", E 36° 16' 42"	KD36	N 26° 55' 03", E 36° 10' 16"	M2	N 27° 17' 47", E 36° 05' 36"	JZ7	N 28° 16' 25", E 35° 11' 13"
TH22	N 26° 44' 09", E 36° 16' 38"	KD37	N 26° 55' 00", E 36° 11' 00"	M3	N 27° 16' 51", E 36° 05' 33"	JZ8	N 28° 16' 49", E 35° 12' 26"
TH23	N 26° 44' 37", E 36° 16' 04"	KD38	N 26° 50' 00", E 36° 11' 00"	M4	N 27° 17' 05", E 36° 03' 52"	JZ9	N 28° 16' 45", E 35° 13' 23"
TH24	N 26° 43' 10", E 36° 16' 19"	KD39	N 26° 47' 12", E 36° 10' 60"	M5	N 27° 16' 48", E 36° 03' 43"	JZ10	N 28° 15' 22", E 35° 13' 31"
TH25	N 26° 42' 20", E 36° 14' 32"	KD40	N 26° 47' 02", E 36° 11' 00"	M6	N 27° 17' 01", E 36° 03' 06"	JZ11	N 28° 15' 13", E 35° 14' 55"
		KD41	N 26° 46' 60", E 36° 11' 26"			JZ12	N 28° 14' 47", E 35° 15' 45"
						JZ13	N 28° 13' 43", E 35° 18' 51"
						JZ14	N 28° 13' 42", E 35° 20' 54"

Explanation: TH, Jabal Thalabah, KD, Jabal Khur Dukhan, M and JM, Jabal Al-Massah, JR, Jabal Raydan, JZ, Jabal az Zuhd plutons

II. Mineralogy

Seventy-four standard thin sections of the rocks were prepared for petrographic study.

Point-counting for determining modal composition

A point counter was used to calculate the modal compositions (Table II.1 and II.2) of selected thin sections that were representative of the granites from the different plutons and the results are given in volume percentage. An average of almost 2500 counts was taken on each section. The presence of perthitic textures in most of the thin-sections made the estimate of % K-feldspar difficult, but an attempt was made to count the plagioclase lamellae (etc.) that are hosted in the larger K-feldspars. The presented tables show recalculated values and the rock names are based on the classification of Streckeisen for plutonic rocks.

Heavy mineral separation

Eight samples (TH14, KD15, KD28, JM31, JR8, JR12, JZ2 & JZ6) of granite were crushed and sieved for mineral separation. A rock splitter was used to split the hand specimens into small fragments to ease the crushing using the fly press. The samples were then sieved and the 250-63μm fraction was subjected to magnetic separation using a hand magnet to remove any magnetic minerals. The remaining material was then subjected to heavy liquid separation using sodium poly-tungstate (SPT) to separate any mineral with a density less than approximately $3g/cm^3$ (quartz, feldspar, mica).

Mineral identification using scanning electron microscopy and electron microprobe analysis

Preliminary identification and semi-quantitative analysis of the separated minerals were carried out using a Hitachi S-3000 scanning electron microscope coupled with a Link Systems energy dispersive X-ray analyzer in the Department of Earth Science, Royal Holloway. For quantitative analysis, polished thin sections were prepared from 6 samples (TH13, JM31, JR8, JR12, KD28 and JZ6) and these were analyzed (Table II.3 to II.9) using a JEOL Superprobe JXA-8100 in the Department of Earth Sciences, University College, London. Calibration was achieved using synthetic standards and accuracy was checked using the BCR international standards.

Table II.1. Modal analyses of the Jabal Al-Massah, the Jabal Raydan and the Jabal az Zuhd granitoids

Sample Number	K-feldspar	Plagioclase	Quartz	Amphibole	Biotite	Rock Name
M4	25.3	48	19.6	1.1	6	Granodiorite
JM33	25.6	48.4	25.3	0.0	0.7	
JM7	31	26.5	39.4	0.0	3.1	Monzogranite
JM24	39.8	28.3	30.5	0.0	1.4	
JM16	43	26	28.5	0.0	2.5	Syenogranite
JM18	43.3	30.5	26	0.0	0.2	
JM13	53.3	2	44.5	0.2	0.0	Alkali granite
JR3E	38.9	36	24	0.0	1.1	Monzogranite
JR12	33.5	28.5	31.9	2.4	2.2	
JR13B	31.3	33.5	28.5	3.5	3.2	
JR3C	38	18.5	43	0.3	0.2	Syenogranite
JR9	44.2	20.6	33.1	0.4	1.7	
JR20	42.8	14.5	42.2	0.3	0.2	
JR19	61.5	7.4	30.6	0.2	0.3	Alkali granite
JZ1A	54.6	25.2	19.8	0.1	0.3	Syenogranite
JZ5	39	15.5	44.3	1	0.2	
JZ2	56.5	5	32.5	2	4	Alkali granite
JZ6	54.2	2.4	31.8	3.5	6.1	
JZ8	57.6	2.2	33.7	2.9	3.6	
JZ10	54.7	6	31.5	4.5	3.3	
JZ13	52.8	6	34.5	3.5	3.2	

Table II.2. Modal analyses of the Jabal Thalabah and the Jabal Khur Dukhan granitoids

Sample Number	K-feldspar	Plagioclase	Quartz	Amphibole	Biotite	Rock Name
TH3	17	38.7	41	0.3	3	Granodiorite
TH4	16.7	34.8	43.5	0.0	5	
TH9	11	53.3	31	0.0	4.7	
TH11	20.7	49.7	25.4	0.0	4.2	
TH14	16.4	43.4	38.3	0.5	1.4	
TH18	15	57.3	27.2	0.0	0.5	
TH19	15	59.9	24.8	0.0	0.3	
TH7`	14.8	59.7	23	0.0	2.5	
TH5	39.2	26.7	32.9	0.2	1	Monzogranite
TH5`	43.3	9.2	46.7	0.0	0.8	Syenogranite
TH10`	51	20.5	28.4	0.1	0.0	
TH12`	60.5	12	27.5	0.0	0.0	
TH13`	60.7	3.5	32.5	1.5	1.8	Alkali granite
TH14`	61.5	7.5	27	2	2	
KD23	7.3	59	25.5	3.2	5.5	Granodiorite
KD11	33.4	27.4	33.2	1.8	4.2	Monzogranite
KD12	35.5	35.6	24.5	0.8	3.6	
KD28	59	14.7	25.6	0.2	0.5	Syenogranite
KD37	61	4	35	0.0	0.0	
KD1	63	2.5	34.5	0.0	0.0	Alkali granite
KD4	67	6.5	26.2	0.3	0.0	
KD41	62	0.8	37.2	0.0	0.0	

Abbreviations: TH, Jabal Thalabah, KD, Jabal Khur Dukhan, JM and M, Jabal Al-Massah, JR, Jabal Raydan, JZ, Jabal az Zuhd.

Table II.3: Electron microprobe analysis of monazite-Ce from Jabal Al-Massah Complex (wt %)

Mg	Si	P	S	Ca	Fe	Ag	La	Ce	Nd	Gd	Th	Total
	1	33		1	1		19	33	8			96
	1	31	1	1			14	31	11		3	93
	1	29	1	1			15	29	10		4	90
0.5	2	30		1		2	15	32	9			92
	2	30	1				16	30	10		4	93
	1	31	1	1		2	14	31	9	2		92
	1	31	1	0.5			17	33	10		2	96
	1	30	1	1			14	30	10		4	91
	1	29	1	1			13	29	10		4	88
	1	31	1	1			15	32	9		2	92

Table II.4: Electron microprobe analysis of Mn-rich Ilmenite from Jabal Al-Massah Complex

Al	Si	Ca	Ti	Mn	Fe	Total
			49	14	27	90
	3	3	49	18	21	94
	8	6	47	15	17	93
0.5	1	1	48	10	30	91
			50	14	27	91

Table II.5: Electron microprobe analysis of allanite from Jabal Raydan Complex

Al	Si	P	Ca	Ti	Fe	Ag	Ba	La	Ce	Nd	Total
3	8	1	5		31			10	24	9	91
2	6	1	4		3	1	2	13	26	9	67
4	10	1	6		4	1	2	11	22	8	69
8	27		8	1	16				11	5	76
9	28		10	1	18				10	4	80

Table II.6: Electron microprobe analysis of thorite from Jabal Raydan Complex

Al	Si	Ca	V	Fe	Y	Ce	Th	U	Total
1	16	1	4	1	4	10	52	6	95
1	15	1	2	8	3	3	57	5	95

Table II.7: Electron microprobe analysis of Mn-rich Ilmenite from Jabal az Zuhd Pluton

Ca	Ti	Mn	Fe	Total
0.4	48	13	33	94
0.4	49	13	34	96
0.4	50	13	34	97

Table II.8: Electron microprobe analysis of fergusonite-Y from Jabal az Zuhd Pluton

Ti	Fe	Rb	Y	Nb	Ce	Nd	Sm	Gd	Dy	Total
1	3		28	49		3	2	3	4	90
1	4	2	29	51		4		2	3	92
1	2	2	29	50	2	3		5	4	98

Table II.9: Electron microprobe analysis of xenotime from Jabal az Zuhd Pluton

P	Ca	Y	La	Pr	Nd	Sm	Gd	Total
33	2	11	15	4	18	4	3	90

Amphibole

The amphibole and other mineral analyses are presented in Tables II.10 to II.15. Analytical totals less than 95% were rejected from further consideration. Amphibole formulae were calculated based on 23 oxygens from Deer et al. (2001). The analysis was calibrated using geochemical reference standards BCR-1, BCR-2, BCR-3 and BCR-4 for both the WED and EDS amphibole analyses.

The analyses are presented in the following tables. Results for analyses of amphibole from Jabal Al Massah were not good and totals were less than 94% (perhaps due to alteration). These have therefore not been presented but their overall character is used in the thesis.

Table II.10: **Sample TH 13**: Amphibole analysis from WDS (analyses and cations)

	Elements	SiO_2	TiO_2	Al_2O_3	FeO	MnO	MgO	CaO	Na_2O	K_2O	F	Cl_2O	Total
Analyses	1	42.11	0.94	5.43	27.19	0.62	5.21	10.42	1.97	0.89	0.54	0.23	95.55
	2	45.16	0.81	4.49	26.72	0.59	5.44	10.43	1.85	0.84	0.54	0.13	97
	3	44.25	1.09	5.63	27.06	0.6	5.01	10.41	2.13	0.99	0.58	0.21	97.96
	4	42.43	1.14	5.83	26.84	0.58	5.12	10.36	2.11	0.99	0.55	0.2	96.15
	5	67.99	0	19.89	0.16	0	0	0	0.25	12.44	0	0.03	100.76
	6	43.75	1.19	5.64	27.08	0.62	5.13	10.27	2.16	0.94	0.6	0.19	97.57
	7	44.01	1.11	5.63	26.94	0.59	5.29	10.19	2.17	0.94	0.58	0.2	97.65
	8	42.86	1.07	6.58	27.26	0.6	4.93	10.38	2.08	1.08	0.45	0.13	97.42
Cations	1	7.17	0.12	1.09	3.87	0.09	1.32	1.9	0.65	0.19	0.15	0.05	
	2	7.48	0.1	0.88	3.7	0.08	1.34	1.85	0.59	0.18	0.14	0.03	
	3	7.29	0.14	1.09	3.73	0.08	1.23	1.84	0.68	0.21	0.15	0.05	
	4	7.16	0.14	1.16	3.79	0.08	1.29	1.87	0.69	0.21	0.15	0.05	
	5	9.09	0	3.13	0.02	0	0	0	0.07	2.12	0	0.01	
	6	7.25	0.15	1.1	3.75	0.09	1.27	1.82	0.69	0.2	0.16	0.04	
	7	7.27	0.14	1.1	3.72	0.08	1.3	1.8	0.69	0.2	0.15	0.05	
	8	7.13	0.13	1.29	3.79	0.08	1.22	1.85	0.67	0.23	0.12	0.03	

Table II.11: **Sample TH 13**: Amphibole analysis from EDS (analyses and cations)

	Elements	SiO_2	TiO_2	Al_2O_3	FeO	MnO	MgO	CaO	Na_2O	K_2O	Cl_2O	Total
Analyses	1	42.32	0.99	5.52	28.32	0.6	4.99	9.65	2.32	0.92	0.15	95.78
	2	42.43	1.52	4.93	28.28	0.6	4.66	9.49	2.45	0.77	0.22	95.35
	3	42.13	1.03	5.5	28.32	0.62	4.57	9.71	2.3	1.03	0.19	95.4
	4	41.88	1.19	5.2	28.9	0.65	4.73	9.05	2.42	0.92	0.18	95.12
	5	42.59	1.22	5.59	28.09	0.38	4.51	9.3	2.4	0.93	0.35	95.36
	6	43.23	1.02	5.45	27.88	0.61	5.31	9.82	2.46	0.84	0.16	96.78
	7	42.18	1.24	5.29	27.75	0.55	4.58	9.52	2.34	0.83	0.26	94.54
	8	44.22	0.75	4.9	28.92	0.61	4.65	9.79	1.67	0.69	0.1	96.3
	9	42.85	1.01	5.85	29.62	0.52	4.2	9.86	2.25	1.05	0.1	97.31
	10	42.46	1.41	5.28	28.4	0.77	4.79	9.67	2.32	0.92	0.26	96.28
	11	44.15	1.21	5.12	28.81	0.64	4.7	9.89	2.15	0.81	0.29	97.77
	12	41.59	1.55	6.38	29.62	0.54	3.9	9.73	2.49	1.04	0.35	97.19
	13	40.76	1.26	6.49	27.93	0.48	4.52	9.67	2.18	1.09	0.35	94.73
	14	43.01	0.97	6.55	27.8	0.42	4.78	7.56	2.25	2.03	0.21	95.58
	15	42.41	1.26	5.65	29.19	0.59	4.27	9.98	2.35	0.95	0.32	96.97
	16	41.54	1.22	6.12	29.53	0.56	4.08	9.7	2.29	0.87	0.28	96.19
	17	41.56	1.45	6.21	28.76	0.33	4.45	9.63	2.51	1.01	0.29	96.2
	18	41.64	1.21	6.33	28.4	0.44	4.3	9.91	2.31	1.1	0.24	95.88
	19	40.7	1.21	6.18	28.37	0.43	4.42	9.67	2.61	0.95	0.25	94.79
	20	40.72	1.56	6.46	27.85	0.43	4.35	9.63	2.68	1.03	0.35	95.06
	21	45.35	0.56	3.63	27.25	0.81	5.5	9.8	1.95	0.7	0.16	95.71
	22	41.17	1.18	6.55	28.6	0.36	4.6	9.82	2.42	1.08	0.21	95.99
	23	42.63	1.16	5.51	28.4	0.56	4.88	9.76	2.25	0.79	0.19	96.13
	24	42.23	1.56	6.75	28.84	0.58	4.11	9.99	2.41	1.05	0.26	97.78
	25	42.74	1.24	5.72	29.03	0.77	4.43	9.91	2.31	1.09	0.25	97.49
Cations	1	7.22	0.13	1.11	4.04	0.09	1.27	1.76	0.77	0.2	0.04	
	2	7.25	0.2	0.99	4.04	0.09	1.19	1.74	0.81	0.17	0.05	
	3	7.23	0.13	1.11	4.06	0.09	1.17	1.78	0.77	0.23	0.04	
	4	7.21	0.15	1.06	4.16	0.09	1.21	1.67	0.81	0.2	0.04	
	5	7.27	0.16	1.13	4.01	0.06	1.15	1.7	0.8	0.2	0.08	
	6	7.26	0.13	1.08	3.91	0.09	1.33	1.77	0.8	0.18	0.04	
	7	7.27	0.16	1.07	4	0.08	1.18	1.76	0.78	0.18	0.06	
	8	7.45	0.1	0.97	4.07	0.09	1.17	1.77	0.54	0.15	0.02	
	9	7.21	0.13	1.16	4.17	0.07	1.05	1.78	0.73	0.23	0.02	
	10	7.22	0.18	1.06	4.04	0.11	1.21	1.76	0.77	0.2	0.06	
	11	7.35	0.15	1	4.01	0.09	1.16	1.76	0.69	0.17	0.07	
	12	7.04	0.2	1.27	4.19	0.08	0.99	1.77	0.82	0.22	0.08	
	13	7.05	0.16	1.32	4.04	0.07	1.17	1.79	0.73	0.24	0.08	
	14	7.29	0.12	1.31	3.94	0.06	1.21	1.37	0.74	0.44	0.05	
	15	7.18	0.16	1.13	4.13	0.09	1.08	1.81	0.77	0.21	0.08	
	16	7.11	0.16	1.23	4.22	0.08	1.04	1.78	0.76	0.19	0.07	
	17	7.09	0.19	1.25	4.1	0.05	1.13	1.76	0.83	0.22	0.07	
	18	7.11	0.16	1.27	4.05	0.06	1.09	1.81	0.76	0.24	0.06	
	19	7.05	0.16	1.26	4.11	0.06	1.14	1.79	0.88	0.21	0.06	
	20	7.03	0.2	1.32	4.02	0.06	1.12	1.78	0.9	0.23	0.08	
	21	7.63	0.07	0.72	3.83	0.12	1.38	1.77	0.64	0.15	0.04	
	22	7.04	0.15	1.32	4.09	0.05	1.17	1.8	0.8	0.24	0.05	
	23	7.24	0.15	1.1	4.03	0.08	1.24	1.78	0.74	0.17	0.04	
	24	7.07	0.2	1.33	4.04	0.08	1.02	1.79	0.78	0.22	0.06	
	25	7.19	0.16	1.13	4.08	0.11	1.11	1.79	0.75	0.23	0.06	

Table II.12: **Sample JR 12**: Amphibole analysis from WDS (analyses and cations)

	Elements	SiO_2	TiO_2	Al_2O_3	FeO	MnO	MgO	CaO	Na_2O	K_2O	F	Cl_2O	Total
Analyses	1	42.43	0.42	7.69	28.21	0.85	3.83	10.94	1.43	1.33	0.27	0.02	97.42
	2	41.08	1.74	7.18	26.57	0.93	4.42	9.95	2.22	0.9	0.22	0.12	95.33
	3	43.05	1.55	6.96	25.97	0.81	4.76	9.94	2.29	0.9	0.23	0.12	96.58
	4	41.86	1.82	8.9	23.76	0.74	5.97	10.65	2.57	0.78	0.35	0.02	97.42
	5	42.43	1.8	8.64	23.61	0.79	6.03	10.34	2.68	0.68	0.45	0.04	97.49
	6	40.86	1.76	8.18	25.12	0.81	5.35	10.68	2.18	0.7	0.26	0.03	95.93
	7	44.25	1.5	6.16	25.82	0.87	5.24	9.99	2.13	0.81	0.29	0.11	97.17
	8	44.23	1.49	6.47	26.65	0.93	4.6	10	1.89	0.84	0.17	0.07	97.34
	9	43.35	1.47	6.32	25.7	0.91	4.89	10.05	2.06	0.84	0.21	0.09	95.89
	10	43.67	1.6	6.8	27.39	1.01	4.37	10.31	2.08	0.88	0.22	0.08	98.41
	11	43.71	1.48	6.93	26.88	0.99	4.7	10.55	2.03	0.99	0.23	0.08	98.57
	12	34.93	2.41	14.1	29.41	0.59	5.77	0.08	0.22	7.57	0.12	0.06	95.26
Cations	1	7.1	0.05	1.52	3.94	0.12	0.96	1.96	0.46	0.28	0.07	0	
	2	7	0.22	1.44	3.78	0.13	1.12	1.82	0.73	0.2	0.06	0.03	
	3	7.17	0.19	1.37	3.62	0.11	1.18	1.77	0.74	0.19	0.06	0.03	
	4	6.86	0.22	1.72	3.25	0.1	1.46	1.87	0.81	0.16	0.09	0	
	5	6.92	0.22	1.66	3.22	0.11	1.47	1.81	0.85	0.14	0.12	0.01	
	6	6.86	0.22	1.62	3.53	0.11	1.34	1.92	0.71	0.15	0.07	0.01	
	7	7.29	0.19	1.2	3.56	0.12	1.29	1.76	0.68	0.17	0.07	0.03	
	8	7.3	0.19	1.26	3.68	0.13	1.13	1.77	0.6	0.18	0.04	0.02	
	9	7.26	0.19	1.25	3.6	0.13	1.22	1.8	0.67	0.18	0.06	0.02	
	10	7.17	0.2	1.32	3.76	0.14	1.07	1.81	0.66	0.18	0.06	0.02	
	11	7.16	0.18	1.34	3.68	0.14	1.15	1.85	0.65	0.21	0.06	0.02	
	12	6.1	0.32	2.9	4.29	0.09	1.5	0.01	0.08	1.69	0.03	0.01	

Table II.13: **Sample JR 12**: Amphibole analysis from EDS (analyses and cations)

	Elements	SiO_2	TiO_2	Al_2O_3	FeO	MnO	MgO	CaO	Na_2O	K_2O	Cl_2O	Total
Analyses	1	41.49	1.69	6.74	27.62	1.12	4.5	9.22	2.08	0.83	0.08	95.37
	2	41.3	1.31	6.81	28.47	1.13	3.92	10.03	1.76	0.84	0	95.57
	3	41.76	1.77	6.48	26.69	0.96	4.82	9.52	1.98	0.91	0.2	95.09
	4	42.09	0.93	6.9	28.31	1.08	3.99	9.86	1.98	1.04	0	96.18
	5	41.61	1.31	6.37	28.96	0.88	3.65	9.9	2.05	0.84	0	95.57
	6	42.45	0.82	6.66	28.65	1.09	4.08	10.3	1.54	0.84	0.13	96.56
	7	34.67	3.46	13	29.44	0.42	4.62	0.12	0.36	9.06	0.03	95.18
	8	34.29	3.52	12.97	29.1	0.83	5.03	0.02	0.14	9.18	0	95.08
	9	34.76	3.72	12.74	29.71	0.61	4.81	0.05	0.27	8.82	0.04	95.53
	10	41.12	0.95	6.84	28.78	1.23	3.81	9.92	2.18	1.14	0	95.97
	11	41.72	0.61	6.91	29.07	1.17	3.83	10.26	1.6	1.14	0.06	96.37
	12	35.26	2.62	13.33	28.44	0.61	5.32	0.22	0.44	8.34	0.1	94.68
	13	34.85	3.28	13.46	28.81	0.48	4.47	0.06	0.26	9.13	0	94.8
	14	40.39	1.82	8.91	26.39	1.03	5.17	10	2.92	0.77	0.08	97.48
	15	41.54	1.88	7.69	25.59	0.72	5.18	9.92	2.72	0.78	0.03	96.05
	16	41.5	1.39	8.31	26.14	0.71	5.07	10.19	2.16	0.78	0.03	96.28
	17	41.83	1.14	6.61	29.82	1.14	3.93	9.67	1.58	1.03	0.04	96.79
	18	34.38	1.7	13.76	29.59	0.6	4.82	0.08	0.39	8.98	0.01	94.31
	19	42.06	0.96	6.55	29.61	1.12	3.85	9.77	1.67	1.15	0	96.74
	20	41.58	1.58	7.07	28.86	0.74	3.77	9.81	1.51	1.01	0.03	95.96
	21	41.62	1.1	6.69	28.75	0.92	3.9	9.87	1.7	1.14	0	95.69
	22	41.69	1.44	6.56	28.11	0.91	4.12	9.47	2.24	0.87	0.1	95.51
	23	42.37	1.57	6.68	26.98	0.97	4.81	9.2	1.99	0.87	0.05	95.49
	24	43.36	0.97	5.38	29.08	1.14	4.15	10.22	1.38	0.71	0	96.39
	25	42.05	1.76	6.69	27.32	0.84	4.6	9.8	2.36	0.82	0.07	96.31
	26	40.77	0.16	9.02	29.49	0.9	3.09	10.19	1.22	1.16	0.01	96.01
Cations	1	7.14	0.22	1.37	3.98	0.16	1.01	1.7	0.59	0.18	0.02	
	2	7.03	0.17	1.37	4.05	0.16	1.11	1.83	0.62	0.18	0	
	3	7.17	0.23	1.31	3.83	0.14	1.02	1.75	0.66	0.2	0.05	
	4	7.03	0.12	1.36	3.96	0.15	1.58	1.77	0.17	0.22	0	
	5	7.53	0.18	1.36	4.38	0.14	0	1.92	0.04	0.19	0	
	6	7.11	0.1	1.31	4.01	0.15	1.4	1.85	0.12	0.18	0.03	
	7	6.13	0.46	2.71	4.35	0.06	1.22	0.02	0.12	2.04	0.01	
	8	6.09	0.47	2.71	4.32	0.13	1.33	0	0.05	2.08	0	
	9	6.13	0.49	2.65	4.38	0.09	1.26	0.01	0.09	1.98	0.01	
	10	7.05	0.12	1.38	4.13	0.18	0.97	1.82	0.73	0.25	0	
	11	7.1	0.08	1.39	4.14	0.17	0.97	1.87	0.53	0.25	0.01	
	12	6.22	0.35	2.77	4.19	0.09	1.4	0.04	0.15	1.88	0.02	
	13	6.17	0.44	2.81	4.26	0.07	1.18	0.01	0.09	2.06	0	
	14	6.73	0.23	1.75	3.68	0.14	1.29	1.79	0.94	0.16	0.02	
	15	6.97	0.24	1.52	3.59	0.1	1.3	1.78	0.88	0.17	0.01	
	16	6.95	0.17	1.64	3.66	0.1	1.27	1.83	0.7	0.17	0.01	
	17	7.1	0.15	1.32	4.23	0.16	0.99	1.76	0.52	0.22	0.01	
	18	6.14	0.23	2.89	4.42	0.09	1.28	0.01	0.14	2.04	0	
	19	7.14	0.12	1.31	4.2	0.16	0.97	1.78	0.55	0.25	0	
	20	7.07	0.2	1.42	4.1	0.11	0.96	1.79	0.5	0.22	0.01	
	21	7.12	0.14	1.35	4.11	0.13	0.99	1.81	0.56	0.25	0	
	22	7.12	0.18	1.32	4.02	0.13	1.05	1.73	0.74	0.19	0.02	
	23	7.17	0.2	1.33	3.82	0.14	1.21	1.67	0.65	0.19	0.01	
	24	7.34	0.12	1.07	4.12	0.16	1.05	1.85	0.45	0.15	0	
	25	7.09	0.22	1.33	3.85	0.12	1.16	1.77	0.77	0.18	0.02	
	26	6.97	0.02	1.82	4.22	0.13	0.79	1.87	0.4	0.25	0	

Table II.14: **Sample JZ 6**: Amphibole analysis from WDS (analyses and cations)

	Elements	SiO_2	TiO_2	Al_2O_3	FeO	MnO	MgO	CaO	Na_2O	K_2O	F	Cl_2O	Total
Analyses	1	51.09	0.2	0.91	33.11	0.51	2.17	0.57	6.33	0.78	0.09	0.01	95.77
	2	50.2	0.29	1.1	32.5	0.53	2.3	0.84	6.62	0.86	0.25	0.01	95.5
	3	46.66	0.24	1.97	31.94	0.55	1.95	0.9	5.63	0.93	0.17	0.01	90.95
	4	50.45	0.19	1.13	32.24	0.54	2.51	1.02	6.67	0.98	0.32	0.01	96.06
	5	51.81	0.39	0.25	28.46	0.33	0.38	3.83	11.15	0.01	0	0	96.61
	6	51.48	0.41	0.27	28.82	0.3	0.37	3.74	11.29	0	0	0	96.68
	7	52.64	0.21	0.29	29.38	0.2	0.33	2.59	12.22	0	0	0.01	97.87
	8	51.58	0.24	0.34	29.55	0.26	0.39	3.27	11.61	0.03	0	0.01	97.28
	9	51.24	2.16	0.21	28.8	0.6	0.35	4.96	10.47	0.01	0	0	98.8
	10	52.37	0.43	0.26	28.72	0.41	0.42	5.95	10.24	0	0	0	98.8
	11	51.16	0.79	0.23	27.77	0.37	0.38	5.66	9.96	0.02	0	0.02	96.36
Cations	1	6.05	0.02	0.13	3.28	0.05	0.38	0.07	1.45	0.12	1	0	
	2	8.5	0.04	0.22	4.6	0.08	0.58	0.15	2.17	0.19	0	0	
	3	8.34	0.03	0.42	4.77	0.08	0.52	0.17	1.95	0.21	0	0	
	4	8.49	0.02	0.22	4.54	0.08	0.63	0.18	2.18	0.21	0	0	
	5	8.62	0.05	0.05	3.96	0.05	0.09	0.68	3.6	0	0	0	
	6	8.58	0.05	0.05	4.02	0.04	0.09	0.67	3.65	0	0	0	
	7	8.65	0.03	0.06	4.04	0.03	0.08	0.46	3.89	0	0	0	
	8	8.57	0.03	0.07	4.11	0.04	0.1	0.58	3.74	0.01	0	0	
	9	8.38	0.27	0.04	3.94	0.08	0.08	0.87	3.32	0	0	0	
	10	8.54	0.05	0.05	3.92	0.06	0.1	1.04	3.24	0	0	0	
	11	8.54	0.1	0.05	3.88	0.05	0.09	1.01	3.22	0	0	0.01	

Table II.15: **Sample JZ 6**: Amphibole analysis from EDS (analyses and cations)

	Elements	SiO_2	TiO_2	Al_2O_3	FeO	MnO	MgO	CaO	Na_2O	K_2O	Cl_2O	Total
Analyses	1	49.9	0.48	1.16	34.42	0.63	2.15	1.13	6.88	1.19	0.06	98
	2	49.3	0.11	1.1	34.49	0.55	1.86	0.87	6.79	0.91	0.12	96.1
	3	49.5	0.25	1.27	34.1	0.6	2.15	1.2	6.78	1.01	0	96.86
	4	48.37	0.73	1.11	33.51	0.74	2.09	1.16	7.06	1.12	0.06	95.95
	5	49.36	0.16	1.09	33.56	0.8	2.09	1.13	6.87	1.2	0.04	96.3
	6	48.15	0.32	1.22	33.5	0.54	2.04	1.18	6.81	1.24	0.07	95.07
	7	46.92	1.08	1.05	34.07	0.93	1.99	1.28	6.48	1.36	0	95.16
	8	48.67	0.38	1.17	32.55	0.8	2.03	1.56	6.44	1.51	0.03	95.14
	9	48.34	1.04	1.12	33.45	0.88	2.1	1.37	6.8	1.43	0	96.53
	10	48.02	0.5	0.92	32.94	0.91	2.24	1.43	6.49	1.45	0.01	94.91
	11	48.81	0.19	1.32	34.05	0.47	2.04	1.04	7.01	0.83	0.03	95.79
	12	50.85	0.44	0.34	29.85	0.19	0.32	4.01	11.15	0.09	0	97.24
	13	50.99	0.49	0.42	31.42	0.14	0.41	1.49	13.16	0	0.06	98.58
	14	51.39	0.01	0.36	32.46	0.14	0.1	0.48	13.58	0.04	0.06	98.62
	15	48.13	0.22	0.37	29.48	0.43	0.44	4.24	10.57	0.04	0.13	94.05
	16	50.81	0.71	0.25	29.71	0.26	0.41	5.45	10.75	0	0.06	98.41
	17	50.11	0.67	0.57	28.74	0.4	0.42	5.09	10.72	0.01	0.06	96.79
	18	47.21	1.85	0.97	33.41	0.96	2.41	1.29	6.72	0.97	0.03	95.82
	19	50.45	0.08	0.36	30.75	0.25	0.42	2.79	12.58	0	0	97.68
	20	51.69	-0.01	0.5	30.19	0.1	0.27	3.84	12.25	0.07	0	98.9
	21	51.9	0.28	0.47	29.51	0.37	0.34	2.54	12.79	0	0.05	98.25
	22	50.37	0.92	0.3	29.43	0.42	0.3	4.94	10.87	0.01	0	97.56
	23	48.11	0.95	1.07	33.24	0.81	2.21	1.25	6.61	1.05	0	95.3
	24	47.74	0.31	1.27	33.33	0.63	2.06	1.18	6.79	1.16	0.05	94.52
	25	47.24	1.55	0.92	33.09	0.99	2.22	1.4	6.38	1.27	0.07	95.13
	26	49.62	0.31	0.94	33.65	0.89	2.27	1.05	6.97	0.97	0	96.67
	27	49.4	0.22	0.95	30.05	0.33	0.41	1.97	12.49	0.01	0.04	95.87
	28	50.26	0.3	0.38	30.52	0.12	0.32	2.6	12.7	0.03	0	97.23
	29	49.59	0.34	0.34	29.96	0.29	0.32	5.02	10.73	0.01	0	96.6
Cations	1	8.32	0.06	0.23	4.8	0.09	0.53	0.2	2.22	0.25	0.01	
	2	8.39	0.01	0.22	4.91	0.08	0.47	0.16	2.24	0.2	0.03	
	3	8.36	0.03	0.25	4.82	0.09	0.54	0.22	2.22	0.22	0	
	4	8.26	0.09	0.22	4.79	0.11	0.53	0.21	2.34	0.24	0.01	
	5	8.38	0.02	0.22	4.77	0.12	0.53	0.2	2.26	0.26	0.01	
	6	8.3	0.04	0.25	4.83	0.08	0.52	0.22	2.28	0.27	0.02	
	7	8.14	0.14	0.21	4.94	0.14	0.52	0.24	2.18	0.3	0	
	8	8.34	0.05	0.24	4.67	0.12	0.52	0.29	2.14	0.33	0.01	
	9	8.24	0.13	0.23	4.77	0.13	0.53	0.25	2.25	0.31	0	
	10	8.3	0.06	0.19	4.76	0.13	0.58	0.26	2.16	0.32	0	
	11	8.33	0.02	0.26	4.86	0.07	0.52	0.19	2.34	0.18	0.01	
	12	8.48	0.06	0.07	4.16	0.03	0.08	0.72	3.72	0.02	0	
	13	8.45	0.06	0.08	4.35	0.02	0.1	0.26	4.39	0	0.01	
	14	8.53	0	0.07	4.5	0.02	0.02	0.09	4.53	0.01	0.01	
	15	8.37	0.03	0.07	4.29	0.06	0.12	0.79	3.52	0.01	0.03	
	16	8.42	0.09	0.05	4.12	0.04	0.1	0.97	3.45	0	0.01	
	17	8.38	0.08	0.11	4.02	0.06	0.11	0.91	3.48	0	0.01	
	18	8.11	0.24	0.2	4.8	0.14	0.62	0.24	2.24	0.21	0.01	
	19	8.45	0.01	0.07	4.31	0.04	0.1	0.5	4.08	0	0	
	20	8.49	0	0.1	4.15	0.01	0.07	0.68	3.9	0.01	0	
	21	8.56	0.04	0.09	4.07	0.05	0.08	0.45	4.09	0	0.01	
	22	8.4	0.12	0.06	4.11	0.06	0.07	0.88	3.52	0	0	
	23	8.26	0.12	0.22	4.77	0.12	0.57	0.23	2.2	0.23	0	
	24	8.3	0.01	0.26	4.84	0.09	0.54	0.22	2.29	0.26	0.01	
	25	8.28	0.05	0.19	4.85	0.15	0.58	0.26	2.17	0.28	0.02	
	26	8.39	0.01	0.19	4.76	0.13	0.57	0.19	2.29	0.21	0	
	27	8.43	0.01	0.19	4.29	0.05	0.1	0.36	4.13	0	0.01	
	28	8.46	0.01	0.08	4.3	0.02	0.08	0.47	4.14	0.01	0	
	29	8.4	0.01	0.07	4.25	0.04	0.08	0.91	3.53	0	0	

III. Geochemistry

Normative Study

The normative compositions (Table III.1) were determined from the chemical analyses using the 'Minpet' software programme.

Sample Preparation for ICP Analyses

Eighty-one samples were crushed and ground for the ICP analyses. A rock splitter was used to split the hand specimens into smaller rock pieces to ease the crushing and to precisely choose a part of each sample for analysis. The samples were then further broken using a fly press and/or a hammer and anvil. Approximately 15g of dis-aggregated material were placed in a vibratory disc mill (Tema) using an agate 'pot' at a speed of 700 rpm.

During the analysis by ICP some international and internal standards (Table III.2 and 3) were also analysed. The international standards were NIM-G (granite), NIM-L (lujavrite), SCO-1 (shale) and RGM-1, while the internal standards were KC10, KC11 and KC12. The standards used for the checks were chosen based on their concentrations in order to cover all ranges of the analyses. Due to the possible occurrence of interferences, some elements were measured either with the AES or with the MS.

For most of the trace elements the powder was dissolved in HF and perchloric acid, evaporated to dryness and then made up with a solution of HCl. The solution was then run on an ICP-AES model Optima 3300RL or ICP-MS 7500cx Series. For the major elements and some other trace elements in resistant phases, a Li-metaborate fusion was carried out and the glass beads were dissolved in HNO_3.

The chemical analyses of the local and international standards (Table III.2 and 3) indicate that the relative difference from the accepted values mostly does not exceed 10%, which means that the accuracy is acceptable for most elements.

Table III.1. The normative values of the studied granitoids

Sample Number	Quartz (%)	Orthoclase (%)	Albite (%)	Sample Number	Quartz (%)	Orthoclase (%)	Albite (%)
TH2`	31.9	31.13	28.66	JM13	28.83	31.17	36.52
TH5`	32.82	18.71	41.18	JM16	30.13	26.16	37.04
TH7`	25.81	13.94	41.45	JM17	29.27	26.41	35.68
TH8`	27.62	16.27	40.75	JM18	31.02	31.1	35.3
TH10`	33.91	22.2	40.22	JM20	23.71	29.32	42.67
TH11`	22.81	25.59	39.3	JM24	29.4	26.7	40.85
TH12`	32.62	27.08	34.69	JM27	29.96	32.09	33.86
TH13`	21.27	25.14	39.78	JM31	30.12	30.77	32.74
TH14`	23.37	25.63	37.89	JM33	26.82	26.94	38.24
TH3	35.15	18.97	38.23	JM4	23.61	33.85	35.66
TH9	30.46	13.93	37.45	JM7	19.75	32.22	41.66
TH18	28.2	14.06	38.38	M2	33.26	26.41	32.12
TH19	29.04	16.07	38.21	M3	18.92	21.67	42.02
KD1	33.43	29.03	34.55	M5	33.07	34.31	29.71
KD2	38.17	27.89	30.51	JR12	25.15	27.17	39.07
KD4	30.01	38.14	26.51	JR13B	27.32	25.09	34.8
KD9	35.56	22.77	32.61	JR17	41.36	5.82	40.48
KD10A	26.3	13.38	37.73	JR19	26.36	28.92	36.21
KD10B	26.38	26.22	36.6	JR20	35	21.24	40.63
KD11	26.9	27.61	35.12	JR3C	33.07	23.13	40.27
KD12	35.46	24.1	32.07	JR3D	20.86	27.18	41.23
KD13	29.88	25.91	34.28	JR3E	34.41	25.97	34.31
KD14	22.36	16.1	39.79	JR9	29.63	29.81	36.72
KD15	35.8	26.93	32.92	JZ1A	29.55	23.72	35.68
KD17	30.17	28.9	33.46	JZ1B	23.14	22.36	37.76
KD21	33.35	29.24	31.69	JZ5	32.03	28.03	25.78
KD22	26.61	26.35	31.02	JZ2	44.48	25.62	8.87
KD23	26.84	23.24	33.29	JZ4	47.05	31.9	7.54
KD28	16.57	35.62	38.7	JZ6	41.29	29.6	9.06
KD29	30.69	29.56	33.63	JZ8	41.98	29.76	8.52
KD34	31.23	30.54	33.37	JZ10	47.07	30.28	8.22
KD36	33.94	29.11	32.27	JZ12	47.1	26.49	8.39
KD37	33.06	30.31	33.23	JZ14	50.34	30.3	7.03
KD38	21.46	35.42	34.62				
KD41	23.81	0.47	69.55				

Abbreviations: TH, Jabal Thalabah, KD, Jabal Khur Duhan, JM and M, Jabal Al-Massah, JR, Jabal Raydan, JZ, Jabal az Zuhd

Table III.2. The local standards for the ICP-AES and MS analyses

	KC 10				KC 11				KC 12			
	During the run	Accepted	Absolute difference	Relative difference	During the run	Accepted	Absolute difference	Relative difference	During the run	Accepted	Absolute difference	Relative difference
SiO_2	48.44	48.00	0.44	0.009	55.99	55.55	0.44	0.008	69.44	69.00	0.44	0.006
Al_2O_3	18.41	17.40	1.01	0.058	16.48	16.51	-0.03	-0.002	15.60	15.20	0.40	0.026
FeO(t)	10.47	9.90	0.57	0.058	9.03	8.71	0.32	0.037	3.18	2.80	0.38	0.136
MgO	8.18	7.70	0.48	0.062	4.08	3.99	0.09	0.022	1.28	1.20	0.08	0.070
CaO	12.09	11.90	0.19	0.016	7.19	6.86	0.33	0.049	1.96	1.80	0.16	0.088
Na_2O	2.46	2.40	0.06	0.026	3.34	3.30	0.04	0.013	4.16	4.20	-0.04	-0.009
K_2O	0.24	0.22	0.02	0.101	2.19	2.15	0.04	0.017	4.20	4.30	-0.10	-0.023
TiO_2	0.82	0.84	-0.02	-0.025	1.10	1.10	0.00	-0.001	0.36	0.35	0.01	0.026
P_2O_5	0.13	0.11	0.02	0.207	0.34	0.32	0.02	0.060	0.12	0.12	0.00	-0.038
MnO	0.13	0.13	0.00	0.029	0.14	0.14	0.00	0.008	0.04	0.05	-0.01	-0.126
Ba	140	126	14.40	0.114	505	491	13.92	0.028	1651	1600	50.75	0.032
Cu	168	170	-1.77	-0.010	107	108	-1.04	-0.010	23	27	-4.04	-0.149
Li	1	6	-5.35	-0.891			0.00		5	8	-3.45	-0.432
Ni	101	104	-3.35	-0.032	281	280	0.80	0.003	11	15	-3.60	-0.240
Sr	354	360	-5.71	-0.016	371	370	1.18	0.003	462	460	1.77	0.004
Y	12	13	-0.84	-0.065	28	28	-0.10	-0.004	5	6	-0.65	-0.108
Zn	73	60	13.32	0.222	117	119	-1.60	-0.013	42	42	0.07	0.002
Rb	4	4	-0.35	-0.088	274	270	4.30	0.016	59	61	-2.14	-0.035
Zr	39	38	1.40	0.037	150	145	4.88	0.034	146	160	-14.24	-0.089
Nb	2	2	-0.14	-0.067	11	12	-0.74	-0.062	3	4	-0.34	-0.097
Mo	1				1				1			
Sn	0		0.20		9				1			
Hf	1	1	-0.65	-0.461	3	3	-0.10	-0.030	3	4	-0.31	-0.089
Ta		<0.1			6	5	0.94	0.188	0	<0.1		
Pb	9	8	0.54	0.067	14		14.33		16	10	6.32	0.632
Th					3	2	0.59	0.244	15	14	0.92	0.066
U	0	0	0.14	0.657	2	2	0.23	0.128	0	0	0.17	0.509
La	6	4	1.95	0.454	25	23	1.54	0.067	38	37	0.73	0.020
Ce	10	9	0.99	0.108	48	49	-1.26	-0.026	65	70	-5.29	-0.076
Pr	1	2	-0.15	-0.091	6	6	-0.14	-0.023	7	7	-0.47	-0.065
Nd	7	7	0.41	0.061	25	27	-1.14	-0.043	26	27	-1.41	-0.052
Sm	2	2	-0.02	-0.010	5	5	0.06	0.011	4	3	0.29	0.086
Eu	1	1	-0.01	-0.011	2	1	0.11	0.079	1	1	0.29	0.261
Gd	2	2	-0.32	-0.171	4	5	-0.63	-0.125	3	2	0.50	0.236
Tb					1				0		0.31	
Dy	2	2	-0.08	-0.041	4	4	-0.32	-0.071	1	1	-0.03	-0.026
Ho	0	0	-0.03	-0.077	1	1	-0.18	-0.183	0	0	-0.02	-0.075
Er	1	1	-0.13	-0.101	2	3	-0.49	-0.182	1	1	-0.13	-0.156
Tm					0		0.36		0			
Yb	1	1	0.01	0.014	2	2	0.11	0.048	0	1	-0.09	-0.187
Lu	0	0	0.02	0.129	0	0	0.03	0.080	0	0	0.04	0.720

Table III.3. The international standards for the ICP-AES and MS analyses

	MIN-G				NIM-L				RGM-1			
	During the run	Accepted	Absolute difference	Relative difference	During the run	Accepted	Absolute difference	Relative difference	During the run	Accepted	Absolute difference	Relative difference
SiO_2	75.98	75.7	0.28	0.004	53.05	52.4	0.65	0.01	73.76	73.5	0.26	0.003
Al_2O_3	12.35	12.1	0.25	0.02	13.27	13.6	-0.33	-0.02	13.78	13.7	0.08	0.006
FeO(t)	2.01	2	0.01	0.007	10.1	9.9	0.2	0.02	1.88	1.8	0.08	0.044
MgO	0.06	0.1	-0.04	-0.418	0.26	0.3	-0.04	-0.14	0.29	0.3	-0.01	-0.043
CaO	0.8	0.8	0	-0.002	3.17	3.2	-0.03	-0.01	1.19	1.2	-0.01	-0.009
Na_2O	3.45	3.4	0.05	0.016	7.5	8.4	-0.9	-0.11	4.05	4.1	-0.05	-0.012
K_2O	5.12	5	0.12	0.025	5.45	5.5	-0.05	-0.01	3.9	4.3	-0.4	-0.093
TiO_2	0.09				0.44	0.5	-0.06	-0.13	0.26	0.3	-0.04	-0.137
P_2O_5					0.04	0.1	-0.06	-0.63	0.05	0.05	0	-0.079
MnO	0.02	0.02		-0.108	0.66	0.8	-0.14	-0.18	0.04	0.04	0	-0.101
											SCO-1	
Ba					417	450	-32.88	-0.07	582	570	12.36	0.02
Cu					30	13	17.39	1.34	28	29	-0.31	-0.01
Li					53	48	4.63	0.1	56	45	11.18	0.25
Ni					0	2	-2.2	-1	26	27	-0.92	-0.03
Sr					4837	4600	237.18	0.05	167	174	-6.65	-0.04
Y					22	26	-3.98	-0.15	22	22	0.29	0.01
Zn					336				93	103	-10.02	-0.1
Rb	313.1	325	-11.9	-0.037	185	190	-4.7	-0.02	106	112	-6.4	-0.06
Zr	299.4	300	-0.6	-0.002					163	160	3.49	0.02
Nb	52.17	53	-0.83	-0.016	973	960	12.9	0.01	13	12	0.64	0.05
Mo	3.012	2.84	0.17	0.061	2	1	0.75	0.62	2	1	0.27	0.2
Sn	5.0458	3.3	1.75	0.529	8	7	0.21	0.03	3	4	-0.71	-0.19
Hf	11.58	12.4	-0.82	-0.066	205	231	-26.3	-0.11	4	5	-0.7	-0.15
Ta	4.397	4.9	-0.5	-0.103	22	25	-2.92	-0.12	1	1	-0.22	-0.24
Pb	42.79	40	2.79	0.07	60	43	17.26	0.4	35	31	3.56	0.11
Th	45.05	51	-5.95	-0.117	58	66	-7.76	-0.12	9	10	-0.32	-0.03
U	13.89	15	-1.11	-0.074	14	14	-0.09	-0.01	3	3	-0.33	-0.11
La	104.2	109	-4.8	-0.044	216	250	-33.6	-0.13	29	30	-0.47	-0.02
Ce	186.8	195	-8.2	-0.042	268	240	27.9	0.12	51	62	-10.99	-0.18
Pr	18.43	19.5	-1.07	-0.055	18	16	1.88	0.11	6	7	-0.55	-0.08
Nd	67.77	72	-4.23	-0.059	47	48	-0.78	-0.02	25	26	-0.86	-0.03
Sm	14.81	15.8	-0.99	-0.063	5	5	-0.43	-0.09	5	5	-0.39	-0.07
Eu	0.3566	0.35	0.01	0.019	1	1	-0.08	-0.06	1	1	-0.02	-0.02
Gd	13.2	14	-0.8	-0.057	5	4	1.77	0.49	4	5	-0.62	-0.14
Tb	2.821	3.1	-0.28	-0.09	1	1	-0.07	-0.1	1	1	0.02	0.03
Dy	15.86	17	-1.14	-0.067	3	3	-0.31	-0.1	4	4	-0.69	-0.16
Ho	3.386	3.6	-0.21	-0.059	1	1	-0.29	-0.32	1	1	-0.27	-0.28
Er	9.827	10.5	-0.67	-0.064	2	3	-0.62	-0.24	2	3	-0.53	-0.21
Tm	1.858	2	-0.14	-0.071					0	0	-0.07	-0.18
Yb	13.02	14.2	-1.18	-0.083	3	3	-0.39	-0.13	2	2	-0.24	-0.1
Lu	1.871	2	-0.13	-0.065	0	0	0.06	0.14	0	0	0.01	0.02

Sample Preparation for XRF Analysis

Some samples (mostly from the Jabal Raydan and Jabal az Zuhd granitoids) did not show good totals from the ICP analysis. Therefore, X-ray fluorescence was used to check these values. In addition, some trace element values were also confirmed by XRF. For this a PANalytical Axios sequential X-ray fluorescence spectrometer was used. Calibration was achieved using international rock standards and accuracy was determined using additional rock standards.

For the trace elements, 6-8 drops of the binding agent (Mowiol) were added to 7g ± .2g of the sample powder and the resulting mixture compressed into a pellet using a tungsten carbide platen (10 tons for one minute). Major elements were analysed on fused Li-metaborate discs. During the analysis some internal standards were used to check the accuracy.

Chemical analyses of some xenoliths are given below.

Table III.4. Chemical analysis of xenoliths from Jabal Al-Massah (JM and M) and Jabal Khur Dukhan (KD) in wt %

Sample Number	JM21H	M6	KD10B
SiO_2	50.82	56.96	72.96
Al_2O_3	14.52	15.64	13.53
Total Fe as FeO	16.03	6.76	2.31
MgO	4.64	4.25	0.39
CaO	10.94	4.34	1.15
Na_2O	0.85	3.07	4.22
K_2O	0.16	6.26	4.30
TiO_2	0.86	1.29	0.23
P_2O_5	0.25	0.88	0.06
MnO	0.22	0.11	0.03
LOI	0.52	0.40	0.40
Total	99.81	99.96	99.60

IV. Isotopic analysis

Methodology for U-Pb Zircon dating

Five samples (TH14`, KD28, JM31, JR13 & JZ6) were used for this analysis. After crushing, the samples were subjected to heavy mineral separation using Na polytungstate. The heavy fraction was then subjected to a Frantz magnetic separator which removed the magnetic fraction. The non-magnetic fraction consisted of zircon together with some allanite, apatite, fluorite and xenotime. Di-iodomethane heavy liquid was also used to separate any mineral with a density less than 3.3g/cm. Zircons were then identified and selected using a binocular microscope and separated by hand using tweezers. The separated grains were then mounted in a resin block and the top surface polished.

Zircons were analysed by laser ablation ICPMS in the Department of Earth Sciences, University College, London. The equipment used was an Agilent Technologies 7700 series ICP-MS coupled with a 213 nanometer NewWave laser ablation system and helium carrier gas. Laser spot size was 40 microns. Plesovice zircon and NIST SRM 612 glass were used as a reference material (Slama *et al*., 2008). Results were processed and refined first using the 'Glitter' software and then plotted using the software programe 'Isoplot'.

Some non-zircon minerals were also analysed in error because of the difficulty of distinguishing zircon from other minerals such as allanite and titanite. These were detected by their different trace element characteristics or anomalously high ages (e.g. > 3000 Ma).

Methodology for Rb-Sr Age dating

Twenty samples representative of the five plutons were selected for Rb-Sr analysis (TH10`, TH12`, TH13`, TH14`, KD13, KD28, KD37, KD41, JZ10, JZ8, JZ6, JZ2, JR9, JR12, JR3C, JR3E, JM31, JM27, JM18, JM16). Selection was based on sample type and a range of Rb/Sr ratios.

Powders were dissolved in a HF-HNO_3 mixture and the Sr was separated using a standard ion-exchange procedure (Thirlwall, 1982; 2002). The separated Sr was loaded on to Ta filaments. The international standard SRM987 was also analysed as a check on the analyses. Samples were then analysed using a VG354 Thermal Ionisation Mass Spectrometer (TIMS) in the Department of Earth Sciences, Royal Holloway. Multidynamic analysis was used to eliminate transmission differences between collectors to achieve a 2sd reproducibility of ±0.000014 for $^{87}Sr/^{86}Sr$. The Rb and Sr contents and Rb/Sr ratios were previously determined by Inductive Coupled Plasma-Atomic Emission Spectrometer (ICP-AES). During the course of this study, the ratio of $^{87}Sr/^{86}Sr$ for the SRM987 international standards was 0.710256 ± 11 for the first sets. For the second sets, the average of SRM 987 and standard values were $^{87}Sr/^{86}Sr$ = 0.710264 ± 12 and 0.710266 ± 10. These results are acceptable as the accepted value is 0.71034 ±0.00026. Isochrons were plotted and calculated using the 'Isoplot' software.

Table IV.1. Isotopic ratio of TH14` and standard values

Analysis	Pb207/Pb206	Pb206/U238	Pb207/U235	Pb208/Th232	Pb208/Pb206	Th232/U238	U238/Si29
STDCZ1	0.05324	0.05404	0.39711	0.01794	0.03323	0.10072	0.01181
STDCZ2	0.0518	0.05477	0.39622	0.01575	0.02878	0.1007	0.01156
STDCZ3	0.05325	0.05315	0.38945	0.01585	0.03042	0.10264	0.01195
TH14-1	0.0605	0.09219	0.78296	0.02872	0.15506	0.5006	0.0018
TH14-2	0.28178	0.13728	5.26353	0.24095	0.7495	0.42938	0.00291
TH14-3	0.06798	0.09706	0.90963	0.03079	0.19425	0.61564	0.00124
TH14-4	0.05989	0.09611	0.7961	0.0288	0.1652	0.55401	0.0056
TH14-5	0.06069	0.08677	0.72478	0.02677	0.19639	0.63972	0.00543
TH14-6	0.06006	0.09515	0.77747	0.03196	0.21059	0.62994	0.00229
TH14-7	0.06306	0.08748	0.77728	0.02887	0.17454	0.53116	0.00347
TH14-8	0.06624	0.09879	0.92539	0.03011	0.19365	0.63819	0.00193
TH14-9	0.05994	0.09293	0.76955	0.02856	0.1966	0.64229	0.00343
TH14-10	0.05946	0.09034	0.74563	0.02936	0.19821	0.61235	0.00429
TH14-11	0.08641	0.09873	1.18102	0.04673	0.22562	0.47857	0.00136
TH14-12	0.06084	0.09947	0.86883	0.02893	0.14789	0.51032	0.00172
TH14-13	0.06492	0.08636	0.74946	0.0324	0.16095	0.4306	0.00304
TH14-14	0.06734	0.08915	0.81057	0.03113	0.13084	0.37599	0.00329
TH14-15	0.06155	0.09935	0.84939	0.0301	0.15636	0.51776	0.00245
TH14-16	0.22808	0.11699	3.5893	0.10782	0.52326	0.56967	0.00212
TH14-17	0.06378	0.10464	0.91822	0.03107	0.14253	0.48148	0.00347
TH14-18	0.06801	0.0986	0.91002	0.03252	0.19708	0.59937	0.00299
STDCZ4	0.05326	0.05407	0.39783	0.01679	0.02973	0.09603	0.01075
STDCZ5	0.05332	0.05222	0.38315	0.01722	0.03341	0.10161	0.0125
STDCZ6	0.05318	0.05515	0.40353	0.01724	0.03293	0.10564	0.01245
GLASS1	0.88501	0.26603	102.16848	0.58784	2.13467	0.96893	0.00024
GLASS2	0.88878	0.2643	110.69237	0.58796	2.13917	0.96444	0.00024

Table IV.2. Isotopic ratio of one sigma uncertainty of TH14` and standards values

Analysis	Pb207/Pb206	Pb206/U238	Pb207/U235	Pb208/Th232	Pb208/Pb206	Th232/U238	U238/Si29
STDCZ1	0.00154	0.00044	0.01903	0.00059	0.00112	0.00121	0.00004
STDCZ2	0.00142	0.00043	0.01863	0.0005	0.00095	0.00119	0.00003
STDCZ3	0.00174	0.00047	0.01962	0.00062	0.00122	0.00127	0.00004
TH14-1	0.00292	0.00099	0.04911	0.00086	0.00489	0.00618	0.00001
TH14-2	0.00711	0.00144	0.25102	0.00577	0.01918	0.0055	0.00001
TH14-3	0.00396	0.00124	0.06515	0.001	0.00671	0.00796	0.00001
TH14-4	0.00152	0.00075	0.03645	0.00069	0.00417	0.00628	0.00002
TH14-5	0.00179	0.00074	0.03507	0.00067	0.00522	0.00734	0.00002
TH14-6	0.00329	0.00115	0.05306	0.001	0.00698	0.00794	0.00001
TH14-7	0.00327	0.00111	0.05117	0.00099	0.00625	0.00684	0.00002
TH14-8	0.00322	0.00108	0.05841	0.00093	0.00626	0.00781	0.00001
TH14-9	0.00244	0.00091	0.04342	0.00083	0.00595	0.00758	0.00001
TH14-10	0.00237	0.0009	0.04157	0.00087	0.00611	0.00726	0.00002
TH14-11	0.00346	0.00107	0.06671	0.00146	0.00732	0.00593	0.00001
TH14-12	0.00406	0.00135	0.06868	0.00117	0.00616	0.00685	0.00001
TH14-13	0.00391	0.00117	0.0545	0.00128	0.00657	0.00578	0.00002
TH14-14	0.00294	0.00099	0.04757	0.00113	0.00485	0.00473	0.00002
TH14-15	0.00388	0.00139	0.06437	0.00125	0.00669	0.00706	0.00002
TH14-16	0.01221	0.00255	0.26855	0.00446	0.02315	0.01016	0.00002
TH14-17	0.00283	0.00119	0.05464	0.00117	0.00548	0.0061	0.00002
TH14-18	0.00246	0.00098	0.04802	0.00113	0.00693	0.00717	0.00001
STDCZ4	0.00181	0.00049	0.02014	0.0007	0.00124	0.00116	0.00004
STDCZ5	0.0018	0.00047	0.01932	0.0007	0.00136	0.00122	0.00005
STDCZ6	0.00185	0.00051	0.02063	0.00073	0.00138	0.00128	0.00005
GLASS1	0.03028	0.00426	13.38469	0.02222	0.08197	0.01532	
GLASS2	0.03039	0.00401	14.92524	0.02266	0.08319	0.01472	

Table IV.3. Age determinations (Ma) of TH14` and standard values

Analysis	Pb207/Pb206	Pb206/U238	Pb207/U235	Pb208/Th232
STDCZ1	339.2	339.3	339.5	359.5
STDCZ2	276.6	343.8	338.9	315.9
STDCZ3	339.5	333.9	334	317.8
TH14-1	621.5	568.5	587.2	572.3
TH14-2	3372.8	829.3	1863	4363.4
TH14-3	867.8	597.1	656.9	612.9
TH14-4	599.5	591.5	594.6	574
TH14-5	628.2	536.4	553.5	533.9
TH14-6	605.9	586	584	635.8
TH14-7	710.4	540.6	583.9	575.4
TH14-8	814	607.3	665.2	599.5
TH14-9	601.4	572.8	579.5	569.2
TH14-10	583.8	557.6	565.7	584.9
TH14-11	1347.3	607	791.8	923
TH14-12	633.4	611.3	634.9	576.5
TH14-13	771.8	534	567.9	644.4
TH14-14	848.3	550.5	602.8	619.6
TH14-15	658.3	610.6	624.3	599.5
TH14-16	3038.6	713.2	1547.2	2069.5
TH14-17	734.2	641.5	661.4	618.5
TH14-18	868.9	606.2	657.1	646.9
STDCZ4	339.7	339.5	340.1	336.5
STDCZ5	342.2	328.1	329.4	345.1
STDCZ6	336.2	346.1	344.2	345.6
GLASS1	5065.1	1520.6	4707.7	9345.6
GLASS2	5071.1	1511.8	4788.3	9347.1

Table IV.4. Isotopic ratio of one sigma uncertainty of age estimate (Ma) of TH14` and standards values

Analysis	Pb207/Pb206	Pb206/U238	Pb207/U235	Pb208/Th232
STDCZ1	64.13	2.7	13.83	11.68
STDCZ2	61.58	2.65	13.55	9.99
STDCZ3	72.5	2.89	14.34	12.39
TH14-1	100.88	5.85	27.97	16.85
TH14-2	38.79	8.15	40.69	94.04
TH14-3	116.24	7.28	34.64	19.7
TH14-4	53.86	4.41	20.61	13.57
TH14-5	62.31	4.38	20.65	13.29
TH14-6	114.29	6.76	30.31	19.64
TH14-7	106.42	6.58	29.23	19.35
TH14-8	98.37	6.35	30.8	18.23
TH14-9	85.91	5.35	24.92	16.29
TH14-10	84.39	5.3	24.18	17.09
TH14-11	75.39	6.29	31.06	28.21
TH14-12	137.55	7.89	37.31	22.92
TH14-13	121.78	6.93	31.63	25.06
TH14-14	88.15	5.86	26.68	22.12
TH14-15	129.71	8.17	35.34	24.55
TH14-16	83.25	14.72	59.42	81.43
TH14-17	91.26	6.97	28.92	23.03
TH14-18	73.25	5.75	25.53	22.13
STDCZ4	75.14	2.99	14.63	13.89
STDCZ5	74.59	2.88	14.18	13.93
STDCZ6	77.01	3.11	14.93	14.43
GLASS1	47.56	21.68	131.73	282.82
GLASS2	47.53	20.44	135.68	288.47

Table IV.5. Isotopic ratios of KD28 and standard values

Analysis	Pb207/Pb206	Pb206/U238	Pb207/U235	Pb208/Th232	Pb208/Pb206	Th232/U238	U238/Si29
STDCZ1	0.05317	0.05302	0.38653	0.01656	0.02936	0.09425	0.01027
STDCZ2	0.05342	0.05426	0.39937	0.01775	0.03463	0.10619	0.01284
STDCZ3	0.05306	0.05333	0.39169	0.01651	0.03082	0.09989	0.01226
KD28-1	0.10351	0.10467	1.46308	0.04893	0.18305	0.39289	0.00088
KD28-2	0.06317	0.09747	0.85134	0.02775	0.07731	0.27249	0.00367
KD28-3	0.06241	0.08263	0.71328	0.01558	0.10276	0.5471	0.01622
KD28-4	0.08646	0.03084	0.36799	0.00803	0.24029	0.92675	0.06039
KD28-5	0.06163	0.10417	0.88631	0.02539	0.09571	0.39424	0.00449
KD28-6	0.14853	0.12772	2.40535	0.09256	0.2576	0.35694	0.00361
KD28-7	0.06012	0.1007	0.83626	0.02644	0.07794	0.29816	0.00304
KD28-8	0.06016	0.09765	0.81418	0.02599	0.09048	0.34132	0.00392
KD28-9	0.06233	0.08054	0.69213	0.02498	0.07527	0.24377	0.00605
KD28-10	0.06927	0.04927	0.46936	0.00388	0.08721	1.11305	0.07038
KD28-11	0.08737	0.04338	0.52133	0.0125	0.14628	0.50989	0.01312
KD28-12	0.07918	0.10473	1.00007	0.00756	0.16765	2.33218	0.00574
KD28-13	0.05968	0.08543	0.70153	0.02029	0.21164	0.89475	0.0289
KD28-14	0.0622	0.10834	0.91384	0.02401	0.06413	0.29043	0.00392
KD28-15	0.07508	0.09392	0.97383	0.03177	0.12278	0.36425	0.00671
KD28-16	0.06799	0.09451	0.87214	0.02758	0.12438	0.42767	0.00142
KD28-17	0.07204	0.10069	1.00627	0.0321	0.11525	0.36252	0.00264
KD28-18	0.06099	0.09905	0.82563	0.02622	0.08966	0.33957	0.00368
KD28-19	0.05916	0.0955	0.7791	0.02466	0.04418	0.17148	0.01954
STDCZ4	0.05331	0.05277	0.38839	0.01684	0.03049	0.09573	0.01143
STDCZ5	0.05308	0.05586	0.40859	0.0172	0.03097	0.10072	0.01188
STDCZ6	0.05342	0.05223	0.38344	0.01729	0.03664	0.11081	0.01222
GLASS1	0.90036	0.30202	110.95963	0.65471	1.76767	0.8156	0.00019
GLASS2	0.88958	0.30228	110.11222	0.66716	1.78325	0.80762	0.00019

Table IV.6. Isotopic ratio of one sigma uncertainty of KD28 and standards values

Analysis	Pb207/Pb206	Pb206/U238	Pb207/U235	Pb208/Th232	Pb208/Pb206	Th232/U238	U238/Si29
STDCZ1	0.0006	0.00037	0.01649	0.00014	0.00028	0.0009	0.00001
STDCZ2	0.00057	0.00037	0.01693	0.00012	0.00029	0.00101	0.00001
STDCZ3	0.00058	0.00037	0.01662	0.00012	0.00027	0.00095	0.00001
KD28-1	0.00129	0.00076	0.06281	0.00036	0.00165	0.00381	
KD28-2	0.00084	0.0007	0.03671	0.00024	0.00079	0.00266	
KD28-3	0.00065	0.00056	0.03007	0.00009	0.00081	0.00529	0.00001
KD28-4	0.00088	0.00021	0.01548	0.00005	0.00186	0.00899	0.00004
KD28-5	0.00067	0.00072	0.03742	0.00017	0.0008	0.00385	
KD28-6	0.00566	0.00198	0.14494	0.00219	0.00662	0.00526	0.00005
KD28-7	0.00069	0.00069	0.03537	0.00019	0.0007	0.00295	
KD28-8	0.00068	0.00067	0.03436	0.00018	0.0008	0.00339	
KD28-9	0.0008	0.00057	0.02948	0.00021	0.00077	0.00245	0.00001
KD28-10	0.00075	0.00033	0.01967	0.00003	0.00076	0.01113	0.00009
KD28-11	0.00095	0.00029	0.02184	0.00008	0.00128	0.00513	0.00001
KD28-12	0.00169	0.0009	0.04627	0.00009	0.00244	0.0242	0.00002
KD28-13	0.00063	0.00057	0.02927	0.00013	0.00184	0.00908	0.00002
KD28-14	0.00091	0.00078	0.03933	0.00028	0.00085	0.00303	0.00001
KD28-15	0.00084	0.00063	0.04069	0.00022	0.00114	0.00374	0.00001
KD28-16	0.00116	0.00072	0.03831	0.0003	0.00159	0.00452	
KD28-17	0.00093	0.0007	0.04256	0.00027	0.00123	0.00379	
KD28-18	0.00074	0.00067	0.03461	0.00021	0.00092	0.00355	
KD28-19	0.00065	0.00064	0.03236	0.00018	0.00043	0.0018	0.00002
STDCZ4	0.00062	0.00035	0.01618	0.00015	0.00033	0.00101	0.00001
STDCZ5	0.00063	0.00037	0.01702	0.00015	0.00035	0.00107	0.00001
STDCZ6	0.00066	0.00035	0.01601	0.00016	0.00043	0.00119	0.00001
GLASS1	0.01062	0.00225	4.94547	0.00522	0.01906	0.00905	
GLASS2	0.0105	0.00222	4.84823	0.00537	0.01946	0.00898	

Table IV.7. Age determinations (Ma) of KD28 and standard values

Analysis	Pb207/Pb206	Pb206/U238	Pb207/U235	Pb208/Th232
STDCZ1	335.8	333.1	331.8	331.9
STDCZ2	346.8	340.6	341.2	355.5
STDCZ3	331.3	334.9	335.6	330.9
KD28-1	1688	641.7	915.3	965.6
KD28-2	714	599.6	625.4	553.3
KD28-3	688.3	511.8	546.7	312.4
KD28-4	1348.4	195.8	318.2	161.6
KD28-5	661.5	638.8	644.4	506.8
KD28-6	2329	774.9	1244.2	1789.3
KD28-7	608	618.5	617.1	527.4
KD28-8	609.2	600.6	604.8	518.7
KD28-9	685.4	499.3	534.1	498.6
KD28-10	906.8	310.1	390.7	78.2
KD28-11	1368.7	273.7	426	251
KD28-12	1176.6	642.1	703.8	152.2
KD28-13	592.7	528.4	539.7	405.9
KD28-14	681	663.1	659.1	479.5
KD28-15	1070.7	578.7	690.4	632.1
KD28-16	868.2	582.2	636.7	549.8
KD28-17	987.3	618.4	707	638.7
KD28-18	638.9	608.8	611.2	523.1
KD28-19	573.1	588	585	492.4
STDCZ4	341.8	331.5	333.2	337.5
STDCZ5	332.3	350.4	347.9	344.7
STDCZ6	346.6	328.2	329.6	346.4
GLASS1	5089.4	1701.3	4790.7	
GLASS2	5072.4	1702.6	4783	

Table IV.8. Isotopic ratio of one sigma uncertainty of age estimate (Ma) of KD28 and standards values

Analysis	Pb207/Pb206	Pb206/U238	Pb207/U235	Pb208/Th232
STDCZ1	25.48	2.27	12.07	2.76
STDCZ2	23.73	2.29	12.29	2.41
STDCZ3	24.41	2.26	12.12	2.44
KD28-1	22.78	4.43	25.89	6.94
KD28-2	28	4.12	20.13	4.8
KD28-3	22.02	3.36	17.82	1.87
KD28-4	19.61	1.31	11.49	0.94
KD28-5	23.28	4.18	20.14	3.26
KD28-6	63.89	11.3	43.22	40.53
KD28-7	24.73	4.07	19.56	3.76
KD28-8	24.41	3.94	19.23	3.57
KD28-9	27.17	3.38	17.69	4.22
KD28-10	22.1	2.05	13.6	0.52
KD28-11	20.79	1.82	14.58	1.65
KD28-12	41.76	5.27	23.49	1.89
KD28-13	22.23	3.4	17.47	2.58
KD28-14	30.86	4.53	20.86	5.61
KD28-15	22.21	3.74	20.93	4.36
KD28-16	34.96	4.21	20.78	5.91
KD28-17	25.88	4.11	21.54	5.34
KD28-18	25.71	3.95	19.25	4.11
KD28-19	23.68	3.74	18.47	3.54
STDCZ4	26.06	2.17	11.84	2.9
STDCZ5	26.42	2.28	12.27	3.03
STDCZ6	27.44	2.16	11.75	3.23
GLASS1	16.57	11.13	44.85	63.81
GLASS2	16.59	10.99	44.3	65.09

Table IV.9. Isotopic ratio of JR13 and standard values

Analysis	Pb207/Pb206	Pb206/U238	Pb207/U235	Pb208/Th232	Pb208/Pb206	Th232/U238	U238/Si29
GLASS1	0.88957	0.3248	125.36349	0.7463	1.90221	0.83133	0.00009
GLASS2	0.89475	0.31485	116.63236	0.76696	1.90083	0.78359	0.00009
JR13-1	0.05907	0.10571	0.85678	0.02917	0.12577	0.45763	0.01218
JR13-2	0.06102	0.10801	0.90443	0.03067	0.14405	0.50946	0.0141
JR13-3	0.06629	0.1078	0.95588	0.03344	0.12189	0.39458	0.00058
JR13-4	0.086	0.09576	1.09642	0.04831	0.16261	0.32365	0.00078
JR13-5	0.07298	0.09949	0.98736	0.03914	0.10341	0.26393	0.00075
JR13-6	0.05909	0.10628	0.86391	0.02935	0.14015	0.50958	0.01346
JR13-7	0.06203	0.10302	0.88141	0.03053	0.12028	0.40755	0.01005
JR13-8	0.05859	0.10746	0.8754	0.03213	0.1272	0.42727	0.01746
JR13-9	0.06022	0.10532	0.87503	0.0331	0.10325	0.32988	0.00738
JR13-10	0.0608	0.10457	0.87942	0.03355	0.10407	0.32573	0.01079
JR13-11	0.06437	0.10001	0.88461	0.03097	0.11804	0.38273	0.00995
JR13-12	0.06705	0.10091	0.9311	0.03167	0.14919	0.4774	0.00472
JR13-13	0.06097	0.10087	0.84651	0.02583	0.11152	0.43727	0.0142
JR13-14	0.05923	0.10162	0.82942	0.02642	0.10863	0.41957	0.01355
JR13-15	0.06335	0.08931	0.77819	0.02639	0.18349	0.62353	0.02239
JR13-16	0.0643	0.08724	0.77305	0.02444	0.15802	0.56654	0.01896
JR13-17	0.06135	0.10371	0.87445	0.02987	0.15359	0.53551	0.00443
JR13-18	0.0588	0.11043	0.89291	0.03072	0.08625	0.31138	0.01328
JR13-19	0.06233	0.11047	0.91363	0.0345	0.09916	0.31884	0.00049
JR13-20	0.07531	0.09798	1.01376	0.1085	0.06443	0.05843	0.03359
JR13-21	0.0891	0.06979	0.85984	0.02376	0.19988	0.58946	0.0211
JR13-22	0.06027	0.10526	0.87555	0.0295	0.11868	0.42527	0.00771
JR13-23	0.08163	0.10014	1.12923	0.0276	0.1674	0.60998	0.00408
JR13-24	0.07357	0.06361	0.64922	0.01602	0.25392	1.01257	0.02413
JR13-25	0.05936	0.10745	0.88301	0.02949	0.20245	0.7408	0.02169
JR13-26	0.1139	0.10914	1.68293	0.09452	0.20347	0.23594	0.00096
STDCZ1	0.05349	0.05383	0.39712	0.01727	0.03402	0.10647	0.01192
STDCZ2	0.05323	0.05352	0.39359	0.01685	0.0314	0.10019	0.01193
STDCZ3	0.05327	0.05385	0.39443	0.01734	0.03273	0.10207	0.01167

Table IV.10. Isotopic ratio of one sigma uncertainty of JR13 and standards values

Analysis	Pb207/Pb206	Pb206/U238	Pb207/U235	Pb208/Th232	Pb208/Pb206	Th232/U238	U238/Si29
GLASS1	0.00975	0.00244	5.76227	0.00533	0.01884	0.00906	
GLASS2	0.00979	0.00235	5.26953	0.00547	0.01878	0.00852	
JR13-1	0.00062	0.00072	0.03665	0.0002	0.00119	0.00483	0.00001
JR13-2	0.00064	0.00074	0.03869	0.00021	0.00136	0.00537	0.00001
JR13-3	0.00095	0.00079	0.04209	0.00032	0.00143	0.00423	
JR13-4	0.0011	0.00069	0.04767	0.0004	0.00176	0.00345	
JR13-5	0.00129	0.00079	0.04485	0.00051	0.00154	0.00291	
JR13-6	0.00062	0.00072	0.03695	0.0002	0.00133	0.00537	0.00001
JR13-7	0.00065	0.0007	0.03771	0.00021	0.00114	0.0043	0.00001
JR13-8	0.00061	0.00073	0.03743	0.00022	0.0012	0.00451	0.00001
JR13-9	0.00064	0.00072	0.03745	0.00023	0.00099	0.00348	0.00001
JR13-10	0.00064	0.00071	0.03762	0.00023	0.00099	0.00344	0.00001
JR13-11	0.00068	0.00068	0.03784	0.00021	0.00112	0.00404	0.00001
JR13-12	0.00092	0.00073	0.04081	0.00028	0.00166	0.00509	0.00001
JR13-13	0.00064	0.00069	0.03621	0.00017	0.00106	0.00461	0.00001
JR13-14	0.00062	0.00069	0.03548	0.00018	0.00103	0.00443	0.00001
JR13-15	0.00066	0.00061	0.03327	0.00018	0.00173	0.00658	0.00002
JR13-16	0.00067	0.00059	0.03306	0.00016	0.00149	0.00598	0.00001
JR13-17	0.00066	0.00071	0.03749	0.00021	0.00148	0.00565	
JR13-18	0.00062	0.00075	0.0382	0.00021	0.00082	0.00329	0.00001
JR13-19	0.00104	0.00084	0.04106	0.0004	0.00135	0.00346	
JR13-20	0.00078	0.00067	0.04334	0.00074	0.00061	0.00062	0.00003
JR13-21	0.001	0.00048	0.03697	0.00017	0.00197	0.00623	0.00004
JR13-22	0.00064	0.00072	0.03749	0.0002	0.00114	0.00449	0.00001
JR13-23	0.00088	0.00069	0.0484	0.00019	0.00161	0.00644	
JR13-24	0.00079	0.00044	0.0278	0.00011	0.00242	0.01068	0.00003
JR13-25	0.00062	0.00073	0.03775	0.0002	0.00191	0.00781	0.00002
JR13-26	0.00132	0.00077	0.0726	0.00072	0.00207	0.00252	
STDCZ1	0.00058	0.00037	0.01703	0.00014	0.00035	0.00113	0.00001
STDCZ2	0.00059	0.00037	0.0169	0.00014	0.00033	0.00106	0.00001
STDCZ3	0.00059	0.00037	0.01694	0.00014	0.00035	0.00108	0.00001

Table IV.11. Age determinations (Ma) of JR13 and standard values

Analysis	Pb207/Pb206	Pb206/U238	Pb207/U235	Pb208/Th232
GLASS1	5072.4	1813.1	4913.6	
GLASS2	5080.6	1764.5	4840.9	
JR13-1	569.7	647.8	628.4	581.2
JR13-2	640	661.2	654.1	610.5
JR13-3	815.7	659.9	681.2	664.8
JR13-4	1338.1	589.5	751.6	953.7
JR13-5	1013.5	611.4	697.4	776.1
JR13-6	570.4	651.1	632.3	584.7
JR13-7	675.1	632.1	641.7	607.8
JR13-8	552	658	638.5	639.1
JR13-9	611.5	645.5	638.3	658.2
JR13-10	632.3	641.1	640.7	667
JR13-11	753.8	614.5	643.5	616.6
JR13-12	839.5	619.8	668.2	630.2
JR13-13	638.2	619.5	622.7	515.5
JR13-14	575.5	623.9	613.3	527.1
JR13-15	719.9	551.4	584.5	526.5
JR13-16	751.4	539.2	581.5	488
JR13-17	651.5	636.1	638	594.9
JR13-18	559.6	675.2	647.9	611.5
JR13-19	685.3	675.5	659	685.6
JR13-20	1076.7	602.5	710.8	2082
JR13-21	1406.3	434.9	630	474.7
JR13-22	613.3	645.2	638.6	587.6
JR13-23	1236.5	615.2	767.4	550.2
JR13-24	1029.6	397.5	508	321.2
JR13-25	580.3	657.9	642.6	587.4
JR13-26	1862.6	667.8	1002.1	1825.4
STDCZ1	349.7	338	339.6	346.1
STDCZ2	338.6	336.1	337	337.7
STDCZ3	340.3	338.1	337.6	347.4

Table IV.12. Isotopic ratio of one sigma uncertainty of age estimate (Ma) of JR13 and standards values

Analysis	Pb207/Pb206	Pb206/U238	Pb207/U235	Pb208/Th232
GLASS1	15.42	11.86	46.3	61.71
GLASS2	15.38	11.51	45.49	62.58
JR13-1	23.17	4.2	20.04	3.86
JR13-2	22.37	4.28	20.63	4.05
JR13-3	29.65	4.58	21.85	6.22
JR13-4	24.46	4.03	23.09	7.78
JR13-5	35.49	4.6	22.91	9.97
JR13-6	22.91	4.22	20.13	3.87
JR13-7	22.3	4.1	20.35	4.05
JR13-8	22.6	4.26	20.27	4.22
JR13-9	22.68	4.19	20.28	4.43
JR13-10	22.4	4.16	20.32	4.44
JR13-11	21.99	3.99	20.39	4.11
JR13-12	28.41	4.27	21.46	5.43
JR13-13	22.39	4.03	19.91	3.44
JR13-14	22.66	4.05	19.69	3.52
JR13-15	21.91	3.6	19	3.47
JR13-16	21.87	3.52	18.93	3.23
JR13-17	23.09	4.15	20.31	4.06
JR13-18	22.7	4.37	20.49	4.1
JR13-19	35.09	4.87	21.78	7.87
JR13-20	20.76	3.92	21.86	13.5
JR13-21	21.36	2.92	20.18	3.37
JR13-22	22.79	4.19	20.29	3.97
JR13-23	20.95	4.02	23.08	3.76
JR13-24	21.46	2.64	17.12	2.16
JR13-25	22.44	4.26	20.36	3.86
JR13-26	20.8	4.47	27.48	13.36
STDCZ1	24.46	2.26	12.38	2.71
STDCZ2	24.84	2.25	12.31	2.77
STDCZ3	24.9	2.26	12.33	2.85

Table IV.13. Isotopic ratio of JZ6 and standard values

Analysis	Pb207/Pb206	Pb206/U238	Pb207/U235	Pb208/Th232	Pb208/Pb206	Th232/U238	U238/Si29
GLASS1	0.82987	0.29728	105.40056	0.59151	1.40199	0.68549	0.00009
GLASS2	0.82208	0.29381	96.58147	0.57299	1.39583	0.69632	0.00009
JZ6-1	0.05694	0.08372	0.65829	0.02036	0.11326	0.45317	0.01417
JZ6-2	0.08084	0.10289	1.12998	0.02731	2.36633	8.67277	0.00029
JZ6-3	0.09175	0.09906	1.23043	0.01806	3.07525	16.41532	0.0007
JZ6-4	0.7264	1.14861	109.73186	0.47166	1.28366	3.04123	0.00002
JZ6-5	0.0558	0.09611	0.74016	0.02394	0.08757	0.34205	0.01158
JZ6-6	0.05765	0.09759	0.78258	0.02384	0.63321	2.52194	0.00433
JZ6-7	0.05812	0.09962	0.80318	0.01899	0.67812	3.46119	0.00399
JZ6-8	0.05618	0.08983	0.69772	0.02211	0.09181	0.36288	0.01265
JZ6-9	0.06331	0.09945	0.85601	0.02291	5.87471	24.81453	0.00048
JZ6-10	0.05799	0.09289	0.74595	0.02085	0.1228	0.5323	0.00883
JZ6-11	0.16829	0.09857	2.22918	0.07941	0.28881	0.34877	5.40109
JZ6-12	0.05508	0.07505	0.57093	0.01302	0.01235	0.06926	0.0168
JZ6-13	0.06873	0.06431	0.61334	0.01615	0.12158	0.47093	0.01828
JZ6-14	0.0956	0.10259	1.36649	0.02855	0.392	1.3702	0.00116
JZ6-15	0.05536	0.09194	0.7025	0.02418	0.02703	0.09996	0.01052
JZ6-16	0.05574	0.07049	0.54261	0.0151	0.02112	0.09594	0.01516
JZ6-17	0.06855	0.09393	0.87925	0.01616	0.64104	3.62544	0.00252
JZ6-18	0.05652	0.08742	0.68522	0.01968	0.14029	0.60625	0.00547
JZ6-19	0.05517	0.09437	0.71934	0.0225	0.09772	0.39873	0.00918
JZ6-20	0.0667	0.09593	0.88287	0.02586	0.12353	0.44578	0.00593
JZ6-21	0.07254	0.10223	1.02963	0.03078	0.12554	0.40567	0.0012
STDCZ1	0.04872	0.05269	0.35675	0.01365	0.02396	0.08998	0.01107
STDCZ2	0.06036	0.05525	0.46023	0.02376	0.04882	0.11046	0.01238
STDCZ3	0.053	0.05328	0.38876	0.01674	0.03853	0.11933	0.01366

Table IV.14. Isotopic ratio of one sigma uncertainty of JZ6 and standards values

Analysis	Pb207/Pb206	Pb206/U238	Pb207/U235	Pb208/Th232	Pb208/Pb206	Th232/U238	U238/Si29
GLASS1	0.00842	0.00217	4.37309	0.00346	0.01065	0.00637	
GLASS2	0.00842	0.00217	3.99463	0.00339	0.01071	0.0065	
JZ6-1	0.00055	0.00055	0.02524	0.00011	0.00079	0.00403	0.00001
JZ6-2	0.00163	0.00087	0.04853	0.00016	0.0211	0.07919	
JZ6-3	0.00139	0.00075	0.04977	0.0001	0.02438	0.14774	
JZ6-4	0.00781	0.01007	4.8767	0.00298	0.0104	0.03158	
JZ6-5	0.00053	0.00063	0.02837	0.00013	0.00061	0.00304	0.00001
JZ6-6	0.00059	0.00065	0.03013	0.00013	0.00444	0.02243	
JZ6-7	0.00058	0.00066	0.03089	0.0001	0.00473	0.03078	
JZ6-8	0.00054	0.00059	0.02675	0.00012	0.00064	0.00323	0.00001
JZ6-9	0.00117	0.00078	0.03587	0.00012	0.04745	0.22402	
JZ6-10	0.00056	0.00061	0.02861	0.00011	0.00086	0.00473	0.00001
JZ6-11	0.00158	0.00064	0.08533	0.00041	0.00199	0.0031	0.02704
JZ6-12	0.00053	0.00049	0.0219	0.00009	0.0001	0.00062	0.00001
JZ6-13	0.00066	0.00042	0.0235	0.00009	0.00085	0.00419	0.00001
JZ6-14	0.00118	0.00072	0.0537	0.00017	0.00312	0.01229	
JZ6-15	0.00053	0.0006	0.02694	0.00014	0.0002	0.00089	0.00001
JZ6-16	0.00054	0.00046	0.0208	0.00009	0.00016	0.00085	0.00001
JZ6-17	0.00077	0.00064	0.03416	0.00009	0.00465	0.03231	
JZ6-18	0.00056	0.00058	0.02633	0.00011	0.001	0.00539	
JZ6-19	0.00054	0.00062	0.02762	0.00012	0.0007	0.00355	0.00001
JZ6-20	0.00066	0.00063	0.03392	0.00014	0.00089	0.00397	0.00001
JZ6-21	0.00082	0.00069	0.04003	0.0002	0.00101	0.00364	
STDCZ1	0.00049	0.00035	0.01371	0.00009	0.00019	0.0008	0.00001
STDCZ2	0.0006	0.00036	0.01769	0.00015	0.00037	0.00099	0.00001
STDCZ3	0.00057	0.00036	0.01503	0.00012	0.00033	0.00107	0.00002

Table IV.15. Age determinations (Ma) of JZ6 and standards values

Analysis	Pb207/Pb206	Pb206/U238	Pb207/U235	Pb208/Th232
GLASS1	4973.9	1677.8	4739	9392.3
GLASS2	4960.5	1660.5	4651.2	9155.7
JZ6-1	488.4	518.3	513.6	407.3
JZ6-2	1217.5	631.3	767.7	544.6
JZ6-3	1462	608.9	814.5	361.7
JZ6-4	4783.9	4930.3	4779.5	7809.8
JZ6-5	444.1	591.6	562.5	478.1
JZ6-6	516.3	600.3	587	476.2
JZ6-7	533.8	612.2	598.6	380.2
JZ6-8	458.8	554.6	537.4	442.1
JZ6-9	718.7	611.2	627.9	457.8
JZ6-10	529.1	572.6	565.9	417
JZ6-11	2540.8	606	1190.3	1544.5
JZ6-12	415.5	466.5	458.6	261.5
JZ6-13	890.6	401.8	485.7	323.9
JZ6-14	1539.9	629.6	874.7	569.1
JZ6-15	426.4	567	540.3	483
JZ6-16	441.5	439.1	440.1	302.9
JZ6-17	885.1	578.8	640.6	324
JZ6-18	472.1	540.2	529.9	393.9
JZ6-19	419	581.3	550.3	449.7
JZ6-20	828.3	590.5	642.5	516.1
JZ6-21	1001.1	627.4	718.7	612.7
STDCZ1	134.4	331	309.8	274
STDCZ2	616.6	346.6	384.4	474.6
STDCZ3	328.8	334.6	333.5	335.5

Table IV.16. Isotopic ratio of one sigma uncertainity of age estimate (Ma) of JZ6` and standards values

Analysis	Pb207/Pb206	Pb206/U238	Pb207/U235	Pb208/Th232
GLASS1	14.34	10.78	41.73	43.92
GLASS2	14.48	10.79	41.57	43.51
JZ6-1	21.37	3.27	15.46	2.15
JZ6-2	39.16	5.11	23.13	3.13
JZ6-3	28.69	4.41	22.66	1.95
JZ6-4	15.32	30.21	44.72	40.9
JZ6-5	20.73	3.71	16.56	2.52
JZ6-6	21.81	3.79	17.16	2.47
JZ6-7	22.25	3.86	17.39	1.97
JZ6-8	21.21	3.49	16	2.33
JZ6-9	38.8	4.57	19.62	2.42
JZ6-10	21.43	3.6	16.64	2.2
JZ6-11	15.66	3.78	26.83	7.69
JZ6-12	21.27	2.96	14.15	1.77
JZ6-13	19.56	2.55	14.79	1.69
JZ6-14	23.03	4.23	23.04	3.43
JZ6-15	21.29	3.56	16.07	2.78
JZ6-16	20.78	2.79	13.69	1.77
JZ6-17	23.08	3.75	18.45	1.75
JZ6-18	21.92	3.42	15.86	2.12
JZ6-19	21.57	3.66	16.31	2.43
JZ6-20	20.51	3.72	18.29	2.81
JZ6-21	22.76	4.06	20.03	3.93
STDCZ1	23.37	2.13	10.26	1.8
STDCZ2	21.48	2.23	12.3	2.86
STDCZ3	24.21	2.17	10.99	2.43

References:

ABDELSALAM, M.G. and STERN, R.J., 1996. Sutures and shear zones in the Arabian Shield. *Journal of African Earth Sciences*, **23**, 289-310.

ADAMS, C.J.; PANKHURST, R.J., MAAS, R. and MILLAR, I.L., 2005. Nd and Sr isotopic signatures of metasedimentary rocks around the South Pacific margin, and implications for their provenance. *Geological Society of London, Special Publication,* **246**, 113-142.

AGAR, R.A., 1986. Structural geology of felsic plutonic rocks in the Arabian Shield; styles, modes and levels of displacement. *Journal of African Earth Sciences,* **4**, 105-121.

ALDERTON, D. and MOORE, F., 1981. New determinations of tin and tungsten in granites from south-west England. *Mineralogical Magazine*, **44**, 354-356.

ALI, B.H., WILDE, S.A. and GABR, M.M.A., 2009. Granitoid evolution in Sinai, Egypt, based on precise SHRIMP U–Pb zircon geochronology. *Gondwana Research,* **15**(1), 38-48.

ALKANE RESOURCES LTD., 2012. The Dubbo Zirconia Project. An advanced strategic and alternate supply for the zirconium, niobium and rare earths industries, Australian Uranium and Rare Earth Conference. Available from: www.alkane.com.au/presentations/pdf/20120719.pdf

ALKANE RESOURCES LTD., 2012. The Dubbo Zirconia Project. Long term production of zirconium, hafnium, niobium, tantalum, yttrium and rare earths, Geological setting. Available from*:* www.alkane.com.au/projects/nsw/dubbo/DZP-Summary-March-10.pdf

AL-SHANTI, A.M.S, 1993. The Geology of the Arabian Shield. *Center for Scientific Publishing King Abdulaziz University*, Saudi Arabia. 192 p.

AL-SHANTI, A. M.S., 2003. The Geology of the Arabian Shield: General geology. *King Abdulaziz University Press*, 3-7. 204 p.

AL-SHANTI, A.M.S., ABDEL-MONEM, A.A. and MARZOUKI, F.H., 1984. Geochemistry, petrology and Rb-Sr dating of trondhjemite and granophyre associated with Jabal Tays Ophiolite, Idsas area, Saudi Arabia. *Precambrian Research,* **24**(3-4), 321-334.

AL TAYYAR, J., JACKSON, N.J. and AL-YAZIDI, S., 1986. Geology and mineralization of the Jabalat alkali-feldspar granite, northern Asir region, Kingdom of Saudi Arabia. *Journal of African Earth Sciences*, **4**, 183-188.

ARZAMASTSEV, A.A., BEA, F., ARZAMASTSEVA, L.V. and MONTERO, P., 2002. Rare earth elements in rocks and minerals from alkaline plutons of the Kola Peninsula, NW Russia, as indicators of alkaline magma evolution. *Russian Journal of Earth Sciences*, **4** (3), 187-209.

AUSTRALIAN MINES ATLAS., 2011.Niobium, resources. Available from: www.australianminesatlas.gov.au/aimr/commodity/niobium.html

AVALON RARE METALS INC., 2012. Metals for clean technology, NI 43-101 Resource Estimate. Available from: www.avalonraremetals.com/projects/thor_lake/ni_43-101/

AYDOĞAN, M.S., ÇOBAN, H., BOZCU, M. and AKINCI, Ö., 2008. Geochemical and mantle-like isotopic (Nd, Sr) composition of the Baklan Granite from the Muratdağı Region (Banaz, Uşak), western Turkey: Implications for input of juvenile magmas in the source domains of western Anatolia Eocene–Miocene granites. *Journal of Asian Earth Sciences,* **33**(3-4), 155-176.

BARBARIN, B., 2005. Mafic magmatic enclaves and mafic rocks associated with some granitoids of the central Sierra Nevada batholith, California: nature, origin, and relations with the hosts. *Lithos,* **80**(1-4), 155-177.

BARBARIN, B and STEPHENS, E. 2001. The Fourth Hutton Symposium on the Origin of Granites and Related Rocks. Alkali- calcic and alkaline post-orogenic granite

magmatism: petrologic constraints and geodynamic setting. *The Geological Society of America,* 319 p.

BARTON, M.D. and JOHNSON, D.A., 1996. Evaporitic-source model for igneous-related Fe oxide–(REE-Cu-Au-U) mineralization. *Geology*, **24,** 259-262.

BATCHELOR, R. A., and BOWDEN, P., 1985, Petrogenetic interpretation of granitic rock series using multi-cationic parameters. *Chemical Geology*, **48**, 43-55.

BAXTER, S. and FEELY, M., 2002. Magma mixing and mingling textures in granitoids: examples from the Galway Granite, Connemara, Ireland. *Mineralogy and Petrology*, **76**, 63-74.

BEA, F. 1996.Residence of REE, Y, Th and U in Granites and Crustal Protoliths; Implications for the Chemistry of Crustal Melts. *Journal of Petrology*, **37** (3), 521-552.

BE`ERI-SHLEVIN, Y., KATZIR, Y. and WHITEHOUSE, M., 2009. Post-collisional tectonomagmatic evolution in the northern Arabian–Nubian Shield: time constraints from ion-probe U–Pb dating of zircon. *Journal of the Geological Society,* **166** (1), 71-85.

BI, X., CORNELL, D.H. and HU, R., 2002. REE composition of primary and altered feldspar from the mineralized alteration zone of alkaline intrusive rocks, western Yunnan Province, China. *Ore Geology Reviews*, **19**(1-2), 69-78.

BOKHARI, M. M., JACKSON, N. J and AL-OWEIDI, K., 1986. Geology and mineralization of the Jabal Umm Al Suqian albitized apogranite, southern Najd region, Kingdom of Saudi Arabia. *Journal of African Earth Sciences,* **4**, 189-198.

BORTNIKOV, N.S., GORELIKOVA, N.V. and KOROSTELEV, P.G., 2007. REE behavior in tin-bearing hydrothermal-magmatic systems: An example of deposits of the Far East. *Doklady Earth Sciences*, **415** (2), 950-953

BRITISH GEOLOGICAL SURVEY., 2011. Rare Earth Elements Profile. Major deposits classes. Available from*:* www.bgs.ac.uk/downloads/start.cfm?id=1638.

BROSKA, I., HARLOV, D., TROPPER, P. and SIMAN, P., 2007. Formation of magmatic titanite and titanite-ilmenite phase relations during granite alteration in the Tribec Mountains, Western Carpathians, Slovakia. *Lithos*, **95** (1-2), 58-71.

BROWN, W. L., 1984. Feldspars and Feldspathoids. Structures, properties and occurrences. Series C, mathematical and physical science: exsolution and coarsening. *Springer,* **137,** 328-360

BROWN, G.F. and JACKSON, R.O., 1960. The Arabian Shield. International Geological congress, 21st, Copenhagen, *Proceedings*, pt. 9: 69-77.

BUDDINGTON, A.F., FAHEY, J., and VLISIDIS, A., 1963. Degree of Oxidation of Adirondack Iron Oxide and Iron-Titanium Oxide Minerals in Relation to Petrogeny. *Journal of Petrology*, **4** (1), 69-138.

CALVEZ, J.Y., ALSAC, C., DELFOUR, J., KEMP, J. and PELATON, C., 1982. Geological evolution of western, central and eastern parts of the northern Precambrian Shield, Kingdom of Saudi Arabia. *Precambrian Research,* **16** (4), 48.

CAMP, V.E., 1984. Island arcs and their role in the evolution of the western Arabian Shield. *the Geological Society of America Bulletin*, **95**, 913-921.

CASTOR, S.B., 2008. The Mountain Pass rare-earth carbonatite and associated ultrapotassic rocks, California. *Canadian Mineralogist*, **46**, 779-806.

CASTOR, S.B and HEDRICK, J.B., 2006. Rare earth elements, in KOGEL, J.E., TRIVEDI, N.C., BARKER, J.M., and KRUKOWSKI, S.T., Industrial minerals and rocks: Commodities, markets, and uses. *Society for Mining, Metallurgy, and Exploration,* (7th edition), 769-792.

CASTOR, S.B., and NASON, G.W., 2004. Mountain Pass rare earth deposit, California, in CASTOR, S.B., PAPKE, K.G., and MEEUWIG, R.O., Betting on industrial minerals, Proceedings of the 39th Forum on the Geology of Industrial Minerals. *Nevada Bureau of Mines and Geology*, Special Publication, **33**, p. 68–81.

CHANG, L.L.Y, HOWIE, R.A and ZUSSMAN, J., 1995. Rock-forming minerals: Non-silicates: Sulphates, Carbonates, Phosphates, Halides. *Geological Society*, **5**b (2nd edition), 382 p.

CHAPPELL, B.W. and WHITE, A.J.R., 1974. Two contrasting granite types. *Pacific Geology*, **8**, 173-174.

CHAROY, B. & RAIMBAULT, L., 1994. Zr-, Th-, and REE-rich biotite differentiates in the A-type granite pluton of Suzhou (eastern China): the key role of fluorine, *Journal of Petrology*. **35** (4), 919-962.

CLARK, M.D., 1986. Explanatory notes to the geologic map of the Al Bad quadrangle, sheet 28A, Kingdom of Saudi Arabia. *Saudi Arabian Directory for Mineral Resources*, Geologic Map GM-81, scale 1:250,000, 46 p.

CLEMENS, J. and BEA, F., 2012. Landmark Papers: Granite Petrogenesis. *The Mineralogical Society*, No.4, p.343.

CONRAD, W., NICHOLLS, I and WALL, V., 1988. Water-Saturated and –Undersaturated Melting of Metaluminous and Peraluminous Crustal Compositions at 10 kb: Evidence for the Origin of Silicic Magmas in the Taupo Volcanic Zone, New Zealand, and other Occurrences. *Journal of Petrology*, **29** (4), 765-803.

COOPER, J.A., STACEY, J.S., STOESER, D.C. and FLECK, R.J., 1979. An evaluation of the zircon methods of isotopic dating in the southern Arabian craton. *Contributions to Mineralogy and Petrology*, **86**, 429-439.

COX, K.G., BELL, J.D. and PANKHURST, R.J., 1979. The interpretation of igneous rocks. *Allen and Unwin*, 464 p.

CRAIG, J. R. and VAUGHAN, D. J, 1981. Ore Microscopy and Ore Petrography. *Wiley and Sons*. 406 p.

DAVIES, F.B., 1980. Reconnaissance geology of the Duba quadrangle, sheet 27/35D, Kingdom of Saudi Arabia. *Saudi Arabian Deputy Ministry for Mineral Resources,* Geologic Map GM-57, scale 1:100,000. 30p.

DAVIES, F.B., 1982. Pan-African granite intrusion in response to tectonic volume changes in a ductile shear zone from northern Saudi Arabia. *Journal of Geology,* **90**, 467–484.

DAVIES, F.B., 1983. Geology of the Al Wajh quadrangle, sheet 26B, Kingdom of Saudi Arabia. *Saudi Arabian Deputy Ministry for Mineral Resources,* Open-File Report DGMR-OF-03-8. 81p.

DAVIES, F.B. and GRAINGER, D.J., 1983. Explanatory notes to the geological map of the Al Muwaylih quadrangle, sheet 27A, Dabbagh complex. *Saudi Arabian Deputy Ministry for Mineral Resources,* scale 1:250,000. 61 p.

DAVIES, F.B., and GRAINGER, D.J., 1985. Explanatory notes to the geologic map of the Al Muwaylih quadrangle, sheet 27A, Kingdom of Saudi Arabia. *Saudi Arabian Deputy Ministry for Mineral Resources,* Geological Map GM-82, scale 1:250,000, 32 p.

DEER, W., ZUSSMAN, J. and HOWIE, R., 2001. Rock-forming Minerals: Framework silicates, feldspars: Alkali feldspars are present in the granite, monzodiorite and diorites of the Ballachulish igneous complex. *The Geological Society,* 4A (2nd Edition), 972p.

DE LA ROCHE, H., LETERRIER, J., GRANDCLAUDE, P., and MARCHAL, M., 1980. A classification of volcanic and plutonic rocks using R1-R2 diagram and major element analyses- Its relationships with current nomenclature. *Chemical Geology*, **29**, 183-210.

DELFOUR, J., 1979. Geology of the Halaban quadrangle, sheet 23G, Kingdom of Saudi Arabia. *Saudi Arabian Directorate of Mineral Resources,* Geologic Map GM-46-A, Scale 1:250 000.

DELFOUR, J., 1981. Geologic, tectonic and metallogenic evolution of the northern part of the Precambrian Arabian Shield. *Bulletin du Bureau de Researches et Minieres* (1-2) Section II, 1980-1981, 1-19.

DELFOUR, J., 1983. Geology and mineral resources of the northern Arabian Shield. *BRGM Technical Record*, BRGM-TR-03-1.

DEMPSTER, T.J., JENKIN, G.T., and ROGERS, G., 1994. The Origin of Rapakivi Texture. *Journal of Petrology*, **35** (4), 963-981.

DOUCH, C.J., 1986. Ratamah specialized granite, Midyan region, Kingdom of Saudi Arabia; rock types, geochemistry and rare-metal distribution. *Journal of African Earth Sciences*, **4**, 177-182.

DOUCE, P.A.E., 1999. What do experiments tell us about the relative contributions of crust and mantle to the origin of granitic magmas? In: Understanding granites. *Geological Society Special Publications*, **158**, 55-75.

DRYSDALL, A.R., 1980. Geology and mineral potential of the granites of N.W. Hijaz, interim report No.1. *Saudi Arabian Deputy Ministry for Petroleum and Mineral Resources*, Open-File Report DGMR-722.

DRYSDALL, A.R. and DOUCH, C.J., 1986. Nb-Th-Zr mineralization in microgranite—microsyenite at Jabal Tawlah, Midyan region, Kingdom of Saudi Arabia. *Journal of African Earth Sciences*, **4**, 275-288.

DRYSDALL, A.R., JACKSON, N.J., RAMSAY, C.R., DOUCH, C.J. and HACKETT, D., 1984. Rare Element Mineralization Related to Precambrian Alkali Granites in the Arabian Shield. *Economic Geology*, **79**, 1366-1377.

DRYSDALL, A.R., and ODELL, J., 1982. Geochemical discrimination of the granitoids of Midyan, northwest Hijaz, Saudi Arabia. *Saudi Arabian Ministry for Petroleum and Mineral Resource*, 69-76.

DRYSDALL, A.R. and RAMSAY, C.R., 1986. Introduction. *Journal of African Earth Sciences*. **4**, 1-9.

DRYSDALL, A.R., RAMSEY, CR. and STOESER, D.B., 1986. Felsic plutonic rocks and associated mineralization of the Kingdom of Saudi Arabia. *Journal of African Earth Sciences*, **4**, 291 p.

Du BARY, E.A., 1986. Jabal Silsilah tin prospect, Najd region, Kingdom of Saudi Arabia. *Journal of African Earth Sciences*, **4**, 237-247.

Du BRAY, E.A., 1986. Specialized granitoids in the southeastern Arabian Shield - case history of a regional assessment. *Journal of African Earth Sciences*, **4**, 169-176.

DUYVERMAN, H.J., 1984. Late Precambrian granitic and volcanic rocks and their relation to cratonization of the Arabian Shield. *Faculty of Earth Sciences Bulletin* 4, 50-96.

DUYVERMAN, H.J., HARRIS, N.B.W. and HAWKESWORTH, C.J., 1982. Crustal accretion in the Pan African: Nd and Sr isotope evidence from the Arabian Shield. *Earth and Planetary Science Letters*, **59**(2), 315-326.

EBADI, A. and JOHANNES, W., 1991. Beginning of melting and composition of first melts in the system Qz-Ab-Or-H_2O-CO_2. *Contribution to Mineral Petrology*, **106**, 286-295.

EBY, G.N., 1992. Chemical subdivision of the A-type granitoids: Petrogenetic and tectonic implications. *Geology*, **20**, 641-644.

ELLIOTT, J.E., AL-YAZIDI, S., AL-EISSA, A., AL-SHAMMERI, A., HASHEM, H.I. and TARABULSI, Y. Exploration of the Ghurayyah Radioactive Granite, Kingdom of Saudi Arabia, *Saudi Geological Survey*, Open-File Report, SGS-OF-2001-7.

ESFAHANI, M.M., KHALILI, M., KOCHHAṘ., N. and GUPTA, L.N., 2010. A-type granite of the Hassan Robat area (NW of Isfahan, Iran) and its tectonic significance. *Journal of Asian Earth Sciences*, **37** (3), 207-218.

FAURE, G. and POWELL, J.L., 1972. Strontium Isotope Geology. *Springer-Verlag*, 188 p.

FEELY, M., SELBY, D., HUNT, J. and CONLIFFE, J., 2010. Long-lived granite-related molybdenite mineralization at Connemara, western Irish Caledonides. *Geological Magazine*, 886-894.

FITTON, J.G. and UPTON, B.G.J., 1987. Alkaline igneous rocks, alkaline rocks and their inclusions: a window on the Earths interior. *Geological Society Special Publication,* **30**, 15-27.

FLECK, R.J., GREENWOOD, W.R., HADLEY, D.G., ANDERSON, R.E., and SCHMIDT, D.L., 1979. Rubidium-strontium geochronology and plate tectonics of the southern part of the Arabian Shield. *U.S.G.S.*, Saudi Arabian Project Report 245.

FROST, C.D., 2001. A geochemical classification of granitic rocks. *Journal of Petrology*, **42**, 2033-2048.

FROST, B.R., BARNES, C.G., COLLINS, W.L., ARCULUS, R.J., ELLIS, D. and FROST, C.D., 2001. A geochemical classification for granitic rocks. *Journal of petrology*, **42** (11), 2033-2048.

FROST, B.R., CHAMBERLAIN, K.R. and SCHUMACHER, J.C., 2001. Sphene (titanite): phase relations and role as geochronometer. *Chemical Geology*, **172** (1-2), 131-148.

FROST, C.D. and FROST, B.R., 1997. Reduced rapakivi-type granites: the tholeiite connection. *Geology*, **25**, 647-650.

FROST, C.D. and FROST, B.R., 2010. On Ferroan (A-type) Granitoids: their Compositional Variability and Modes of Origin. *Journal of Petrology,* 1-15.

FROST, B. R. and LINDSLEY, D. H., 1991. Occurrence of iron–titanium oxides in igneous rocks. Oxide Minerals: Petrologic and Magnetic Significance. *Reviews in Mineralogy,* **25**, 433–486.

GASS, I.G., 1981. Chapter 15 Pan-African (Upper Proterozoic) plate Tectonics of the Arabian—Nubian Shield. In: A. KRÖNER. *Developments in Precambrian Geology*, 387-405.

GENNA, A., NEHLIG, P., LE GOFF, E., GUERROT, C. and SHANTI, M., 2002. Proterozoic tectonism of the Arabian Shield. *Precambrian Research,* **117**(1-2), 21-40.

GRAINGER, D.J., and HANIF, M.R., 1989. Explanatory notes to the geologic map of the Shaghab quadrangle, sheet 27B, Kingdom of Saudi Arabia. *Saudi Arabian Directory for Mineral Resources*, Geological Map GM-109, scale 1:250,000, 31 p.

GREENWOOD, W.R., ANDERSON, R.E., FLECK, R.J. and ROBERT, R.J., 1980. Precambrian geologic history and plate tectonic evolution of the Arabian Shield. *Saudi Arabian Directorate of Mineral Resources Bulletin* 24, 35p.

GREENWOOD, W.R., HADLEY, D.G., ANDERSON, R.E., FLECK, R.J. and SCHMIDT, D.L., 1976. Late Proterozoic cratonization in the southwestern Saudi Arabia. *Proterozoic Transactions of the Royal Society of London*, A.280: 517-527.

GROMET, L.P., SILVER, L.T., 1983. Rare earth element distributions among minerals in a granodiorite and their petrogenetic implications. *Geochimica et Cosmochimica Acta*, **47**, 925-940.

GUILLOT, S., LE FORT, P., PECHER, M., BARMAN, R., and APRAHAMIAN, J., 1994. Contact metamorphism and depth of emplacement of the Manaslu granite (central Nepal): Implications for Himalayan orogenesis. *Tectonophysics*, **241**, 99-119.

HACKETT, D., 1986. Mineralized aplite-pegmatite at Jabal Sa`id, Hijaz region, Kingdom of Saudi Arabia. *Journal of African Earth Sciences,* **4**, 257-267.

HALDEN, N.M., MANDZIUK, W.S., YOUNG, J., CLARK, G.S. and YANG, P., 2007. LAM-ICP-MS zircon dating of the Falcon Lake Intrusive Complex and Caddy Lake granite, southeastern Manitoba, Canada. *Proceedings of the Geologists' Association,* **118**(1), 25-35.

HALLIDAY, A.N., STEPHENS, W.E. and HARMON, R.S., 1980. Rb-Sr and O isotopic relationships in 3 zoned Caledonian granitic plutons, Southern Highlands, Scotland: evidence for varied sources and hybridization of magma. *Journal of the Geological Society*, **137,** 329-348.

HAMIDULLAH, S. and BOWES, D., 1986. Calcium Amphibole From Igneous Rocks: Mineralogical pressure indicators. *Geological Bulletin*, **19**, 13-29.

HAMMARSTROM, J.M. and ZEN, E.A., 1986. Aluminium in hornblende: An empirical igneous geobarometer, *American Mineralogist*, **71**, 1297-1313.

HARBEN, P.W. and KUZVART. M.,1996. Industrial Minerals: A Global Geology. *Metal Bulletin Books Ltd*. 462 p.

HARLEY, S.L. and KELLY, N.M., 2007. Zircon: Tiny but timely. *Elements.*, **3**, 13-18.

HARLOV, D.E., PROCHAZKA, V., FORSTER, H. and MATEJKA, D., 2008. Origin of monazite-xenotime-zircon-fluorapatite assemblages in the peraluminous Melechov granite massif, Czech Republic. *Mineralogy and Petrology*, **94** (1-2), 9-26.

HARRIS, N. B. W., 1981. The role of fluorine and chlorine in the petrogenesis of a peralkaline complex from Saudi Arabia. *Chemical Geology*, **31,** 303-310.

HARRIS, N.B.W., 1985. Alkaline complexes from the Arabian Shield. *Journal of African Earth Sciences,* **3**(1-2), 83-88.

HARRIS, N.B.W. and MARRINER, G.F., 1980. Geochemistry and petrogenesis of a peralkaline granite complex from the Midian Mountains, Saudi Arabia. *Lithos,* **13**(4) 325-337.

HARRIS, N.B.W., PEARCE, J.A. and TINDLE, A.G., 1986. Geochemical characteristics of collision-zone magmatism. *Geological Society,* Special Publications, **19**(1), 67-81.

HASSANEN, M. A., 1997. Post-collision, A-type granites of Homrit Waggat Complex, Egypt: petrological and geochemical constraints on its origin. *Precambrian Research,* **82**(3-4), 211-236.

HASSANEN, M.A. and HARRAZ, H.Z., 1996. Geochemistry and Sr- and Nd-isotopic study on rare-metal-bearing granitic rocks, central Eastern Desert, Egypt. *Precambrian Research,* **80**(1-2), 1-22.

HAWTHORNE, F.C. and OBERTI, R., 2007. Classification of the amphiboles. *Mineralogy and Geochemistry,* **67**(1), 55-88.

HELVACI, C., and GRIFFIN, W.L., 1984. Rb-Sr geochronology of the Bitlis Massif, Avnik (Bingol) area, S.E. Turkey, *in*, Dixon, J.E., and Robertson, A.H.F., The Geological Evolution of the Eastern Mediterranean. *Blackwell Scientific Publication,* 403 – 414.

HENRIQUEZ, F. and MARTIN, R., 1978. Crystal-Growth Textures in Magnetite Flows and Feeder Dykes, El Laco, Chile. *Canadian Mineralogist*, **16**, 581-589.

HERVE, F., PANKHURST, R., DEMANT, A. and RAMIRREZ, E., 1996. Age and Al-in-hornblende geobarometry in the north Patagonian Batholith, Aysen, Chile. *Third ISAG, St Malo (France)*, 579-582.

HIMMELBERG, G.R., 1977. Iron-titanium oxides of the Dufek intrusion, Antarctica. *American Mineralogist*, **62**, 623-633.

HOFMANN, A.W., 1988. Chemical differentiation of the Earth: the relationship between mantle, continental crust and oceanic crust. *Earth Planet Science Letters,* **90**, 297-314.

HUMPHRIES, M., 2010. Rare earth elements: The global supply chain. Available from: http://www.fas.org/sgp/crs/natsec/R41347.pdf

Info mine research group. Upper case? 2008. Union of Independent Experts in the Field of Mineral Resources, Metallurgy and Chemical Industry. Zirconium Resources Market Research in the CIS. Available from: www.infomine.ru/otchets/en_zrraw-en.pdf .

JACKSON, N.J., 1986. Mineralization associated with felsic plutonic rocks in the Arabian Shield. *Journal of African Earth Sciences,* **4**, 213-227.

JACKSON, N.J., 1986. Petrogenesis and evolution of Arabian felsic plutonic rocks. *Journal of African Earth Sciences,* **4**, 47-59.

JACKSON, N. J. and DOUCH, C. J., 1986. Jabal Hamra REE-mineralized silexite, Hijaz region, Kingdom of Saudi Arabia. *Journal of African Earth Sciences,* **4**, 269-274.

JACKSON, N.J. and RAMSAY, C.R., 1980. Time-space relationships of Upper Precambrian volcanic and sedimentary units in the central Arabian Shield. *Journal of the Geological Society of London,* **137**, 617-628.

JACKSON, N.J., WALSH, J.N. and PEGRAM, E., 1984. Geology, geochemistry and petrogenesis of late Precambrian granitoids in the Central Hijaz Region of the Arabian Shield. *Contributions to Mineralogy and Petrology,* **87**(3), 205-219.

JANARDHAN, A. S., NEWTON, R. C., and HANSEN, E. C., 1982.The transformation of amphibolite facies gneiss to charnockite in southern Karnataka and northern Tamil Nadu, India. *Contributions to Mineralogy and Petrology*, **79** (2), 130-14.

JANOTS, E., ENGI, M., RUBATTO, D., BERGER, A., GREGORY, C. and RAHN, M., 2009. Metamorphic rates in collisional orogeny from in situ allanite and monazite dating. *Geology*,. **37** (1), 11-14.

JOHANNES, W and HOLTZ, F., 1990**.** Formation and composition of H2O-undersaturated granitic melts. High temperature metamorphism and crustal anatexis. *Unwin Hyman*, 87-104.

JOHNSON, P.R., 1983. A preliminary lithofacies map of the Saudi Arabian Shield, an interpretation of the lithofacies and lithostratigraphy of the late Proterozoic layered

rocks of Saudi Arabia. Scale 1:1000,000, in two sheets, kingdom of Saudi Arabia. . *Saudi Arabian Directorate of Mineral Resources*, Technical Record, RF-TR-03-2.

JOHNSON, P.R., 2003. Post-amalgamation basins of the NE Arabian shield and implications for Neoproterozoic III tectonism in the northern East African orogen. *Precambrian Research*, **123**(2-4), 321-337.

JOHNSON, P.R., 2006. Explanatory notes to the map of Proterozoic geology of western Saudi Arabia. *Saudi Geological Survey,* Technical Report SGS-TR-2006-4, 62 p.

JOHNSON, M. C., and RUTHERFORD, M. J., 1989. Experimental calibration of the aluminum-in-hornblende geobarometer with application to Long Valley caldera (California), *Geology*, **17**, 837–841.

JONES, A.P., WALL, F. and WILLIAMS, C.T., 1996. Rare Earth Minerals: Chemistry, Origin and Ore Deposits. Mineralogical Society, Series 7, *Chapman and Hall.* 384p.

JUNG, S., MEZGER, K. and HOERNES, S., 1998. Petrology and geochemistry of syn- to post-collisional metaluminous A-type granites—a major and trace element and Nd–Sr–Pb–O-isotope study from the Proterozoic Damara Belt, Namibia, *Lithos*, **45**(1-4), 147-175.

KARKKAINEN, N. and APPELQVIST, H., 1999. Genesis of a low-grade apatite-ilmenite-magnetite deposit in the Kauhajarvi gabbro, western Finland. *Mineralium Deposita*, **34**, 754-769.

KAWAKATSU, K., and YAMAGUCHI, Y., 1987. Successive zoning of amphiboles during progressive oxidation in the Daito-Yokota granitic complex, San-in belt, southwest Japan. *Geochimica et Cosmochimica Acta*, **51**, 535–540.

KEBEDE, T. and KOEBERL, C., 2003. Petrogenesis of A-type granitoids from the Wallagga area, western Ethiopia: constraints from mineralogy, bulk-rock chemistry, Nd and Sr isotopic compositions. *Precambrian Research,* **121**(1-2), 1-24.

KELLOGG, K.S. and SMITH, C.W., 1986. Geology and tin-greisen mineralization of the Akash granite, northern Arabian Shield. *Journal of African Earth Sciences,* **4**, 205-210.

KEMP, J., 1981. Geology of the Wadi Al`Ays quadrangle, sheet 25C, Kingdom of Saudi Arabia. *Saudi Arabian Deputy Ministry for Mineral Resources,* Geologic Map GM-53-A, scale 1:250,000, with text, 39 p.

KEMP, J., PELLATON, C. and CALVEZ, J. Y., 1980. Geochronological Investigations and geological history in the Precambrian of northwestern Saudi Arabia. *Saudi Arabian Deputy Ministry for Petroleum and Mineral Resources,* Open-File Report BRGM-OF-01-1.

KEMP, J., PELLETON, C. and CALVEZ, J.Y., 1982. Cycles in the chelagenic evolution of the Precambrian Shield in part of northwestern Saudi Arabia. *Saudi Arabia Deputy Ministry for Mineral Resources,* Professional Paper no. pp-1, 27-42.

KIM, C. and KIM, G., 1997. Petrogenesis of the early Tertiary A-type Namsan alkali granite in the Kyongsang Basin, Korea. *Geoscience Journal,* **1**(2), 99-107.

KINNAIRD, J.A., BOWDEN, P., IXER, R.A. and ODLING, N.W.A., 1985. Mineralogy, geochemistry and mineralization of the Ririwai complex, northern Nigeria. *Journal of African Earth Sciences,* **3**(1-2), 185-222.

KOKSAL, S., MOLLER, A., GONCUOGLU, M.C., FREI, D. and GERDES, A., 2012. Crustal homogenization revealed by U–Pb zircon ages and Hf isotope evidence from the Late Cretaceous granitoids of the Agaçören intrusive suite (Central Anatolia/Turkey). *Contributions to Mineralogy and Petrology,* **163** (4), 725-743.

KOVALENKO, V.I. and YARMOLYUK, V.V, KOZLOVSKY, A.M., KOVACH, V. P., SAL'NIKOVA, KOTOV, A. B. and VLADYKIN, N.V., 2007. Two Types of Magma Sources of Rare-Metal Alkali Granites. *Geology of Ore Deposits,* **49** (6), 442–466.

KRAUSKOPF, K., 1979. Introduction to geochemistry. *McGraw-Hill Book Company,* (2nd edition), 601p.

KRAUSKOPF, K., and BIRD, D.K., 1995. Introduction to geochemistry. *McGraw-Hill, Inc.,* (3rd edition), 633 p.

KÜSTER, D., 2009. Granitoid-hosted Ta mineralization in the Arabian–Nubian Shield: Ore deposit types, tectono-metallogenetic setting and petrogenetic framework. *Ore Geology Reviews,* **35**(1), 68-86.

KÜSTER, D. and HARMS, U., 1998. Post-collisional potassic granitoids from the southern and northwestern parts of the Late Neoproterozoic East African Orogen: a review. *Lithos,* **45**(1-4), 177-195.

LEAKE, B.E., 1978. Nomenclature of amphiboles. *Canadian Mineralogists*, **16**, 501–520.

LEAKE, B.E., WOOLLEY, A.R., ARPS, C.S., BIRCH, W.D., GILBERT, M.C., GRICE, J.D., HAWTHORNE, F.C., KATO, A., KISCH H.J., KRIVOVICHEV, V.G., LINTHOUT, K., LARIRD, J., MANDARINO, J.A., MARESCH, W.V., NICKEL, E.H., ROCK, N.S., SCHUMACHER, J.C., SMITH, D.C., STEPHENSON, N.N., UNGARETTI, L., WHITTAKER, E.W and GUO, Y., 1997. Nomenclature of amphiboles: Report of the subcommittee on amphiboles of the International Mineralogical Association, Commission on New Minerals and Mineral Names. *Canadian Mineralogists*, **35**, 219–246.

LEITE, R.J., JANASI, V A.,Creaser, R.A. and Heaman, L.M., 2007. The late-to postorogenic transition in the Apiaı´domain, SE Brazil Constraints from the petrogenesis of the Neoproterozoic Agudos Grandes Granite Batholith. *Journal of South American Earth Sciences*, **23**, 213–235.

Le MAITRE, R.W., BATEMAN, P., DUDEK, A., KELLER, J., LAMEYRE, J., LE BAS, M.J., SABINE, P.A., SCHMID, R., SORENSEN, H., STRECKEISEN, A., WOOLLEY, A.R., ZANETTIN, B., 1989. A Classification of Igneous Rocks and Glossary of Terms. *Blackwell*, 193p.

LEVIN, V. and Park, J., 2000. Shear zones in the Proterozoic lithosphere of the Arabian Shield and the nature of the Hales discontinuity. *Tectonophysics*, **323**, 131–148.

LIU, W., 2002. Fluid–rock interaction during subsolidus microtextural development of alkali granite as exemplified by the Saertielieke pluton, Ulungur of the northern Xinjiang, China. *Chemical Geology*, **182**(2-4), 473-482.

LIU, S., HU, R., GAO, S., FENG, C., QI, Y., WANG, T., FENG, G. and COULSON, I.M., 2008. U–Pb zircon age, geochemical and Sr–Nd–Pb–Hf isotopic constraints on age and origin of alkaline intrusions and associated mafic dikes from Sulu orogenic belt, Eastern China. *Lithos*, **106**(3-4), 365-379.

LOISELLE, M.C. and WONES, D.S., 1979. Characteristics and origin of anorogenic granites. *Geological Society of America Bulletin*, **11**, 468p.

MAALOE, S and WYLLIE, P.J., 1975. Water content of a granite magma deduced from the sequence of crystallization determined experimentally with water-undersaturated conditions. *Contributions to Mineralogy and Petrology*, **52**, 175-191.

MACKENZIE, D.E., BLACK, L.P. and SUN, S., 1988. Origin of alkali-feldspar granites: An example from the Poimena Granite, northeastern Tasmania, Australia. *Geochimica et Cosmochimica Acta*, **52**(10), 2507-2524.

MANIAR, P.D. and PICCOLI, P.M., 1989. Tectonic discrimination of granitoids. *Geological Society of America Bulletin*, **101**, 635-643.

MARKS, M., and MARKL, G., 2001. Fractionation and Assimilation Processes in the Alkaline Augite Syenite Unit of the Ilímaussaq Intrusion, South Greenland, as Deduced from Phase Equilibria. *Journal of Petrology*, **42** (10), 1947-1969.

MARTIN, R., 2007. Amphiboles in the Igneous Environment. *Reviews in Mineralogy and Geochemistry*, **67**, 323-358.

MENGEL, F and RIVERS, T., 1991. Decompression Reactions and P-T Conditions in High-grade Rocks, Northern Labrador: P-T-t Paths from Individual Samples and

Implications for Early Proterozoic Tectonic Evolution. *Journalof Petrology*. **32** (1), 139-167.

Minerals Announces Resource Estimates for Foxtrot Rare Earth Element Project., 2011 Available from: http://www.newswire.ca/en/story/898503/search-minerals-announces-resource-estimates-for-foxtrot-rare-earth-element-project

MITCHELL, R. H., 1990. A review of the compositional variation of amphiboles in alkaline plutonic complexes. *Lithos*, **26**, 135-156.

MITCIIELLI, R.H. and CHAKHMOURADIAN, A.R., 1996. Composition variation of Loparite from Helovozero Alkaline Complex, Russia. *Canadian Mineralogist*, **34**, 977-990.

MOGHAZI, A.M., HARBI, H.M. and ALI, K.A., 2011. Geochemistry of the Late Neoproterozoic Hadb adh Dayheen ring complex, Central Arabian Shield: Implications for the origin of rare-metal-bearing post-orogenic A-type granites. *Journal of Asian Earth Sciences,* **42** (6), 1324-1340.

MOHAMED, F.H. and EL-SAYED, M.M., 2008. Post-orogenic and anorogenic A-type fluorite-bearing granitoids, Eastern Desert, Egypt: Petrogenetic and geotectonic implications. *Chemie der Erde - Geochemistry,* **68**(4), 431-450.

MUCKE, A., 2003. Fayalite, pyroxene, amphibole, annite and their decay products in rnafic clots within the Younger Granites of Nigeria: Petrography, mineral chemistry and genetic implications. *Journal of African Earth Sciences*, **36**, 55-71.

MÜLLER, A., SELTMANN, R., HALLS, C., SIEBEL, W., DULSKI, P., JEFFRIES, T., SPRATT, J. and KRONZ, A., 2006. The magmatic evolution of the Land's End pluton, Cornwall, and associated pre-enrichment of metals. *Ore Geology Reviews,* **28**(3), 329-367.

NAGUDI, B., KOEBERL, C. and KURAT, G., 2003. Petrography and geochemistry of the Singo granite, Uganda, and implications for its origin. *Journal of African Earth Sciences,* **36**(1-2), 73-87.

NAKASHIMA, K., and IMAOKA, T., 1998. Niobian and zincian ilmenites in syenites from Cape Ashizuri, Southwest Japan. *Mineralogy and Petrology*, **63**, 1-17.

NALINI, H.A. Jr., BILAL, E. and CORREIA-NEVES, J.M., 2000. Syn-collisional peraluminous magmatism in the Rio Doce region: mineralogy, geochemistry and isotopic data of the Neoproterozoic Urucum Suite (Eastern Minas Gerais State, Brazil). *Brasilian Geosciences*. **30**, 120–125.

PEARCE, *J.A., 1996. Sources and settings of granitic rocks.* Episodes 19, 120-125.

PEARCE, J.A., BENDER, S.E., DE LONG, W.S.F., LOW, P.J., GUNER, Y., SAROGLU, F., YILMAZ, Y., MOORBATH, S and MITCHELL, J.G. 1990. Genesis of collision volcanism in Eastern Anatolia, Turkey. *Journal of Volcanology and Geothermal Research*, **44**, 189-229.

PEARCE, J.A., HARRIS, N.B.W. and TINDLE, A.G., 1984. Trace Element Discrimination Diagram for the Tectonic Interpretation of Granitic Rocks. *Journal of Petrology*, **25** (4), 956-983.

PE-PIPER, G., 2007. Relationship of amphibole composition to host-rock geochemistry: the A-type gabbro-graniteWentworth pluton, Cobequid shear zone, eastern Canada. *European Journal of Mineralogy*, **19**, 29–38.

PETRIK, I. and KONECNY, P., 2009. Metasomatic replacement of inherited metamorphic monazite in a biotite-garnet granite from the Nizke Tatry Mountains, Western Carpathians, Slovakia: Chemical dating and evidence for disequilibrium melting. *American Mineralogist*, **94** (7), 957-974.

PITCHER, W.S., 1982. Granite type and tectonic environment: Mountain Building Processes. *Academic Press*, 19-40.

POLLARD, P., 1995. A Special Issue Devoted to the Geology of Rare Metal Deposits, Geology of Rare Metal Deposits: An Introduction and Overview. *Economic Geology*, **90**, 489-494.

PONOMARENKO, A.N., VLADYKIN, N.V, KRYVDIK, S.G. and DUBYNA, A.V., 2011. Geochemistry and ore-bearing ability of alkaline rocks of the Ukrainian and the Aldan Shields, Abstracts of International conference. *N.P. Semenenko Institute of geochemistry, mineralogy and ore formation NAS of Ukraine.*

PRYER, L.L. and ROBIN, P.-.F., 1996. Differential stress control on the growth and orientation of flame perthite: A palaeostress-direction indicator. *Journal of Structural Geology,* **18**(9), 1151-1166.

PUTNIS, A. and McCONNELL, J.D.C., 1980. Principles of mineral behavior, Fig. 7.8. *Blackwell Scientific Publications*, 257 .

RADAIN, A. A. M., 1980. Petrogenesis of some peralkaline and non-peralkaline post-tectonic granites in the Arabian Shield, Kingdom of Saudi Arabia. *Faculty of Earth Sciences Research Series*, **16**, 195p.

RADAIN, A.A.M., ALI, S., O. NASSEEF, A. and A. ABDEL-MONEM, A., 1987. Rb-Sr geochronology and geochemistry of plutonic rocks from the Wadi Shuqub quadrangle, west-central Arabian Shield. *Journal of African Earth Sciences,* **6**(4), 553-568.

RADAIN, A.A.M., FYFE, W.S. and KERRICH, R., 1981. Origin of peralkaline granites of Saudi Arabia. *Contributions to Mineralogy and Petrology*, **78**, 358-366.

RAMEZANI, J., and TUCKER, R.D., 2003, The Saghand region, central Iran: U-Pb geochronology, petrogenesis and implications for Gondwana tectonics. *American Journal of Science,* **303**, 622–665.

RAMSAY, C.R., 1982. Geology and mineral resource potential of Pan-African granitoid rocks, northern Midyan region, Saudi Arabia. *Saudi Arabian Deputy Ministry for Petroleum and Mineral Resources,* Open-File Report DGMR-OF-02-11.

RAMSAY, C.R., 1983. Geology of the Rabigh quadrangle, sheet 22D, Kingdom of Saudi Arabia. *Saudi Arabian Deputy Ministry for Petroleum and Mineral Resources,* Open-File Report DGMR-OF-03-15.

RAMSAY, C.R., 1986. Specialized felsic plutonic rocks of the Arabian Shield and their precursors. *Journal of African Earth Sciences,* **4**, 153-168.

RAMSAY, C.R., JACKSON, N.J. and ROOBOL, M.J., 1979. Structural-lithological provinces in Saudi Arabian Shield geotravers. *Institution of Applied Geology Bulletin* 3, **1**: 63-84

RAMSAY, C.R., ODELL, J. and DRYSDALL, A.R., 1986. Felsic plutonic rocks of the Midyan region, Kingdom of Saudi Arabia—II. Pilot study in chemical classification of Arabian granitoids. *Journal of African Earth Sciences,* **4**, 79-85.

RAPELA, C.W., HEAMAN, L.M., and McNUTT, R.H., 1982, Rb-Sr geochronology of granitoid rocks from the Pampean Ranges, Argentina. *Journal of geology*, **90**, 574-582.

RARE ELEMENT RESOURCES LTD., 2012. Targeting rare earth elements and gold, *New releases.* Available from: www.rareelementresources.com/s/NewsReleases.asp?ReportID=499417&_Title=Rare-Element-Reports-38-Percent-Increase-of-M-I-Rare-Earth-Mineral-Resource

ROBB, L.J., FREEMAN, L.A. and ARMSTRONG, R.A., 2000. Nature and longevity of hydrothermal fluid flow and mineralisation in granites of the Bushveld Complex, South Africa. *Geological Society of America* Special Papers**, 350**, 269-281.

ROGERS, J. J. W., and GREENBERG, J. K., 1990. Late-orogenic, post-orogenic, and anorogenic granites: distinction by major element and trace element chemistry and possible origins. *Journal of Geology*, **98**, 291-309.

ROLLINSON, H., 1993. Using Geochemical Data: Evaluation, Presentation, Interpretation. *Wiley and Sons,* 352 p.

ROOBOL, M.J. and WHITE, D.L., 1986. Cauldron-subsidence structures and calderas above Arabian felsic plutons. *Journal of African Earth Sciences*, **4**, 123-134.

ROWAIHY, N.M., 1985. Geologic map of the Haql quadrangle, sheet 29A, Kingdom of Saudi Arabia. *Saudi Arabian Directory for Mineral Resources,* Geological Map GM-80, scale 1:250,000, 15 p.

RUIZ, C., FERNÁNDEZ-LEYVA, C. and LOCUTURA, J., 2008. Geochemistry, geochronology and mineralisation potential of the granites in the Central Iberian Zone: The Jalama batholith. *Chemie der Erde - Geochemistry,* **68**(4), 413-429.

RUMBLE, D. and FINNERTY, T., 1974. Devonian Grossularite-Spessartine Overgrowth on Ordovician Almandine from Eastern Vermont. *American Mineralogist*, **59**, 558-562.

SALEH, G.M., 2006. Geologic relationships and mineralization of peralkaline/alkaline granite-syenite of the Zargat Na' am ring complex, Southeastern Desert, Egypt. *Chinese Journal of Geochemistry,* **25 (2),** 97-111.

SALVI, S., FONTAN, F., MONCHOUX, P., WILLIAMS-JONES, A.E., and MOINE, B., 2000. Hydrothermal mobilization of high field strength elements in alkaline igneous systems: Evidence from the Tamazeght Complex, Morocco. *Economic Geology*, **95**, 559-576.

SALVI, S. and WILLIAM-JONES, A.E., 2006. Alteration, HFSE mineralization and hydrocarbon formation in peralkaline igneous system: Insights from the Strange Lake Pluton, Canada. *Lithos*, **91** (1-4), 19-34.

SASAKI, M., FUJIMOTO, K., SAWAKI, T., TSUKAMOTO, H., KATO, O., KOMATSU, R., DOI, N. and SASADA, M., 2003. Petrographic features of a high-temperature granite just newly solidified magma at the Kakkonda geothermal field, Japan. *Journal of Volcanology and Geothermal Research,* **121**(3-4), 247-269.

SATO, K., SANTOSH, M., TSUNOGAE, T., KON, Y., YAMAMOTO, S. and HIRATA, T., 2010. Laser ablation ICP mass spectrometry for zircon U–Pb

geochronology of ultrahigh-temperature gneisses and A-type granites from the Achankovil Suture Zone, southern India. *Journal of Geodynamics*, **50**(3-4), 286-299.

SAUDI GEOLOGICAL SURVEY, 2012.Geology: Arabian Shield. Available from: www.sgs.org.sa/English/Geology/Pages/ArabianShield.aspx

SAUDI GEOLOGICAL SURVEY, 2012. Geology: Sedimentary rocks. Available from: Available from:
www.sgs.org.sa/English/Geology/Phanerozoic/Pages/default.aspx

SAUDI GEOLOGICAL SURVEY, 2012.Geology: Tectonic and Structure. Available from*:* www.sgs.org.sa/English/Geology/Pages/TectonicStructure.aspx

SAUNDERS, C.M, and TUACH, J., 1989. Zr-Nb-Y-REE mineralization in the Cross Hills Plutonic Suite. *Geological Survey of Newfoundland*, report 894, 181-192.

SCHARER, U. and ALLERGRE, C.J., 1983. The Palung granite (Himalaya); high-resolution U-Pb systematics in zircon and monazite. *Earth and Planetary Science Letters*, **63** (3), 423-432.

SCHMIDBERGER, S.S and HEGNER, E., 1999. Geochemistry and isotope systematics of calc-alkaline volcanic rocks from the Saar-Nahe basin (SW Germany)-implication for Late-Variscan orogenic development. *Contribution to Mineral Petrology*, **135**, 373-385.

SCHMIDT, D.L., HADLEY, D.G., GREENWOOD, W.R., GONZALEZ, LOUIS, COELMAN, R.J. and BROWN, G.F., 1973. Stratigraphy and tectonism of the southern part of the Precambrian Shield of Saudi Arabia. *Saudi Arabian Directorate General of Mineral Resources Bulletin*, **8**, 13p.

SCHMIDT, D.L., HADLEY, D.G. and STOESER, D.B., 1979. Late Proterozoic crustal history of the Arabian Shield, southern Najd province, Kingdom of Saudi Arabia, in Evolution and Mineralization of the Arabian-Nubian Shield, King Abdulaziz University. *Institute of Applied Geology Bulletin*, **3**, 2: Pergamon Press, 41-58.

SHEARD, E.R., WILLIAM-JONES, A.E., HEILIGMANN, M., PEDERSON, C. and TRUEMAN, D.L., 2012.Controls on the Concentration of Zirconium, Niobium, and the Rare Earth Elements in the Thor Lake Rare Metal Deposit, Northwest Territories, Canada. *Economic Geology*, **107** (1), 81-104.

SLAMA, J., KOSLER, J., CONDON, D., CROWLEY, J.L., GERDES, A., HANCHAR, J.M., HORSTWOOD, M.S.A., MORRIS, G.A., NASDALA, L., NORBERG, N., SCHALTEGGER, U., SCHOENE, B., TUBRETT, M.N. and WHITEHOUSE, M.J. 2008. Plesovice zircon-A new natural reference material for U-Pb and Hf isotopic microanalysis. *Chemical geology*, **249**, 1-35.

SMITH, J. V., 1974. Feldspar minerals. Chemical and textural properties. *Springer*, 690p.

SMITH, J.W., 1979. Geology of the Wadi Azlam quadrangle, sheet 27/36C, Kingdom of Saudi Arabia. *Saudi Arabian Deputy Ministry for Petroleum and Mineral Resources*, Geological map GM-36, with text, 36 p.

SOLIMAN, M.M., 1987. The younger granites and ring complexes of the Southeastern Desert of Egypt and their relation to mineralization. *Journal of African Earth Science*s, **6** (5), 745-754.

SORENSEN, S., 1991. Petrogenetic significant of zoned allanite in garnet amphibolites from a paleo-subduction zone in Catalina Schist, southern California. *American Mineralogist*, **76**, 589-601.

STERN, R. and JOHNSON, P., 2010. Continental lithosphere of the Arabian Plate: A geologic, petrologic, and geophysical synthesis. *Earth Sciences Reviews*, **101**(1-2), 29-67.

STERN, R.J., JOHNSON, P.R., KRÖNER, A. and YIBAS, B., 2004. Neoproterozoic Ophiolites of the Arabian-Nubian Shield. *Developments in Precambrian Geology*, 95-128.

STOESER, D.B., 1986. Distribution and tectonic setting of plutonic rocks of the Arabian Shield. *Journal of African Earth Sciences*, **4**, 21-46.

STOESER, D.B. and CAMP, V.E., 1984. Pan-African microplate accretion of the Arabian Shield, *U.S.G.S.* Mission, D.G.M.R., TR-4-1-R-670.

STOESER, D.B., and ELLIOTT, J.E., 1980. Post-orogenic peralkaline and calc-alkaline granites and associated mineralization of the Arabian shield. In: Evolution and Mineralization of the Arabian-Nubian Shield. *Institute for Applied Geology Bulletin* 3, 4 (1-23) Oxford, Pergamon Press Ltd, **4**, 168p.

STOESER, D.B. and FROST, C.D., 2006. Nd, Pb, Sr, and O isotopic characterization of Saudi Arabian Shield terranes. *Chemical Geology*, **226,** 163– 188.

STOESER, D.B., JACKSON, N.J., RAMSAY, C.R., DRYSDALL, A.R., Du BRAY, E.A. and DOUCH, C.J., 1985. Map of Plutonic Rocks in The Arabian Shield, Kingdom of Saudi Arabia (northern sheet). *U.S.G.S*

STRECKEISEN, A., 1976. To each plutonic rock its proper name. *Earth Science Reviews*, 12, 1-33 p.

SYLVESTER, P.J., 1989. Post-Collisional Alkaline Granites. *Journal of Geology*, **97**(3), 261-280.

TADESSE, T., HOSHINO, M., SUZUKI, K. and IIZUMI, S., 2000. Sm-Nd, Rb-Sr and Th-U-Pb zircon ages of syn- and post-tectonic granitoids from the Axum area of northern Ethiopia. *Journal of African Earth Sciences*, **30**(2), 313-327.

TARASSOV, M., TARASSOVA, E. and PIROEVA, I., 2008. Alteration of monazite in the Igralishte granite pluton, Southwestern Bulgaria. *Bulgarian Geological Society*, 25-26.

TASEKO MINES LIMITED, 2011 Taseko Announces Inferred Resource at Aley Niobium Project. Available from: www.tasekomines.com/tko/NewsReleases.asp?ReportID=478487

TAYLOR, S.R. and McLENNAN, S.M., 1985. The Continental Crust: Its Composition and Evolution. *Blackwell*, p. 312.

TEKLAY, M., KRÖNER, A. and MEZGER, K., 2001. Geochemistry, geochronology and isotope geology of Nakfa intrusive rocks, northern Eritrea: products of a tectonically thickened Neoproterozoic arc crust. *Journal of African Earth Sciences,* **33**(2), 283-301.

THIRLWALL, M.F., 1982. A triple filament method for rapid and precise analyses of rare earth elements by isotope dilution. *Chemical Geology*, 35, 155-166.

THIRLWALL, M.F., 2002. Multicollector ICP-MS analysis of Pb isotopes using a 207Pb-204Pb double spike demonstrates up to 4000 ppm/amu systematic errors in Tl-normalization. *Chemical Geology*, 184, 255-279.

TISCHENDORF, G., 1977. Geochemical and petrographic characteristics of silicic magmatic rocks associated with rare-element mineralization. In: Metallization Associated with Acid Magmatism. *Czechoslovakian Geologic Survey,* **2**, 41-96.

TOWNSEND, K.J., MILLER, C.F., D`ANDREA, J.L., AYERS, J.C., HARRISON, T.M. and COATH, C.D., 2000. Low temperature replacement of monazite in the Ireteba granite, Southern Nevada: geochronological implications. *Chemical Geology*, **172**, 95-112.

TSURUMI, J., HOSONUMA, H. and KANAGAWA, K., 2003. Strain localization due to a positive feedback of deformation and myrmekite-forming reaction in granite and aplite mylonites along the Hatagawa Shear Zone of NE Japan. *Journal of Structural Geology,* **25**(4), 557-574.

TULLOCH, A.J., and CHALLIS, G.A., 2000. Emplacement depths of Paleozoic-Mesozoic plutons from western New Zealand estimated by hornblende-Al geobarometry. *New Zealand Journal of Geology and Geophysics,* **43**, 555-567.

VAIL, J.R., 1989. Ring complexes and related rocks in Africa. *Journal of African Earth Sciences,* **8**(1), 19-40.

VERNON, R.H., 1991. Questions about myrmekite in deformed rocks. *Journal of Structural Geology*, **13**(9), 979-985.

VERNON, H.R., 2004. A practical Guide to Rock Microstructure. *Cambridge University Press*, 594 p.

WANG, Q., McDERMOTT, F., XU, J. F., BELLON, H., ZHU, Y. T., 2005. Cenozoic K rich adakitic volcanics in the Hohxil area, northern Tibet: lower crustal melting in an intra-continental setting. *Geology* **,33**, 465–468.

WANG, Q., WYMAN, D.A., LI, Z., BAO, Z., ZHAO, Z., WANG, Y., JIAN, P., YANG, Y. and CHEN, L., 2010. Petrology, geochronology and geochemistry of ca. 780 Ma A-type granites in South China: Petrogenesis and implications for crustal growth during the breakup of the supercontinent Rodinia. *Precambrian Research*, **178**(1-4), 185-208.

WANG, X-L., ZHOU, J-C., GRIFFIN, W.L., WANG, R-C, QIU, J-S, O`REILLY, S.Y., XU, X., LIU, X-M. and ZHANG, G-L., 2007. Detrital zircon geochronology of Precambrian basement sequences in the Jiangnan orogen: Dating the assembly of the Yangtze and Cathaysia Blocks. *Precambrian Research*, **159**, 117-131.

WANG, X., ZHOU, J., QIU, J., ZHANG, W., LIU, X and ZHANG, G., 2006. LA-ICP-MS U-Pb zircon geochronology of the Neoproterozoic igneous rocks from Northern Guangxi, South China: Implications for tectonic evolution. *Precambrian Research,* **145,** 111–130.

WILSON, M., 1989. Igneous Petrogenesis. *Unwin Hyman*, London. 466p.

WU, Y., ZHENG, Y., TANG, J., GONG, B., ZHAO, Z. and LIU, X., 2007. Zircon U–Pb dating of water–rock interaction during Neoproterozoic rift magmatism in South China. *Chemical Geology,* **246**(1-2), 65-86.

YAMAGUCHI, Y., 1985. Homblende-cummingtonite and hornblende-actinolite intergrowths from the Koyama calc-alkaline intrusion, Susa, southwest Japan. *American Mineralogist,* **70**, 980-986.

YANG, K.F., FAN, H.R., SANTOSH, M, HU, F.F. and WANG, K.Y., 2011. Mesoproterozoic carbonatitic magmatism in the Bayan Obo deposit, Inner Mongolia, North China: Constraints for the mechanism of super accumulation of rare earth elements. *Ore Geology Reviews*, **40,** 122-131.

YUGUCHI, T. and NISHIYAMA, T., 2008. The mechanism of myrmekite formation deduced from steady-diffusion modeling based on petrography: Case study of the Okueyama granitic body, Kyushu, Japan. *Lithos,* **106** (3-4), 237-260.

ZAW, K., 1990. Geological, petrogical and geochemical characteristics of granitoid rocks in Burma: with special reference to the associated W-Sn mineralization and their tectonic setting. *Journal of Southeast Asian Earth Sciences,* **4**(4), 293-335.

ZENTENO, D., CHAVEZ, P., and TOLSON, G., 1996.Uplift and subduction erosion in southwestern Mexico since the Oligocene: pluton geobarometry constraints. *Earth and Planet Science Letters,* **141** (1-4), 51-65.

ZHAO, X., ZHOU, M., LI, J. and WU, F., 2008. Association of Neoproterozoic A- and I-type granites in South China: Implications for generation of A-type granites in a subduction-related environment. *Chemical Geology,* **257** (1-2), 1-15.